ACS NANO

www.acsnano.org

NANO FOCUS

Diverse Applications of Nanomedicine

Beatriz Pelaz,[†] Christoph Alexiou,[‡] Ramon A. Alvarez-Puebla,[§,∥] Frauke Alves,[#,¶,□] Anne M. Andrews,[■,○,Φ] Sumaira Ashraf,[†] Lajos P. Balogh,[●] Laura Ballerini,[△] Alessandra Bestetti,[▲] Cornelia Brendel,[▽] Susanna Bosi,[▼] Monica Carril,[⬡,⬢] Warren C. W. Chan,[$] Chunying Chen,[∞] Xiaodong Chen,[⊗] Xiaoyuan Chen,[∫] Zhen Cheng,[‡] Daxiang Cui,[ℏ] Jianzhong Du,[∀] Christian Dullin,[¶] Alberto Escudero,[†,ǎ] Neus Feliu,[∂] Mingyuan Gao,[ϕ] Michael George,[Π] Yury Gogotsi,[◑] Arnold Grünweller,[⊕] Zhongwei Gu,[&] Naomi J. Halas,[¤] Norbert Hampp,[Φ] Roland K. Hartmann,[⊕] Mark C. Hersam,[⌀] Patrick Hunziker,[◊,◊] Ji Jian,[◆] Xingyu Jiang,[∞] Philipp Jungebluth,[◨] Pranav Kadhiresan,[$] Kazunori Kataoka,[⊡] Ali Khademhosseini,[††] Jindřich Kopeček,[‡‡] Nicholas A. Kotov,[§§] Harald F. Krug,[⊥⊥] Dong Soo Lee,[¶¶] Claus-Michael Lehr,[□□,■■] Kam W. Leong,[○○] Xing-Jie Liang,[∞,●●] Mei Ling Lim,[∂] Luis M. Liz-Marzán,[⬡,⬢,△△] Xiaowei Ma,[●●] Paolo Macchiarini,[▲▲] Huan Meng,[■,▼▼] Helmuth Möhwald,[▽▽] Paul Mulvaney,[▲] Andre E. Nel,[■,▼▼] Shuming Nie,[⬡⬡] Peter Nordlander,[¤] Teruo Okano,[⬢⬢] Jose Oliveira,[$$] Tai Hyun Park,[∞∞,⊗⊗] Reginald M. Penner,[∫∫] Maurizio Prato,[▼,⬡,⬢] Victor Puntes,[∥,‡‡,ΦΦ] Vincent M. Rotello,[ℏℏ] Amila Samarakoon,[$] Raymond E. Schaak,[∀] Youqing Shen,[ǎǎ] Sebastian Sjöqvist,[∂] Andre G. Skirtach,[▽▽,∂∂] Mahmoud G. Soliman,[†] Molly M. Stevens,[ϕϕ] Hsing-Wen Sung,[⊕⊕] Ben Zhong Tang,[ΠΠ] Rainer Tietze,[‡] Buddhisha N. Udugama,[$] J. Scott VanEpps,[§§] Tanja Weil,[&&,◑◑] Paul S. Weiss,[■,○,¤¤] Itamar Willner,[ΦΦ] Yuzhou Wu,[◑◑,⌀⌀] Lily Yang,[$$] Zhao Yue,[†] Qian Zhang,[†] Qiang Zhang,[◊◊] Xian-En Zhang,[◊◊] Yuliang Zhao,[∞] Xin Zhou,[◆◆] and Wolfgang J. Parak*[,†,⬡]

[†]Fachbereich Physik, [▽]Fachbereich Medizin, [⊕]Fachbereich Pharmazie, and [Φ]Department of Chemistry, Philipps Universität Marburg, 35037 Marburg, Germany

[‡]ENT-Department, Section of Experimental Oncology & Nanomedicine (SEON), Else Kröner-Fresenius-Stiftung-Professorship for Nanomedicine, University Hospital Erlangen, 91054 Erlangen, Germany

[§]Department of Physical Chemistry, Universitat Rovira I Virgili, 43007 Tarragona, Spain

[∥]ICREA, Pg. Lluís Companys 23, 08010 Barcelona, Spain

[#]Department of Haematology and Medical Oncology, [¶]Department of Diagnostic and Interventional Radiology, University Medical Center Göttingen, 37075 Göttingen Germany

[□]Department of Molecular Biology of Neuronal Signals, Max-Planck-Institute for Experimental Medicine, 37075 Göttingen, Germany

[■]California NanoSystems Institute, [○]Department of Chemistry and Biochemistry and [Φ]Department of Psychiatry and Semel Institute for Neuroscience and Human Behavior, [▼▼]Division of NanoMedicine and Center for the Environmental Impact of Nanotechnology, and [¤¤]Department of Materials Science and Engineering, University of California, Los Angeles, Los Angeles, California 90095, United States

[●]AA Nanomedicine & Nanotechnology Consultants, North Andover, Massachusetts 01845, United States

[△]International School for Advanced Studies (SISSA/ISAS), 34136 Trieste, Italy

[▲]School of Chemistry & Bio21 Institute, University of Melbourne, Parkville, Victoria 3010, Australia

[▼]Department of Chemical and Pharmaceutical Sciences, University of Trieste, 34127 Trieste, Italy

[⬡]CIC biomaGUNE, Paseo de Miramón 182, 20014, Donostia - San Sebastián, Spain

[⬢]Ikerbasque, Basque Foundation for Science, 48013 Bilbao, Spain

[$]Institute of Biomaterials and Biomedical Engineering, University of Toronto, Toronto, Ontario M5S 3G9, Canada

[∞]CAS Center for Excellence in Nanoscience and CAS Key Laboratory for Biomedical Effects of Nanomaterials and Nanosafety, National Center for Nanoscience and Technology of China, Beijing 100190, China

Received: September 7, 2016
Published: March 14, 2017

DOI: 10.1021/acsnano.6b06040
ACS Nano 2017, 11, 2313−2381

[⊗]School of Materials Science and Engineering, Nanyang Technological University, Singapore 639798
[∫]Laboratory of Molecular Imaging and Nanomedicine, National Institute of Biomedical Imaging and Bioengineering, National Institutes of Health, Bethesda, Maryland 20892, United States
[‡]Molecular Imaging Program at Stanford and Bio-X Program, Canary Center at Stanford for Cancer Early Detection, Stanford University, Stanford, California 94305, United States
[ℏ]Institute of Nano Biomedicine and Engineering, Department of Instrument Science and Engineering, School of Electronic Information and Electronical Engineering, National Center for Translational Medicine, Shanghai Jiao Tong University, 200240 Shanghai, China
[∀]Department of Polymeric Materials, School of Materials Science and Engineering, Tongji University, Shanghai, China
[ϡ]Instituto de Ciencia de Materiales de Sevilla. CSIC, Universidad de Sevilla, 41092 Seville, Spain
[∂]Department of Clinical Science, Intervention, and Technology (CLINTEC), Karolinska Institutet, 141 86 Stockholm, Sweden
[∮]Institute of Chemistry, Chinese Academy of Sciences, 100190 Beijing, China
[Π]Nanion, 80636 München, Germany
[&]College of Polymer Science and Engineering, Sichuan University, 610000 Chengdu, China
[◑]Department of Materials Science and Engineering and A.J. Drexel Nanomaterials Institute, Drexel University, Philadelphia, Pennsylvania 19104, United States
[¤]Departments of Physics and Astronomy, Rice University, Houston, Texas 77005, United States
[⌀]Departments of Materials Science and Engineering, Chemistry, and Medicine, Northwestern University, Evanston, Illinois 60208, United States
[⟠]University Hospital, 4056 Basel, Switzerland
[◊]CLINAM, European Foundation for Clinical Nanomedicine, 4058 Basel, Switzerland
[⧫]Department of Polymer Science and Engineering and [ϡϡ]Center for Bionanoengineering and Department of Chemical and Biological Engineering, Zhejiang University, 310027 Hangzhou, China
[◨]Thoraxklinik Heidelberg, Universitätsklinikum Heidelberg, 69120 Heidelberg, Germany
[⊡]The University of Tokyo, Bunkyo, Tokyo 113-8654, Japan
[††]Havard University, Cambridge, Massachusetts 02139, United States
[‡‡]Biomedical Polymers Laboratory, University of Utah, Salt Lake City, Utah 84112, United States
[§§]Emergency Medicine, University of Michigan, Ann Arbor, Michigan 48019, United States
[⊥⊥]EMPA, Federal Institute for Materials Science and Technology, CH-9014 St. Gallen, Switzerland
[¶¶]Department of Molecular Medicine and Biopharmaceutical Sciences and [∞∞]School of Chemical and Biological Engineering, Seoul National University, Seoul, South Korea
[□□]Department of Pharmacy, Saarland University, 66123 Saarbrücken, Germany
[■■]HIPS - Helmhotz Institute for Pharmaceutical Research Saarland, Helmholtz-Center for Infection Research, 66123 Saarbrücken, Germany
[○○]Department of Biomedical Engineering, Columbia University, New York City, New York 10027, United States
[●●]Laboratory of Controllable Nanopharmaceuticals, Chinese Academy of Sciences (CAS), 100190 Beijing, China
[△△]Biomedical Research Networking Center in Bioengineering Biomaterials and Nanomedicine, Ciber-BBN, 20014 Donostia - San Sebastián, Spain
[▲▲]Laboratory of Bioengineering Regenerative Medicine (BioReM), Kazan Federal University, 420008 Kazan, Russia
[▽▽]Department of Interfaces, Max-Planck Institute of Colloids and Interfaces, 14476 Potsdam, Germany
[⬡⬡]Emory University, Atlanta, Georgia 30322, United States
[⬢⬢]Tokyo Women's Medical University, Tokyo 162-8666, Japan
[$$]SMALL, Wiley-VCH, Weinheim, German
[⊗⊗]Advanced Institutes of Convergence Technology, Suwon, South Korea
[∫∫]Department of Chemistry, University of California, Irvine, California 92697, United States
[‡‡]Institut Català de Nanotecnologia, UAB, 08193 Barcelona, Spain
[ΦΦ]Vall d'Hebron University Hospital Institute of Research, 08035 Barcelona, Spain
[ℏℏ]Department of Chemistry, University of Massachusetts, Amherst, Massachusetts 01003, United States
[∀∀]Department of Chemistry, The Pennsylvania State University, University Park, Pennsylvania 16802, United States
[∂∂]Department of Molecular Biotechnology, University of Ghent, B-9000 Ghent, Belgium
[∮∮]Department of Materials, Department of Bioengineering, Institute for Biomedical Engineering, Imperial College London, London SW7 2AZ, United Kingdom
[ΠΠ]Hong Kong Branch of Chinese National Engineering Research Center for Tissue Restoration and Reconstruction, Hong Kong, China

DOI: 10.1021/acsnano.6b06040
ACS Nano 2017, 11, 2313−2381

⊕⊕Department of Chemical Engineering and Institute of Biomedical Engineering, National Tsing Hua University, Hsinchu City, Taiwan, ROC 300

&&Institut für Organische Chemie, Universität Ulm, 89081 Ulm, Germany

◑◑Max-Planck-Institute for Polymer Research, 55128 Mainz, Germany

ΦΦInstitute of Chemistry, The Center for Nanoscience and Nanotechnology, The Hebrew University of Jerusalem, Jerusalem 91904, Israel

⌀⌀School of Chemistry and Chemical Engineering, Huazhong University of Science and Technology, 430074 Wuhan, China

◊◊School of Pharmaceutical Science, Peking University, 100191 Beijing, China

◊◊National Laboratory of Biomacromolecules, CAS Center for Excellence in Biomacromolecules, Institute of Biophysics, Chinese Academy of Sciences, 15 Datun Road, Chaoyang District, Beijing, 100101, China

♦♦Key Laboratory of Magnetic Resonance in Biological Systems, State Key Laboratory of Magnetic Resonance and Atomic and Molecular Physics, National Center for Magnetic Resonance in Wuhan, Wuhan Institute of Physics and Mathematics, Chinese Academy of Sciences, Wuhan 430071, China

ABSTRACT: The design and use of materials in the nanoscale size range for addressing medical and health-related issues continues to receive increasing interest. Research in nanomedicine spans a multitude of areas, including drug delivery, vaccine development, antibacterial, diagnosis and imaging tools, wearable devices, implants, high-throughput screening platforms, *etc.* using biological, nonbiological, biomimetic, or hybrid materials. Many of these developments are starting to be translated into viable clinical products. Here, we provide an overview of recent developments in nanomedicine and highlight the current challenges and upcoming opportunities for the field and translation to the clinic.

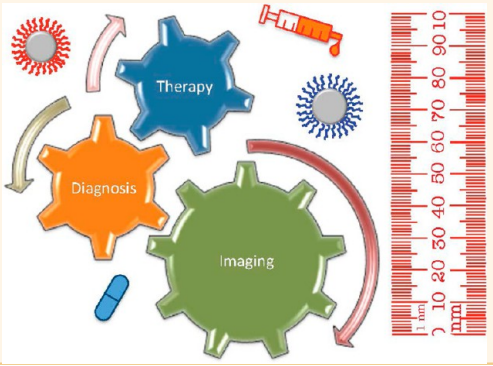

Medicine is the science, engineering, and practice of diagnosing, treating, curing, monitoring, predicting, and preventing diseases. Most people associate nanomedicine with pharmaceutical formulations, where soft or hard particles of nanometer dimensions are injected into humans for diagnosis and treatment. However, this field covers a broader range of research and development. Nanomedicine differs from other types of medicine in that it involves the development and application of materials and technologies with nanometer length scales to function in all the ways described below.[1−5]

Properties of nanoscale objects are transitional between molecular and bulk regimes. Nanoscale properties exist for all materials, regardless of whether they are found in nature or are synthetic. However, only synthetic objects are typically considered part of "nanoscience and engineering", whereas the study of biological nanoscale structures is often thought as part of characterization without considering biological properties. Because of the transitional nature of "nanoscale" materials, it is difficult to limit a material's reach and define its borders by strict definitions and solid numbers (*e.g.*, larger than atoms or small molecules, but smaller than 100 nm). More importantly, nanoscale particles can demonstrate new properties that can be exploited for the design of new therapeutic effects and diagnostics.

Nanomedicine is an interdisciplinary field, where nanoscience, nanoengineering, and nanotechnology interact with the life sciences. Given the broad scope of nanomedicine, we expect it eventually to involve *all* aspects of medicine. Moreover, nanomedicine, like medicine, can enter the clinics and can be part of conventional clinical practice assuming all aspects of translation are satisfied, including safety, regulatory, and ethical requirements. It is expected that nanomedicine will lead to the development of better devices, drugs, and other applications for early diagnoses or treatment of a wide range of diseases with high specificity, efficacy, and personalization, with the objective being to enhance patients' quality of life. In this Nano Focus, we do not attempt to define nanomedicine but rather to provide an overview of recent achievements, materials, and technologies belonging to nanomedicine.

Nanoparticles (NPs) are key components of nanomedicine, and currently, a large variety of nanoparticle types exist. However, no standardized nomenclature exists in the literature; therefore, terms such as engineered nanomaterials, nonbiological complex drugs (NBCDs), nanomedicals/nanomedicines, *etc.* are used freely. Many nanomaterials can replicate some functions of globular biological macromolecules.[6] Examples are lipid micelles,[7] different polymeric nanostructures,[8] protein constructs,[9] ribonucleic acid (RNA) NPs (RNPs),[10] carbon dots (C-dots),[11] nanodiamonds (NDs),[12] carbon nanotubes (CNTs),[13] graphene,[14] as well as inorganic materials such as mesoporous silica NPs (MSNP), superparamagnetic iron oxide NPs (SPIONs),[15] quantum dots (QDs),[16] plasmonic NPs,[17] gold nanoclusters (GNCS),[18] upconverting NPs (UCNPs),[19] *etc.* Many of these nanoscale materials have unique size- and shape-dependent optical, electronic, and magnetic properties, and these properties are dependent upon methods to synthesize, to purify, and to characterize them.[20−23] Many researchers note that small changes in size and shape can significantly affect the properties of the NPs. Precision syntheses are therefore necessary to produce samples with tightly focused distributions in order to achieve the targeted functions specifically and to correlate observed functions with specific NP characteristics. Detailed characterization of NP samples that are used in a medical application is also critical because one must know and understand what is being injected into the body. A sample of NPs may be heterogeneous with distinct subpopulations after synthesis.[24,25] Microscopic imaging is conventionally used, but this technique may be insufficient

DOI: 10.1021/acsnano.6b06040
ACS Nano 2017, 11, 2313−2381

because it is limited to a small number of NPs that may or may not be representative of the whole sample. Thus, microscopic imaging may not provide sufficient information about surface functionalization, composition, and other property-determining features. Other techniques that are starting to become part of the characterization scheme of NPs prior to use in humans are dynamic light scattering, transmission electron microscopy, gel electrophoresis, and ζ-potential analysis. However, there are no standardized characterization requirements of NPs[26] prior to use in humans, and this must be a focus for nanomedicine applications. The main reason is that the biodistribution and interaction of NPs with proteins is strongly size- and surface-dependent, and thus, in a heterogeneous sample, many NPs will distribute differently and may exhibit undesired effects or even toxicity. In addition to characterization, there is also a need to develop new and improved methods of NP separation and purification to produce optimal samples for nanomedical applications and for studying NP behavior inside the body[27,28] (which is important to design optimal NP formulations for medical use).

Despite the need to standardize characterization methods, NPs are expected to improve the detection and diagnosis of diseases. First, smart NPs can be designed to provide contrast at the zone of interest and report information about the local environment after administration into the body. This information can aid in imaging the anatomical fine structures of organs and labeling tissues with certain markers and enables local readout of the concentrations of molecules of interest, which helps to analyze diseases directly inside the human body. Second, NPs are key components of many high-throughput diagnostics machines that can analyze extracted samples (such as blood, tissue, *etc.*) outside of the body for rapidly detecting biological makers and molecular alterations. The ability to analyze multiple biomarkers simultaneously may improve diagnostic precision. Moreover, multifunctional or theranostic NPs that can simultaneously diagnose, treat, and even monitor therapeutic efficacy are being engineered.[29]

Nanoparticles are also being developed for the treatment of disease; NPs are used as delivery vehicles for pharmaceutical agents,[30] as bioactive materials, or as important components in implants.[31] In the case of delivery, NP-based carrier systems have a unique ability to cross biological barriers. Thus, NPs can enter tumors *via* their localized leaky vasculature and are retained due to poor lymphatic drainage in the tumor microenvironment.[32] This passive targeting is called the enhanced permeation and retention (EPR) effect.[33] There is an ongoing debate in the literature about the effectiveness of active, *i.e.*, ligand/receptor-mediated targeting, *versus* passive targeting, but any carrier has to be delivered to the designated site before it can bind to cell surface receptors or be retained by other effects.[34]

In addition to using nanomedicine to diagnose and to treat diseases, it is also important to establish NPs' efficacy and safety in biological systems. After the NP has functioned as designed after administration into the body, what happens to the carrier particle when the drug has been delivered or the tissue imaged? Elimination of the particles can potentially occur *via* renal or hepatobiliary clearance. If they do not get cleared, the long-term fate of the NPs is not clear. These particles may degrade and get cleared renally because they are small enough to transport through the kidney's filtration slits,[35−37] or they may accumulate in different organs and interact with off-target cells. The *in vivo* fate of NPs can potentially be a dynamic process, and thus, there is a need to understand nanobiokinetics (nanopharmacokinetics and pharmacodynamics), which may relate to unique and interesting toxicological responses of NPs.

Nanomedicine is not limited to colloidal materials and technologies to evaluate them for *in vivo* applications. Nanomedicine developments go beyond the "magic particulate bullet" concept.[38] Nanomedicine could involve the design of new scaffolds and surfaces for engineering sensors or implantable systems and electronics to aid in the regeneration of tissues (*i.e.*, regenerative medicine). Many of these concepts are still at the early stages of development, but some have already reached clinical practice.

This Nano Focus article is organized into four subsections that are focused on specific applications of materials or systems with nanoscale properties: (a) *in vivo* diagnostics, (b) *in vitro* diagnostics, (c) *in vivo* therapeutics, and (d) implantable nanomaterials.

IN VIVO DIAGNOSIS ("SMART IMAGING")

A key focus in nanomedicine involves the use of nanomaterials as contrast agents for anatomical and functional imaging. Using nanomaterials as contrast agents enables visualization of structures inside the human body and helps clinicians to delineate healthy from diseased tissues and to recommend proper treatment. Nanoparticles can be engineered with different contrast properties. The most common modalities are computed tomography (CT); magnetic resonance imaging (MRI); imaging of radioactivity, such as positron emission tomography (PET) or single photon emission computed tomography (SPECT); fluorescence imaging; and photoacoustic imaging. For all these techniques, material development is crucial because the NPs are contrast agents that enable visualization of biological tissues. For this application, NPs can be engineered to localize in specific tissues and potentially produce high contrast.

A key focus in nanomedicine involves the use of nanomaterials as contrast agents for anatomical and functional imaging.

Computed Tomography. X-ray-based imaging enables high-resolution anatomical and, in the case of CT also three-dimensional (3D), imaging of mostly skeletal tissues at unlimited depth in human applications. Computed tomography imaging is the work-horse in clinical diagnostics due to the simplicity of the technique, the comparable low demands on infrastructure, the rapid image generating, and the low costs for a standard examination.

In recent years, around 250 out of every 1000 people in the United States underwent CT imaging.[39] Classical X-ray imaging harnesses the tissue-specific attenuation of X-ray energy to generate contrast in the recorded radiographs. Therefore, bones generate more contrast than soft tissue because of the larger relative electron density of bone. In order to boost the low contrast of soft tissue, contrast agents with elements such as iodine and barium characterized by a high-electron density are typically applied to visualize blood vessels in gastrointestinal (GI) tract, tumors, and other soft tissues. In contrast to typical functional imaging techniques such as PET and SPECT, in CT, the photons/X-rays are produced outside the body and only modulated by the tissues through which they travel. Thus, the large photon flux enables a high signal-to-noise ratio, leading CT to outperform other 3D imaging techniques in terms of spatial

DOI: 10.1021/acsnano.6b06040
ACS Nano 2017, 11, 2313−2381

resolution. However, the weak interaction between tissue and the incident X-ray beam results in comparably limited sensitivity of CT, which might explain why specifically targeting contrast strategies are virtually non-existent.

This poor sensitivity has encouraged nanomedicine researchers to develop nanoparticles as contrast agents for X-ray imaging. Gold nanoparticles (AuNPs) are central to this development. Due to its high atomic number and electron density (79 and 19.32 g/cm^3, respectively, *versus* the typical X-ray contrast agent, iodine, with values of 53 and 4.9 g/cm^3, respectively), AuNPs have higher attenuation coefficients and can be used as contrast agents for X-ray imaging, CT, and micro-CT.[40] The AuNPs are typically coated with targeting molecules such as folic acid so that they can highlight distinct tissue structures. Gold nanoclusters (NCs), which are smaller structures than AuNPs, are also being developed as CT contrast agents.[18,40] Folic-acid-conjugated AuNCs with silica shells were demonstrated to exhibit good biocompatibility and could actively target the folic acid receptor (+) *in vitro* of MGC-803 cells and *in vivo* gastric cancer tissues with 5 mm diameter in nude mice models. The researchers showed that the use of NCs exhibited excellent contrast for CT imaging. In addition to CT imaging, these NCs can also be used for molecular imaging since red fluorescence emission was observed.[41,42] These NCs also penetrated the tumor and were retained, but their small size enabled them to be cleared renally.[41,42] Thus, these NPs are promising candidates for future clinical use.

Besides gold, NPs composed of other materials with a high atomic number are also suited for CT. One example is $NaGdF_4$-based UCNPs. Besides providing contrast for CT, these NPs can be imaged optically (see Figure 1). In addition to their ability to provide contrast for CT, potential toxicity of NPs plays an important role toward translation to clinics (*vide infra*).

In parallel to the development of new CT contrast agents, there has also been progress in instrumentation relating to the preparation and detection of the agents. Novel X-ray sources such as synchrotrons provide tremendously more flux and a higher degree of coherence and therefore enable the exploitation of the wave nature of X-rays for imaging purposes. These novel X-ray sources have led to new applications like phase contrast CT, diffraction enhanced imaging, and holotomography, to name a few.[44−46] For example, phase contrast CT provides 10−200 times more contrast in soft tissue applications than classical absorption-based CT.[47,48] This gain in contrast directly translates into an increase in sensitivity. By coupling this increased sensitivity with the use of target-specific contrast agents, submicrometer-scale 3D spatial resolution can be achieved. This technique can be applied to gather structural

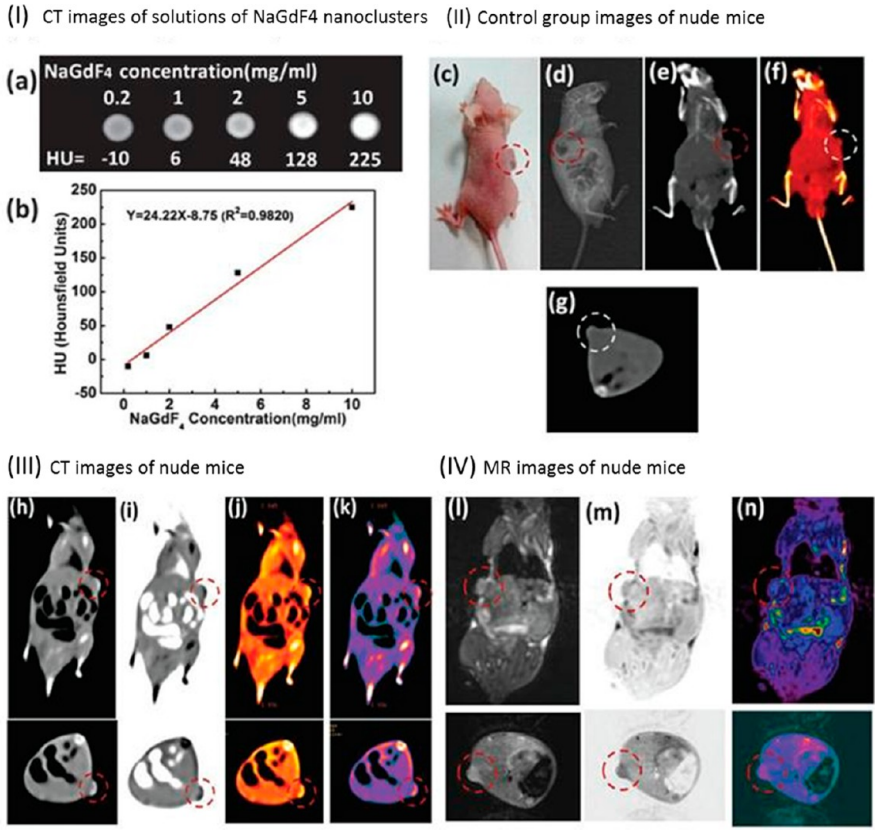

Figure 1. (I) *In vitro* CT images of (a) lanthanide-doped $NaGdF_4$ upconversion "nanoclusters" (<5 nm) suspended in aqueous solution. (b) CT attenuation plot (given in Hounsfield units, HU) of $NaGdF_4$ NPs in dependence of the concentration of each sample from 0.2 to 10 mg/mL to further investigate the CT contrast effect. (II) Images of a control group before injection of NPs: (c) photograph of a nude mouse loaded with gastric cancer MGC-803 cells; (d) X-ray image, and (e−g) CT images of nude mice from the control group. (III) (h−k) CT images and (IV) (l−n) MRI images of mice after intravenous injection with $NaGdF_4$ UCNPs, making use of passive targeting (EPR effect). The pulse sequence: electromagnetic conversion (EC) = 1/141.7 kHz; repetition time (TR time) = 2000; echo time (TE time) = 65.6/Ef (echo frequency). Parameters of transverse plane: the pulse sequence, EC = 1/141.7 kHz; TR time = 2000; TE time = 43.8/Ef. It took about 6 h to acquire one image. The relaxivity value of $NaGdF_4$ UCNPs at 1.5 T is about 4.5 mMs^{-1}. Adapted with permission from ref 43. Copyright 2015 Royal Society of Chemistry.

DOI: 10.1021/acsnano.6b06040
ACS Nano 2017, 11, 2313−2381

information indicative of asthma within the lung of a mouse.[49] It can also be applied in the visualization of macrophages loaded with barium sulfate after intracheal instillation.[49] In a study by Dullin *et al.*, the researchers achieved 9 μm resolution, which enabled the visualization of macrophage function within the local 3D environment.[46] The spatial resolution could be further improved to 400 nm by using holotomography (see Figure 2).[50]

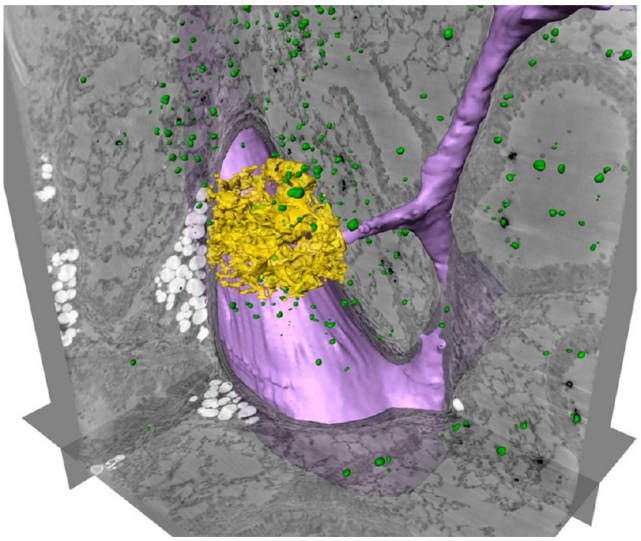

Figure 2. Three-dimensional localization of labeled macrophages in a 500 μm thick lung section of a healthy mouse, scanned by holotomography. Three orthogonally oriented slices are shown, together with automatically labeled barium clusters (green), representing macrophages loaded with barium sulfate and alveolar walls in a small region of interest (ROI, yellow). A part of a blood vessel has been marked semi automatically (purple). Adapted with permission from ref 50. Copyright 2015 Nature Publishing Group.

The NP-based CT imaging technologies can potentially change the way we perform CT-based clinical diagnosis.[51] Currently, soft tissue imaging *via* CT requires a large dose of iodine- or barium-containing contrast agents to overcome poor sensitivity. However, the high dose may not be well tolerated by patients. Furthermore, it is difficult to design traditional contrast agents to target specifically and to bind to cellular biomarkers or accumulate in tissues of interest such as sites of inflammation or primary tumors and metastasis. Combining targeted AuNPs with the recent development of energy-resolved detectors,[52] the discrimination of a multitude of different materials in a single CT scan should be possible in the near future. Therefore, the challenge facing the field is to design and to engineer small NP probes of high-atomic-number materials like iodine, gold, or barium, conjugated to targeting moieties that specifically label certain cell types *in vivo*, similar to probes used in optical imaging. Moreover, since novel CT techniques do not focus on X-ray attenuation but on phase shift or scattering as sources of contrast, other types of NPs like hollow spheres[53] or NPs with X-ray scattering properties will become increasingly important. Despite the negative effects of the applied X-ray dose, CT is the most applied technique in clinical diagnosis (*e.g.*, ~50% of imaging-based diagnostics performed in Germany in 2013 were by CT).[54] Improved detectors and the implementation of novel algorithms, especially newly developed reconstruction techniques, have already dramatically lowered X-ray doses.[55] Techniques like limited angle reconstruction and zoom tomography will further aid in this development.[50,56]

Magnetic Resonance Imaging. Magnetic resonance imaging is widely used for *in vivo* applications, due to its safety, spatial resolution, soft tissue contrast, clinical relevance, and ability to record anatomical and functional information about soft tissues and organs. Notably, MRI-responsive contrast agents provide physiological information that complements routine anatomical images. Since the technology is based on the interaction of nuclei with surrounding molecules in a magnetic field, MRI has no need for ionizing radiation and possesses unlimited depth of penetration and unparalleled soft tissue contrast.[57] However, MRI has relatively poor sensitivity in comparison to nuclear and optical modalities, thus leading to longer acquisition time and use of large amounts of contrast agents. Although the introduction of higher magnetic fields (higher than 4.7 T) could increase the signal-to-noise ratio, thereby permitting higher resolution and faster scanning, the safety of high static magnetic field strengths on human health is of great concern.[58,59] The development of hyperpolarized MRI (*i.e.*, polarization of the nuclear magnetic moments far beyond thermal equilibrium conditions)[60] has improved the sensitivity of the desired nuclei and enables quantitative *in vivo* imaging and real-time metabolic profiling using stable isotope precursors.[60] Current contrast agents such as paramagnetic agents or SPIONs play important roles in enhancing contrast in T_1 or T_2 images, which provide higher MRI sensitivity and accuracy for imaging living subjects. These agents accelerate the rate of T_1 and T_2 relaxation, thereby enhancing local contrast.[61] Paramagnetic agents (*e.g.*, gadolinium-based agents) principally accelerate longitudinal T_1 recovery, generating positive contrast, while superparamagnetic agents (*e.g.*, iron oxide-based agents such as SPIONs) primarily increase the rate of dephasing or transverse T_2 decay, resulting in negative contrast effects.[61] However, both types of agents have been associated with toxic effects, which needs to be taken into account for their use on humans and in veterinary medicine (*vide infra*).[62,63]

Conventional T_1 contrast agents such as paramagnetic complexes (based on Gd^{3+}, Mn^{2+}, or Fe^{3+}) are small molecules that leave the vascular system within minutes and are renally cleared. The short circulation time makes it difficult to acquire a high-resolution image of desired sites. Biocompatible NP-based T_1 contrast agents have been developed because they have a number of advantages over conventional T_1 contrast.[64,65] Researchers can tailor the size, shape, and composition; circulation time; target cells and tissues; and optical and physical properties to meet the biological requirements for optimizing imaging. For example, Gd(III)−nanodiamond conjugates enable contrast enhancement with a much smaller amount of Gd compared to other agents used.[66] For example, melanin has been intensively studied as a target for melanoma imaging and was recently a major focus for designing a multimodal imaging nanoplatform. Melanin NPs with diameters of 4.5 nm not only retain their unique optical properties but also have natural binding capability with various metal ions. After chelation with Fe^{3+} ions and subsequent conjugation with cyclic arginine-glycine-aspartic acid (RGD) molecules, melanin NPs serve as T_1 contrast agents for targeted MRI of U87MG glioblastoma.[67,68] In another example, a noncytotoxic asymmetrical cancer-targeting polymer vesicle based on R-poly(L-glutamic acid)-*block*-poly(ε-caprolactone) [R is folic acid or diethylenetriaminepentacetatic acid (DTPA)], as shown in Figure 3, was reported as a T_1 MRI contrast agent with enhanced sensitivity, and it also served as a delivery vehicle for cancer chemotherapy.[69] Such asymmetrical vesicles have a cancer-targeting outer corona

DOI: 10.1021/acsnano.6b06040
ACS Nano 2017, 11, 2313−2381

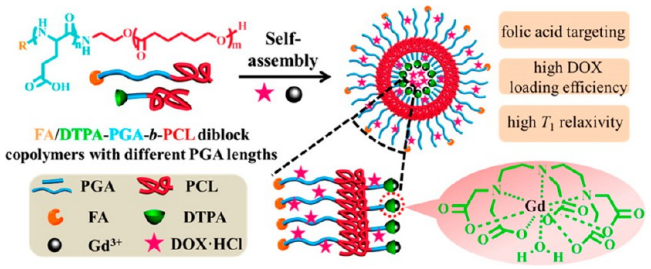

Figure 3. Illustration of multifunctional asymmetrical polymer vesicles for ultrasensitive T_1 MRI and effective cancer targeted drug delivery. Adapted from ref 69. Copyright 2015 American Chemical Society.

coupled with a Gd(III)-chelating and drug-loading-enhancing inner corona. Liu and colleagues demonstrated that such vesicles exhibited an extremely high T_1 relaxivity (42.39 mM^{-1} s^{-1}, 8-fold better than that of DTPA-Gd) and anticancer drug loading efficiency (52.6% for doxorubicin hydrochloride, DOX·HCl).[69] Moreover, the DOX-loaded vesicles exhibited 2-fold better antitumor activity than free DOX.[69]

As T_2 contrast agents, SPIONs establish a substantial locally perturbed dipolar field to shorten proton relaxation of the surrounding tissues significantly. The magnetism of NPs under normal magnetic field strengths is dependent on the magneto-crystalline anisotropy and the size of the NPs. In comparison to their spherical counterparts, for example, iron oxide NPs with an octapod shape exhibit an ultrahigh transverse relaxivity value, and dramatically increase the sensitivity of MRI for early stage cancer detection, largely due to their effective radius and the local field inhomogeneity of the magnetic core.[70] Because of the negative contrast effect and magnetic susceptibility artifacts, it is still a major challenge to distinguish the region of signals induced by iron oxide NPs from low-level background magnetic resonance (MR) signals originating from adjacent tissues such as bone, vasculature, calcification, fat, hemorrhage, blood clots, *etc.* As a combination of paramagnetic and SPIONs, *e.g.*, in core/shell structures,[71] dual-mode T_1/T_2 contrast agents have been developed for dual T_1 and T_2 mode MRI because they help validate reconstruction and visualization of the data in an accurate and reliable way. However, interference inevitably occurs when both T_1 and T_2 contrast agents are integrated into a single nanostructure in close proximity. The magnetic field induced by the T_2 contrast material perturbs the relaxation process of paramagnetic T_1 contrast materials, leading to undesirable quenching of the T_1 signal. Core/shell structures can efficiently reduce their magnetic coupling by introducing a separating layer between the superparamagnetic core and paramagnetic shell. Such magnetically decoupled dual-mode T_1/T_2 contrast agents not only provide superior MR contrast effects in both modes, but also enable self-confirmation of images and essentially function as an "AND logic gate" to reduce susceptibility artifacts from the raw images to enhance accuracy of the MRI.[72,73] In contrast to core/shell structures, dumbbell hybrid nanostructures combine T_1 and T_2 contrast agents together in a nanocomposite *via* a bridge NP, which spatially separates two contrast agents at a certain distance to reduce their magnetic coupling.[74] Unlike core/shell structures where T_2 contrast agents are sequestered within a supporting matrix, dumbbell nanostructures allow both T_1 and T_2 contrast agents to be exposed to their immediate environment without compromising their magnetic properties. Moreover, both surfaces of T_1 and T_2 contrast agents are available for subsequent surface coating for targeting molecular imaging.

Besides being "mere" contrast agents for MRI,[75,76] activatable or "smart" NPs can respond to a change in tumor microenvironment to instigate the therapeutic and diagnostic mechanism.[77,78] The most common triggers for activatable NPs are stimuli such as pH, temperature, redox reactions,[79] metabolites, ions, proteases, ultrasound, and light.[80] The tumor microenvironment regulates tumor progression and the spread of cancer in the body. Responsive agents capable of reporting diagnostically relevant physicochemical properties of the microenvironment in which the contrast agent distributes have gained tremendous attention. Various nanocarriers have been tested in combination with a myriad of imaging contrast agents, payload drugs, and targeting moieties, leading to the formulation of theranostic NPs capable of delivering therapy concomitant with diagnosis. In the case of MRI, different "smart" NP probes have been demonstrated. The design of pH-responsive probes is of great interest, since it is an important physiological parameter and pH dysregulation can be a cancer marker. Gao and colleagues reported a smart pH-activatable ^{19}F-probe for detecting specific and narrow pH transitions ranging from 5.5 to 7.4 in biological systems.[81] They developed micelles composed of fluorinated polymers with tertiary amines having different pK_a values. The protonation of such amines at pH below their pK_a results in micelle disassembly and ^{19}F-MRI/nuclear magnetic resonance spectroscopy (NMR) signal activation. They were able to determine the pH through the identification of the corresponding activated ^{19}F-reporter. In another related example, hypoxia in the tumor microenvironment results in lactic acid production and, hence, acidic conditions. Zhou and colleagues fabricated pH-triggered NPs for ^{19}F-MRI and fluorescence imaging (MRI-FI) of cancer cells.[82] ^{19}F was attached to AuNPs by acid-labile hydrazone linkers. Fluorescence imaging revealed highly selective uptake of these NPs by lung cancer cells. The "trick" to these NPs involves selective release of ^{19}F-MRI contrast agent after the NPs have reached the tumor environment. In the acidic intracellular compartments of cancer cells the ^{19}F detached from the AuNPs and appreciably enhances the intracellular ^{19}F-MRI signal, as shown in Figure 4.

Temperature differences between tissues is a common feature in pathological conditions, especially in tumors. Thus, a second class of "smart" NP probes for MRI uses hypersensitive detection of temperature changes in different tissues.[83] Langereis and colleagues[84] reported a combined temperature-sensitive liposomal ^{1}H chemical exchange saturation transfer (CEST)[85] and ^{19}F magnetic resonance (MR) contrast agent as a potential carrier system for MRI-guided drug delivery. The liposomes contain both a chemical shift agent as well as a highly fluorinated compound. Upon reaching the melting temperature of the agents' lipid membrane, the lipo-CEST contrast enhancement vanishes, due to the release of the chemical shift agent. Simultaneously, the ^{19}F-MRI probe is freed from the influence of the paramagnetic shift agent causing an appearance of a ^{19}F-MRI signal. The combined CEST and ^{19}F-MR temperature-sensitive liposomal carrier provides CEST-based contrast enhancement, which can be switched on and off, to localize the liposomes before release, while the ^{19}F-MR signal can potentially quantify local drug release of drugs with MRI.

Redox reactions play crucial roles in biological processes, and abnormal redox reactions are implicated in various conditions including liver damage and human immunodeficiency virus (HIV). A third class of "smart" NP probes for MRI uses redox

DOI: 10.1021/acsnano.6b06040
ACS Nano 2017, 11, 2313−2381

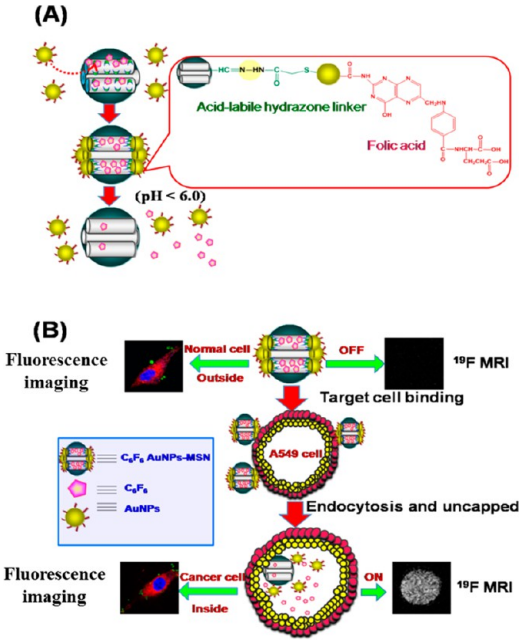

Figure 4. (A) Synthesis of AuNPs capped with folic acid and ^{19}F contrast agent. Folic acid with a high tumor affinity due to the overexpression of its receptors on the cancer cells was conjugated onto the surface of the AuNPs. ^{19}F contrast agent was covalently conjugated onto the AuNPs *via* acid-labile hydrazone linkers. (B) pH-triggered release of the ^{19}F contrast agent from the AuNPs to the cytosol *via* the selective removal of the pH-labile cap in the acidic intracellular compartments of cancer cells. Adapted with permission from ref 82. Copyright 2014 Royal Society of Chemistry.

reactions in the tumor microenvironment for cleavage of atoms from the NP structure. Kikuchi and co-workers designed redox activatable NPs to image reducing environments.[86] Gd^{3+} complexes were attached to the surface of ^{19}F containing NPs by disulfide linkers. Vicinity of the Gd^{3+} to ^{19}F reduces the transveral relaxation time T_2 of the fluorine compounds by the paramagnetic relaxation enhancement effect, which attenuates the ^{19}F NMR/MRI signal (see Figure 5). When the disulfide

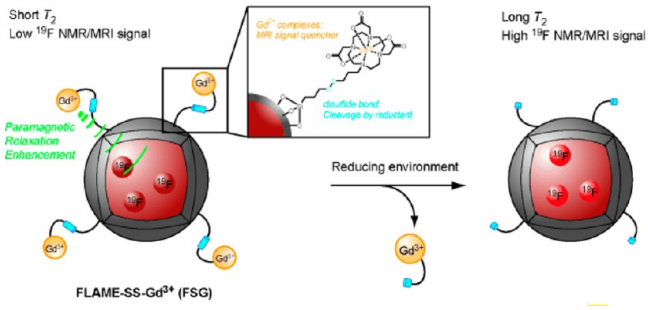

Figure 5. Design of redox activatable NPs. Adapted with permission from ref 86. Copyright 2015 Wiley-VCH Verlag GmbH & Co.

bonds enabling attachment of Gd^{3+} are reduced, the Gd^{3+} complexes are cleaved from the NP surface. Then, the T_2 NMR/MRI signal of the encapsulated ^{19}F compounds increases, indicating the presence of the NPs in redox active environment.

Imaging Radiolabels. There has been rapid progress in the development of NP-based radiolabels.[87] Chelators such as 1,4,7,10-tetraazacyclododecane-1,4,7,10-tetraacetic acid (DOTA) and 1,4,7-triazacyclononane-1,4,7-trisacetic acid are commonly used to label diagnostic positron emitters, *e.g.*, ^{68}Ga or ^{64}Cu, or therapeutic beta-emitters, *e.g.*, ^{177}Lu or ^{90}Y. The sequential use of different poly(ethylene glycol) (PEG) -coated emitters, *e.g.*, ^{68}Ga and ^{177}Lu enable multiplexed labeling, as well as improved circulation time. For this purpose, micelle encapsulation was introduced for combining a mixture of amphiphiles comprising chelators bearing the radiolabels, ligands for targeting, and PEG for surface passivation with originally hydrophobic NPs.[88] The same method could successfully be applied for different types of NPs, such as SPIONs, plasmonic NPs, and core/shell UCNPs. Sometimes the NPs can be labeled postsynthetically without the use of chelators for radiometals.[89] The resulting radiolabeled NPs enable researchers to trace their biodistribution when administered systemically, and to study fundamental NP *in vivo* process (*e.g.*, determining the contribution of active *versus* passive tumor targeting in mouse models).[90]

In fact, radiolabels are particularly suited for quantitative biodistribution studies. γ-emission is barely absorbed by tissue, and radioactivity is independent of the probe's local environment, *i.e.*, there are no substantial quenching effects such as in the case of fluorophores, which often exhibit pH-dependent emission. Using radiolabels produces excellent signals and, therefore, a low dose can yield sufficient image quality to make a diagnostic interpretation. One additional advantage is the ability for multiplexed read-out of radiolabels with different γ-emission energies in parallel. This has been recently used for recording the biodistribution of several compounds of NPs independently.[37] Most NPs are hybrid structures composed of their functional part (*i.e.*, contrast for imaging) and an organic surface coating that provides colloidal stability and targeting capability, as well as the corona of adsorbed proteins.[91,92] By adding radiolabels of different energies to different parts of the NPs, the NPs could disintegrate after *in vivo* administration, *i.e.*, the organic surface capping may come off the functional particle core.[37] Such studies in the future will enable imaging of the different NP components to elucidate the fate of the different parts of the NP. This will be important for understanding the biodegradability of all different parts of a NP and their elimination. This is decisive for guiding the design of NPs for use in *in vivo* delivery applications. However, when different labeling methods and radioisotopes are used to label NPs to study their fate, it is crucial to ensure that the radioisotopes are incorporated onto the NPs with little impact on their original biological behavior.

Fluorescence Imaging. Fluorescence is a useful imaging modality because the emission of the probes after excitation can be visualized by the naked eye or at higher resolution with optical microscopy. There is an abundance of available fluorophores that can be tailored to specific applications. Many traditional organic fluorophores suffer from aggregation-caused quenching (ACQ), thereby limiting design schemes where specific interactions promote fluorophore localization. This has forced researchers to use dilute solutions (often at the nanomole level) of fluorophores. Given the minuscule amount of fluorophore, they can be easily photobleached, which imposes a limit on the achievable contrast. Contrary to ACQ, aggregation-induced emission (AIE) is where increased aggregation yields a stronger fluorescent signal.[93] This makes AIE fluorogens (AIEgens) good candidates for bioimaging applications.[94] The accumulation of AIEgens at regions of interest results in the formation of nanoaggregates (AIE dots), which intensifies the fluorescence signal. The AIE dots are resistant to photobleaching, enabling high-quality bioimaging over a wide time window. They are suitable for long-term tracking of theranostic processes such as tumor-metastasis

DOI: 10.1021/acsnano.6b06040
ACS Nano 2017, 11, 2313−2381

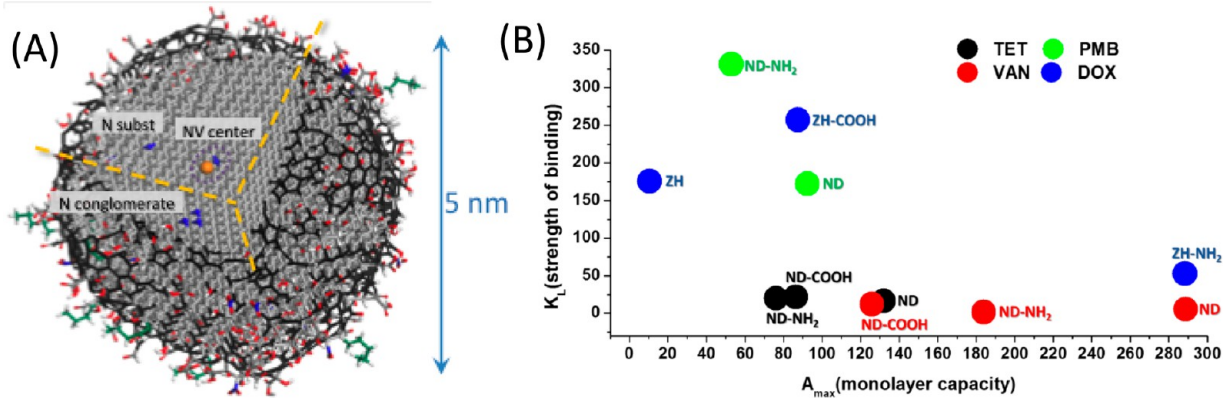

Figure 6. (A) Schematic model of a 5 nm ND with a fluorescent NV center and a variety of surface terminations after oxidative purification is shown. The diamond core is covered by a layer of surface functional groups that stabilize the NP by terminating its dangling bonds. The surface can also be stabilized by the conversion of sp^3 carbon to sp^2 carbon. Adapted with permission from ref 118. Copyright 2012 Nature Publishing Group. (B) Plot showing the strength of binding (K_L) *versus* the monolayer capacity (A_{max}) based on a Langmuir model for DOX, polymyxin B, tetracycline, and vancomycin adsorbed on detonation-produced ND from two sources (ZH and ND) with different surface chemistries: the as-received surface, like in the right picture, carboxylated (−COOH) and aminated ($-NH_2$) surfaces. Adapted with permission from refs 125 and 126. Copyright 2016 Elsevier and copyright 2013 American Chemical Society, respectively.

monitoring, drug delivery/release, and stem-cell therapy.[95] Organic AIE dots enjoy almost all advantages of inorganic QDs,[96,97] yet are free of the disadvantages of the latter (*e.g.*, cytotoxicity[98,99]). In addition, AIE molecules and nanoaggregates can be decorated by functional groups with binding specificity to particular receptors that enables active targeting.[94,96,97] Integration of an RGD unit with the AIEgen structure, for example, has generated integrin-specific fluorescence turn-on bioprobes for tumor cell targeting, image-guided drug delivery, *in situ* monitoring of therapeutic effect, *etc.*[100,101]

Two decades ago, fluorescent semiconductor QDs were introduced for the fluorescent labeling of biological molecules and cells.[102,103] Due to their narrow emission bands, QDs are suited for multiplexed read-out, as detailed below.[104,105] Semiconductor QDs are also bright and show reduced photobleaching, which makes them suitable for long-term imaging at the single-molecule level.[106−108] However, semiconductor QDs can be cytotoxic toward cells due to the release of metal ions[98,99] and many researchers take this fact into consideration in designing QDs for their long-term imaging studies.[109−111] For example, CdSe QDs can be coated with ZnS polymer shells or SiO_2 layers to suppress the dissolution of possibly toxic semiconductor core materials.[99] Details about the mechanism for potential toxicity are still under discussion.

Rare earth (RE)-based nanophosphors, which consist of a host inorganic matrix doped with luminescent lanthanide (Ln) cations, constitute another type of luminescent materials. Their main advantages are their low toxicity, high photostability, high thermal and chemical stability, high luminescence quantum yield, and sharp emission bands.[112] However, they normally show low luminescence intensity, which is caused by the low absorption of the parity-forbidden Ln^{3+} 4f−4f transitions.[113] The optical properties of such NPs can be further modified by doping, as shown recently in the case of Eu^{3+}, Bi^{3+} codoped $REVO_4$ (RE = Y, Gd) NPs. Intense red luminescence was achieved by using indirect excitation of the Eu^{3+} cations *via* the vanadate anions. The incorporation of Bi^{3+} into the $REVO_4$ structure resulted in a shift of the original absorption band corresponding to the vanadate toward longer wavelengths, yielding nanophosphors excitable by near-ultraviolet and visible light.[114]

Carbon dots are another class of fluorescent NPs. Carbon dots are zero-dimensional carbon nanomaterials and possess the advantageous characteristics of QDs over organic fluorophores, such as high photostability, tunable emission, and large two-photon excitation cross sections.[11] Moreover, C-dot fluorescence does not blink. They are water-soluble, can be functionalized, can be produced economically, and have excellent cell permeability and biocompatibility, making them attractive for intracellular sensing.[11,115,116] Also, C-dots without heavy metal content are environmentally friendly and can be much safer for biological applications than traditional Cd-containing QDs.[11,115,116] In a recent study, C-dots were subjected to a systematic safety evaluation involving acute toxicity, subacute toxicity, and genotoxicity experiments (including a mouse bone marrow micronuclear test and a *Salmonella typhimurium* mutagenicity test).[117] Carbon dot dosages of 51 mg/kg weight body showed no significant toxic effects, *i.e.*, no abnormality or lesions, and no genotoxicity in the organs of the animals.

Nanodiamonds, another group of carbon NPs, are receiving growing interest for drug delivery and other biomedical applications because they have good biocompatibility.[118] Intravenously administered ND complexes at high dosages did not change serum indicators of liver and systemic toxicity.[119] Nanodiamond powder produced by detonation (5−6 nm, see Figure 6) or other methods (20−50 nm) are readily available in commercial quantities at moderate cost and are among the most promising carbon nanomaterials for drug delivery, imaging, and theranostic applications. Fluorescence of NDs due to nitrogen-vacancy (NV) centers (see Figure 6) that are composed of a substitutional nitrogen and a next neighbor vacancy enables biomedical imaging.[120,121] Fluorescent NPs can also be produced by linking or adsorbing various fluorophores onto NDs. For example, bright blue fluorescent NDs were produced *via* covalent linking of octadecylamine to carboxylic groups on the ND surface (ND-ODA).[122] In biomedical imaging, fluorescent NDs combine the advantages of semiconductor QDs (small NP size, high photostability, and bright multicolor fluorescence) with biocompatibility, lack of toxicity, and tunable surface chemistry. Therefore, they are promising for *in vivo* imaging. Since the sizes of ND particles can be smaller than 5 nm NPs, they can be removed by renal excretion without leaving any toxic residue in the body.[123,124]

DOI: 10.1021/acsnano.6b06040
ACS Nano 2017, 11, 2313−2381

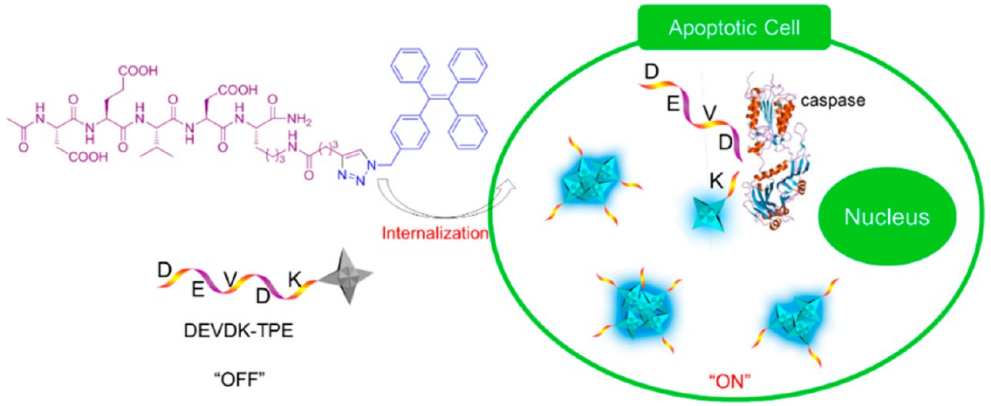

Figure 7. Diagrammatic illustration of the real-time monitoring of cell apoptosis process by DEVDK-TPE, an AIE-active fluorescent bioprobe. Adapted from ref 131. Copyright 2012 American Chemical Society.

Besides using fluorescent NPs as contrast labels for imaging, "smart" fluorophores that change their fluorescence signal depending on the local environment can be designed. By integrating pH-sensitive fluorophores on the surfaces of NPs, information about their local environment can be gained, for example, whether they are located extracellularly in neutral pH or intracellularly inside acidic endosomes/lysosomes.[127,128] By combining analyte-sensitive fluorophores with NPs, the concentrations of different analytes in the vicinity of the NPs can be determined.[129,130]

Fluorescent NPs based on AIE offer another concept in this direction. The AIE process has been utilized to develop light-up biosensors. Cell apoptosis, for example, has been followed in real time by making use of the AIE process (see Figure 7).[131] Tetraphenylethene (TPE), an archetypical AIEgen, has been functionalized by a short oligopeptide (DEVDK) through click chemistry, affording DEVDK-TPE, a peptide–AIEgen adduct. DEVDK-TPE is soluble in aqueous buffers and hence emits no fluorescence (*i.e.*, no residual emission). It remains nonfluorescent in intracellular media after cells internalize it. During apoptosis, caspase enzyme cleaves the DEVD segment. The residual segment (K-TPE) is not hydrophilic enough to be dissolved in aqueous media and thus forms intracellular nanoaggregates. The aggregate formation turns on the fluorescence of TPE, which is gradually intensified with the progress of apoptosis. This enables real-time and *in situ* monitoring of the biological process of programmed cell death.[131]

For cellular and *in vivo* cancer imaging, Nie, Gao, and their co-workers have developed a class of activatable NPs based on the use of copolymer materials with ionizable tertiary amine groups and covalently conjugated fluorescence dyes.[132,133] The self-assembled NP structures undergo a dramatic and sharp transition within a narrow range of pH (often less than 0.2 pH units). This pH-induced transition leads to rapid and complete dissociation of the nanomicelles. As a result, the covalently linked dyes change from a self-quenched "off" state to a highly emissive bright "on" state. This supersensitive and nonlinear response to external pH enables targeting acidic organelles in cancer cells as well as the acidic microenvironment in solid tumors. This feature is important in addressing the tumor heterogeneity problem, which is a major challenge for various imaging and therapeutic approaches based on molecular or receptor targeting. By targeting the common "hallmarks" of tumors (*i.e.*, the acidic habitat or microenvironment and the growth of new blood vessels or angiogenesis), this work has opened exciting opportunities in detecting and potentially treating a broad range of human solid tumors. This approach leads to improved detection sensitivity because each NP contains multiple dye molecules, which are turned on (restored to fluorescence) in an all-or-none fashion, leading to amplified fluorescence signals that are many times brighter than those of single dye molecules.

LABORATORY-BASED DIAGNOSIS ("HIGH-THROUGHPUT SCREENING")

Nanoparticles can also be used for detection of molecules, cells, and tissues outside the human body. In this diagnostic application, the function of the NP is to identify unique biological molecules in biological fluids that are associated with the health of the patient. The NPs act as transducers and are coated with ligands to enable the biorecognition of unique biological molecules in the fluid in the *in vitro* sensing applications. For example, AuNPs have been modified with ligands that specifically bind to a complementary protein. The presence of these proteins induces the cross-linking of the NPs (*i.e.*, agglutination). This controlled agglomeration can be observed colometrically by the change of color of the NP solution.[134,135] These concepts have been later refined, for example in rapid colorimetric DNA sensing.[136,137] This AuNP-based diagnostic technology has advanced to testing of patient samples and is now used in the clinic.[138] Nanotechnology presents an opportunity to improve the overall diagnostic process by lowering the limit of detection, thus enabling high throughput and multiplexed detections of biological targets with high sensitivity.

> Nanoparticles can also be used for molecular detection of molecules, cells, and tissues outside the human body.

Screening Based on Fluorescence Read-Out. Quantum dots are frequently used as fluorescence labels in proteins or nucleic acid assays. One example in this direction is a QD-based fluorescence polarization assay for screening of antigen surface epitopes.[139] In this example, a method for quickly screening and identifying dominant B cell epitopes was developed using hepatitis B virus (HBV) surface antigen as a target. Eleven amino acid fragments from the HBV surface antigen were synthesized by 9-fluorenylmethoxy carbonyl solid-phase peptide synthesis strategy, and then CdTe QDs were used to label the N-terminals

DOI: 10.1021/acsnano.6b06040
ACS Nano 2017, 11, 2313–2381

of all peptides. After optimizing the factors for this fluorescence polarization (FP) immunoassay, the antigenicities of synthetic peptides were determined by analyzing the recognition and combination of peptides and standard antibody samples. The results of the FP assays confirmed that 10 of the 11 synthetic peptides had distinct antigenicities. In order to screen dominant antigenic peptides, the FP assays were carried out to investigate the antibodies against the 10 synthetic peptides of the HBV surface antigen in 159 samples of anti-HBV surface antigen-positive antiserum. The results showed that 3 of the 10 antigenic peptides might be immunodominant, because the antibodies against them existed more widely among the samples and their antibody titers were higher than those of other peptides. Using three dominant antigenic peptides, 293 serum samples were detected for HBV infection by the FP assays. The results showed that the antibody-positive ratio was 51.9%, and the sensitivity and specificity were 84.3% and 98.2%, respectively. This QD-based FP assay is a simple, rapid, and convenient method for determining immunodominant antigenic peptides and has potential in applications such as epitope mapping, vaccine designing, or clinical disease diagnosis.

Another application of QDs is multiplexed detection, as described by Nie and co-workers. Quantum dots have been incorporated into microbeads to generate barcodes, where unique optical emission for each bead can be generated by different amounts and sizes of QDs.[140] Fluorescent QDs are ideal optical coders, because they have narrow fluorescence line widths, size- and shape-tunable emission, photostability, and all fluorescence emission can be excited with a single wavelength. Thus, barcodes can be designed with high coding precision, cost-effective instrumentation can be used by simplifying the optical components and excitation source for read out, and, finally, it has been suggested that over 1 million unique barcodes can be generated using different emitting QDs and intensities. There are several methods to prepare QD barcodes: (a) the "swelling" technique, where polystyrene beads are mixed in a solvent to enable beads to increase in volume, which allows the diffusion of hydrophobic QDs into the outermost layer,[140] (b) layer-by-layer (LbL) assembly of different emitting QDs onto the surface of the beads,[141] (c) incorporation of QDs inside a silica NP with a hydrophobic core,[142,143] and (d) microfluidic flow focusing to incorporate QDs inside the microbeads.[144−146] Each method of barcode preparation has a different fluorescence signal stability. Some formulations tend to expose QDs to small ions in the buffer, which leads to high read-out variability.[147] Hence, careful selection of preparation method is required for reproducibility in the biological assay. This optimization is important for the use of barcodes in diagnosing patient samples as outlined in the following examples.

To make use of barcodes for biological applications, the surface of the barcodes typically needs to be coated with bio-recognition molecules (*e.g.*, oligonucleotides or antibodies). Panels of different, uniquely emitting barcodes can be designed for detecting "sets" of diseases. For example, a mixture of five unique emitting barcodes with three distinct target proteins has been designed for diagnosing patients with HIV, hepatitis B, and hepatitis C. The two other barcodes were used as positive and negative controls. These five barcodes can be mixed with a patient's plasma and secondary probes. If the patient presents the antigen that recognizes the antibody on the barcode surface and the secondary probe, molecular assembly forms sandwich complexes of barcode−patient antigen−secondary probes. The overall optical signal of the barcode for positive detection changes upon the assembly process, and can be distinguished by using flow cytometry[148] or a smartphone camera.[149] A demonstration of the use of QD barcodes for diagnosing patient samples was reported by Ming *et al.*, who found that barcodes could be used to detect the genetic targets of patients infected with HIV and hepatitis B.[149] Kim *et al.* described the clinical sensitivity and specificity for QD barcode diagnostic analysis of hepatitis B to be greater than 90%.[150] This is a promising step for the clinical translation of this technology. The QD barcode is an example of a number of emerging nanotechnology-based diagnostic devices, where multiplexing occurs by the design of the barcoding system (*e.g.*, Raman-based barcodes, graphic barcodes).[151,152]

Novel approaches in instrumentation have also been developed to enable automation of barcode-based diagnostic assays. Microfluidic chips are an ideal platform for high-throughput multiplexed read-out. This approach has been demonstrated by coupling microfluidics with traditional Western blots (WBs) in protein identification.[153] Parallel microfluidic channels are designed to incorporate the internal molecular weight marker, loading control, and antibody titration in one protocol. Compared to the conventional WB that detects only one protein, the microfluidic WB (μWB) can analyze at least 10 proteins simultaneously from a single sample, while requiring only about 1% of the amount of antibody used in conventional WB. For nucleic acid analyses, microcapillary and loop-mediated isothermal amplification are incorporated (cLAMP) to achieve straightforward, robust, multiplexed, and point-of-care testing (see Figure 8). The cLAMP uses capillaries (glass or plastic) to introduce and to house samples/reagents, segments of water droplets to prevent contamination, pocket warmers to provide heat, and a hand-held flashlight for visual read-out of the fluorescence signal. It enables the simultaneous detection of two regions of the HIV genome from multiple plasma samples. As few nucleic acid detection methods can be wholly independent of external power supply and equipment, the cLAMP holds great promise for point-of-care applications in resource-poor settings.[154] To enhance the throughput for detection and to integrate the analysis of proteins and nucleic acids into one protocol, barcode-based bioassays that are capable of encoding and decoding are introduced. A single barcoded microchip can carry out tens of individual protein/nucleic acid assays (encode), and immediately yield all assay results by a portable barcode reader or a smartphone (decode). The applicability of barcoded microchips has been demonstrated by HIV immunoassays for simultaneous detection of three targets (anti-gp41 antibody, anti-gp120 antibody, and anti-gp36 antibody) from six human serum samples. However, the barcode-based assay can also be applied for the simultaneous detection of pathogen-specific oligonucleotides by a single chip containing both positive and negative controls.[155]

Another multiplex detection technology that is gaining interest is "chemical nose" sensors.[156] Array-based "chemical nose" sensors have been designed where individual spots are coated with chemical agents to recognize specific molecules in a complex analyte mixture. These systems use selective recognition of analytes, a complementary approach to traditional biomarker-based strategies. Nanoparticle-based chemical noses have been used for sensing of sera,[157] cell-surface based discrimination of bacteria,[158] and genotyping of cancer cells.[159] These systems used separate recognition elements to generate the selectivity-based pattern required for analyte identification. Recently, an alternative multiplexing strategy was used to create a high-throughput multichannel sensor that was able to determine the mechanism of chemotherapeutics within minutes,[160] instead of

DOI: 10.1021/acsnano.6b06040
ACS Nano 2017, 11, 2313−2381

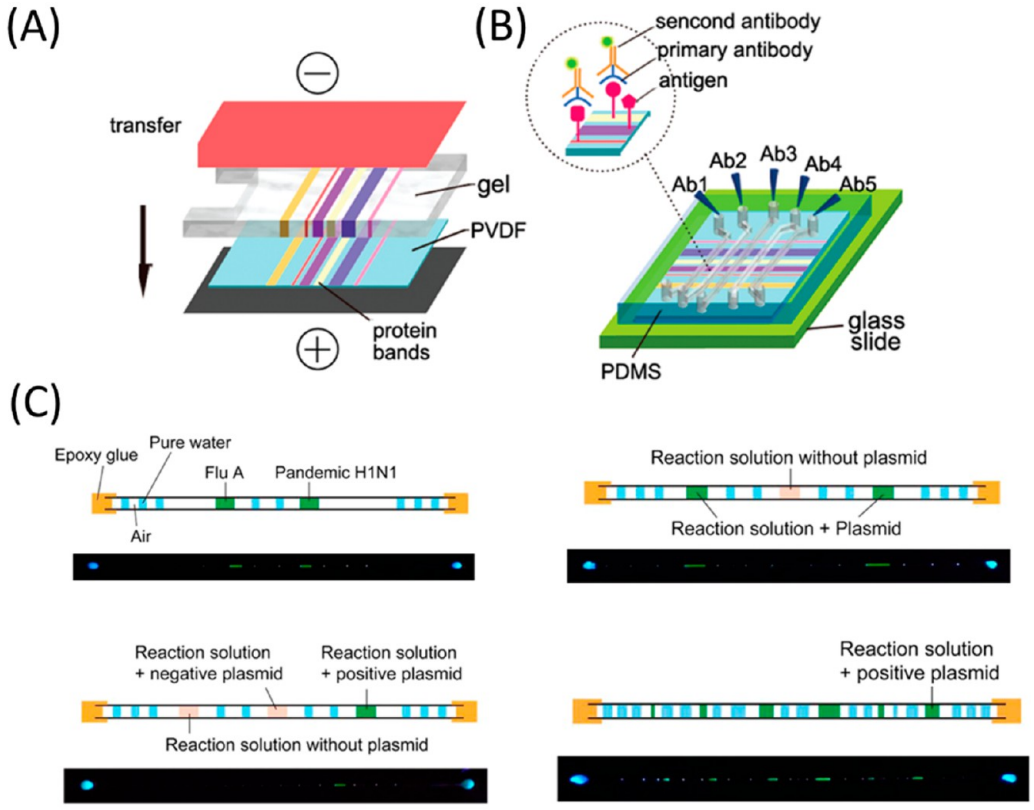

Figure 8. Illustration of μWB and multiplexed cLAMP carried out in a variety of forms by means of microcapillaries. (A) Proteins are transferred from a polyacrylamide gel to a polyvinylidene fluoride (PVDF) membrane by electroblotting. (B) μWB chip is assembled by incorporating a polydimethylsiloxane (PDMS) microfluidic network with the blotted PVDF membrane. Panels (A) and (B) adapted from ref 153. Copyright 2010 American Chemical Society. (C) Microfluidic channels are oriented perpendicular to the protein bands on the membrane. Antibodies for specific proteins are introduced in parallel microfluidic channels. Adapted from ref 154. Copyright 2014 American Chemical Society.

the weeks required for traditional biochemical approaches (see Figure 9). The multiplexed platform complexed a single AuNP with three different fluorescent proteins (FPs) to detect drug-induced physicochemical changes on cell surfaces. This result demonstrates the ability of nanomaterials to sense minute changes in cell surfaces rapidly, enabling high-throughput screening. These systems are promising for a wide variety of applications, including diagnostics for wound biofilms.[161]

While in the above example, the fluorophores were merely used as passive labels, they can also be used for active sensing in intracellular assays. The functionalization of luminescent NPs and their incorporation into cells provide versatile means to image cells. However, the design of functional NPs that quantitatively respond to specific cellular biomarkers or intracellular conditions remains challenging. Several recent reviews have addressed advances in the application of luminescent NPs for intracellular sensing.[162−164] Quantum dots have been widely applied as luminescent transducers for the development of optical biosensors.[165,166] Quantum dots can be functionalized with moieties that alter their fluorescence properties in response to particular cellular conditions or cellular biomarkers. This approach can be used to develop intracellular sensors. As an example, core/shell CdSe/ZnS QDs were functionalized with a dopamine-conjugated peptide monolayer to act as pH sensors (see Figure 10A). Under aerobic conditions, the dopamine ligands are oxidized to quinone units, which quench the transfer of electrons. The quenching efficiency of the QDs is dependent on the redox potential of quinone units, which, in turn, are pH-dependent.[167] By altering the pH, the quenching efficiency of the QDs can be tuned.[167] The ability of the QDs to respond to intracellular pH changes was demonstrated experimentally by Medintz *et al.*[167] By subjecting COS-1 cells loaded with QDs to extracellular nystatin, which induces pH changes in the cells, the intracellular pH changes could be quantified using an *in vitro*-derived calibration curve (see Figure 10B).

Similarly, cytochrome *c* functionalized CdSe/ZnS QDs can be used for detection of the reactive oxygen species (ROS) superoxide radical ($O_2^{\bullet-}$). The $O_2^{\bullet-}$-mediated reduction of cytochrome *c* enhances the fluorescence of QDs. The ability of the QDs to respond to intracellular changes in $O_2^{\bullet-}$ was demonstrated experimentally by Li *et al.*[168] By subjecting HeLa and HL-7702 cells to phorbol myristate-induced generation of $O_2^{\bullet-}$, the resulting fluorescence could provide a quantitative measure of the time-dependent concentration of $O_2^{\bullet-}$ in the cells.[168]

Quantum dots can also be applied for the detection of dihydronicotinamide adenine dinucleotide (NADH).[169] CdSe/ZnS QDs were functionalized with a monolayer of Nile Blue (NB^+), which quenches the fluorescence *via* an energy transfer mechanism (see Figure 11A). Freeman *et al.* demonstrated that NADH, a cofactor generated *via* the metabolic Krebs cycle, induced reduction of NB^+ to the colorless NBH reduced state, which resulted in the recovery of QD fluorescence (see Figure 11B). The metabolism of HeLa cells can be inhibited by anticancer drugs, *e.g.*, taxol, which substantially lowers the intracellular NADH concentration to yield low fluorescence

DOI: 10.1021/acsnano.6b06040
ACS Nano 2017, 11, 2313−2381

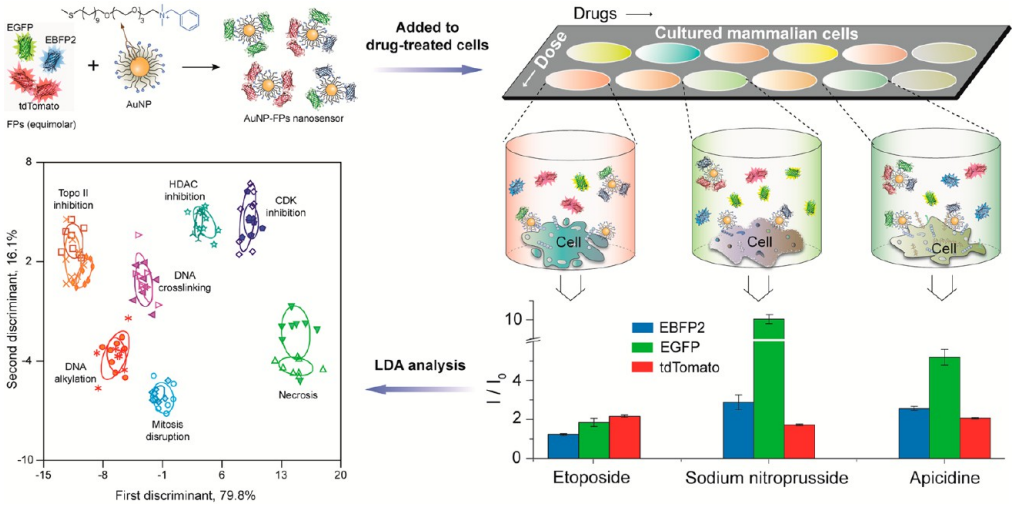

Figure 9. Multichannel AuNP fluorescent protein sensor, generating different responses for drug-induced phenotypes. Clustering of the mechanisms was performed using linear discriminant analysis, enabling identification of new drugs as "known" or "novel". Adapted from ref 160. Copyright 2015 Nature Publishing Group.

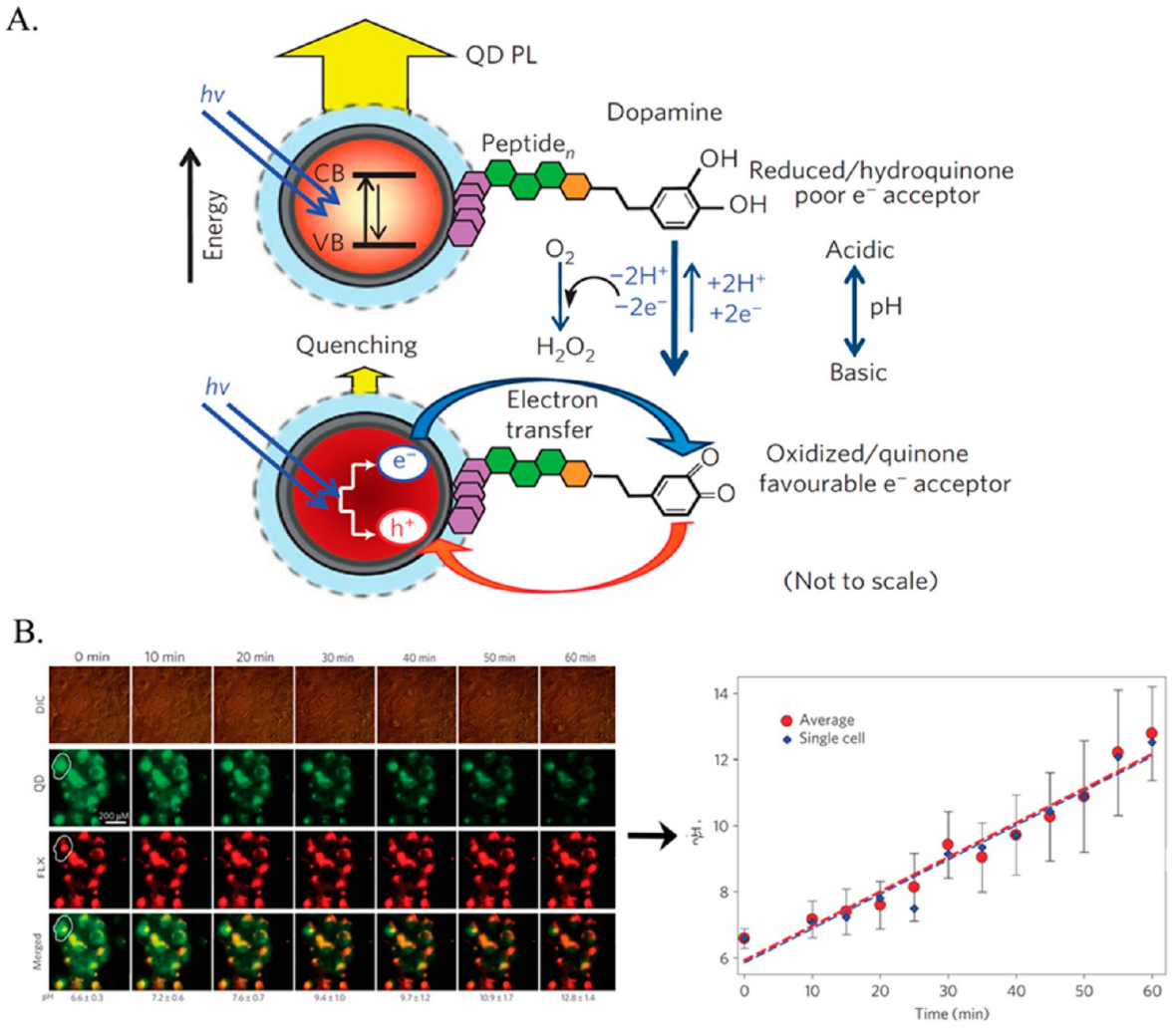

Figure 10. (A) Dopamine-functionalized QDs for the photoluminescence (PL) sensing of pH *via* the pH-dependent oxidation of dopamine to the quinone derivative, and the accompanying electron-transfer quenching of the QDs. (B) Differential interference contrast (DIC) and fluorescence confocal imaging of pH-changes in COS-1 cell subjected to internalized pH-responsive dopamine-functionalized QDs (fluorescence at 550 nm) and co-incorporated red fluorescent Fluorophorex (FLX) 20 nm nanospheres acting as an internal strand, emitting at 680 nm. The calibration curve corresponding to the intracellular fluorescence changes derived from the confocal fluorescence images is displayed at the bottom. Adapted with permission from ref 167. Copyright 2010 Nature Publishing Group.

DOI: 10.1021/acsnano.6b06040
ACS Nano 2017, 11, 2313−2381

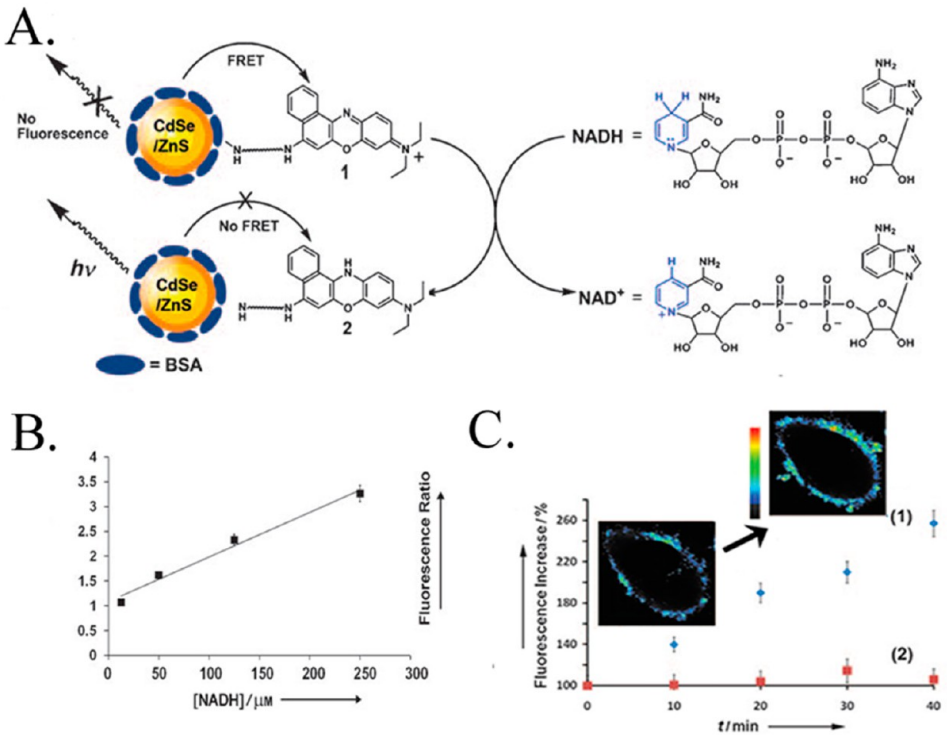

Figure 11. (A) Schematic analysis of NADH using NB^+-functionalized CdSe/ZnS QDs. (B) Calibration curve corresponding to the fluorescence changes of the CdSe/ZnS QDs upon analyzing different concentrations of NADH. (C) Time-dependent fluorescence changes observed upon the glucose (50 mM)-stimulated activation of the metabolism in HeLa cancer cells loaded with NB^+-functionalized CdSe/ZnS QDs in (1) untreated HeLa cells, (2) Taxol-treated HeLa cells. Inset: Time-dependent confocal microscopy images of a HeLa cell (without Taxol treatment) upon triggering the metabolism with glucose 50 mM. Adapted with permission from ref 169. Copyright 2008 John Wiley & Sons, Inc.

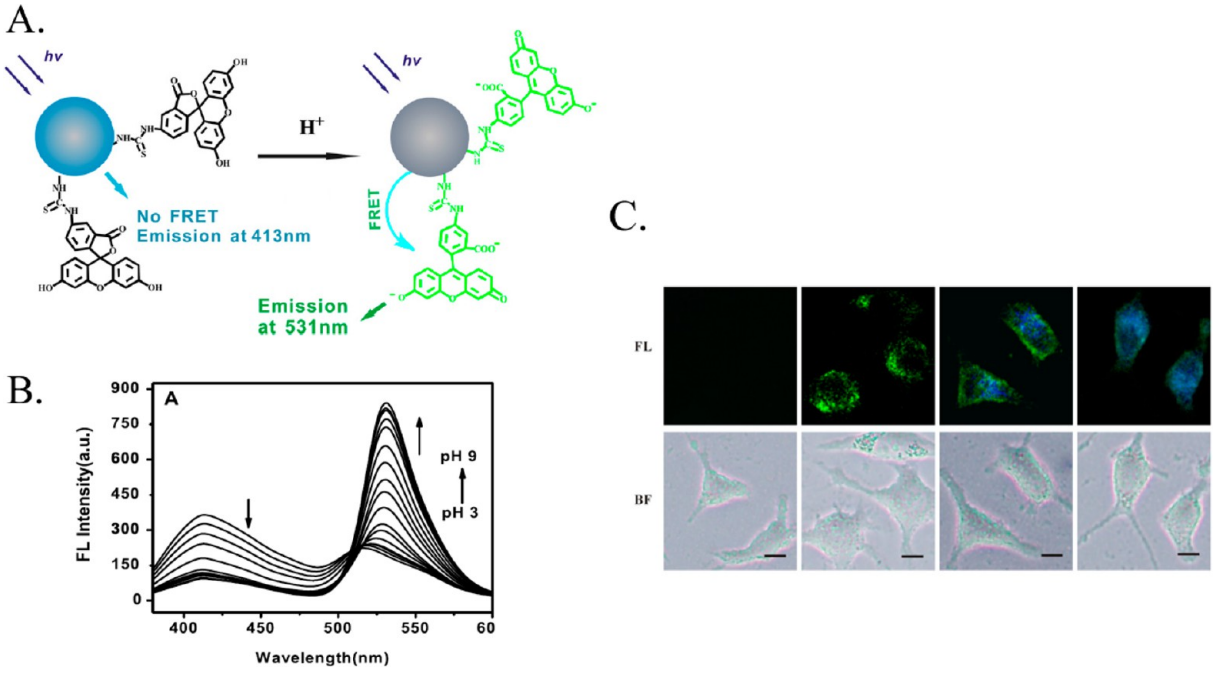

Figure 12. (A) Schematic pH-stimulated fluorescence changes of fluorescein isothiocyanate (FITC)-functionalized C-dots. (B) Fluorescence spectra of the FITC-modified C-dots at different pH values. (C) Confocal microscopy images (fluorescence, FL, and bright-field BF) following the spatial pH changes in L929 cells loaded with the FITC-modified C-dots. Adapted with permission from ref 170. Copyright 2013 IOP Publishing.

(see Figure 11C). This latter example highlights the potential use of intracellular QDs biosensors for drug screening applications.[169]

The potential toxicity associated with the intracellular application of QDs can be avoided by using alternatives such as C-dots. Figure 12 illustrates the application of fluorescein-modified

DOI: 10.1021/acsnano.6b06040
ACS Nano 2017, 11, 2313−2381

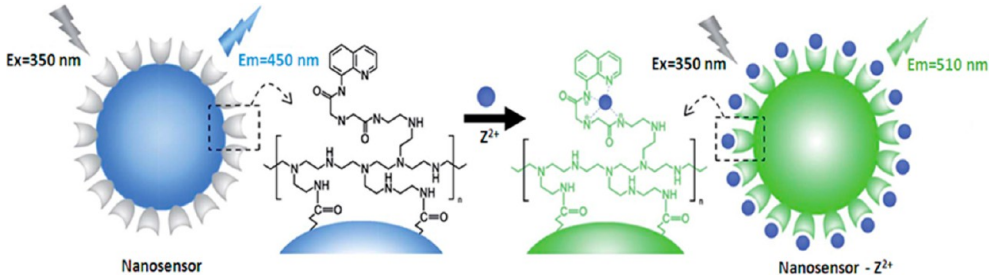

Figure 13. Carbon-dot-based sensor for the intracellular sensing of Zn^{2+} ions. Adapted from ref 177. Copyright 2014 Royal Society of Chemistry.

C-dots as optical transducers in the fluorescence resonance energy transfer (FRET)-based detection of intracellular pH.[170] Carbon dots serve as the donor in the FRET pairing with fluorescein to provide a ratiometric detection of pH within a region of pH = 4.0 to pH = 8.0 (Figure 12B). Similar experiments have been performed with QDs modified with a pH-sensitive fluorophore,[171] demonstrating that the concept of active pH sensing can be carried out with a variety of different NP materials. Du *et al.*[170] demonstrated the use of fluorescein-functionalized C-dots in monitoring temporal and spatial intracellular pH changes in L929 cells using fluorescence spectroscopy (see Figure 12C).

In addition to the sensor mentioned above, several other intracellular fluorescent C-dot-based pH sensors have also been reported.[172,173] The quantification of intracellular pH is particularly interesting since abnormal pH values are often associated with certain diseases such as cancer or Alzheimer's disease.[174,175] Moreover, functionalized C-dots have been modified for intracellular sensing of metal ions.[176,177] For example, quinoline-functionalized C-dots were applied to sense Zn^{2+} ions in the intracellular environment (see Figure 13).[177]

Organic and inorganic polymer NPs have been implemented as functional units for intracellular sensing applications. For example, silica NPs have been widely used to transport fluorophores for the intracellular sensing of oxygen levels,[178] pH,[179] or metal ions.[180] In these systems, the fluorophore embedded within the SiO_2 NPs responds selectively to the intracellular analyte, thus providing an optical output in response to stimuli. Often the combination of two fluorophores, where only one fluorophore responds to the respective analyte, are integrated with the NPs, to enable the ratiometric detection of the analyte. For example, the pH-sensitive FITC and pH-insensitive $Ru(bpy)_3^{2+}$ fluorophores were incorporated into SiO_2 NPs. The labeled NPs were then applied for sensing the drug-induced lysosomal pH changes in murine macrophages stimulated by chloroquine, and for the dexamethasone-induced acidification in apoptotic HeLa cells.[181] A sense-and-treat SiO_2 NPs system was demonstrated by the immobilization of Atto 647 dye and a DOX-functionalized polymer on the SiO_2 NP. The functionalized NPs were incorporated in Hep-G2 cells, and the pH-induced release of the DOX in endosomal and lysosomal domains of the cells was probed by the two fluorophores, while releasing the anticancer DOX drug.

Organic polymer NPs exhibit several advantages for transporting intracellular sensing moieties. Many different nontoxic polymer matrices are available and their hydrophilic/hydrophobic properties can be tailored for optimal cell permeation. Furthermore, the versatile methods available to modify polymer NPs enable the functionalization of recognition ligands, fluorophores, and cell-targeting ligands and functionalities, and minimize nonspecific adsorption. Figure 14 illustrates two

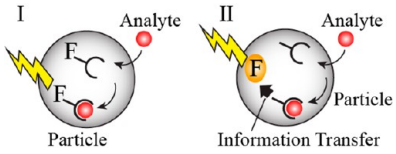

Figure 14. Chemically modified polymer NPs for intracellular sensing: (I) NPs function as optically responsive ligands. (II) Particles functionalized with an analyte recognition unit and an optical-transducing element. The recognition event activates the optical transducer.

general strategies to assemble polymer-based NPs for intracellular sensing applications. One type of sensing NPs involves the incorporation of a fluorophore into the NP matrices where it serves as both binding ligand and optical transducer, panel I. The second type of intracellular optical sensors involves the modification of the NPs with two functional elements: (i) a recognition ligand that binds the analyte and (ii) a transducer that responds optically to the recognition event, panel II. This two-element NP composite is known as an opt(r)ode, in analogy to electrochemical sensing electrodes. In this approach, electrochemical reactions stimulated by the recognition complex or intracellular environmental changes, *e.g.*, pH changes, induced by the sensing events, trigger the optical transducer in the NPs.

Fluorescent sensors for the intracellular detection of specific ions such as Cu^{2+}, Mg^{2+}, and Zn^{2+} were developed[182−184] using ion-responsive fluorophores embedded in polymer NPs (Figure 14, panel I). An interesting optical sensor that follows the principle shown in Figure 14, panel I, and probes intracellular levels of H_2O_2 is depicted in Figure 15. Polyacrylonitrile (BPAN) NPs modified with the Schiff base ligands of aminopyridine boronate ester (50 nm diameter) were used as the sensor NPs (Figure 15A). In the presence of H_2O_2, oxidative cleavage of the boronate ester units occurred, leading to the formation of the hydroxy-pyridine-substituted polymer nanoparticles, which exhibited a characteristic fluorescence band at λ = 400 nm. The intensity of the fluorescence band was correlated with the concentration of H_2O_2 (Figure 15B), and other ROS species did not interfere with it.[185]

In yet another example, researchers developed bifunctional polymer NPs that acted as optrodes to probe intracellular levels of H_2O_2, according to the principle shown in Figure 14, panel II.[186] They modified PEG hydrogel nanospheres (250−350 nm) with horseradish peroxidase (HRP) and the Amplex Red (10-acetyl-3,7-dihydroxy phenoxazine) transducer (Figure 16A). In the presence of stress-induced and intracellular formation of H_2O_2, the HRP-catalyzed oxidation of Amplex Red proceeds, yielding the fluorescent resorufin transducer.[186] The hydrogel NPs were introduced into macrophages, and these responded to exogenous H_2O_2 (100 μM) or endogenous peroxide stimulated by lipopolysaccharides (1 $\mu g \cdot mL^{-1}$).

DOI: 10.1021/acsnano.6b06040
ACS Nano 2017, 11, 2313−2381

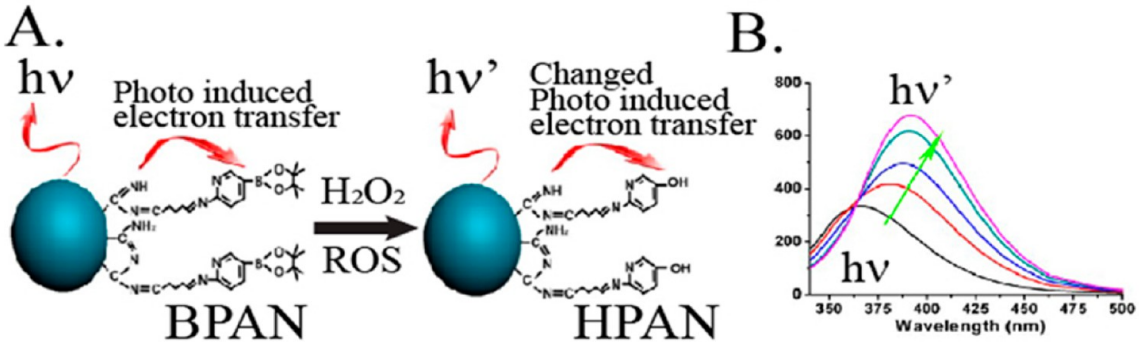

Figure 15. (A) Chemically modified boronate ester-functionalized BPAN NPs for intracellular fluorescence probing H_2O_2. (B) Fluorescence spectra changes of the modified polymer NPs upon interaction with increasing amounts of H_2O_2: 0, 20, 40, 60, and 80 μM. Adapted from ref 185. Copyright 2012 American Chemical Society.

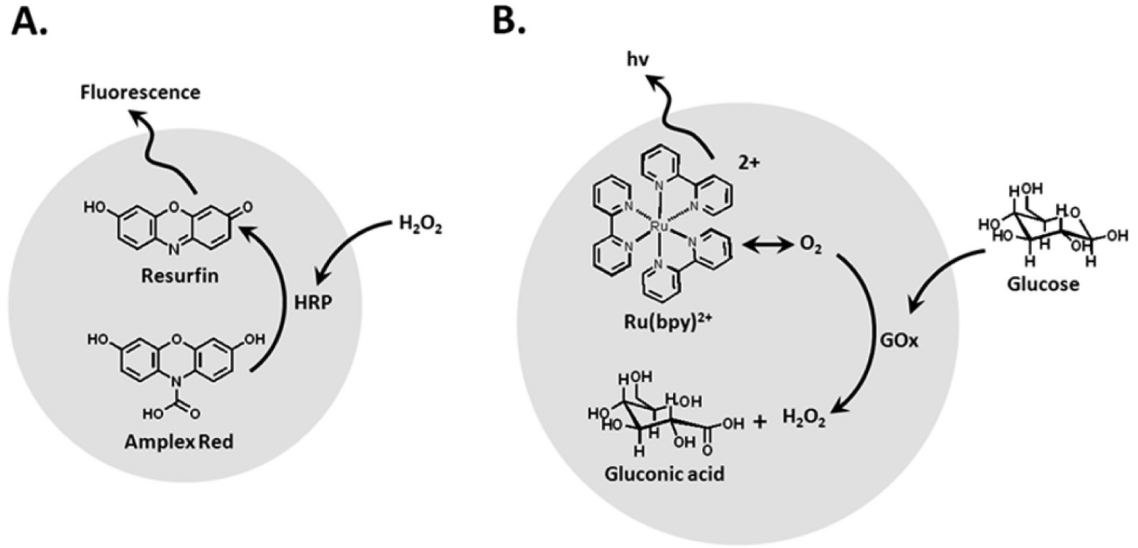

Figure 16. Bifunctional recognition/dye polymer NPs for sensing: (A) Sensing of H_2O_2 *via* the HRP-driven oxidation of Amplex-Red to the fluorescent Resorufin product. (B) Sensing of glucose by the depletion of O_2 by the GOx-mediated oxidation of glucose, using $Ru(bpy)_3^{2+}$ as auxiliary fluorescent probe.

Similarly, a nanosensor capable of monitoring intracellular glucose levels is depicted in Figure 16B). Polyacrylamide NPs were implemented as a carrying matrix for glucose oxidase, GOx, and the Ru(II)-tris-bipyridine, $Ru(bpy)_3^{2+}$, transducer. While the $Ru(bpy)_3^{2+}$ fluorescence is quenched by intracellular O_2 levels, the O_2-driven GOx-catalyzed oxidation of glucose depletes the O_2 levels, resulting in the triggered-on fluorescence of the $Ru(bpy)_3^{2+}$ luminescent probe. As the degree of O_2 depletion by the biocatalytic process is controlled by the concentration of glucose, the resulting fluorescence of the transducer provided a quantitative measure for the concentration of glucose.[187] The use of composite polymer NPs carrying enzymes and optical transducers as bifunctional sensing elements is particularly attractive since the products generated by many enzyme-driven processes may activate optical (fluorescent) transducers. The use of such intracellular nanosensors should be implemented with caution, however, since intracellular environmental conditions, *e.g.*, changes in pH, might alter the enzyme activities, thus perturbing the intracellular nanosensor performances.

Screening Based on Surface Plasmon Resonance. Plasmonic NPs are also designed for optical read-out,[188−192] in particular, in the form of colorimetric responses. The aggregation of AuNPs shifts the absorption maximum to longer wavelengths. Aggregation can be induced by the selective binding of analyte molecules to the functionalized surfaces of AuNPs.[193] The most popular example in this research direction is DNA detection, as developed by Mirkin and co-workers.[136,194,195] There are now many similar assays. For example, Stevens and co-workers used AuNPs to detect the enzyme phospholipase A_2 at a concentration of 700 pM.[190] A more complex scheme was used by Pompa and co-workers to detect cancer-related point mutations in the Kirsten rat sarcoma viral oncogene homologue (KRAS) gene.[189] In this case, AuNP aggregates form when the target gene hybridizes with the complementary single-stranded capture probes functionalized to AuNPs. Subsequently, the AuNP−target-gene complex undergoes a secondary binding event with DNA-functionalized magnetic Fe_3O_4 microparticles. In addition to nucleic acid detection, AuNPs functionalized with capture antibodies and patterned onto dielectric surfaces can be used to fabricate a protein biosensor.[192] The characteristic surface plasmon resonance (SPR) of such AuNPs is shifted by the binding of target proteins, and this spectral shift can be detected using conventional SPR imaging spectrometers. Tamiya and co-workers demonstrated a 300-channel version of this device, capable of label-free detection of targets down to 100 pg/mL.[192]

DOI: 10.1021/acsnano.6b06040
ACS Nano 2017, 11, 2313−2381

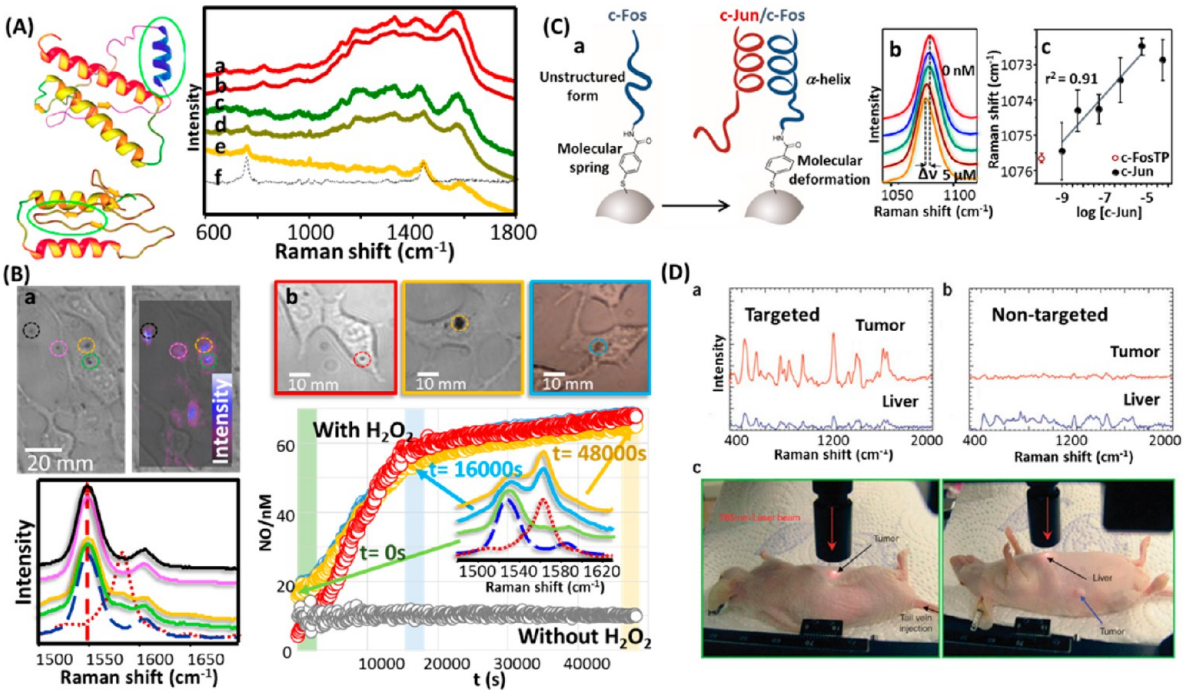

Figure 17. (A) Scheme showing prion mutation and prion ultradetection in human blood. Surface-enhanced Raman spectra (SERS) of (a) natural and (b) spiked human blood; (c) natural and (d) spiked human plasma; (e) spiked human plasma after spectral subtraction of the matrix (human plasma); (f) the scrambled prion. Adapted with permission from ref 205. Copyright 2011 National Academy of Sciences. (B) (a) Optical spectra and SERS (mapped at 1548 cm^{-1}, as marked with the arrow below) images of 3T3 cells in the presence of capsules. The SERS spectra (bottom) show the signals for the colored circles in the image (top). (b) Optical images and intracellular NO formation over time (obtained through the $I_{1583}/(I_{1583} + I_{1548})$ relation) for three different samples upon NO induction with hydrogen peroxide (H_2O_2). A control sample without the presence of H_2O_2 is also shown for comparison. Representative normalized SERS spectra obtained at different times are shown. The SERS dashed (blue) and dotted (red) spectra represent the reference vibrational pattern for aminobezenethiol and hydroxybenzenethiol, respectively. Adapted with permission from ref 212. Copyright 2013 John Wiley & Sons, Inc. (C) (a) Outline of the c-Fos/c-Jun dimerization on the metal surface and the resulting deformation of the Raman label structure. (b) Details of the 1000−1100 cm^{-1} spectral regions of the SERS of the molecular spring (benzenethiol) interfacing the NP and the protein c-Fos.(c) Spectral shift of the benzenethiol band at *ca.* 1075 cm^{-1} as a function of c-Jun concentration (logarithmic scale) in HEPES buffer. Adapted from ref 215. Copyright 2013 American Chemical Society. (D) (a) *In vivo* cancer targeting and SERS detection by using ScFv-antibody-conjugated AuNPs that recognize the tumor biomarker epidermal growth factor receptor (EGFR). Top: Photographs showing a laser beam focusing on the tumor site or on the anatomic location of liver. Bottom: SERS spectra obtained from the tumor and the liver locations by using (a) targeted and (b) nontargeted NPs. Two nude mice bearing human head and neck squamous cell carcinoma (Tu686) xenograft tumors (3 mm diameter) received 90 mL of ScFv EGFR-conjugated SERS tags or PEGylated SERS tags (460 pM). The NPs were administered *via* tail vein single injection. SERS spectra were taken 5 h postinjection. *In vivo* SERS spectra were obtained from the tumor site (red) and the liver site (blue) with 2 s signal integration and at 785 nm excitation. The spectra were background-subtracted and shifted for better visualization. The Raman reporter molecule was malachite green, with distinct spectral signatures as labeled. Adapted with permission from ref 216. Copyright 2008 Nature Publishing Group.

Taking advantage of the high cross-section absorbance of plasmonic NPs, their SPR can also be used in plasmonic-driven thermal sensing. Qin *et al.* presented an improved lateral flow immunoassay using AuNPs, which improved the analytical sensitivity of the method 32-fold, achieving similar sensitivity to an enzyme-linked immunosorbent assay (ELISA).[196] Furthermore, Polo *et al.* reported a SPR-based detection of carcinoembryonic antigen (CEA) with a sensitivity 3 orders of magnitude better than standard ELISAs using anisotropic AuNPs.[197]

One of the emerging techniques related to plasmon resonance that demonstrated high sensitivity and versatility is the chiroplasmonic method developed by Kotov and Xu.[198−200] This technique is based on the giant polarization rotation characteristic of nanoscale assemblies highly polarizable metallic nanoparticles. The chiroptical effects in these structures are several orders of magnitude higher than in small organic molecules due to high polarizability of the inorganic nanomaterials and larger dimension. Notably, the physics of chiroplasmonic detection differs from that of red-blue plasmon coupling assays or screening with Raman scattering based (see below). Polarization rotation in NP assemblies is primarily based on interactions of the electromagnetic field with asymmetric nanostructures rather than on the formation of so-called 'hot spots' or plasmon coupling.[201] This difference is essential for biomedical diagnostics because it enables detection of long strands of DNA and large proteins. For instance, translation-inspiring sensitivity was obtained for prostate specific antigen using this method.[202] Most recently, this method in combination with UCNPs also enabled dual detection of one of the most promising diagnostic targets micro RNAs (miRNA) at the levels sufficient for its application in cancer diagnostics.[203]

Screening based on surface-enhanced Raman scattering. Surface-enhanced Raman scattering (SERS) is another class of NP-based molecular detection.[204,205] Surface-enhanced Raman scattering is an ultrasensitive molecular spectroscopy technique that benefits from the electromagnetic fields generated upon excitation of plasmons in nanomaterials. Despite the

DOI: 10.1021/acsnano.6b06040
ACS Nano 2017, 11, 2313−2381

impressive detection limits of SERS, down to the single molecule level,[206] its application in diagnosis has been restricted until recently by the inherent complexity of biological samples. Thus, direct SERS detection of disease markers have typically been carried out either in lab samples, where the marker was diluted in a controlled solution, or in biological samples, where the marker is characterized by an extraordinary affinity for the plasmonic surfaces, such as the use of SERS detection for Creutzfeldt-Jakob prionic diseases (see Figure 17A).[205] The use of chemoreceptors, intermediary molecular species with selective affinity for the molecular target (*i.e.*, the disease marker),[207] has notably increased the applicability of SERS as an efficient diagnostic tool. Surface-enhanced Raman scattering has therefore been applied to *ex vivo* detection of drugs,[208] proteins,[209] metabolites indicative of disease,[210] or even toxic ions,[211] but also to *in vitro* monitoring of relevant small inorganic molecules such as nitric oxide[212] or pH levels[213] inside living cells (see Figure 17B). In this approach, SERS detection is achieved indirectly as the spectral changes for the chemoreceptor are monitored before and after reaction with the target analyte, rather than directly detecting the analyte. Ideally, the chemoreceptor needs to show a recognizable spectral change, either structural or electronically, upon conjugation with its target. Although this property can be found easily in small aromatic molecules, such as aromatic thiols and amines, porphyrins, and dyes, macromolecules such as peptides and proteins usually do not present spectrally discernible differences. In such cases, however, the use of molecular springs as an interface between the metallic surface and the protein chemoreceptor can be employed to monitor the interactions with the analytical target. This strategy has been demonstrated successfully in the quantification of the oncogenic protein c-JUN in cell lysates by using the transcription factor FOS[214] coupled with mercaptobenzoic acid as the molecular spring (see Figure 17C).[215] An alternative approach to the use of SERS for diagnostics and bioimaging relies on the highly intense signals that can be obtained from plasmonic NPs labeled with molecules featuring large SERS cross sections. This strategy, pioneered by Shuming Nie, has been demonstrated extensively for bioimaging of tumors in mice (see Figure 17D) and for use as a contrast agent for the multiplex labeling in tissue preparations.[217] The use of different Raman labels in combination with different antibodies can further expand the multiplexing capability of these systems. Moreover, a variety of membrane receptors can be targeted specifically to obtain pertinent spatial information.[218] Surface-enhanced Raman scattering NP tags have also been used for multiplexed detection of circulating tumor cells and cardiovascular protein biomarkers in blood samples.[219] Nie and co-workers developed a sandwich-type assay involving magnetic capturing beads and SERS tags for measuring a panel of four cardiac protein biomarkers (sVCAM-1, suPAR, HSP70, and CRP). The magnetic beads enable easy purification while the SERS tags enable simultaneous quantification. Due to multiplexing, high sensitivity, and the large dynamic range of SERS, multiple biomarkers can be assessed over a wide concentration range in a single tube. Since this system removes many purification and enrichment steps, SERS-based assays can provide better positive and negative predictive values in high-risk patients. In the context of coronary arterial disease, a major clinical problem is the prediction of sudden cardiac events such as plaque rupture and myocardial infarction. Hence, it is important to develop assays to distinguish high-risk populations for plaque rupture that require immediate intervention and treatment.

Screening Based on Electronic Read-Out. Nanowires[220−229] are enabling a novel class of biosensors that are capable of detecting disease markers in blood, saliva, and urine, and able to convert the detection events into electronic signals. Semiconductor nanowire field-effect transistors (FETs) make use of nanowires that are sensitive to surface-binding events.[230] This sensitivity is derived from the proximity of the binding sites to the charge carriers within the nanowire.[231−233] Nanoengineered FETs differ considerably from conventional, microlithography-based FETs for solution-based detection.[234−236] For example, nanoengineering enables miniaturization and also enables the detector to be close to the target. Silicon nanowires can detect proteins at 10 fM concentrations in low ionic strength buffers; however, the detection of analyte molecules by nanowire FETs in high ionic strength (>mM) solutions, including all physiological solutions of interest, has posed problems. In such solutions, the Debye length is reduced to 0.2−2.0 nm and the screening of analyte charge by the electrolytes either reduces sensitivity or, more often, prevents detection of the analyte altogether.[221,237] Andrews, Weiss, and Yang showed that aptamer-functionalized FETs can operate in full ionic strength buffer, presumably because of the proximity of the charged backbone to the gated semiconductor, and thus show promise for *in vivo* measurements.[238,239] A recent study demonstrated[230] that backfilling antibody-functionalized silicon nanowires with a PEG layer extends the Debye length, enabling the detection of prostate-specified antigen at a concentration of 10 nM in 100 mM phosphate buffer.[230] Nanowires composed of conductive polymers (*e.g.*, polyaniline[240−243]) have also been adapted for electrical biosensing using either FET-based transduction[244,245] or chemoresistive transduction.[228,229] In these systems, the binding sites are either antibodies or virus particles displaying peptide motifs, both of which are capable of recognizing and binding analyte molecules. Conveniently, either of these two "receptors" can be entrained in the polymer from the polymerization solution during nanowire fabrication. In contrast to nanowire FETs, transduction of analyte binding to polymer nanowires is not completely understood. Carbon nanotubes have been also used as transducers for biosensing.[246] All these biosensors are "label-free"—capable of providing a signal correlated to the concentration of analyte by immersion in a solution without added reagents or process steps. Thus, these devices are ideally suited for use in point-of-care disease diagnostics.

An electrically responsive NP sensing scheme requires electrical contact. One approach described by Gadopadhyay *et al.*[240] involves the incorporation of AuNPs into polyaniline films on electrode surfaces.[240] In this case, AuNPs facilitate the attachment of single-stranded DNA (ssDNA) capture strands to the nanowire, using a thiol-based immobilization scheme. Binding of target DNA to the ssDNA capture strands impedes the redox responsiveness of polyaniline and reduces peak currents by providing an insulating layer to the electrode surface.[240] Gadopadhyay *et al.* demonstrated that target nucleotide concentrations down to 10^{-18} M can be detected by monitoring changes in peak currents. Similarly, QDs have been used as transducer in electrochemistry based detection schemes.[247−254]

Biological molecules can also act as transducers that directly convert binding events into electrical signals. This action can be in the form of ion channels, which open in response to binding events and subsequently result in a signal cascade.[255] Olfactory receptors, for example, can be used for the development of sensitive and selective odor-sensing biosensors.[256−258] These biosensors can screen numerous volatile compounds generated

DOI: 10.1021/acsnano.6b06040
ACS Nano 2017, 11, 2313−2381

by the human body, such as exhaled breath and body odors, to detect diseases and health conditions.[259,260] Olfactory receptors have also been combined with various transducers such as quartz crystal microbalance,[261−263] SPR sensors,[264,265] microelectrodes,[266,267] NPs,[268] graphene,[269,270] and nanotubes[271−277] to generate different types of read-outs. For example, a biosensor with an electrical read-out was constructed by immobilizing olfactory receptors on nanotubes.[271,272] Similarly, a nanovesicle-based olfactory biosensor, where nanovesicles with surface olfactory receptors were immobilized on nanotubes, was successfully used for cancer diagnosis.[263,276,277] In addition to olfactory receptors, others, such as hormone receptors,[268] taste receptors,[278,279] and peptides[280] can also efficiently be used in biosensors that can detect components of saliva, tears, blood, urine, cerebral spinal fluid, mucous, and even tissues.[281,282]

Similarly, whole cells can be used as transducers, whereby electric currents of electrically excitable cells are recorded.[283] Primary cells[284] and stem cells[285] from patients have become interesting targets that can be used as potential tools for personalized medicine. In addition to whole cells, specific ion channels can also be used as transducers. Ion channels are involved in electrical signal conduction (such as in the nervous or cardiac systems) as well as in other disease areas such as oncology,[286] cystic fibrosis,[287] diabetes,[288] and infection.[289] The gold standard for monitoring ion channel currents is the patch clamp technique,[290] which provides highly accurate functional recordings from single or multiple ion channels in cells. However, the low throughput and the need for highly trained operators exclude the classical patch clamp technique from many screening applications. This situation changed with the development of the planar patch clamp technique.[291,292] The latest generations of planar patch clamp devices like the SyncroPatch 384PE (2013 by Nanion Technologies) enable recordings of up to 768 cells at a time, and can be integrated into high-throughput screening cascades of the pharmaceutical industry. Nanotechnology has had a leading role in shaping these technologies by providing nanopores responsible for sealing the cell and the detector surface. Such nanopores can be used not only for electrophysiological measurements of cells, but also have been used in the context of DNA detection.[293] In most cases, electrophysiological detection is used for monitoring overexpressing ion channels, which has implications in primary drug targeting or for eliciting dangerous side effects. One prominent example is the cardiac herG channel that plays an important role in heart arrythmia and QT-prolongation.[284,285,294−296]

At the tissue and organ levels, indicators like electrophysiological signals have been widely employed for evaluation of organ function. However, conventional electrodes are confronted with the mismatch between rigid/planar electrodes and soft/curvilinear tissues. By designing gold nanobelts with sinusoidal structures on flexible tripod substrates, one is able to create stretchable biointegrated electrodes for direct recording of electrophysiological signals of rat cerebral cortex with desirable sensitivity and stability.[297] The transfer of thin, flexible electronics onto polymers also enables conformal placement and measurements.[298] Given the abundance of material candidates and nanofabrication techniques, more novel and smart tools capable of monitoring function and quantity would emerge and boost the development of nanomedicine and its transition into practical applications.

Biomechanical Assays. Nanoenabled tools can be designed for diagnostics and therapies based on the mechanical properties of cells.[299] At the subcellular and cellular levels, many biophysical properties have recently emerged as indicators of cell physiology and pathology, as complementary or regulatory alternatives for disease development. Cell migration, for example, can be traced by removing the trail of adherent cells left on a substrate coated with AuNPs[300,301] or with QDs.[110] The morphology of the trails correlates with the metastatic potential of the cells.[302] The force that adherent cells exert on a substrate can also be measured. For example, cell-traction-force microscopy based on the deformation of the polymer substrates on which cells are grown is able to spatiotemporally map cell traction force as precise as a nanonewton.[303−305] It can also be used to uncover previously hidden details of drug−cell interactions and mechanical contributions during cell migration.[303−305] For example, previously retarded cell migration upon NP uptake was attributed to cytoskeleton disruption. However, the uptake of the NPs actually transforms cells from the motile phenotype into an adhesive phenotype, as revealed by the increased cell traction force and altered patterns of cell traction force.[306] More importantly, ultrasensitive cell traction force microscopy could be competitive to traditional cell biology methods such as the 3-(4,5-dimethylthiazol-2-yl)-2,5-diphenyltetrazolium bromide assays,[307] WB, and flow cytometry, since early changes can be readily observed under cell-traction-force microscopy.

IN VIVO TREATMENT ("PARTICLE-BASED DELIVERY")

Nanoparticles have been designed to treat many diseases, but the most prominent disease focus has been in cancer. The literature is replete with large sets of *in vivo* data obtained from animals, and some NP formulations for cancer treatment have already been approved by regulatory agencies and have reached hospitals, showing much reduced adverse effects compared to bare drugs.[308] However, their therapeutic efficacies are most often not or only marginally improved.[309,310] Thus, there are ongoing efforts to develop systems with high therapeutic efficacies.[311] The key in such developments is to improve the design of the nanodelivery system by precisely controlling the functions/properties of the materials.

Nanoparticles have been designed to treat many diseases, but the most prominent disease focus has been in cancer.

Nanoparticles as Anticancer Drugs. The cancer drug delivery process to a solid tumor consists of five critical steps, termed the CAPIR cascade: **c**irculation in blood, **a**ccumulation and **p**enetration into the tumor, cellular **i**nternalization, and intracellular drug **r**elease. Thus, the overall therapeutic efficiency of a nanomedicine is determined by its efficiency in each step (see Figure 18).[312] A nanomedicine efficiently accomplishing the whole CAPIR cascade should have a high therapeutic index. Correspondingly, such a nanomedicine should have 2R2SP properties, the abbreviation of "drug retention *vs* release (2R)", "surface stealthy *vs* sticky (2S)" and "tumor penetration (P)".[313] The 2R indicates the required properties of the nanomedicine in terms of the loaded drug, *i.e.*, it must tightly retain the drug without burst release during the transport in blood compartments and tumor tissues, while efficiently releasing the drug at the intracellular target to exert its pharmaceutical action. Similarly, the 2S gives the needed properties in terms of the NP surface, which should be stealthy while in blood circulation for

DOI: 10.1021/acsnano.6b06040
ACS Nano 2017, 11, 2313−2381

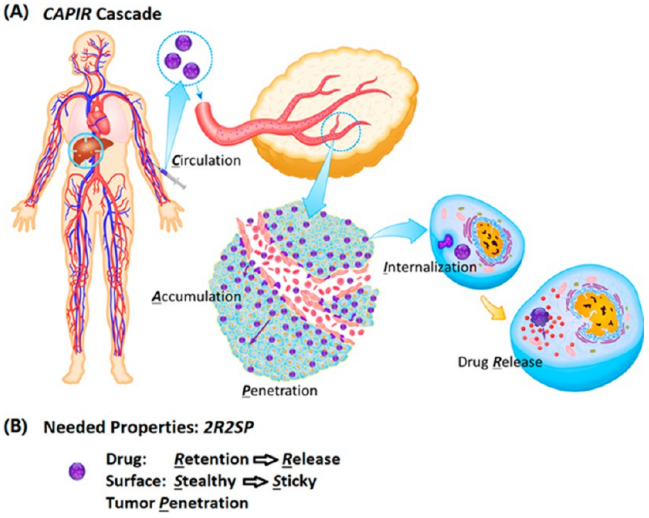

Figure 18. (A) Five-step CAPIR cascade in targeted cancer drug delivery. Reprinted with permission from ref 312. Copyright 2014 John Wiley & Sons, Inc. (B) Needed properties of a nanomedicine capable of accomplishing the cascade.

passive tumor accumulation, whereas it should become sticky once nearby the tumor cells to interact with them for efficient cellular uptake. Besides the 2R2S properties, the nanomedicine should be able to penetrate in tumor tissues to reach remote tumor cells from blood vessels. Only if a nanomedicine possesses 2R2SP properties will it be able to accomplish the CAPIR cascade successfully and to deliver active drugs at the right time and place to provide an overall high therapeutic efficacy and favorable prognosis.[312,313] Therefore, the current focus on developing nanomedicines of high therapeutic index lies on tailoring the basic physiochemical properties of NPs, *i.e.*, "size, surface properties, and stability (3S nanoproperties)" to achieve 2R2SP properties to accomplish the CAPIR cascade efficiently.

A demonstration of such a 2R2SP nanomedicine is a dendrimer core−lipid shell nanoassembly mimicking a "cluster-bomb", which shows enhanced efficacy, as demonstrated by Sun *et al.*[312] The nanocomplex is able to cruise to a tumor, shed "bomblets" to penetrate into the tumor, and then "fire" at tumor cells to accomplish the CAPIR cascade. A sixth-generation nontoxic degradable polyaminoester dendrimer with a diameter of 5 nm was chosen as the "bomblet" because of its ability to carry anticancer drugs and, more importantly, its pH-dependent 2-(*N*,*N*-diethylamino)ethyl termini.[312,314,315] The lipid shell was composed of fusogenic DOPE phospholipids, PEGylated DSPE-PEG lipids, and cholesterol in order to keep the nanoassembly stable and to provide a stealth surface in the blood compartment. The 45 nm NPs contained ~27 5 nm dendrimers surrounded by a PEGylated lipid layer. The NPs could circulate in blood and accumulate in the tumor *via* the EPR effect. Once in the tumor, the fusion of the lipid layer with the cell membrane released the dendrimers intracellularly or extracellularly. The nearly neutral dendrimers were shown to penetrate into tumor tissues easily due to their size, where the extracellular pH is acidic (pH ~6−7). The dendrimers were then protonated and became positively charged, efficiently triggering fast cellular uptake, and releasing the drug inside the cells. The dendrimer−lipid nanoassembly efficiently accomplished the CAPIR cascade and thus exerted strong anticancer activity in DOX-resistant tumor compared with typical PEG−PCL micelles.[312]

Nanoparticulate Delivery Vehicles. A vast number of classes of nanoparticulate delivery vehicles have been reported.[316−351] As demonstrated by Huynh *et al.*,[317] drug-loaded delivery vehicles are attractive because they can be passively or actively targeted to cancer tissues to improve anticancer drug selectivity and thereby reduce severe side effects. Liposomes[316] are perhaps one of the most advanced delivery vehicles concerning clinical translation, with several formulations approved by the U.S. Food and Drug Administration (FDA).[316] Liposome-based systems encapsulating drugs are already used in some cancer therapies (*e.g.*, Myocet, Daunoxome, Doxil). However, liposomes have some significant drawbacks: they have a low capacity to encapsulate lipophilic drugs, they are manufactured through processes involving organic solvents, they are often leaky and are unstable in biological fluids and aqueous solutions.[317]

Polymeric micelles embedded with drugs can also reduce undesirable side effects. Micelle formation involves the self-assembly of amphiphilic molecules in which, upon separation of hydrophilic and hydrophobic moieties, hollow capsules are formed. In water, the interior of those micelles forms the hydrophobic container, whereas the outside imposes the hydrophilic interface. Encapsulation of anticancer drugs within micelles can reduce toxicity and improve circulation.[318,352,353] For example, nephrotoxicity is significantly reduced by loading cisplatin into polymeric micelles.[318] Shielding the cisplatin-loaded core with PEG improves longevity in blood circulation by reducing acute kidney accumulation of polymeric micelles. In this regard, the secondary structure of the micelle core also plays a critical role in stabilizing polymeric micelles in diluted conditions in the blood. For example, since the core-forming segment in this formulation is poly(L-glutamic acid) (PLG), cisplatin binding to the side chain of the PLG segment induces α-helix formation. Regular assembly of cisplatin-bound helical bundles in the core is key to keeping the micellar structure intact during blood circulation.[319] Five different formulations of polymeric micellar drugs based on poly(ethylene glycol)-poly(amino acid) block copolymers, developed by Kataoka and colleagues, are already in clinical translation in Asia and North America.[320] Specifically, a polymeric micellar drug loaded with paclitaxel is close to completing its Phase III clinical trial, and is expected to be up for approval soon. Polymeric micelles thus provide a mature platform with numerous advantages to improve patient compliance appreciably, including outpatient treatment without hospitalization.

Micelles can also be jointly fabricated with polymers as well as lipids. Microfluidic chips can be used for the controlled production of these micelles for the delivery of therapeutic agents.[321,322] By adopting a microfluidic platform (see Figure 19), NPs of varying water content and rigidity but with the same chemical composition, size, and surface properties can be synthesized. It is important to be able to vary the properties of these micelles efficiently since cellular uptake can be entirely dependent on these characteristics. For example, rigid or "hard" NPs, with less interfacial water between the polymeric core and lipid shell, can enter cells more easily than those that are flexible ("soft"). In contrast, bigger particles have poor accumulation in cells.[128,323] In this regard, a hollow-structured rigid nanovesicle (RNV) was fabricated to entrap various hydrophilic reagents effectively by multistage microfluidic chips in one step, without complicated synthesis, extensive use of emulsifiers or stabilizers, or laborious purification procedures. The RNVs contain a hollow water core, a rigid poly(lactic-*co*-glycolic acid) (PLGA) shell, and an outermost lipid layer. The entrapment efficiency of

DOI: 10.1021/acsnano.6b06040
ACS Nano 2017, 11, 2313−2381

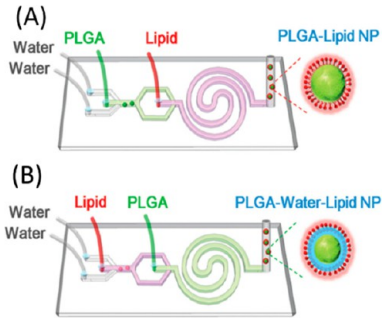

Figure 19. Scheme of a two-stage microfluidic platform for assembling polymer–lipid hybrid NPs with varying amounts of water. (a) Nanoparticles composed of the lipid shell and PLGA core are produced by injecting the PLGA solution in the first stage and lipid–PEG solution in the second stage (mode 1, P–L NPs). (b) Nanoparticles composed of the lipid shell, interfacial water layer, and PLGA core are produced by injecting the lipid–PEG solution in the first stage and the PLGA solution in the second stage (mode 2, P–W–L NPs). Adapted with permission from ref 322. Copyright 2015 John Wiley & Sons, Inc.

hydrophilic reagents such as calcein, rhodamine B, and small interfering ribonucleic acid (siRNA) inside the hollow water core of RNVs was approximately 90%.[42]

Unlike micelles, polymer capsules provide a delivery platform for encapsulating hydrophilic drugs. Polymer capsules can be formed with entirely hydrophilic polymers, for example, the LbL approach can form these capsules by templating particles.[324,325,354] While such capsules are often on the micrometer scale, smaller polymer NPs can be obtained from polymer capsules by thermal shrinkage.[327] In this approach, hollow capsules "filled" with a desired medicine with an even polyelectrolyte layer number are subjected to elevated temperatures (above the temperature of the glass transition temperature of the polyelectrolyte complex, *i.e.*, ∼40 °C). At temperatures above 60 °C, polymeric NPs are formed.

In contrast to the aforementioned NPs, where lab-made synthesis is required, exosomes are naturally occurring nano-sized-vesicles endogenously secreted by cells.[328] They are involved in intercellular and tissue-level communication by transferring biological material (*i.e.*, microRNAs [miRNAs], siRNA) among cells. Exosomes exhibit great potential as nanocarriers for a wide range of therapies, including inflammatory diseases and cancer,[329] as well as for diagnosis.[330]

Nanocarriers are not always in the form of vesicles; there are numerous other types of delivery vehicles including water-soluble polymers, dendrimers, and even polysaccharides.[331,334,340,341] Water-soluble polymers in a random coil conformation can be efficient carriers of anticancer drugs.[324,331] Recently, backbone degradable *N*-(2-hydroxypropyl)methacrylamide (HPMA) copolymer–drug conjugates synthesized by reversible addition–fragmentation chain transfer copolymerization demonstrated high efficacy in treating solid tumors. These conjugates contain a degradable oligopeptide sequence (GFLG) in the backbone and drug in the backbone and at the termini. This design permits the use of high molecular weight, long-circulating polymer carriers without impairing their biocompatibility (the carrier will degrade into fragments that will be eliminated from the body).[355] Consequently, as a result of maintaining the concentration gradient (blood to tumor) for an extended period of time, the EPR effect is considerably more effective: the drug can accumulate in solid tumor to a higher extent. Conjugates with epirubicin,[332] DOX,[333] and a combination of conjugates with gemcitabine (GEM) and paclitaxel[8] were highly effective in the treatment of experimental ovarian cancer using this platform.

Dendrimers[334] are another form of polymeric NPs, which have the advantage of being nearly monodisperse, in contrast to polymerization products, while having a defined structure and composition.[334,335] Remarkably, dendrimers with adequate hydrophilicity, unlike liposomes and polymer micelles, do not have a critical micelle concentration.[336] Therefore, dendrimers should not "in principle" fragment upon dilution.[337] Additionally, the number of functional groups grows exponentially as the number of generations increases. These features make dendrimers a powerful platform for drug delivery. Drugs can be loaded into the dendrimers in different ways, such as by encapsulation or by covalent binding of the drug. Drug encapsulation can be realized in unimolecular micelles or in supramolecular assemblies.[338] This approach enables encapsulation of the most widely used chemotherapeutic agents, *e.g.*, DOX, methotrexate, paclitaxel, and campthothecin.[335] The covalent binding of drugs is traditionally used to overcome the encapsulation problems, and the drugs are linked to the dendrimer surface using groups that will be cleaved following cellular uptake (*e.g.*, *cis*-aconityl or acyl hydrazine groups, ester groups or disulfide groups).[335] All these characteristics distinguish these materials as potential carriers for different therapeutic applications.[339]

Another class of carrier vehicles is based on polysaccharides, such as chitosan, which are promising carriers for oral delivery of therapeutic proteins.[356] The oral route is considered to be the most convenient and comfortable means of drug administration for patients.[357] Chitosan is a biocompatible polysaccharide derived from the shells of crustaceans. It is a mucoadhesive agent and a permeation enhancer that is able to mediate the opening of tight junctions between epithelial cells reversibly.[358] A NP carrier system formed by self-assembly of positively charged chitosan and negatively charged poly(γ-glutamic acid) in an aqueous milieu has been developed for delivering protein drugs orally.[340,341] The as-prepared chitosan NPs are pH-responsive in the intestines, because the pK_a of chitosan is approximately 6.5. The working mechanism for this oral delivery system is that the mucoadhesive chitosan NPs adhere to and infiltrate the mucus layer on the intestinal surface. The infiltrated NPs can transiently open the tight junctions between epithelial cells while becoming unstable and disintegrated, owing to their pH-responsiveness, and releasing the loaded protein. The released protein then permeates the paracellular pathway *via* opened tight junctions, ultimately absorbing into the systemic circulation.[342] However, the enhanced absorption of therapeutic proteins, as delivered by chitosan NPs, occurs mainly in the duodenum, most likely because chitosan is insoluble in a neutral/basic pH environment in the jejunum and ileum.[343] Additionally, these chitosan NPs are not able to protect the released protein from degradation by the proteases present in the mucus layer. One strategy of inhibiting intestinal protease activities is to remove essential metal ions such as Ca^{2+} from the enzyme structure using chelating agents such as ethylene glycol tetraacetic acid (EGTA). Furthermore, the use of chelating agents for removing extracellular Ca^{2+} can disrupt intercellular junctions and increase paracellular permeability. According to reported experiments, EGTA-conjugated chitosan NPs can significantly reduce enzymatic degradation by the specific removal of extracellular Ca^{2+} from the intestinal lumen. This enhanced stability causes intracellular internalization of junctional components, and thereby increases the

DOI: 10.1021/acsnano.6b06040
ACS Nano 2017, 11, 2313–2381

absorption of protein throughout the small intestine.[344] A recent large animal study performed with beagle dogs revealed that EGTA-conjugated chitosan NPs could successfully deliver proteins into the plasma.[345] Although chitosan-based NPs are promising for oral delivery of therapeutic proteins, further preclinical studies are required to test their efficacy and safety.

Proteins can themselves form the basis of another class of drug carriers.[346] The abundant plasma protein, serum albumin, has been successfully converted into a drug transporter and was launched to the market in 2005 for delivering the anticancer drug paclitaxel (Abraxane).[347] Serum albumin is a nontoxic, nonantigenic, and biodegradable material. In fact, albumins are excellent charge-reversible materials. Albumins have characteristic isoelectric points, due to the existence of both carboxylic acid and amino groups. When the environmental pH is higher than the pI, albumins have more negative charge on their surface, otherwise albumins are more positively charged. In addition, the pI of albumins can be adjusted by changing the ratio between the carboxylic acid and amino groups through chemical modifications. By tuning charge, albumin NPs have been successfully used to deliver negatively charged nucleic acids as biomolecules for gene therapy.[359] Recent approaches broadened the applicability of this successful platform and there is further development of novel features that aims to advance intelligent drug delivery. Boronic-acid-rich albumin NPs have been equipped with targeting peptides cRGD on the surface and DOX encapsulated inside the NPs.[348] The boronic acid groups enhance the recognition of NPs to cancer cells, since the boronic acids reversibly interact with overexpressed sialic acid residues. Encouraged by the success of albumin NPs, other endogenous proteins are being investigated such as milk casein,[349] or the iron-transport protein ferritin.[350] Proteins in their denatured form reproducibly enable the attachment of PEG chains as well as drug molecules to improve circulation times and solubility. In this way, polypeptide−PEG copolymers of human serum albumin have been obtained that can form small micelles. These micelles were able to transport and to release multiple copies of the drug DOX in leukemia cells *via* a two-step release mechanism.[351]

Similar to protein carriers, ribonucleic acid (RNA) nanotechnology has emerged as a potential platform for drug delivery applications. This use is largely due to the ability to design structures with high thermodynamic stability, and favorable and distinctive *in vivo* attributes.[360] RNA can act both as a delivery vehicle as well as an active therapeutic agent. As an example, Qiu *et al.* combined the bacteriophage phi29 DNA packaging motor pRNA three-way junction (3WJ) with folic acid, a near-infrared (NIR) marker, and BRCAA1 (breast cancer associated antigen 1, AF208045) siRNA (see Figure 20).[43] These RNA NPs comprise functionality for targeting, imaging, delivery, gene silencing, and regression of gastric cancer. *In vitro* assays revealed that the RNA NPs specifically bind to gastric cancer MGC803 cells. The siRNA incorporated in the RNA NPs thereby significantly silences the BRCAA1 gene. The apoptosis of gastric cancer cells was observed as a result of silencing the antiapoptosis factor BCl-2 and up-regulation of the proapoptosis factor Rb and Bax expression. Animal trials using a gastric tumor-bearing nude mice model confirmed that these RNA NPs could be used to image gastric cancer *in vivo*, while showing little accumulation in crucial organs and tissues several hours postsystemic injection. The growth of the gastric tumor noticeably decreased during the course of treatment. No damage to important organs by the RNA NPs was detected. All results show that RNA nanotechnology can overcome some conventional cancer therapeutic limitations

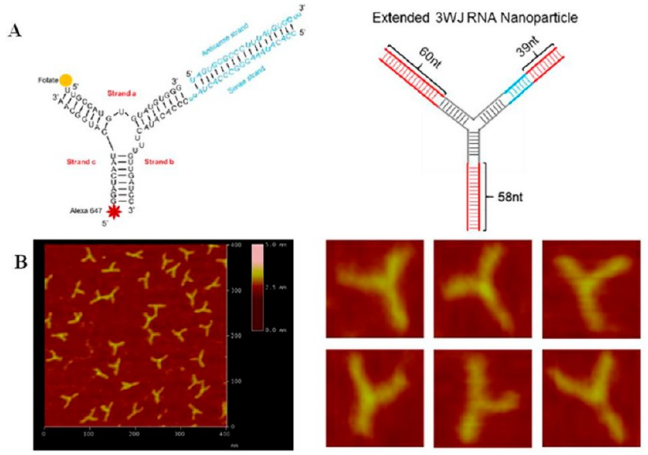

Figure 20. Global structure of therapeutic RNA NPs with BRCAA1 siRNA. (A) Design of the RNA NPs. The left image shows the NP structure as used in animal trials. On the right, an extended structure imaged by atomic force microscopy (AFM) is shown. (B) AFM image of extended 3WJ RNA NPs. The RNA complex as shown in (A) on the left is estimated to be around 10 nm in size. Due to convolution of the tip size (~10 nm in diameter) in AFM images, features smaller than the size of the tip cannot be resolved. To characterize the structure of the RNA constructs, the 3WJ NPs were extended by 39−60 base pairs (in red color, A, on the right), which is within the persistence length of dsRNA and will not affect the 3WJ folding as described before by Shu *et al.*,[362] to generate the AFM image as shown. Adapted with permission from ref 360. Copyright 2015 Nature Publication Group.

and open new opportunities for specific delivery of therapeutics such as siRNA, miRNA, and/or chemotherapeutic drugs to stomach cancer. In recent work, siRNA attached to glucose-modified AuNPs (AuNP@PEG@glucose@siRNA) were applied *in vitro* to a luciferase-CMT/167 adenocarcinoma cancer cell line and *in vivo* to the lungs of B6 albino mice.[361] The siRNA-bearing NPs induced the expression of pro-apoptotic proteins such as Fas/CD95 and caspases 3 and 9 in CMT/167 adenocarcinoma cells in a dose-dependent manner, independent of the inflammatory response. Moreover, *in vivo* pulmonary delivered siRNA-bearing NPs were capable of targeting c-Myc gene expression (a crucial regulator of cell proliferation and apoptosis) *via in vivo* RNA interference (RNAi) in tumor tissue. This led to an ~80% reduction in tumor size without associated inflammation. Overall, RNA NPs can improve therapeutic efficacy while reducing toxicity and side effects and therefore provide an avenue for use in clinical tumor therapy in the near future.

Nanodiamonds are among the most promising carbon nanomaterials for drug delivery, as well as imaging and theranostic applications. Nanodiamonds that are ~5 nm have a large accessible surface and tailorable surface chemistry, combined with unique optical, mechanical, and thermal properties.[118] In drug delivery, the rational surface modification of NDs allows for enhanced adsorption and chemical binding of the drugs for sustained or triggered drug release. Both the amount of drug adsorbed and the strength of adsorption can be controlled by the surface chemistry. By attaching drugs to the surface of NDs and by achieving controlled release, it is possible to renew the potency of anticancer chemotherapeutics.[125] Similarly, the development of NDs for targeted delivery of antibiotics and other drugs may also restore the drug efficiency and reduce systemic toxicity. Currently, NDs are being investigated for the delivery and sustained release of anticancer chemotherapeutics,[119,363]

DOI: 10.1021/acsnano.6b06040
ACS Nano 2017, 11, 2313−2381

nucleic acids,[364] and insulin.[365] Nanodiamonds have also been demonstrated for covalent binding of proteins, sometimes enhancing their activity.[366]

Similarly, inorganic NPs are frequently used as delivery vehicles. Among the inorganic nanocarriers, mesoporous silica nanoparticles (MSNPs) have emerged as a multifunctional platform that enables the development of custom-designed treatment modalities for disease-specific applications. One example is the use of MSNPs to address cancer-specific challenges such as the dysplastic stroma of pancreatic ductal adenocarcinoma (PDAC). The stroma serves as a treatment barrier due to inaccessible tumor blood vessels as well as the expression of cytidine deaminase, which is responsible for rapid degradation of the first line chemotherapeutic agent, GEM. It is possible to use a variety of MSNP designs to address the stromal barrier, including drug delivery to decrease the stromal abundance or negotiating vascular access by interfering with the action of pericytes that closely adhere to vascular fenestrations in the stromal blood vessels (see Figure 21A).[367−370] In one formulation, a MSNP carrier was developed to deliver a small-molecule inhibitor of the TGF-β receptor kinase, which is responsible for providing the cellular signal for the adherence of pericytes to endothelial cells.[371] This was accomplished by placing a polycationic polymer on the NP surface to interact with the small molecule inhibitor *via* hydrogen bonding. Under acidic conditions, the small molecule inhibitor was rapidly released in the tumor stroma. When used as a first-wave carrier, this NP construct opened vascular fenestrations within 1−2 h, thereby making it possible for a second-wave carrier (*e.g.*, a liposome) to deliver GEM to the tumor site (see Figure 21B).[371] Another formulation included the development of a dual delivery carrier, where a lipid-bilayer-coated MSNP (LB-MSNP) was used to codeliver a synergistic GEM/paclitaxel combination to the site of orthotopic human tumor implants in the pancreas of a murine model.[372] This dual-delivery MSNP carrier was ∼10× more potent than Abraxane, which recently received FDA approval in combination with GEM. Not only did the ratiometric-designed carrier suppress the tumor stroma, but it also decreased the expression of cytidine deaminase, enabling increased uptake of activated GEM at the cancer site (see Figure 21C).[372] The LB-MSNP could also be used with considerable efficacy to deliver irinotecan to the pancreatic cancer site. This result can be achieved using a remote loading method in which the drug is imported for high loading efficiency across the lipid bilayer through the use of a proton gradient.[373] This carrier was more effective than a liposomal equivalent that was recently approved by the FDA, but it also improved safety because of its more stable drug retention. Together, these examples demonstrate the use of multifunctional MSNPs for the treatment of pancreatic cancer.

Naturally there are many more types of NPs used for delivery applications, such as CNTs, graphene, and also the already mentioned inorganic NPs such as SPIONs, plasmonic NPs, *etc.* However, due to their sheer number, it is impossible to describe them all in this Nano Focus.

Targeting. Targeting of NPs refers to delivery to specific tissues and cells *in vivo*. Nanoparticles can be designed to be stealthy to escape immune clearance and avoid nonspecific cell uptake but should also be capable of being sticky to target tissues and interacting with and/or be taken up by desired cells. Nanoparticles can passively or actively accumulate in the desired tissue *via* transport through leaky vessels and unique intraorgan pressures, or adhere to specific biological structures in the targeted tissue *via* molecule recognition to surface-bound

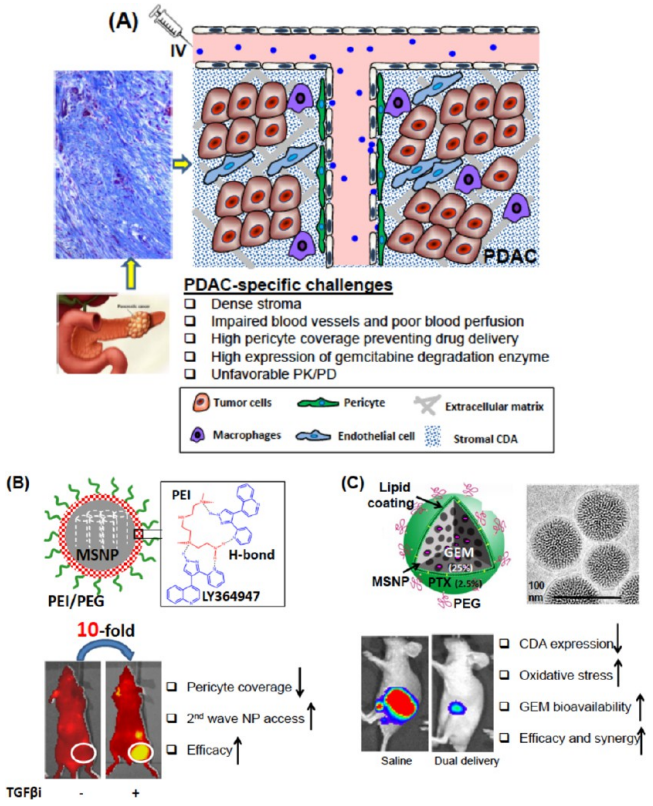

Figure 21. (A) Schematic to show the barriers and challenges that are responsible for failed chemotherapy in PDAC. This includes abundant dysplastic stroma, which serves as a physical and biological barrier, interference in vascular access and the presence of a high local concentration of deaminase activity, which leads to in activation of GEM. Trichrome staining of human PDAC is also shown: blue staining is collagen deposition. (B) Two-wave approach for PDAC treatment. PEI/PEG-MSNP binds to the TGFβ inhibitor, LY364947. The complexation is highly stable in the physiological conditions, but can be disrupted in the acidic stromal environment. NIR-labeled particles retention was increased 10-fold prior to injecting the TGFβi carrier into mice with BxPC3 xenografts (circle), with significantly decreased pericyte coverage on endothelial cells in tumor blood vessel. Reprinted from ref 371. Copyright 2013 American Chemical Society. (C) Schematic describing GEM trapping in MSNP pores, which are sealed off by the LB that contains a subtoxic dose of paclitaxel (PTX). Ratiometric codelivery of GEM/PTX by LB-MSNP inhibits PANC-1 orthotopic tumor growth through increased delivery of GEM at the tumor site. GEM/PTX loaded LB-MSNP leads to CDA inhibition in parallel with increased oxidative stress. Adapted from ref 372. Copyright 2015 American Chemical Society.

ligands.[374] Recently, researchers designed smarter NPs that can turn from stealthy to sticky. Switching between these two properties may enhance the biodistribution and targeting of NPs to diseased tissues.

Researchers have found inspiration in nature by using principles of viruses, transport proteins and their interactions with cell membranes, to achieve "stealthy and sticky" properties. Mimicking envelope-type viruses, different envelope-type[375,376] or shell-sheddable nanocarriers[377,378] have been explored to enhance the distribution of NPs in target tissue. Polymers with strong antifouling properties, such as PEG or zwitterionic polymers, were tethered onto NPs by cleavable anchor groups that are responsive to different stimuli, *e.g.*, pH, redox, and proteolytic enzymes. The NPs with the stealthy shell had prolonged circulation times and enhanced accumulation in solid

DOI: 10.1021/acsnano.6b06040
ACS Nano 2017, 11, 2313−2381

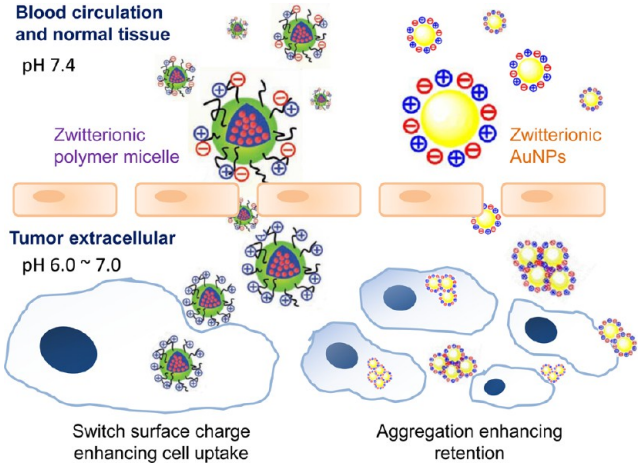

Figure 22. Interchange between "stealthy and sticky" for zwitterionic polymer micelles (left) and the mix-charged AuNPs (right). Adapted with permission from ref 379 and 380. Copyright 2012 and 2014 John Wiley & Sons, Inc.

tumors due to the EPR effect, *i.e.*, passive targeting. The unique stimuli within the targeting tissue enable the NP to release the shell, thus converting from stealthy into sticky. In a similar direction, zwitterionic surfaces containing mixed positive and negative charges have received great attention due to their unique stealthy properties and their similarity to proteins. Many proteins behave stealthily to most cells and they can have long circulation times *in vivo*. However, they can alternate between "stealthy and sticky" under even a slight stimulus such as a minor change in pH.[379] Although the detailed mechanism of this change has not been elucidated and might indeed be complex, the zwitterionic properties of amino acids and the mixed-charge structures of proteins might contribute to this feature. By exploiting pH changes in different structures (*e.g.*, in tumor tissues, 6.5−6.8; in endosomes, 5.5−6.8; and in lysosomes, 4.0−5.0), zwitterionic polymer-based NPs, capable of altering their charge densities in different tissues, can be prepared. This responsiveness involves introducing a surface moiety sensitive to tumor extracellular acidity (pH ~6.8)[379] as the anionic part of the zwitterionic polymer (see Figure 22).

Nanoparticles can also be covered by neoglycoconjugates, or sugar-like functional groups and other functionalities such as thiol groups, to convert the NPs from stealthy to sticky. Though typically uncharged, such glycan-based ligands provide extremely high stability in biofluids, while minimizing nonspecific cell internalization. Whereas much research has been carried out with nanometer-size AuNPs,[381] these moieties have only recently been shown to work for larger AuNPs with various morphologies, including nanorods.[375,382] Interestingly, even though the stealthiness was shown to be superior to that of PEG ligands, specific protein-binding was retained, enabling the AuNPs to target cell types that overexpress certain protein receptors. The NPs thus exhibit prolonged circulation times due to the pronounced antifouling properties of the zwitterionic polymer. However, when the NPs are in an acidic tumor environment, surface charges change from negative to positive, leading to enhanced cellular uptake and accumulation of the NPs within tumor tissue. Compared with the NPs that switch their charge states by cleavage of the responsive covalent bonds, charge conversion of weakly electrolytic groups at different pH proceeds rapidly and better mimics the changes in charge density of amino acid segments within proteins. Surface engineering of inorganic NPs *via* mix-charged ligands can enhance NP retention in tumors by modulating the aggregation of NPs.[380,383,384] The mixed-charge modified AuNPs present not only a transition from stealthy to sticky under the acidic extracellular pH of solid tumors, but also a significant aggregation of NPs with much higher tumor accumulation, retention, and cellular internalization. Aggregation of AuNPs can also shift the surface plasmon band to the near-infrared wavelengths for photothermal therapy.[385] Moreover, recent studies on 3D spheroids of liver cells made in inverted colloidal crystals demonstrated that targeted nanotubes display unusually fast passive diffusion in the tissues.[386] Such an effect originates from the effective two-dimensional (2D) translation of nanotubes over the surface of the cells in the tissues when the attractive forces between nanotubes are balanced with electrostatic repulsion. This finding suggests that nanoscale design of drug delivery vehicles can result in deep and effective penetration into the tumors.

In addition to tailoring the surface properties of NPs, optimizing the sizes of NPs is also particularly important for tumor accumulation, penetration, and finally treatment efficacy,[387] particularly in targeting stroma-rich tumors.[388] By using micelles, ranging from 20 to 300 nm with the same chemical structure and physical properties, Wang *et al.* found that the blood circulation time and tumor accumulation of micelles increased with an increase in their diameters; with optimal diameters ranging from 100 to 160 nm. However, higher tumor accumulation of the large micelles (100 nm) did not result in significantly improved therapeutic efficacy, because larger micelles had poorer tumor penetration than did smaller micelles (30 nm). An optimal size that balances drug accumulation and penetration in tumors is critical for improving the therapeutic efficacy of nanoparticulate formulations.[387] The size effect is more pronounced in pancreatic tumors, which usually have thicker stroma and hypovascular characteristics that limit NP penetration. In the same direction, Kataoka and co-workers discovered that tuning the size of polymeric micelles in the range below 50 nm significantly improved the penetrability into stroma-rich pancreatic tumor and consequently improved antitumor efficacy.[367] In addition, 30 nm polymeric micelles loaded with cisplatin have proceeded onto Phase III clinical trials for the treatment of pancreatic cancer patients by extending survival times in Phase I/II compared to standard treatment using GEM.

Apart from passive targeting, as described above, there are also exciting recent developments in actively targeting NPs. As one of the early studies in designing integrin-targeted nanomedicines, RGD-modified stealth liposomes achieved higher intracellular levels of DOX.[389] In recent years, more novel ligands against various tumor targets have been employed by making use of different targeting motifs, including alpha-conotoxin ImI, PHSCNK, lanreotide, octreotide and chlorotoxin for alpha 7 nAChR, integrin $\alpha_5\beta_1$, somatostatin receptors, and chloride channels.[390−394] However, receptor redistribution induced by ligand binding decreases receptor affinity for ligands. A special dimeric RGD with proper distance between two RGD motifs was used to circumvent this problem.[395] On the other hand, an electrically neutral but hydrophobic penetration peptide was introduced to modify NPs against different breast cancer cell phenotypes irrespective of their receptor expression, displaying lasting accumulation and better inhibition of the tumor.[396] Still, there are ongoing discussions about the benefits of active *versus* passive targeting.[34,397]

Besides ligand-mediated active targeting, active physical targeting has also been demonstrated. Magnetic focusing can

DOI: 10.1021/acsnano.6b06040
ACS Nano 2017, 11, 2313−2381

enrich iron oxide NPs in the tumor region. Materials most commonly used for magnetic drug delivery contain metal or metal oxide NPs, such as SPIONs. Superparamagnetic iron oxide NPs consist of an iron oxide core, often coated with organic materials such as fatty acids, polysaccharides, or polymers to improve colloidal stability and to prevent separation into NPs and carrier medium.[398,399] For some applications, a permanent magnet is placed in the targeted region prior to the administration of magnetic NPs. This has been done for ferric steel implants, which were placed in the subarachnoid space in an *in vitro* human spine model prior to NP administration into the spine.[400] Similarly, dilute microferrimagnetic wires implanted within blood vessels in combination with an externally applied magnetic field can provide specific enrichment of simultaneously administered ferromagnetic NPs.[401] The challenge of NP enrichment in deeper body regions was addressed by He and co-workers, who deployed Halbach-like magnet arrays.[402] Nacev *et al.* also developed a sophisticated approach based on fast magnetic pulses on ferromagnetic rods that led to reversing the sign of the potential energy term in Earnshaw's theorem. This process enabled a quasi-static, stable trap between magnets, resulting in the concentration of ferromagnetic rods on a central target.[403] These concepts are still far away from clinics. Magnetic drug targeting (MDT), based on intra-arterial administration of drug-loaded SPIONs, is closer to application in patients. This technology involves enriching SPIONS *via* a strong external magnetic field. A proof-of-principle preclinical study was conducted to demonstrate successful application of SPIONs for cancer treatment.[404] Simultaneous injection of Mitoxantone−SPIONs into the tumor-supplying vessel in rabbits and the application of a strong external magnetic field over a VX2 squamous cell led to complete tumor remissions without side effects. By applying only 5−10% of the conventional chemotherapeutic dose, complete tumor remissions were achieved. The distribution profile after MDT displayed 57.2% of the total recovery of administered drug: with 66.3% of the particles localized in the tumor region with magnetic targeting, compared to less than 1% of drug and NPs reaching the tumor region during conventional intravenous application. Magnetic drug targeting enables better enrichment of drug formulations and, consequently, enables more specific treatment. The majority of magnetic material is based on magnetic NPs either encapsulated or coated by different inorganic core/shell coatings[405] or by various polymer-based matrices, which are from natural[406−408] or artificial origin.[409,410] To translate these magnetic nanoparticles for clinical applications, the development of methods for large-scale synthesis is required. A promising approach to synthesizing fatty acid-coated SPIONs, shielded with albumin and functionalized with adsorptive mitoxantrone, was developed with easy scale-up synthesis pathways in order to obtain antitumor-effective magnetic NPs.[411] Nanoparticles derived from this process have proven to be stable under appropriate storage conditions.[412]

Delivery of Macromolecular Biopharmaceuticals across Biological Barriers. Nanomedicines are also being developed for diagnosing and treating infectious, neurodegenerative, or cardiovascular diseases.[413] Anticancer drugs are typically small organic molecules; however, the number and impact of macromolecular biopharmaceuticals (*i.e.*, polypeptides and polynucleotides) are increasing enormously. Their size and complexity impose significant challenges to their use as safe and effective medicines, including fast elimination and poor metabolic stability. Furthermore, this class of compounds notoriously suffers from limited permeability across biological barriers, such as cellular membranes or epithelial tissues (see Figure 23).[414] On the other hand, their medical use offers not only the ability to ameliorate symptoms, but also the opportunity to cure or to prevent diseases, either by directly correcting hormonal disorders (*e.g.*, insulin in diabetes) or by correcting, inhibiting, or reprogramming genetically disordered cells. The delivery of macromolecular biopharmaceuticals, preferentially *via* noninvasive ("needle free") approaches, is therefore another important future application of nanomedicines. This approach takes advantage of the fact that NPs can both stabilize and protect the therapeutic cargo, while translocating across epithelial tissue barriers like those of the gastrointestinal (GI) tract, skin, or lungs.[415]

Similar to the EPR effect, which occurs at the endothelium of tumor blood vessels, NPs can also accumulate in inflamed mucosal areas. This phenomenon was demonstrated recently by

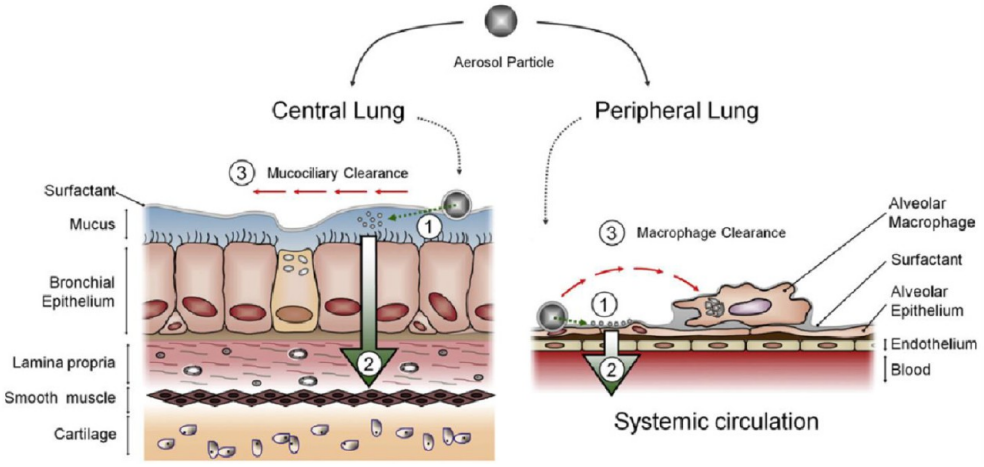

Figure 23. Cellular and noncellular barriers of the lung: after landing on lung lining fluids, (1) the drug (or eventually entire NPs) must cross the pulmonary epithelium (2) in order to reach the underlying tissue or the systemic circulation, respectively. Besides, inhalation, nanopharmaceuticals must also overcome effective clearance processes (3) provided by either mucus in the central lung (bronchi) or by macrophages in the peripheral lung (alveoli). Reprinted with permission from ref 414. Copyright 2014 Elsevier.

DOI: 10.1021/acsnano.6b06040
ACS Nano 2017, 11, 2313−2381

confocal laser endoscopy in colitis patients.[416] In several colitis mouse models, oral administration of enteric-coated NPs that encapsulated an anti-inflammatory compound showed significant alleviation of symptoms and inflammatory markers compared to the same dose of free drug and nanocarriers without enteric coating. At the same time, adverse effects elicited by drugs can be reduced through targeted delivery, which reduces the dosing frequency as well as adverse side effects.[417,418]

Nanoparticles can also accumulate in hair follicles and skin folds after transport through the stratum corneum (SC). This phenomenon depends on the NP size and shape. As a medical application, it offers the potential to reach the perifollicular antigen-presenting cells without impairing the SC barrier. Transfollicular delivery of ovalbumin using polymeric NPs was recently shown to induce a significant cellular and humoral immune response, without compromising the SC barrier by any pretreatment, when combined with innovative adjuvants.[419−421]

Lastly, pulmonary delivery of inhalation nanopharmaceuticals is an area of emerging interest for the treatment of both systemic and pulmonary diseases. Market approval of several inhalative formulations demonstrates the preference of the public for less invasive means of drug delivery. However, the lung features several biological barriers that normally protect our bodies against potentially noxious substances, which need to be overcome for effective delivery.[422]

Transport of biomolecular pharmaceuticals across barriers such as biofilms has also been a topic of focus. For example, patients suffering from cystic fibrosis, a genetic disorder, typically get infections by opportunistic bacteria, most notably *Pseudomonas aeruginosa*. These Gram-negative bacteria protect themselves from attacks from the immune system by forming biofilms. Interfering with their so-called quorum sensing communication systems by novel types of anti-infectives may prevent biofilm formation, therefore combatting the bacteria while minimizing the development of resistance. Using solid lipid NPs (<100 nm), researchers observed about a 7-fold increase in potency to reduce the virulence factor pyocyanin compared to the free drug.[423] Nanoparticles can also be used to address respiratory problems with implications for bacterial or viral infections. Aerosolized chitosan-coated PLGA nanoparticles have been used for *in vivo* genome editing by nuclease-encoding RNA of a lethally deficient surface protein B. As opposed to viral vectors, which caused lethal adverse effects in clinical trials, the nanotechnology-based nonviral carriers can be prepared by well-controlled chemical processes and do not bear the typical risks of viral vectors.[424]

Stimuli-Responsive Release. Controlled-release systems can potentially reduce or alter toxicity by selectively controlling the rate of drug release and directly killing diseased cells. Researchers have thus far developed many different controlled-release methods.[30] For instance, transporter polymers containing pH-sensitive groups are protonated or deprotonated in the local microenvironment. This responsiveness again leads to the disruption of the hydrophilic−hydrophobic balance of the nanocarriers, triggering drug release. Alternatively, cleavage of chemical bonds in response to pH can degrade the nanocarrier and release drug molecules. Acid-sensitive polypeptide nanogels have been reported for efficient DOX loading and release. Dual pH-sensitive polymer−drug conjugates that reversed their surface charges from negative to positive at tumor extracellular pH (~6.8) promoted cell internalization and DOX drug release at pH 5.0 (endo/lysosomal pH) by cleaving acid-labile hydrazine bonds.[425]

Besides pH, redox potential has recently emerged as a ubiquitous natural stimulus for intracellular drug and gene delivery because of the large concentration gradient of glutathione (GSH) in healthy (~2−10 mM) and tumor tissues (~10−25 mM). Glutathione-responsive nanocarriers have been designed containing disulfide bonds,[426,427] either in the hydrophobic block of amphiphilic copolymers,[428] at the interconnection of two polymer blocks,[429] or as cross-linkers.[430] The redox potential differences of disulfide and diselenide bonds[431,432] could even facilitate a dual reduction-sensitive polyplex for programmed gene transfection, by sequentially deshielding the reductive conditions of tumor tissues and consequently degrading in response. In addition, thioether bridges of higher chemical stability have been introduced offering better handling and storage compared to disulfide bridges.[433] Cleavage of the thioethers is only triggered by high GSH concentrations above 10 mM, which maximizes the local specificity of redox triggered drug release in tumor cells.

Another powerful stimulus to release NPs are enzymes, which can be in overabundance under pathological conditions such as cancer or inflammation. Elevated local concentrations of matrix metalloproteinases (MMPs), phospholipases, or glycosidases have been exploited to release drug molecules from drug transporters containing the respective enzyme substrates. For instance, MMP-sensitive nanocarriers have been designed by conjugating DOX to silica NPs *via* a MMP-sensitive peptide.[375] The delivery of the nanocarrier to the tumor exposed the carrier to the presence of MMPs in the tumor, which degrades the peptide linker and causes rapid release of the drug DOX from the silica NP.

Tumor cells are characteristically heterogeneous in many aspects.[434] As a result, nanocarriers responding to a single type of signal would release the drug only in the fraction of tumor cells overexpressing that particular signal but not in other tumor cells, thereby decreasing the overall therapeutic efficacy of the drug formulation.[435] For instance, cancer cells may be under reducing conditions as a result of their elevated intracellular GSH levels, which may be several-fold higher than those of normal cells.[436] Also, many tumor cells are reported to overproduce ROS, *e.g.*, perhaps more than 1 order of magnitude higher than healthy cells,[437] and thus increase oxidative stress.[438] These heterogeneous cells may exist in different tumors, but may also coexist in different regions in one tumor. Tumor cells at different stages may also have different GSH/ROS levels.[435,436,438−440] To compensate for this observed tumor heterogeneity, Wang *et al.* proposed an amphiphilic SN38-prodrug formed nanocapsule that could respond to both intracellular GSH and ROS to release the carried drug (see Figure 24).[441] The thioether linker of the prodrug was designed to undergo thiolysis in the presence of GSH or fast hydrolysis due to ROS oxidation of the linker, giving rise to high *in vitro* cytotoxicity and *in vivo* anticancer therapeutic activity. The nanocapsules had a SN38 loading content of 35 wt % and were able to target the tumor passively *via* the EPR effect, making them ideal for translational nanomedicine.[441]

The development of intracellular stimuli-responsive drug-loaded NPs has recently attracted substantial research efforts.[442] Specifically, the intracellular release of drugs by biomarker triggers or intracellular environmental conditions holds great promise as a means to localize the drug in disease-carrying cells. Consequently, this decreases the dose of drugs required for treatment and reduces harmful effects on normal cells. The recognition and catalytic properties encoded in nucleic acids

DOI: 10.1021/acsnano.6b06040
ACS Nano 2017, 11, 2313−2381

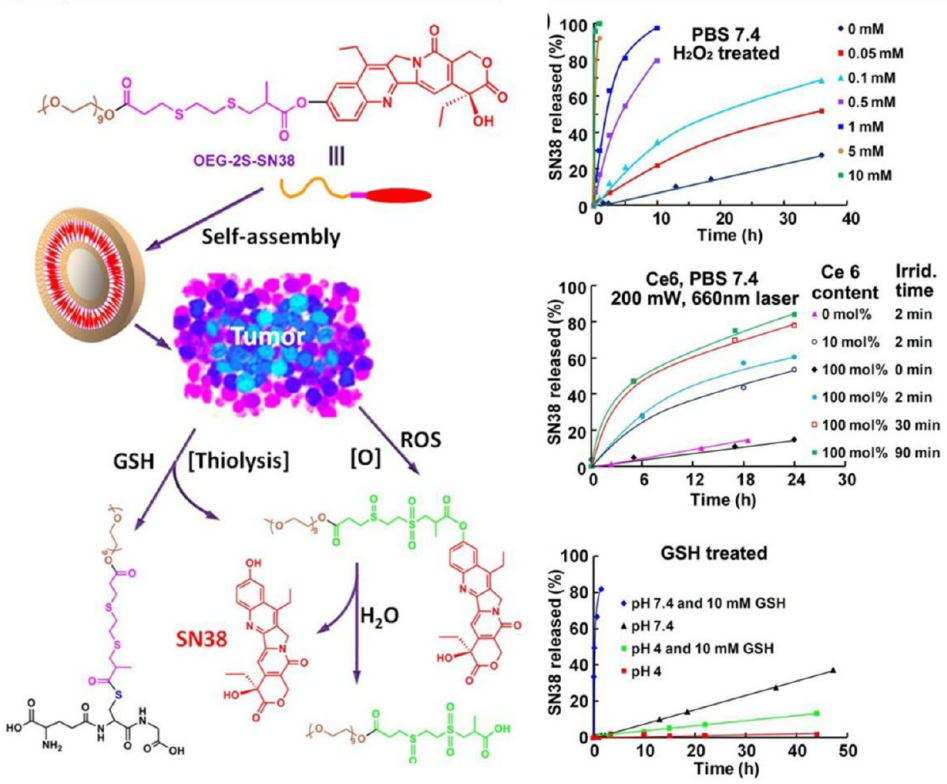

Figure 24. SN38 prodrug formed nanocapsule responsive to tumor GSH/ROS heterogeneity, releasing the parent drug SN38 *via* thiolysis in the presence of GSH or *via* enhanced hydrolysis due to ROS oxidation of the linker. This process thereby gives rise to high *in vitro* cytotoxicity and *in vivo* anticancer therapeutic activity. Reprinted with permission from ref 441. Copyright 2013 John Wiley & Sons, Inc.

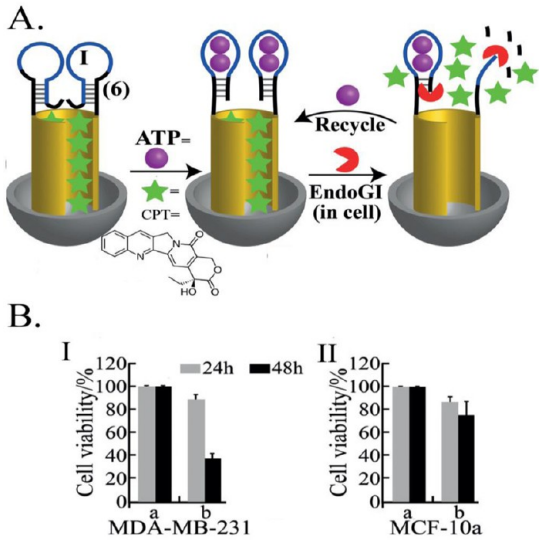

Figure 25. ATP-EndoGI sense-and-treat system involving CPT-loaded mesoporous SiO_2 NPs: (A) Reconfiguring the DNA capping units *via* the formation of ATP−aptamer complexes, followed by the Endo GI digestion of these complexes which leads to the recycling of the ATP biomarker and the release of CPT. (B) Cytotoxicity of the ATP/EndoGI-responsive CPT-loaded SiO_2 NPs toward (I) MDA-MB 231 cells, (II) MCF-10a cells. Entries (a) correspond to treatment of the cells with unloaded NPs and (b) correspond to CPT-loaded SiO_2 NPs. Gray bars correspond to cell viability after 24 h, and black bars represent the cell viabilities after 48 h. Adapted from ref 443. Copyright 2013 American Chemical Society.

have been implemented to develop mesoporous SiO_2 NPs for the intracellular controlled release of anticancer drugs. Figure 25A exemplifies the controlled release of the anticancer drug camptothecin (CPT) from mesoporous SiO_2 NPs (100 nm diameter) using intracellular triggers.[443] The system makes use of the fact that adenosine triphosphate (ATP) is overexpressed in cancer cells due to their enhanced metabolism, and the fact that specific enzymes, such as the exonuclease EndoGI, are produced in certain cancer cells. Accordingly, the mesoporous SiO_2 NPs were loaded with the CPT anticancer drug, and the pores were capped with bulky hairpin nucleic acid units. The hairpin structures included programmed sequence-specific aptamer domains, which recognize the ATP biomarker. The interaction of intracellularly generated ATP with functionalized NPs resulted in the reconfiguration of the hairpin units into ATP−aptamer complexes that were recognized by the secondary intracellular cancer cell biomarker EndoGI. The biocatalytic digestion of the duplex domains of the ATP−aptamer complexes resulted in the regeneration of the ATP biomarker, and the EndoGI-stimulated unlocking of the capped pores, leading to the release of the CPT drug. Figure 25B shows the cytotoxic effects of the stimuli-responsive CPT-loaded mesoporous SiO_2 NPs on MDA-MB-231 breast cancer cells, panel I, and on normal epithelial MCF-10a breast cells, panel II. After a time interval of 48 h, the cell viability of the MDA-MB-231 cells decreased by 65%, whereas the viability of normal cells only decreased by 20%. The effective cell-death of the cancer cells was attributed to the ATP-EndoGI-driven release of CPT in cancer cells.

Mesoporous SiO_2 NPs were also loaded with anticancer drugs, such as DOX, and capped with various other stimuli-responsive nucleic acids responding to substances or environmental

DOI: 10.1021/acsnano.6b06040
ACS Nano 2017, 11, 2313−2381

conditions existing in cancer cells. For example, the *in vitro* release of DOX from mesoporous NPs was triggered by the miR-21 biomarker present in cancer cells[444] or by releasing the i-motif locking units under the acidic conditions available in cancer cells.[445] Similarly, Zhang *et al.* reported the cleavage of DNA-capped, DOX-loaded mesoporous SiO_2 NPs by the ATP-promoted activation of a catalytic Mg^{2+}-dependent DNAzyme that was associated with the capping units.[446] The intracellular release of DOX from DNA-capped mesoporous nanoparticles using photogenerated ROS species has also been demonstrated.[447] In order to realize the potential of these stimuli-responsive NPs fully, toxicity must be evaluated in cells and animals.

Although numerous internal stimuli have been investigated, it remains a challenge to receive a sharp response to subtle changes in environmental conditions. As a result, many exogenous stimuli-responsive drug nanocarriers have been designed to respond to external stimuli such as temperature changes, magnetic or electric fields, and light (*i.e.*, electromagnetic waves) to control the spatial location of drug release.[448,449] Particularly, magnetically responsive transporters have been developed to target tumor tissue under the influence of an external magnetic field.[450] This concept has demonstrated great potential in cancer therapy and increased therapeutic efficacy at lower doses with fewer toxic effects. In addition, magnetic resonance imaging combines diagnostics and therapy in the same system, as we will emphasize in the theranostics section. Light is another attractive stimulus for the construction of stimuli-responsive drug nanocarriers, since this approach enables remote and spatiotemporal drug release by tuning the wavelength, energy, and site of irradiation. The advantages of phototriggered drug release are obvious; however, accessibility of the body for light is limited.[451] Skin treatment is the most obvious application of this technology, but there are numerous other methods used for drug release on or through the skin by epitopical methods. Interestingly, Sykes and co-workers showed that QDs and AuNPs can accumulate and transit through the skin after tail vein injection. Their results suggest that skin may be a depot for light-activated NP drug release.[452] Photochemical drug release has also been studied in the lungs. Practically all organs accessible by endoscopic tools may be treated this way.[453] For the combination of light and interventional therapy, fixed-point drug release can be realized by taking advantage of optical fibers. Near-infrared laser-triggered drug nanocarriers are particularly promising due to deeper tissue penetration, lower scattering properties, and minimal harm imposed on tissues. Thus, NIR-responsive systems are promising platforms for clinical applications.[454−456] Several studies have demonstrated that upon NIR irradiation,[457] AuNPs incorporated in the wall of the polymer-based delivery container can convert light into heat through a series of photophysical processes. The heat can directly destroy cancer cells or facilitate disruption of thermoresponsive NPs, resulting in the release of encapsulated drugs.[458,459] Controlling this process by minimizing heat accumulation can lead to nondestructive opening of capsules and intracellular delivery of medicine.[460−462] However, even though these strategies have proven successful in several examples, deep tissue penetration to reach less accessible targets is still challenging and the accuracy is often low due to complicated tissue and bone environments inside the body. Thus, the future success of this strategy is not only dependent on material design, but also on the development of advanced instruments to position the therapeutic stimulus accurately.

In ophthalmology, there is a need to release drugs for the treatment of secondary cataracts years after implantation of an artificial intraocular lens. In this case, since the cornea is a good ultraviolet light absorber, the use of ultraviolet light is not appropriate for treatment. Photochemical drug release from polymers by two-photon absorption can potentially overcome these problems. In addition to low molecular weight drugs, NPs can similarly be released by two-photon absorption.[463] Examples of such materials have been developed and successfully tested in the lab and in animal models. Thermoresponsive drug nanocarriers have been intensively investigated as drug delivery systems. These transporters reveal high stability at body temperature (~37 °C) but rapidly release their drug cargos within locally heated tissue (~40−42 °C).[464] This approach is particularly attractive in combination with AuNP-assisted NIR plasmonic photothermal therapy.

Alternative Delivery Strategies. An alternative delivery strategy involves combining multiple antitumor drugs in one carrier.[465,466] The poor specificity of most drugs and the complexity of tumors (*e.g.*, multiple targets) contribute greatly to the poor prognosis of chemotherapy. Passively or actively targeted nanopreparations usually enhance the selectivity of anticancer drugs while the combination of therapies against more than one single tumor target improves the therapeutic outcome.[467] Co-delivery of chemotherapeutic drugs and nucleic acids has shown promising results in overcoming multidrug resistance. Simultaneous delivery of small-molecule drugs and nucleic acids is challenging due to the pronounced differences in their physicochemical properties, which may greatly affect their biodistribution and pharmacokinetics. The preparation of delivery systems that enable the delivery of structurally differing drugs with comparable pharmacokinetics is attractive to inhibit tumor growth efficiently. For example, Zhang *et al.* demonstrated that the combined use of octreotide-modified paclitaxel micelles and salinomycin micelles eradicated both breast cancer and cancer stem cells.[468] Zhou *et al.* have shown that treatment of prostate cancer with a combination of two nanoconjugates, one targeting the hedgehog-signaling pathway of stem cells (HPMA copolymer-cyclopamine conjugate) and the other differentiated cells (HPMA copolymer-docetaxel conjugate), improved survival rates.[469] Dai *et al.* reported a strategy combining the mTOR inhibitor, rapamycin, and DOX-loaded octapeptide liposomes to combat triple-negative breast cancer.[470] Feng *et al.* studied the synergistic inhibition of breast cancer by codelivering VEGF siRNA and paclitaxel *via* vapreotide-modified core/shell NPs.[471] Fan *et al.* found that the reduction of tumor interstitial fluid pressure by liposomal imatinib improved the antitumor effect of liposomal DOX.[472] Finally, Wang *et al.* demonstrated the sequential killing of tumor vasculature and tumor cells *via* integrin-targeted polymeric micelles loaded with both combretastatin A4 and DOX.[473]

In addition to intravenous delivery, nanomedicines can be delivered locally. Most chemotherapeutics are delivered systemically, where high doses result in severe side effects and only a limited amount of drug reaches the tumor site. Intratumor or peritumor delivery is thought to improve these issues but the challenge is in simultaneously achieving high drug loading, sustained and stable drug release, and long-term local drug retention. One platform achieved these requirements by incorporating micelles or nanocrystals of a hydrophobic antitumor drug, such as docetaxel and paclitaxel, into a thermosensitive injectable hydrogel.[474,475]

Tumor metastasis accounts for 90% of cancer-associated deaths and is almost inaccessible by chemotherapy, surgical operation, or radiotherapy. A nanomedicine modified with a

DOI: 10.1021/acsnano.6b06040
ACS Nano 2017, 11, 2313−2381

peptide-targeting metastasis can facilitate DOX in inhibiting metastatic tumor growth and prevent the initiation and progression of tumor metastasis.[476] Its targeting to highly metastatic tumors was demonstrated in a double tumor-bearing model with both metastatic and nonmetastatic tumors in the same mouse.[477] Lymph-targeting peptides can enhance nanoparticle delivery to a highly metastatic tumor and its lymphatics.[478] Chlorotoxin, a venom peptide previously used for brain targeting, was found to inhibit metastatic tumor growth and metastasis.[479] After intravenous injection, CPT NPs accumulated in the lungs, a major metastatic site for many types of cancers, which led to greater antimetastatic efficacy.[480] Finally, a macrophage-based biomimetic delivery system inhibited metastasis due to its tumor-homing properties.[481]

Regulating Cells with RNA. Targeting protein-coding messenger RNAs (mRNAs) and regulating noncoding RNAs by delivering therapeutic RNA effectors or modified derivatives has become an important research topic in nanomedicine. In principle, there are four different strategies to deliver nucleic acid effector molecules: (i) through viral vectors that encode RNA effectors such as short hairpin (shRNAs), usually adeno-associated viruses or lentiviruses;[482−484] (ii) *via* NPs based on liposomes (lipoplexes), polycations, or polyamines (polyplexes);[485,486] (iii) as conjugates with hydrophobic molecules (*e.g.*, cholesterol or tocopherol),[487,488] *N*-acetylgalactosamine,[489] or aptamers;[490] and (iv) by gymnotic ("naked") delivery of chemically modified RNA, which means functional delivery into cells without any further formulation.[491] There are various possibilities to form nanoplexes with nucleic acid effectors. For example, chitosans, dendrimers, polyethylenimine, atelocollagen, or cyclodextrin can be used to produce polymeric NPs for delivery. Cationic or neutral liposomes, as well as zwitterionic polymer micelles are available options among liposome-based NPs. Several of these nanoplexes are now in clinical studies, illustrating that RNA-based therapeutics are considered promising for future healthcare. Functionalization of nanoplex delivery sytems opens many perspectives for a more specific delivery of NPs to their target cells.

We will focus our discussion on relatively small nucleic acid effectors, usually not exceeding 50 nucleotides (nt; U1 adaptors, siRNA duplexes) and as short as 8 nt (tiny locked nucleic acids [LNAs]). Such antisense oligonucleotide (ASO) effectors are routinely designed with strategic nucleotide modifications to improve various features, such as stability in biological fluids, cellular uptake, target RNA affinity, and specificity, or to minimize toxicity, nonspecific immune stimulation, and off-target effects.[492] At present, the most effective and widely used chemical modifications are phosphorothioates, ribose 2′-OH modifications (*e.g.*, 2′-O-methyl, 2′-fluoro or 2′-O-methoxyethyl modifications), and LNA residues with their ribose moiety locked in the 3′-endo conformation by a methylene bridge connecting the 2′-oxygen and the 4′-carbon atom (see Figure 26A). Locked nucleic acid modifications make ASOs nuclease-resistant and increase duplex stability with target RNAs more than any other known nucleotide modification, without compromising target specificity as long as immune stimulatory sequences are avoided.[493,494] Gapmers are ASOs carrying an internal stretch of at least 6 DNA oligonucleotides for the recruitment of endogenous RNase H activities that cleave the target RNA in the RNA:DNA hybrid region. The 5′- and 3′-terminal nucleotides of gapmers preferentially modified with LNA residues (termed LNA gapmers)[495] to optimize target affinity and to confer nuclease resistance (see Figure 26B). Such LNA

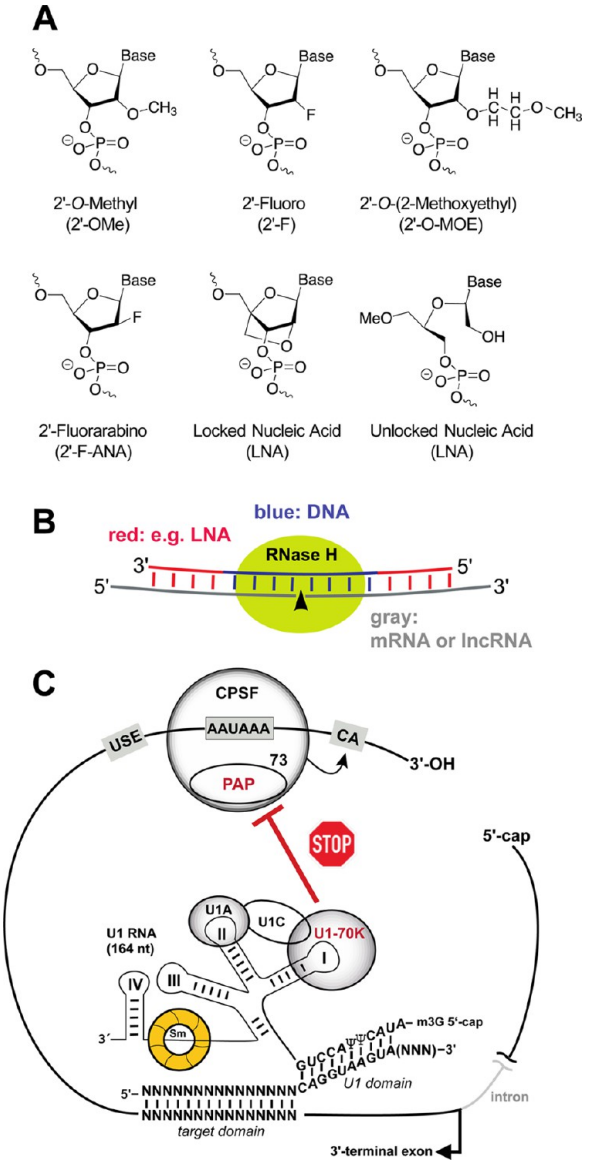

Figure 26. (A) Chemical nucleoside modifications frequently used for nucleic acid effectors. In many cases, phosphorothioate (PS) modifications (one of the two nonbridging oxygens of the phosphodiester replaced with sulfur) are incorporated, to improve the pharmacokinetic properties and cellular uptake. (B) LNA gapmers composed of terminal LNA residues and at least 6 central DNA nucleotides enable cleavage of RNA target strands as part of RNA:DNA hybrids by endogenous RNase H activities. (C) In the U1 adaptor approach, a U1 small nuclear ribonucleoprotein (snRNP) (an abundant spliceosomal RNP) is guided to the 3′-terminal exon of a target pre-mRNA *via* a dual antisense oligonucleotide that simultaneously anneals to the 5′-end of U1 RNA. This blocks polyadenylation *via* an inhibitory interaction between poly(A) polymerase (PAP) and the U1−70K protein. As a result, the pre-mRNA is still cleaved but not polyadenylated, which induces its degradation. Efficient down-regulation by "U1 interference (U1i)" was observed with target domains of 12−15 nt (with up to 15 LNA residues) and 10−13 nt in the U1 RNA binding domain (good efficiency observed with eight 2′-O-methyl and five LNA residues). A PS backbone was also found to be compatible with U1i.[499,500] U1A, U1C, U1−70k and the Sm ring proteins are integral components of the U1 snRNP. PAP: poly(A) polymerase; CPSF: cleavage and polyadenylation specificity factor (including the endonucleolytic subunit 73); CA: cleavage site. Adapted with permission from ref 500. Copyright 2009 John Wiley & Sons, Inc.

DOI: 10.1021/acsnano.6b06040
ACS Nano 2017, 11, 2313−2381

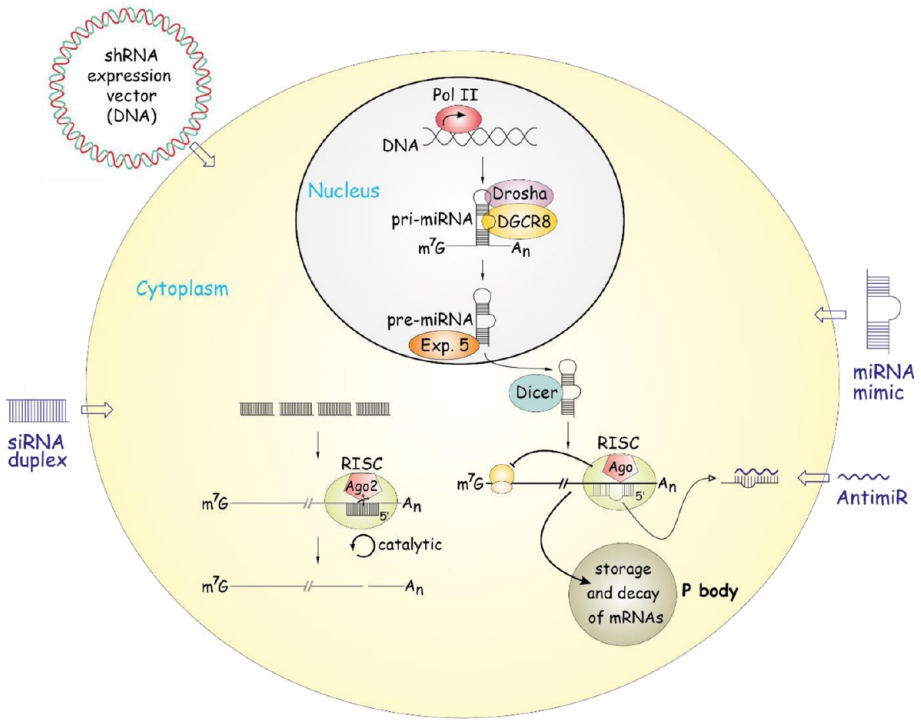

Figure 27. Exogenous RNA effectors utilizing the RNAi machinery of mammalian cells (siRNA duplexes, shRNAs, miRNA mimics) or interfering with the function of endogenous miRNAs (antimiRs). siRNA duplexes, 19 bp long, mimicking the processing products of the RNase Dicer, are incorporated into the RNA-induced silencing complex (RISC). One of the two siRNA strands (termed the guide strand) is selected by RISC to guide the complex to complementary mRNAs sequences that are cleaved by the endonuclease Ago2 followed by mRNA decay. This catalytic process is highly efficient as one siRNA-programmed RISC can cleave many complementary mRNA molecules. In the case of small shRNA expression vectors, a single or multiple shRNAs are usually transcribed from RNA polymerase III promoters after the DNA vector has reached the nucleus; alternatively, miRNA polycistrons can be transcribed from RNA polymerase II (Pol II) promoters. The miRNA primary transcripts (termed pri-miRNAs), vector-encoded shRNAs or polycistronic miRNA transcripts are processed by Drosha and DGCR8 and are exported as precursor intermediates (pre-miRNAs or shRNAs) from the nucleus by the export factor exportin 5 (Exp. 5). The final maturation to short duplexes is catalyzed by the RNase Dicer in the cytoplasm. siRNA and miRNA pathways differ after guide strand selection by RISC: whereas siRNAs are fully complementary to the target mRNA and induce its cleavage, miRNA strands guide the RISC primarily to the 3′-UTR of their target mRNAs where they form only partial base pairing interactions. The prevailing biological miRNA effects are inhibition of the 5′-cap-dependent initiation of protein biosynthesis and/or induction of mRNA transfer into cytoplasmic "processing (P) bodies", where the mRNAs are stored or degraded; m^7G: 7-methyl-guanosine-5′,5′-triphosphate cap at the 5′ end of mRNAs; A_n: poly(A) tail at the 3′-end of mRNAs.

gapmers are applied to knocking down mRNAs and long noncoding RNAs (lncRNAs) which have emerged, like miRNAs (see below), as an abundant class of regulators of gene expression.[496] Aberrant expression of lncRNAs is often causatively linked to pathological processes.[497,498]

The classical RNAi effectors are siRNAs, usually delivered in the siRNA duplex format (19 bp plus 2 nt overhangs at the 3′-ends; see Figure 27), although other formats have been reported, often combined with strategic chemical modifications.[492] siRNAs can be delivered indirectly by using viral vectors (*e.g.*, lentiviral vectors) that encode one or a few shRNAs (see Figure 27). Such approaches have been explored for anti-HIV therapy,[484,501] as they permit controlled expression of shRNAs and increase the duration of the RNAi effect.

The miRNAs, representing the endogenous RNAi effector branch, are interesting targets because their aberrant expression (down- or up-regulation) is also causatively linked to many pathological processes such as tumorigenesis. Here, two different therapeutic strategies have emerged: (i) delivery of so-called miRNA mimics (aiming at restoring the normal levels of a miRNA), and (ii) ASOs that sequester overexpressed mature single-stranded miRNAs, called anti-miRNAs as the overarching term. Classical anti-miRs are complementary to 15 or more nucleotides of the miRNA single strand and are modified with 2′-O-methyl groups and PS internucleotide bonds.[502] Recently, Miravirsen (Roche Innovation Center Copenhagen A/S), a 15-meric miR-122-specific anti-miR with a PS-modified backbone and a mixture of LNA and DNA residues,[503−505] successfully passed a phase 2 clinical trial after significantly reducing hepatitis C virus replication in liver cells.[503−505] As a peculiarity of miRNAs, the essential base-pairing interaction with target mRNAs is confined to the so-called seed region comprising the 5′-terminal 6−8 nt of the miRNA. In fact, there are families of miRNAs whose members share the same seed sequence and are likely to interact with the same target mRNAs. For the sake of a strong therapeutic effect, in many cases it appears reasonable to inactivate all miRNA members of the same family. This inactivation is achieved by a class of anti-miRs termed "tiny LNAs" which are uniformly PS- and LNA-modified 8-mers directed against the miRNA seed region. Tiny LNAs specific to miR-122 have been successfully delivered without any formulation to the livers of primates and nonprimates, where they down-regulated cholesterol levels.[506] In addition, 14-meric fully LNA-modified anti-miRs, termed antiseeds, carrying a natural PO backbone and covering the seed region plus the central part of the target miRNA, were shown to exert a remarkably persistent inhibition

DOI: 10.1021/acsnano.6b06040
ACS Nano 2017, 11, 2313−2381

effect against miRNA families. Such antiseeds can also be delivered as NPs with a branched low-molecular-weight polyethylenimine (PEI LMW-25), whereas tiny LNAs can not.[507] More efficient formulation of longer antiseeds relative to tiny LNAs may be of advantage for NP-based delivery into tissues not accessible by gymnotic delivery. A PO instead of PS backbone may reduce spurious interactions with extra- and intracellular proteins.

Another promising ASO strategy is based on U1 adaptors, which are dual antisense molecules that base-pair with the 3′-terminal region of U1 RNA as part of the highly abundant U1 snRNPs, and with an accessible sequence in the last exon of the target mRNA.[500] This recruitment of the U1 snRNP blocks polyadenylation of the mRNA (but not its cleavage), which consequently results in its degradation by exonucleases[499] (see Figure 26C).[508] It will be interesting to see if the U1 adaptor strategy is applicable to pathologically overexpressed lncRNAs that also undergo polyadenylation.

Here, we have described short nucleic acid effectors. Their potential advantages are (i) cost-effective synthesis, (ii) modulation and control of their properties by introduction of chemical modifications, and (iii) facile incorporation into many NP platforms. Of course, more complex RNA-based therapeutics have been conceived. As an example, Qiu *et al.* combined the bacteriophage phi29 DNA packaging motor pRNA 3WJ with folic acid targeting, a NIR marker for imaging and a BRCAA1 (breast cancer associated antigen 1, AF208045) siRNA for RNAi[43] (see Figure 20).

Inorganic NP-Mediated Cell Death. Most nanoparticle formulations for cancer treatment act as delivery vehicles of cytotoxic agents to induce a cytostatic effect on tumors. Another emerging application of nanomedicine is the direct use of NPs as highly efficient and low-toxic drugs without carrying drug molecules: the inorganic NPs themselves are used as the therapeutic agent. For example, $Gd@C_{82}(OH)_{22}$ with a dose level as low as 10^{-7} mol/kg exhibits an antineoplastic efficiency in tumor-bearing mice.[509] The $Gd@C_{82}(OH)_{22}$ NPs directly possess a strong capacity to improve immunity[510,511] and interfere with tumor metastases *in vivo*,[512−515] with tolerable toxicity *in vivo* and *in vitro*. The high antitumor efficiency of these NPs is not due to direct toxic effects induced on tumor cells, indicating that the anticancer mechanisms are different from classical cancer therapeutics. Results from recent studies suggest a new concept of "caging cancer" with $Gd@C_{82}(OH)_{22}$ NPs, *versus* "killing cancer" by classical therapeutics. The "caging cancer" concept[515,516] refers to rendering the tumor microenvironment inhospitable for tumor growth by forming an induced fibrous layer around the surface of a solid tumor, while using the $Gd@C_{82}(OH)_{22}$ NPs to regulate the diverse components of the tumor microenvironment. By employing this concept, the $Gd@C_{82}(OH)_{22}$ NPs were able to prevent tumor resistance to therapeutic drugs[513] while reducing ROS production in tumor-bearing mice. Furthermore, these NPs mitigated damage to the main organs by decreasing all metalloprotease enzyme activities, while restoring other parameters, such as oxidative stress, close to normal levels.[517,518] These NPs also induced dendritic cells to become functionally mature and increased their capacity to activate allogeneic T cells in tumor-bearing mice.[510,511,519] Tumor angiogenesis can also be inhibited by simultaneously down-regulating more than 20 angiogenic factors.[513] More interestingly, $Gd@C_{82}(OH)_{22}$ NPs were found to be capable of inhibiting triple-negative breast cancer cells by blocking the epithelial-to-mesenchymal transition, resulting in the efficient elimination of cancer stem cells (CSCs) *in vitro* and *in vivo*.[520] In comparison, the use of classical anticancer drugs like paclitaxel resulted in a relatively high enrichment of CSC and promoted

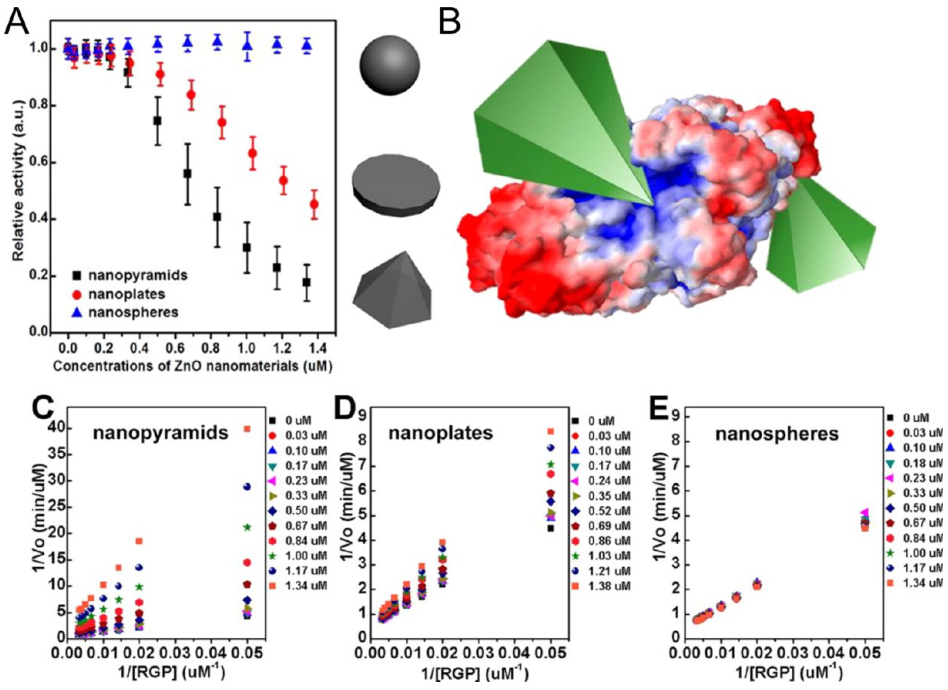

Figure 28. (A) Relative catalytic activity of galactosidase in the presence of three different shapes of ZnO NPs. The relative catalytic activity of galactosidase with each of the ZnO NPs was normalized with respect to free enzyme activity. (B) Pictorial representation of pyramid-shaped NPs interacting with the active site of galactosidase. (C−E) Lineweaver−Burk plots of galactosidase activity with various concentrations of ZnO (C) nanopyramids, (D) nanoplates, and (E) nanospheres. Adapted from ref 524. Copyright 2015 American Chemical Society.

DOI: 10.1021/acsnano.6b06040
ACS Nano 2017, 11, 2313−2381

tumor sphere formation and abrogation of tumor initiation and metastasis, probably due to its selective toxicity to regular tumor cells only but not to CSCs.[520] However, the nontoxic $Gd@C_{82}(OH)_{22}$ NPs selectively target CSCs but not regular tumor cells under hypoxic conditions. Such effects have not been observed in normal stem cells. The direct use of nontoxic nanomedicines with new acting mechanisms like "caging cancer" instead of killing cancer can be considered a potentially revolutionary shift in cancer therapeutics in clinical applications.[521] In the future, such strategies based on shutting down the tumor infrastructure will gain more importance due to their reduced side effects. Despite the broad medical utility of this NP system, the use of Gd-based nanomedicine has recently faced controversy related to potential toxicity issues.[522,523]

In another example, Cha *et al.* proposed ZnO NPs as a therapeutic agent since these NPs can be engineered to specific shapes that act like biomimetic enzyme inhibitors.[524] The ZnO NPs were able to inhibit the activity of beta-galactosidase reversibly in a shape-dependent manner (see Figure 28A). That inhibition was not the result of protein denaturation, but rather a subtler conformational frustration of the enzyme that more closely resembles the mechanism of naturally occurring enzyme inhibitors. Furthermore, Cha *et al.* demonstrated that the NP-based enzyme inhibition can be characterized using the classical Michaelis–Menten and Eadie-Hofstee formalisms (see Figure 28C–E). As many traditional pharmacological therapeutics are enzyme inhibitors, this work opens the door for the design of a new class of degradation-resistant inorganic NP enzyme inhibitors that can be particularly suitable for antibiotic resistant bacteria exemplified by methicillin-resistant *Staphylococcus aureus* (MRSA, see below).

Another approach used to design NP-based drugs to induce apoptosis in malignant cells is based on the cross-linking induction of the surface noninternalizing receptors. Receptor cross-linking involves the biorecognition of high-fidelity natural binding motifs with cell receptors or with side chains of water-soluble polymers. The general design concept of drug-free macromolecular therapeutics is shown in Figure 29. An important feature of these designs is the absence of low-molecular-weight cytotoxic compounds. The concept was validated for the treatment of non-Hodgkin lymphoma (NHL) using nanoconjugates that target CD20 (noninternalizing) receptors on B cells. The system is composed of two nanoconjugates: (a) an anti-CD20 Fab′ fragment covalently linked to a biological moiety (oligopeptide or oligonucleotide) and (b) a polyHPMA grafted with multiple copies of the complementary oligopeptide/oligonucleotide. Exposure of human NHL Raji B cells to anti-CD20 Fab′-Motif 1 decorates the cell surface with peptides/oligonucleotides. Further exposure of the decorated cells to graft copolymer $P\text{-(Motif 2)}_x$ results in heterodimerization or hybridization and triggers the cross-link between CD20 receptors and initiating apoptosis *in vitro* and in a NHL animal model *in vivo*.[525−527] Magnetic resonance imaging and flow cytometry analysis indicated that no residual cancer cells were detectable in long-term survivors (125 days).[527] Multimodality imaging studies investigating the interaction between cellular membranes and nanoconstructs confirmed that self-assembly plays a critical role in this highly specific therapeutic system.[528,529] This new paradigm demonstrated activity in the treatment of cells isolated from patients with chronic lymphocytic leukemia and mantle cell lymphoma.[530,531] This interdisciplinary strategy has potential to overcome rituximab-related resistance and become a new drug development pipeline for the treatment of NHL and other

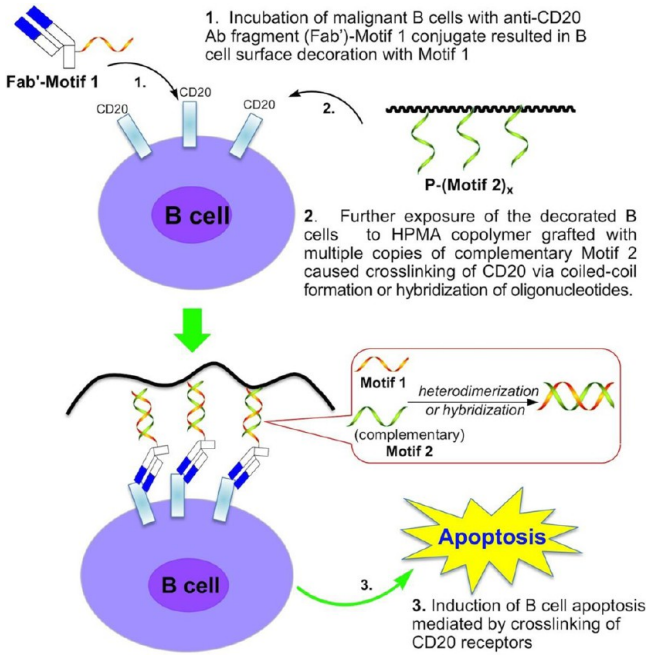

Figure 29. Schematic of overall design and possible mechanism of drug-free macromolecular therapeutics for treatment of NHL. Adapted from ref 527. Copyright 2014 American Chemical Society.

B-cell-derived hematological neoplastic diseases and autoimmune disorders.[532]

Killing Cells with Inorganic NPs upon External Stimuli. Inorganic NPs can respond to external stimuli to elicit tumor cell death. In the following section, we describe three common examples of external stimuli-driven NP therapies, including photodynamic therapy (PDT), photothermal therapy (PTT), and magnetic hyperthermia.[533−535]

In its simplest form, PDT relies on the interaction between a photosensitizer (PS), a light source, and oxygen. A PS is a nontoxic compound capable of absorbing light and producing ROS upon de-excitation, producing ROS. Photosensitizer excitation is usually achieved *via* one-photon transition between its ground state S_0 and a singlet excited state, S_1. At this point, the molecule may return to its ground state *via* emission of a photon (fluorescence), but the excited PS may also generate a triplet state T_1 by intersystem crossing. The lifetime of T_1 is longer (microseconds) than S_1 (nanoseconds), enabling the system to react in one of two ways, called the Type I and Type II mechanisms. The Type I mechanism involves electron transfer between the PS and a substrate, yielding free radicals that can then react with oxygen to form ROS, such as superoxide radical anions. In the Type II mechanism, singlet oxygen is generated *via* an energy transfer between the PS and triplet oxygen.[536]

Desirable characteristics of PSs are (i) high absorption coefficient in the spectral region of the excitation light, preferably in the NIR emission range if PSs are to be used in PDT of cancer states; (ii) a triplet state of appropriate energy (ET > 95 kJ mol^{-1}) to enable efficient energy transfer to ground state oxygen; (iii) high quantum yield (QY) for formation of the triplet state and long triplet state lifetimes ($\tau > 1$ μs); and (iv) high photostability. Organic dyes and aromatic hydrocarbons are one class of molecules that possess these properties. They include dyes such as rose bengal, eosin, and methylene blue that are effective PSs because they possess triplet states of appropriate energy. They have high singlet oxygen yields, with rose bengal

DOI: 10.1021/acsnano.6b06040
ACS Nano 2017, 11, 2313−2381

reaching a value of $\Phi = 0.71$,[537] and strong absorption bands in the green region of the spectrum. Aromatic hydrocarbons such as napthalenes, anthracenes, and biphenyls have also been investigated as PSs. Studies found that the efficiency of energy transfer to triplet oxygen is greatly affected by the substituents on the biphenyl ring and by the polarity of the solvent. Finally, quinones are good PSs, with QYs in the range of 0.11−0.76,[538] but sometimes they lack strong absorption bands at wavelengths shorter than 600 nm. Porphyrins, phthalocyanines, and related tetrapyrroles are another class of molecules that were identified as excellent PSs. Porphyrins and their analogues are ideal PS candidates because they occur naturally in biological systems and therefore generally lack cytotoxicity in the absence of light. These compounds have high QYs and properties that can be easily tuned by changing the substituents on the macrocycle, but they are susceptible to photobleaching. Also worth mentioning are naphthalocyanines, which bear a second benzene ring on the primary phthalocyanine ring. This addition is responsible for an attractive red-shift in absorption from 680 to 770 nm. Chlorins, derived from the porphyrin structure through saturation of one or two double bonds, also have absorbance spectra red-shifted into the therapeutic spectral window. The most studied member of this class is hematoporphyrin, which has high singlet oxygen production QY of 0.65 but unfortunately only a weak absorption band at 630 nm (ε = 3500 M^{-1} cm^{-1}). Some transition metal complexes have been identified as efficient photosensitizers, having singlet oxygen QY comparable to the well-studied organic compounds methylene blue and rose bengal. Ru(II) tris-bipyridine and $[Ru(bpy)_3]^{2+}$, in particular, are effective singlet oxygen producers with a QY of 0.73 in oxygen-saturated deuterated methanol and 0.22 in water.[539] Lastly, little attention has been paid to semiconductor NPs as PSs. However, singlet oxygen production and subsequent cytotoxicity from photoexcited semiconductors such as TiO_2 and ZnO have been reported.[540]

In addition to the aforementioned requirements, the application of PDT to the treatment of cancer or other pathological conditions places other requirements on potential PSs. First, the compound should have low dark toxicity (*i.e.*, it should not be toxic to the organism in the absence of light). Second, it should selectively accumulate into the affected tissue in order to minimize side effects and maximize cytotoxic efficiency. In fact, the half-life of singlet oxygen in biological systems is <0.04 μs, translating into a radius of action of <0.02 μm.[541] Finally, strong absorbance in the red-NIR portion of the spectrum would be advantageous for the PS, as these wavelengths are able to penetrate the deepest into biological tissue (see Figure 30). The ability to excite a PS in this region would increase ROS production efficiency, lowering the number of scattered photons, and achieve maximum attainable treatment depth.

Keeping in mind these requirements, PSs for PDT of cancer have been classified into three generations. (i) The first generation consists of hematoporphyrin derivative (HpD) and its analogues. Beginning in the 1970s, this compound was the first tested and authorized for clinical use. HpD (stage 1) is obtained from hematoporphyrin and is a mixture of ∼10 components. Descending directly from HpD and now one of the most widely used PSs, porfimer sodium (Photofrin, Sinclair) is HpD stage 2, which is HpD purified from its monomeric fraction *via* high performance liquid chromatography. Despite being the most studied, this group of PSs suffers from major drawbacks; their selectivity is poor and only 0.1−3.0% of injected PS is found in tumor tissue.[542] The cutaneous tissue can take up and retain these compounds for up to 10 weeks after intake, thus causing

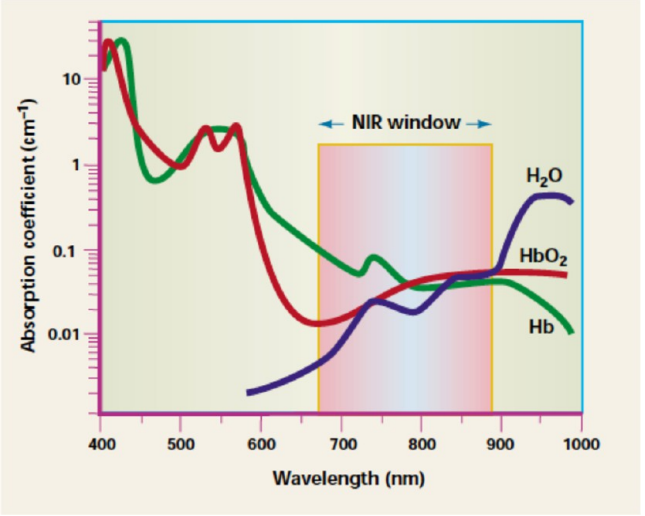

Figure 30. Relative absorbance of body tissue components such as water, hemoglobin (Hb), oxygenated hemoglobin (HbO_2), and melanin. The window that will allow the deepest penetration is the 600−1200 nm region, in the red-NIR. Adapted from ref 547. Copyright 2001 Nature Publishing Group.

photosensitivity in the patient. Furthermore, their absorbance in the NIR optical window is weak, limiting the efficiency of light uptake. (ii) The second generation has been designed with the aim of overcoming previous limitations and includes structurally distinct compounds with long-wavelength absorption and high singlet oxygen QYs. Part of this generation is hematoporphyrin derivatives with enhanced solubility properties for faster clearance from the organism and chlorins. Meso-tetrakis(m-hydroxyphenyl)chlorin (m-THPC/Temoporfin, commercialized as Foscan, Biolitech Pharma), for example, causes less photosensitization than Photofrin but is 100 times more photoactive. Other members of the group are purpurines, which have the disadvantage of being highly hydrophobic, and phthalocyanines. (iii) The third generation focuses on PSs with additional properties through the use of composite structures. Better selectivity toward the tumor tissue is often achieved by conjugation of PSs to monoclonal antibodies or other ligands that bind specifically to the surface of cancerous cells. Also, the use of delivery vehicles like proteins or NPs leads to improved overall hydrophilicity and higher PS loads. (iv) Emerging PDT systems target the development of mesoscale carriers, which can incorporate large numbers of sensitizer molecules. These mesoscale particles are surface modified to minimize removal by immunogenic response mechanisms and reduce nonspecific binding. Specific antibodies attached to these larger functional delivery particles offer advantages over simpler PSs, which have low absorption cross sections and which do not localize specifically to tumors.

There are three main mechanisms by which PDT mediates tumor destruction: direct killing, vascular damage, and activation of an immune response against tumor cells. In the first case, the ROS generated by PDT can kill tumor cells directly. However, complete eradication is not always realized because of the nonhomogeneous distribution of the PS within the tumor, nonhomogeneous penetration of light, and the possibility of limited oxygen availability within the tissue due to the photodynamic process itself. Vascular damage, on the other hand, targets the tumor vasculature system and, therefore, the concentration of nutrients and oxygen that reach it. In this case, the precise action

DOI: 10.1021/acsnano.6b06040
ACS Nano 2017, 11, 2313−2381

mechanism is not yet fully understood, but a biphasic vascular reaction following PDT has been suggested,[543] namely, a first immediate response consisting of vasoconstriction and, after 3 h, a second long-term response characterized by thrombus formation. Both of these effects were correlated with delay or inhibition of tumor growth. Depending on the kind of pathology to be treated, the interval between the sensitizer administration and light exposure might be a deciding factor for one mechanism over the other. When a short interval (minutes) is allowed between drug and light administration, the sensitizer predominantly accumulates in the vascular compartment, thus favoring indirect tumor killing by vascular damage. Conversely, a longer interval (hours) between intravenous drug injection and light administration results in localization of the PS within the extravascular compartment of the tumor and subsequent direct tumor-killing action. Therefore, administration of PSs at multiple time intervals before light activation (fractionated drug-dose PDT) is found to be the most effective way to target both tumor blood vessels and tumor cells. More recent studies in the late 1980s and early 1990s reported infiltration of lymphocytes, leukocytes, and macrophages into PDT-treated tissue, indicating activation of the immune response. Differences in the nature and intensity of the inflammatory reaction between normal and cancerous tissues could contribute to the selectivity of PDT-induced tissue damage.

Photodynamic therapy is a reliable tool for treatment of a variety of diseases, whose clinical use is common and well established. This process involves two major steps, the administration of a PS and the delivery of light. The administration of a PS can be topical or intravenous, depending on the pathology to be treated and the ease of access to the area: skin diseases that allow for topical application will require drugs with different characteristics than will diseases for which an intravenous approach is required. Along with vascular permeability and interstitial diffusion, chemical properties like molecular size, configuration, charge, and the hydrophilic or lipophilic character of the compound will all impact transport and retention of the PS.

Conventionally, PDT is administered as a single treatment using the highest PS dose that avoids systemic toxicity and skin photosensitivity, and the highest light fluence rate that avoids tissue heating and photochemical depletion of oxygen. However, for reasons discussed above, there have been a few studies about *fractionated* PDT, in which the PS administration is spread over time. Preliminary studies have shown improved responses to this kind of metronomic PDT compared to single doses, most likely due to the simultaneous action of direct tumor cell killing and blood vessel damage. Light can be delivered by surface or interstitial irradiation. Surface irradiation includes cases where the light source is external to the body (*e.g.*, treatment of skin lesions), or is placed within and illuminates the inner surface of a body cavity (*e.g.*, a hollow organ or a surgical resection space). Interstitial treatments are usually carried out by placing an optical fiber that carries the light directly into the tissue. Typically, 1−5 W of usable power are required in the 630−850 nm range at irradiances of up to several hundred $mW{\cdot}cm^{-2}$ in order to deliver treatments in tens of minutes. For this reason, there are three main classes of clinical PDT light sources: lasers, light-emitting diodes (LEDs), and filtered lamps (see Figure 31). Lasers are powerful and efficient but they are expensive single-wavelength devices where a separate unit is required for each photosensitizer. In the past few years, LEDs have become a viable technology for PDT, particularly for irradiation of easily accessible tissue surfaces. The main advantages over (diode) laser sources are the low cost and ease of configuring arrays of LEDs into different irradiation geometries. On the other hand, the relatively poor electrical-to-light conversion efficiency (less than 15%) remains an obstacle, because the generated heat must be removed. Finally, a number of lamp systems can be spectrally filtered to match any photosensitizer and they allow flexible geometries. Their drawback is that they are not suitable for endoscopic use because they can be efficiently coupled only into optical fiber bundles or liquid light guides (5−10 mm diameter).[544]

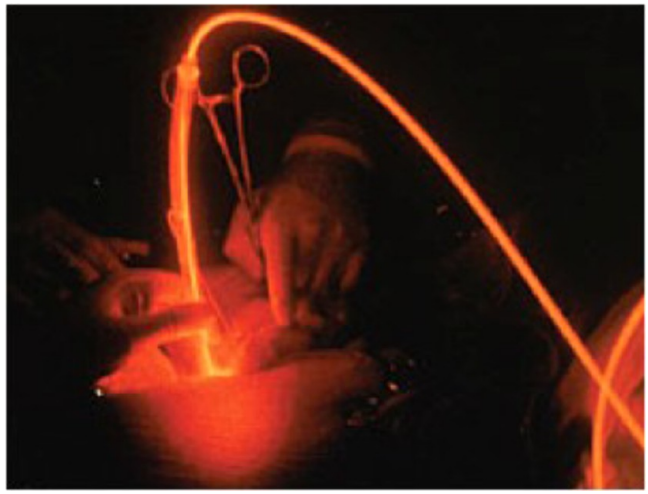

Figure 31. Surgeons delivering laser light through an optical fiber for the treatment of an internal tumor.

Photodynamic therapy design is still a relatively young field and substantial improvements could come from better PSs: higher absorption in the optical window, larger extinction coefficients, more efficient singlet oxygen production, and better chemical and physical properties. Interesting new directions that could overcome some of the intrinsic limitations of current compounds are currently being explored. (i) In two-photon PDT, the PS ground state is able to absorb two photons of NIR light simultaneously, which can be administered in short pulses: the total energy absorbed is the same as that from one-photon absorption at $\lambda_{NIR}/2$ and the resulting photophysical and photochemical processes are the same. This two-photon absorption enables a much wider choice of PS absorbing at high extinction coefficients in the visible, while retaining the possibility of using light in the biological optical window. Also, the quadratic dependence of the two-photon absorption probability can be exploited to give more precise spatial confinement of the PDT effect by high-numerical-aperture focusing of the activating laser beam. One of the drawbacks of this technique is that, in order for the photons to be absorbed simultaneously, the light pulse must typically be shorter than *ca.* 100 fs, a factor that substantially increases the cost of light sources. (ii) Another concept currently being investigated is the use of *molecular beacons* to improve target selectivity. Molecular beacons comprise a targeting moiety, a PS, and, optionally, a quencher. In their simplest form, the targeting group is responsible for accumulation of a higher number of PSs in the cancer cells and therefore higher selectivity. Alternatively, a target-labile linker keeps a PS and a quencher in close proximity, so that FRET prevents activation of the PS. Upon interacting with the target, the linker is either broken or opened so that the PS and quencher are separated, enabling FRET-driven PDT action to occur. (iii) Finally, NP technology provides several

DOI: 10.1021/acsnano.6b06040
ACS Nano 2017, 11, 2313−2381

different novel approaches to PDT. A first approach is the use of NPs as PS carriers, a method already applied to many other imaging contrast agents and therapeutic compounds. The advantages are that the loading of PS molecules per NP can be high and that the NPs can impart new desirable qualities to the compound, such as greater hydrophilicity or targeting ability. Examples include the incorporation of PS into modified silica NPs or into lipoprotein NPs with antibody targeting capabilities, the decoration of AuNPs with PS, or the use of NPs that are themselves photoactive. Another approach is the use of NP−PS conjugates, where the NP serves as the primary light absorber that, through FRET, activates the PS. An issue with all these NP strategies, besides potential toxicity, is the delivery of the NPs or NP−PS conjugates to the target tissues, because the pharmacokinetics are strongly dependent on the NP properties.

In contrast to PDT, which kills cells by the generation of ROS, hyperthermia kills cells by heat. Tumor treatment by heat is one of the oldest ways to cure cancer. The application of pyrogens induces endogenous hyperthermia, where heat is generated by a substance or agent that reacts with the human immune system. This was the standard treatment for inoperable tumors until the middle of the 20th century. After administration of various bacterial toxins (or later on, vaccines) and the subsequent feverish reaction, a significantly higher survival rate was observed. Because of the inability to control the induced fever and the insufficient outcome, it is now applied only rarely.[545] Modern hyperthermia can be performed using plasmonic NPs and light, as well as magnetic NPs and alternating magnetic fields. Inorganic NPs act as local heat sources, triggered by light or alternating magnetic fields. Hyperthermia can be used as a stand-alone approach, or in combination with certain chemotherapeutics.

One of the most promising therapeutic strategies in nanomedicine is that of photothermal cancer therapy.[546]

> One of the most promising therapeutic strategies in nanomedicine is that of photothermal cancer therapy.

In this drug-free therapy, these NPs absorb energy at a wavelength of 700−1000 nm[547] and generate heat. They can burn off the tumor when the irradiation occurs after the particles have accumulated in the tumor. Intensity of the incident laser irradiation, the nature of the NPs (*i.e.*, the localization of the surface plasmon resonance), and the size of NPs are the factors that will determine the efficiency of the localized heating. It was shown at an *in vitro* level that such localized heating can be applied to kill cancer cells.[459,548−552] *In vivo*, the highly localized hyperthermic response induced by resonant laser irradiation results in tumor remission for subcutaneous tumors with high efficacy (see Figure 32).[553] Researchers have demonstrated both passive and active uptake of nanoshells, a type of heat-generating NPs, into tumors.[554,555] In addition to nanoshells, other plasmonic NPs such as gold nanorods and gold nanocages have been shown to be useful for hyperthermia applications.[549,556] In preparation for transition to clinical trials, the toxicity of nanoshells was investigated extensively. No toxic effects were found in this study.[557] Recent improvements in nanoshell design can enhance their clinical utility. The addition and integration of imaging functionalities with the therapeutic function of these NPs resulted in NIR-enhanced fluorescence and NIR-enhanced imaging of tumors.[558−560] Smaller diameter, multilayer NPs known as "nanomatryoshkas", which also have NIR-absorptive

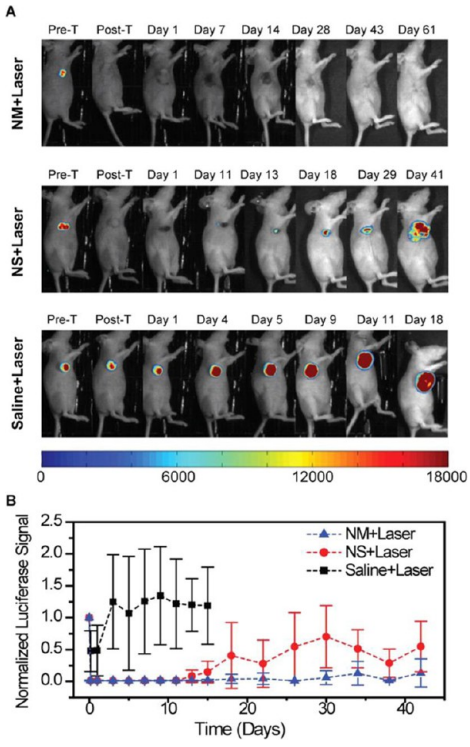

Figure 32. Evaluation of tumor response to PTT by bioluminescence imaging. The bioluminescence signal is generated only in living cancer cells, as a result of luciferase activity. (A) Representative mice of each experimental group showing the luciferase activity in the tumor. The mice injected with nanomatryoshkas or nanoshells and treated with laser experienced loss of bioluminescence in the area illuminated by the laser, as seen after therapy. Mice were euthanized when tumor volume reached 1500 mm^3 or if the tumor persisted at 60 days after treatment. (B) Luciferase activity in the tumor. The luciferase signal was normalized to the signal before treatment. Adapted from ref 563. Copyright 2014 American Chemical Society.

responses, can enhance NIR fluorescence for emitters encased between their inner and outer gold layers.[561] These NPs have shown increased uptake in tumors relative to nanoshells and outstanding remission rates with active targeting of aggressive triple negative breast cancer tumors.[562]

Local heat can also be produced by magnetic NPs upon exposure to alternating magnetic fields.[564−567] The basic precondition for effective magnetic heating is that the NPs have adequate magnetization values. Iron oxides (magnetite/maghemite) are particularly preferred since they have been used as contrast agents in radiology for many years, *e.g.*, in the detection of cancers in the liver and spleen. The generation of heat is based on NP morphology as well as on the energy dissipation during the NPs magnetization process.[568−570] This means that the magnetization reversal of NPs with core diameters larger than 100 nm is governed by the motion of magnetic domain walls. In contrast, cores that are smaller than 100 nm behave like single-domain NPs where no domain walls exist. Even smaller NPs behave as if they are superparamagnetic and the magnetization reversal proceeds either by rotation of the magnetic moment inside the core (Néel relaxation) or by mechanical rotation of the whole NP (Brown relaxation) during exposure to an alternating magnetic field. It has been demonstrated that sufficient thermal energies can be obtained with NPs with core sizes between 10 to 50 nm.[571−573] Concerning NP synthesis, the current challenge is the stabilization of NPs with a

DOI: 10.1021/acsnano.6b06040
ACS Nano 2017, 11, 2313−2381

relatively larger core size distribution.[574] Promising materials in this context are magnetosomes derived from magnetotactic bacteria, which were successfully deployed in a mouse breast cancer model.[575] To enhance treatment efficacy, coapplied chemotherapeutics or drug-carrying magnetic NPs are included. Cisplatin, in combination with magnetic heating, exhibits additive cytotoxic effects, particularly when it reaches its target site of action where it forms DNA adducts after its chloride ions have been displaced by hydroxyl groups.[576] A promising NP formulation with cisplatin payloads was developed by Unterweger *et al.*[406] Most magnetic hyperthermia developments for treating diseases are in the preclinical stage with a few used in the clinic.

Biodegradation. There is increasing awareness of the potential threats of using exogenous nanomaterials *in vivo*. In particular, the development of increasingly sophisticated nanocarriers further increases the risk of undesired side effects, discussed below. Therefore, it is highly desirable that drug delivery vehicles exert only minimal effects on the biological system after their cargo has been delivered, where the vehicles should ideally be eliminated after delivery to target tissues. Consequently, *in vivo* degradation with well-defined rates and with the formation of nontoxic and degradable byproducts that can be excreted becomes increasingly important.[577,578] Currently, there are a number of organic NPs that can be degraded, which will be discussed below.

Water-soluble polymeric drug carriers are one such class of compounds that can be designed to be biodegradable. For these carriers, molecular weight and molecular weight distribution are important factors in their design, impacting both their therapeutic efficacy and their biocompatibility. The higher the molecular weight of the polymer carrier, the higher the accumulation of polymer−drug conjugate in the tumor tissue with concomitant increase in therapeutic efficacy.[331,579] However, the renal clearance threshold limits the molecular weight of nondegradable polymeric carriers (such as HPMA-based) to below 50 kDa.[580] This issue lowers the retention time of the conjugate in circulation with simultaneous decrease in pharmaceutical efficiency. Consequently, higher molecular weight drug carriers with nondegradable backbones deposit and accumulate in various organs, impairing biocompatibility. These concerns can be addressed by the incorporation of degradable polymer backbones, such as those seen in backbone degradable (second generation) HPMA copolymer carriers. These carriers have long circulation times while preserving biocompatibility and are based on the combination of controlled/living radical polymerization and click chemistry.[355,581,582] The backbone degradable HPMA copolymer−drug conjugates provide long-circulating water-soluble therapeutics that effectively accumulate in tumor tissue. They are eliminated from the body after enzymatic cleavage of the oligopeptide segments in the backbone (producing polymer fragments below the renal threshold) and in side chains (releasing the drug). The synthesis procedures proposed are versatile; they provide a platform for the preparation of a large variety of polymer−drug conjugates with tailor-made properties, such as predetermined circulation time and composition.

Controlled degradation—nonspecific cargo release from slow hydrolysis in physiological fluids like the bloodstream—remains a challenge. Therefore, design of biodegradable polymers requires incorporation of fast and efficient polymer degradation at the target site while retaining high stability in circulation and at off-target sites. Polypeptides offer great potential in this aspect, since their stability can be adjusted based on their monomer sequence, their molecular weight, or by attaching stabilizing or degradable side chains along the backbone. The most commonly used hydrophilic polypeptides have protonated amino side chains, *e.g.*, poly(lysine), poly(arginine), poly(glutamate), and poly(aspartate), which ensure excellent water solubility and increase the interaction with the negatively charged cell membrane to facilitate cellular uptake. Amphiphilic block copolymers of two or three homopolypeptides have been prepared with hydrophobic segments such as poly(leucine) and hydrophilic segments such as poly(lysine) that form polymersomes and encapsulate hydrophobic drugs. However, highly positively charged polypeptides often reveal uncontrolled protein absorption, immediate immune responses, opsonization by macrophages, or rapid clearance from the bloodstream by renal or hepatobiliary excretion. To overcome these limitations while taking advantage of the aforementioned properties, innovative materials in biological systems that have a degradable but peptidic nature are highly desirable.

Polymers based on the body's own amino acid sarcosine (*N*-methylated glycine) have been obtained and are one of the first polymers synthesized by living ring-opening polymerization.[583] The polypeptoid polysarcosine offers high water solubility, nonimmunogenicity,[584−586] and protein resistance[587] due to its special characteristics, *e.g.*, weak hydrogen bond acceptor with the lack of hydrogen donor capabilities.[588] Polysarcosine is a nonionic and highly water-soluble polymer that is similar to PEG but potentially offers *in vivo* degradability as suggested from *in vitro* studies under physiologically relevant conditions.[589] The synthesis of block copolymers based on polysarcosine and polylysine, polycysteine, polyglutamic acid, or derivatives thereof, by ring-opening polymerization of the corresponding α-*N*-amino acid carboxyanhydrides in a controlled fashion, offers high end-group integrity, precise control over molecular weight, and low dispersities of around 1.1. The amphiphilic block copolypeptides are nontoxic up to concentrations of 3 mg/mL and stabilize hydrophilic/hydrophobic interfaces in drug formulations and mini emulsion techniques.[589] The deprotected polymers polysarcosine-*block*-polylysine enabled the formation of core/shell polyplexes for efficient *in vitro* transfections.[590] Degradable polypeptide copolymers have been achieved from natural protein precursors. Unlike synthetic polypeptides, which consist of repeating amino acid sequences, the polypeptide backbone of proteins provides a higher diversity of reactive functional groups, which enables further chemical modifications. Moreover, depending on the precursor protein chosen, these polypeptides offer distinctive and adjustable molecular weights, precisely defined sequences, low cytotoxicity, and full degradability. They have been applied for coating fluorescent NPs as well as for the delivery of cytotoxic drug molecules.

A challenge when using inorganic NPs is the ability of the animal to degrade and to eliminate them. Sub-5 nm NPs such as NDs can be eliminated from the body renally without biodegradation and without leaving toxic residues.[591] However, larger inorganic NPs are more difficult to clear from the body. Studies have shown that AuNPs reside in macrophages after uptake and do not appear to be degraded;[592] ZnS-CdSe QDs have also been shown to remain stable in mice and rats after several months.[593,594] There is evidence to suggest that some inorganic NPs (*e.g.*, CdSe QDs and hollow AuNPs) can break down by oxidation or other chemical processes. This process is slow but there is evidence to show they are excreted through the

DOI: 10.1021/acsnano.6b06040
ACS Nano 2017, 11, 2313−2381

kidneys.[35,595,596] The chemistry and design of the inorganic NPs can influence the degradation pattern. Although the core composition is difficult to degrade for most inorganic NPs, the organic surface coating has been shown to degrade *in vivo*. This effect was demonstrated by using multiplexed radiolabels that tag the inorganic core and surface coating with an organic molecule. This labeling strategy enabled the measurements of differential temporal biodistribution of all different parts of a NP after *in vivo* administration. It was discovered that inorganic NPs stabilized by an amphiphilic polymer shell *via* amide bonds lose parts of the organic shell upon enzymatic cleavage *in vivo*.[37] Taking the concept further, a number of researchers have started to use organic molecules to assemble inorganic NPs into complex systems for *in vivo* medical applications. For example, DNA can assemble inorganic NPs into a complex core−satellite system that can target tumors, but these NPs can subsequently enter liver macrophages.[36] The enzymes in these cells degrade the DNA linker and release the inorganic NPs back into the bloodstream to be eliminated through the kidneys. Linker molecules to build nanosystems are not limited to DNA but can also be polymers that can potentially be responsive to enzymatic degradation.[597,598] The clinical translation of inorganic NPs may depend on whether they are cleared from the body, as the long-term toxicity of metal-containing NPs remains unclear. This research area will continue to be active from the fundamental (*i.e.*, understanding the clearance mechanism of inorganic NPs) to the design (*i.e.*, using assembly techniques to build degradable nanosystems containing inorganic NP components) perspectives.

LABORATORY-BASED MATERIAL PRODUCTION FOR TREATMENT ("IMPLANTS MADE WITH NANOTECHNOLOGY")

While some nanomaterials are designed to deliver a drug or an action to diseased tissue and programmed to degrade afterwards, researchers are also synthesizing nanomaterials that can be introduced into the body with the intention "to stay". Surface modeling on the nanoscale can provide new functions and properties to implants, *etc.*[599] Incorporation of nanomaterials with key features for driving tissue engineering is a useful means to achieve unprecedented performance.[600,601] In particular, carbon nanostructures (*e.g.*, single- or multiwall CNTs (SWCNT/MWCNT), graphene, carbon nanohorns, NDs, fullerenes, *etc.*) can provide mechanical strength and useful electronic properties, thanks to their chemical structures.[602] They have been shown to be biocompatible with and to support the growth and proliferation of many classes of cells. Despite the issues associated with CNT use in medicine,[603] there is a growing body of work showcasing their utility in nanomedicine after appropriate chemical functionalization.[604] For example, CNT addition to hydrogels are biomaterials that can be designed to respond to diverse stimuli, *e.g.*, for drug release applications.[605] Some selected examples and applications are detailed below.

Nano- and Microengineered Implants. Nanodiamond−polymer composites can be used in tissue engineering and regenerative medicine, particularly showing potential for restoring damaged tissue. Excellent mechanical properties of NDs in combination with fluorescence, delivery of drugs and biologically active molecules, and biocompatibility are used for reinforcement of implantable polymers to create multifunctional tissue engineering scaffolds. Octadecylamine-modified NDs incorporated into poly L-lactic acid (PLLA) provided fluorescence for monitoring the implant biodegradation (see Figure 33). While biodegradable polymers such as PLLA are not mechanically robust, the incorporation of NDs brings the composite properties close to those of human cortical bone. It increased the composite's mechanical strength and strain to failure, and enabled the use of the composite as a bioresorbable bone-growth scaffold for manufacturing bone fixation devices.[31] In terms of toxicity, murine 7F2 osteoblast morphology and proliferation were unaffected when cultured with the ND-PLLA. These composites possess clinically relevant properties while being nontoxic and highly scalable to produce.[606]

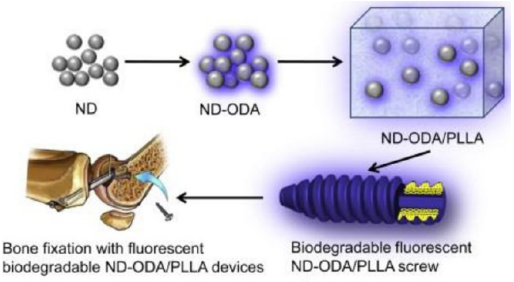

Figure 33. Bone fixation screw made of a biodegradable polymer (PLLA) reinforced with octadecylamine (ODA)-funtionalized fluorescent nanodiamond NPs (ND-ODA) that provide reinforcement, monitoring of biodegradation, and, eventually, drug delivery. Adapted with permission from ref 606. Copyright 2011 Elsevier.

Naturally, for such implants the interface between the implanted devices and surrounding cells and tissues is important. Selection of the geometry offers a useful handle in this direction. Elongated objects, such as nanoneedles, for example, have suitable properties for the delivery of bioactive agents to cells and tissues. This field of nanoneedles for cell-interfacing, which is still emerging, is now growing rapidly and shows great promise. A number of interesting nanoneedles have been developed recently with a multitude of capabilities. Some of these capabilities include transferring biological information to many cells in parallel,[607] sensing intracellular biological signaling such as the presence of enzymes,[608] and measuring intracellular pH at many points across individual cells.[609] The nanoneedles can deliver to the cell cytosol and yet, due to their nanoscale dimensions, are not destructive to the cells. These nanoneedles represent a highly promising technology for intracellular delivery, probing, and interfacing. Porous silicon-based nanoneedles were developed and utilized to deliver DNA and siRNA to cells *in vitro* efficiently and showed transfection efficiencies greater than 90% while silencing (of GAPDH expression) was quantified as 80% effective,[610] encouraging for *in vivo* applications. The authors showed that they could achieve neo-vascularization in the muscles on the backs of mice by using porous silicon nanoneedles to deliver human VEGF165 plasmid DNA.[610] This finding is of interest when considering the potential to prevascularize sites at which tissue engineered implants might be transplanted *in vivo*. It also has the added advantage that nucleic acids can simply be loaded into the nanoneedles and no covalent modifications are required. The nanoneedles are a platform technology that could potentially be used to deliver a wide range of nucleic acids and other bioactive agents for all types of tissues.

Toward Interfacing Electrically Active Tissues. Electrical signals can be used to control the interactions of nanomaterials with tissues. This strategy to control tissue function may be important for many applications such as in the design of neuroprostheses. Below, we describe a number of these applications.

DOI: 10.1021/acsnano.6b06040
ACS Nano 2017, 11, 2313−2381

First attempts for electrically interfacing cells were based on microstructured devices,[611−613] but more recently, nanostructured devices such as nanowires have been used.[614] Two criteria for building successful devices are "wiring" and size, where "wiring" involves the connection of the recording sites to the outside,[615] and size is essential for brain implants to avoid local inflammation.[616] Neuroprosthetic implants made from LbL biomimetic nanocomposites investigated by Kotov and coworkers provide a unique combination of properties that enable manufacturing of smallest possible brain implants that can be safely integrated within brain tissues.[617] Some of these properties include high strength, conductivity, toughness, and biocompatibility.[618,619] Additionally,[615−617] brain implants have been made with gold nanowires.[620]

A major step forward in this field has emerged by exploring the interactions of CNTs with neuronal systems. Indeed, the presence of CNTs influences the electrical activity of neurons, especially in terms of synaptic events. In the past decade, it has been established that CNT-based substrates are able to impact neuronal physiology profoundly from the functional (electrical) point of view. With their exceptional properties of small size, flexibility, strength, inertness, electrical conductivity, and ease of combination with various biological compounds, CNTs are the excellent candidates for interfacing with damaged neuronal tissues. In 2000, it was found that neurons deposited on functionalized CNTs were not only surviving, but also elongating their neurites in all directions.[621] Since then, the study of these materials as functional components of composites for the support of the regeneration of neural tissue has been set up by many research groups.

Carbon nanotubes have high electron mobility, have an affinity for neurons, and can integrate with cell membranes at both dendrites and somas. As a result of these tight interactions, not only neurons, but also entire 3D slices of spinal cord (SC) tissue exhibit desirable behavior.[622−625] The most important results obtained can be summarized in three points: (i) neuronal signaling is enhanced when brain circuits are cultured interfaced to CNT films, (ii) CNT networks are able to induce the formation of a higher number of new synaptic contacts with respect to reference substrates, and (iii) CNT interfaces promote nerve fibers regrowth, potentiating growth cone activity and synaptic responses in entire SC slices: this is an efficient translation from single cell to complex tissues such as SC explants.

It has been found that neonatal hippocampal neurons, laid over a film of CNTs, increase their spontaneous electrical activity. Thereafter high-resolution electron microscopy elucidated the intimate contacts between regrown neuronal processes and CNTs where the boundary line between organic and inorganic matter is ambiguous.[623,625] The most outstanding results concerning the interface between CNTs and neurons are related to the effects on the electrical activity of neuronal networks. Lovat *et al.* compared the electrical activity of hippocampal neuronal networks directly grown on a MWCNT mat with that of networks grown on control substrate by means of the patch-clamp technique.[622] The frequency of spontaneous events (postsynaptic currents) in networks cultured on CNTs was strongly increased (approximately 6-fold) compared with controls. The balance between inhibitory and excitatory components in the neuronal network was not affected.[622] By means of single-cell electrophysiology techniques, electron microscopy analysis and theoretical modeling, it was hypothesized that CNTs can provide a kind of shortcut between the proximal and distal compartments of the neuron.[624] This hypothesis, supported by the observation that neuronal membranes establish tight contacts with the CNT substrate, was further corroborated by other experiments. When cells were forced to fire trains of action potentials, reverberations were detected following depolarization potentials and this reverberation occurred more frequently on CNT-deposited cells than on those grown on inert glassy supports. This type of back-propagating action potential represents a regenerative ability that neurons exhibit in cellular processes, such as the tuning of synaptic activity, the expression of spike-timing-dependent plasticity, the release of modulatory messengers and the modulation of synaptic plasticity.

Another interesting observation concerns the impact of CNTs on the synaptic activity of neuronal networks. The probability of finding synaptically connected pairs of neurons is almost doubled in the presence of the CNT substrate. The synaptic plasticity was also affected because cells grown on CNTs demonstrate potentiated short-term synaptic conditions instead of normal depression in response to afferent presynaptic spike trains. This activity mimicked the high frequency flow of information. All this gain of function is entirely attributable to the peculiar features of conductivity and physiochemical properties of CNTs that affect the network activity and spike propagation.[624]

The ability of CNT substrates to have an effect on central nervous system tissue has been tested by coculturing embryonic spinal cord and dorsal root ganglia multilayered explants chronically interfaced to a film of purified MWCNTs.[625] With respect to the controls, spinal explants cultured on CNTs displayed higher numbers of longer neuronal processes growing in tight contact with substrates bearing higher numbers of growth cones at their tips. These neuronal processes seemed to be slack on the CNT carpet that increased their contact surface but were less stiff than in the control, apparently integrating CNTs as their own supports or exoskeletons. The overall interactions of the spinal tissue with the substrate appear to be intimate and similar to the results reported for isolated cell cultures. When sensory afferent pathways, preserved in spinal explants differentiated *in vitro* were exogenously activated, the resulting synaptic responses recorded from single neurons not in direct contact with the CNT layer were strongly increased. This result indicates that the boosting effects of CNTs at the interface were transferred from the layers of neurons directly exposed to the CNTs to those functionally connected yet physically far from the interface.

In order to improve the biocompatibility of unconstrained CNTs, groups have tried to incorporate CNTs into polymeric scaffolds. In addition to improved biocompatibility, they aim to produce 3D structures that are able to be colonized by neuronal cells and to foster the communication among them, where the CNTs play strengthening and electrically functional roles. To this end, CNTs have been integrated into various biopolymer-based hydrogels as collagen, chitosan,[626] and agarose.[627] In general, all these substrates are good supports for neuronal cells, able to sustain their growth and their ability to extend neurites and growth cones without a remarkable toxicity. None of these scaffolds have yet been tested *in vivo*, however. Similar results have been achieved by CNT composites based on synthetic polymers, mostly polyester polymers such as electrospun fibers of PLGA[628] and of poly(L-lactic acid-*co*-caprolactone).[629] Bosi *et al.* have recently produced a nanocomposite system where CNTs are integrated into a polymeric matrix that can be modeled into different porosities, stiffnesses, and shapes. This nanocomposite consists of a microporous, self−standing, elastomeric scaffold whose skeleton material is made of PDMS, while the

DOI: 10.1021/acsnano.6b06040
ACS Nano 2017, 11, 2313−2381

micrometric cavities are generated by dissolving a sugar template embedded in PDMS.[630] This 3D structure showed viability as a supporting scaffold allowing neuronal colonization and 3D synaptic network reconstruction, but was soft enough to match the viscoelastic nature of native hippocampal neural tissue.[631] The PDMS porous scaffold surfaces was then enriched of MWCNTs, endowing the structure with nanofeatures and implementing its electrical conductivity.

Because of their peculiar electrical features, CNTs are useful as interfaces with other electrically active tissues such as cardiac tissue. Martinelli *et al.*[632] discovered outstanding effects on cardiac cells cultured on CNT substrates. Neonatal rat ventricular myocytes (NRVM) were able to interact with nonfunctionalized MWNTs deposited on glass coverslips by forming tight contacts with the material (see Figure 34). Cardiac

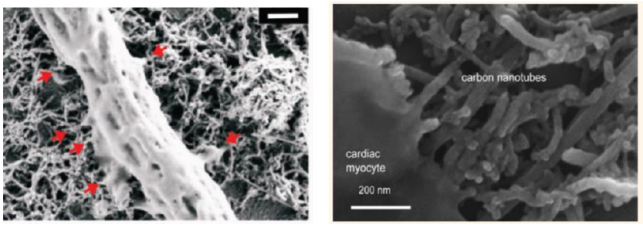

Figure 34. Left: Scanning electron microscopy (SEM) image of a spinal explant peripheral neuronal fiber on a MWCNT substrate. Note the tight and intimate contacts (red arrows) between the neurite membrane and the MWCNTs. Scale bar: 500 nm. Reprinted from ref 625. Copyright 2012 American Chemical Society. Right: SEM image of cardiac myocyte deposited on a layer of MWNT. Adapted from ref 636. Copyright 2013 American Chemical Society.

myocytes modify their viability, proliferation, growth, maturation, and electrophysiological properties when interacting with CNT scaffolds. Two opposing effects on the development appear to take place. Cells prolong the proliferative state, which maintains some cells in an undifferentiated state. They accelerate the maturation of the differentiated cardiac myocytes in terms of a more negative NRVM resting potential compared to the control so that the cells become more "adult-like". By transmission electron microscopy it has been observed that CNTs establish irregular tight contacts with the membranes, in a way that is morphologically similar to neurons cultured on MWNTs.[622] It is not excluded that other modifications indirectly brought about by MWNTs, such as the deposition of the extracellular matrix (ECM) or the cell contact driven cytoskeletal dynamics, are ultimately responsible for the positive effect.

Such an effect holds promise to solve the issue of arrhythmias arising from nonconductive scaffolds, as exemplified also by a chitosan-based hydrogel, where the inserted CNTs act as nanobridges that electrically connect cardiomyocytes.[633] Another interesting cardiac construct has been produced by Shin and colleagues:[634] CNTs were embedded into photo-cross-linkable gelatin methacrylate (Gel-MA) hydrogels, resulting in ultrathin 2D patches where neonatal rat cardiomyocytes were seeded. These cells showed strong spontaneous and stimulated synchronous beating. In addition, a protective effect against DOX (cardiotoxic) and heptanol (cardio-inhibitor) was observed. When released from glass substrates, the 2D cardiac patches (centimeter size) formed 3D soft actuators with controllable linear contractile, pumping, and swimming actuation behaviors. For heart tissue engineering, CNTs can also constitute a templating guide for the electrospinning of hybrid hydrogel nanofibers that form a superb biomimicking scaffold that is capable of matching the orientation index of the left ventricular tissue, thus promoting cardiomyocyte alignment and synchronous beating.[635,636]

The high potential of CNTs in the field of excitable tissue engineering stems from their exceptional nature and the desire to develop synthetic materials with appropriate nanostructure and cell-recognition properties that are able to regulate cell adhesion, survival, and growth. The *in vivo* application of nanotechnology tools and of CNT-based platforms, in particular, is largely directed to basic research applications. However, the extraordinary effects of these materials hint at developing safer devices to promote tissue reconstruction. A major challenge for biomedical applications of CNTs is to overcome the current limitations of CNT degradation time, elimination, and/or safety of use.

Biological Cell-Based Implants. Implants used for regenerative medicine can also be of biological origin. Cell-based therapies offer great potential. For example, stem cells delivered to injured tissue have the potential to regenerate defective tissue.[637,638] One general problem with cell-based therapies, however, is that individually delivered cells have limited retention times in the target tissue. In order to improve retention times, cells can, for example, be delivered in already connected form (so-called cell patches), or they can be seeded into matrices to which they have high binding affinity. Treatment based on connected cell patches instead of isolated cells thus may offer decisive advantages. However, it is not trivial to cultivate cell patches, as at one point connected cells need to be isolated from the culture substrate. Cell adhesion typically can be suspended by enzymatic treatment (*e.g.*, with trypsin) or by depletion in calcium. However, while this enables the collection of cells from culture substrates it also interferes with intracellular contacts. Nanotechnology has helped create culture substrates that enable switching on and off adhesive properties to cells. For example, smart surfaces enable switching from hydrophobic to hydrophilic properties upon changes in temperature. In this way, whole cell patches can be detached from the culture substrate and can be used for transplants.[639] Also, plasmonic heating may be a useful technique in this direction.[640] Such advanced culture methods pave the way for future cell and tissue-engineering therapies. Cell sheet patch therapies were clinically applied to human patients suffering from diseases such as cornea epithelium deficient disease, recovery from endoscopic submucosal dissension surgery for esophageal epithelial cancer, cardiomyopathy,[641,642] periodontal regeneration,[643] and osteoarthritis.[644] While the number of cell layers grown on top of each other within one cell patch is limited as transport of nutrients and oxygen to the cells needs to be warranted,[645] subsequent transplantation of several cell patches of up to ~100 μm thickness is possible and vascularization of the transplants has been demonstrated.[646,647] Cells can also be seeded into matrices resembling replicas of cell surfaces,[648] into decellularized matrices,[649] or even into completely synthetic scaffolds to improve their biocompatibility and engraftment.[650,651] There have been some attempts for translation to the clinic,[652,653] but results have been and are still heavily scrutinized.[654−656] The basic requirements such transplants need to fullfill involve vascularization, in order to warrant continuous blood supply,[657] and, in case of exposure to the environment (*e.g.*, air, food), antimicrobial coatings. Severe skepticism toward the use of these technologies in general is reported.[658]

DOI: 10.1021/acsnano.6b06040
ACS Nano 2017, 11, 2313−2381

Toward Artificial Organs. A current need in medicine is with the construction of whole organs *in vitro* to address the issue of shortages in organ donation.[659] Nanotechnology is emerging as a powerful tool that can help to fulfill this need by assisting in the engineering of artificial organs for regenerative medicine as well as organs-on-a-chip applications.[660,661] The need for nanoscale architecture is derived from the ability of cells to sense the nanoscale structures in their microenvironment.[662] In particular, many ECM molecules that surround cells form nanofibrous structures that help to organize cellular architecture and to induce directional migration and alignment.[663] As outlined in the case of implants, one approach to engineer such nanoscale structures is through the generation of 3D-fibrous scaffolds.[663−665] Techniques like electrospinning and microfluidic-based fiber fabrication have emerged as methods to engineer 3D scaffolds for inducing cellular organization and alignment.[666−669] Furthermore, self-assembling peptides have been used to form nanofibrous structures, which mimic the complex nanoscale architecture of native ECM molecules.

A current need in medicine is the construction of whole organs *in vitro* to address the issue of shortages in organ donation.

Utilization of biomimetic composite coatings made using LbL assembly on inverted colloidal crystal scaffolds on ceramics,[670] gels,[671,672] PLGA polymer[673] enabled, for instance, the creation of *ex vivo* models of bone marrow,[674] thymus,[675] and liver.[676] One of the advantages of the *ex vivo* organs is that they enable multifaceted evaluation of the toxicity of NPs in human tissues in the cellular constructs replicating real organs.[677]

In addition, nanomaterials can be integrated into hydrogels to direct cellular behavior. For example, the integration of nanoscale silicate materials can induce the directed differentiation of mesenchymal stem cells (MSCs) into osteogenic fates.[678] Polymeric nano- and microparticles that release growth factors and cytokines in a controlled manner can be integrated into scaffolds to regulate the surrounding biology. For example, controlled release of angiogenic factors, such as VEGF and PDGF, through polymeric NPs can induce the formation of blood vessels. Other types of nanomaterials such as CNTs and graphene NPs can be incorporated into hydrogels to change their mechanical and electrical properties, as described above. The resulting gels have been shown to enhance the formation of cardiac and skeletal muscle tissues.[634,679,680]

Nanoscale tools also provide means to form tissues with controlled microarchitectures. For example, cell-laden hydrogels can be induced to assemble into particular structures that better mimic the microarchitecture of tissues in the body through the use of nanoscale "programmable glues".[681] In this approach, the various sides of microgels of controlled shapes were coated with adhesive, long, single-stranded DNA where the function of the strands is to induce programmed assembly. It was demonstrated that the resulting DNA strands form nanoscale objects on the surface of gels that uniquely recognized their complementary base-paired strands on other gels to induce assembly. Such structures could 1 day provide scalable ways of engineering tissue structures with predefined architectures.

These and many other examples have shown the power of nanotechnology to direct cellular behavior for inducing tissue formation. It is anticipated that with our increased knowledge of how nanoscale objects interact with cells along with our ability to engineer more controllable nanomaterials will lead to a new era of nanomedicine for regenerative medicine applications.

Antibacterial Coatings. Biofilm formation and dissemination of antibiotic-resistant bacteria by indirect transmission through contaminated surfaces is becoming a major global public health threat. Steel and aluminum surfaces, commonly present in hospital settings as knobs, buttons, frames, taps, *etc.* possess limited or very low antimicrobial activity. A promising approach for limiting indirect transmission is the realization of stable and effective antimicrobial surfaces obtained by nanostructured coatings. Similarly, infections associated with medical devices (catheters, implants, *etc.*) have become a major concern. The adhesion of bacteria to the devices' surfaces during the initial 24 h is believed to be a decisive period for implant-associated infections and the design of optimal antiadhesion of microbes in this period is key. Multilayer coating by LbL self-assembly provides a robust method to design multifunctional dynamic antibacterial surfaces. For example, a multilayer of $(\text{heparin/chitosan})_{10}-(\text{polyvinylpyrrolidone/poly(acrylic acid)})_{10}$ $[(\text{HEP/CHI})_{10}-(\text{PVP/PAA})_{10}]$ provides the properties of contact killing of bacteria due to the underlying $(\text{HEP/CHI})_{10}$ while the top $(\text{PVP/PAA})_{10}$ multilayer film shows a top-down degradable capability in the determined period. This activity leads to almost no adhesion of bacteria within 24 h. The combination of the adhesion resistance and the contact-killing properties shows enhanced antibacterial capability through targeting the "decisive period" of implantation and may have potential for applications in medical implants, tissue engineering, *etc.*[682]

Surfaces with immobilized antimicrobial peptides present high and broad antimicrobial activity.[683] Similarly, a topic worth exploring involves immobilizing antimicrobial ligands onto NPs to enhance their antimicrobial activity. A quaternary ammonium cationic surfactant, didodecyldimethylammonium bromide (DDAB), was immobilized onto silica NPs to develop antimicrobial NPs. These NPs revealed much lower minimal inhibitory concentrations against bacteria and fungi than the soluble surfactant. The electrostatic interaction of the DDAB with the NP is strong since no measurable loss of antimicrobial activity was observed after suspension in aqueous solution for 60 days. This result means that the antimicrobial activity of the NP does not require the leaching of the surfactant from the surface of the NPs. More interestingly, the NP properties expanded to virucidal activity. The versatility, relative facility in preparation, low cost, and large antimicrobial activity of those NPs makes them attractive as coatings for biomedical devices.[684]

Suspensions of ZnO NPs are effective against a broad spectrum of microbial organisms[685−687] but there are many misconceptions about their mechanism(s) of killing bacteria.[524] Generation of ROS was often considered to be the source of antibacterial activity.[688] However, according to analysis of the mechanism of bacterial inhibition by ZnO NPs of different shapes,[524] at least part of the antibacterial activity originates from enzyme inhibition. Anisotropic ZnO and potentially other NPs can mimic biological inhibitors by partially matching their geometries with those of the protein inhibitors. Such activity originates from the similarity of the surface chemistry and size of water-soluble NPs and those of many globular proteins.[6] Applerot *et al.* used ultrasound irradiation to generate ZnO NP-coated surfaces that resist bacterial biofilm formation.[689] Layer-by-layer coatings of ZnO NPs reduce biofilm growth of MRSA by 95%. Silver in bulk and nanomaterial forms has been

DOI: 10.1021/acsnano.6b06040
ACS Nano 2017, 11, 2313−2381

used extensively as medical device coatings but these devices have not lived up to the promise of their *in vitro* data.[690] Silver's antimicrobial function is based on the concentration of silver ions and their associated toxicity.[691,692] Unfortunately, the therapeutic window between efficacy and toxicity for silver is quite narrow, which has led to disappointing clinical effectiveness of silver-coated medical devices.[690] ZnO is significantly less expensive than silver and has selective toxicity for bacteria over mammalian cells.[693,694] ZnO is generally recognized as safe by the FDA.

Nanoparticles can be designed with antibacterial coatings to circulate in the blood to target bacterial infections post-tumor surgery. During chemotherapy, some patients may be more susceptible to bacterial infections.[695,696] This susceptibility cannot be addressed using antibiotics alone, however, as some antibiotics may lead to serious side effects for some patients postsurgery. Abuse of antibiotics has caused the emergence of more resistant and virulent strains of pathogens. As a result, in some cases, clinicians need to prescribe multiple antibiotics in addition to anticancer drugs before and after the surgery. Particles can be engineered with antibacterial properties to target bacteria *in vivo* specifically, which can potentially minimize resistance. For example, a polymer vesicle antibacterial drug carrier has been developed recently. The chitosan-based carrier is grafted with an antibacterial polypeptide and demonstrated to kill both Gram-positive and Gram-negative bacteria (see Figure 35). This polymer vesicle has excellent blood

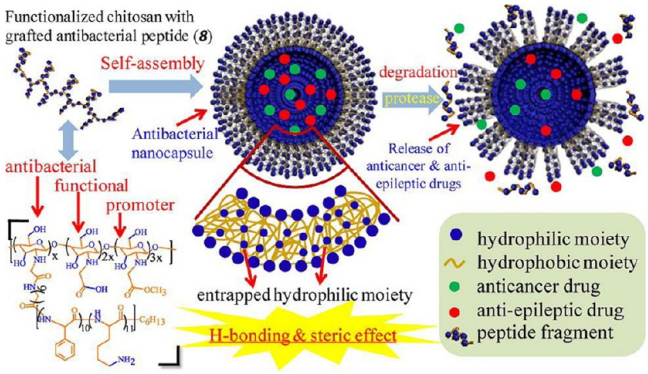

Figure 35. Antibacterial polypeptide-grafted chitosan-based vesicles capable of delivering anticancer and antiepileptic drugs simultaneously. Reprinted from ref 697. Copyright 2013 American Chemical Society.

compatibility and low cytotoxicity, which may benefit patients after tumor surgery.[697,698] The enhanced antibacterial efficacy of polymer vesicles compared with an individual antibacterial polymer chain results from the high concentrations of local positive charges in the polymer vesicles.

IN VIVO COMBINATION OF DIAGNOSIS AND TREATMENT ("THERANOSTICS")

Theranostics involves the combination of both diagnosis and treatment. Image-guided tumor resection is one such application that uses theranostics. The diagnostic use of NPs to label cancer cells, in particular tumor borders and small metastatic regions, can be used to guide the surgeon for subsequent therapeutic surgical removal of the tumors.[699] These diagnostic NPs could also be loaded with therapeutic agents for treating postsurgery. Another interesting application of theranostic agents is NPs that can deliver therapeutic agents into tumors while tracking NP drug delivery.[700] These agents enable noninvasive imaging to provide information on the fate of the drug once they are administered *in vivo*. Theranostics research is an exciting area of research as many different combinations of diagnostic and therapeutic strategies can be built into NP systems.

Image-Guided Surgery. Recently, first-in-human pilot studies have successfully used both passive and active targeting agents for image-guided surgery of human tumors.[701] The specific tumor types studied include breast, lung, ovarian, and pancreatic cancers. Although still preliminary, the results have helped clarify two important issues: (i) most human tumors (but not all) have moderately leaky vasculatures, so the EPR effect provides a general means for passive delivery of imaging agents (5−6 nm albumin-bound indocyanine green) to a broad range of human tumors; (ii) fluorescent dyes such as fluorescein can be conjugated to targeting ligands such as folic acid for specific targeting and high-contrast imaging of human tumors.

In the first approach, passive fluorescent agents do not involve targeting ligands, but rely simply on the biodistribution of the free fluorophore. Singhal and co-workers conducted a small trial on nontargeted NIR dyes, enrolling 5 patients undergoing surgery for removal of their cancers (3 lung nodules, 1 chest wall mass, and 1 anterior mediastinal mass).[701,702] Two surgeons reached a consensus about the clinical stage and operative approach prior to surgery. All enrolled patients were thought to have limited disease, be amenable to surgery, and have no metastases (*i.e.*, potentially curable). Patients were injected with indocyanine green (ICG) prior to surgery.[703] At the time of surgery, the body cavity was opened and inspected. The results demonstrated that NIR imaging can identify tumors from normal tissues, provides excellent tissue contrast, and facilitates the resection of tumors.[701] In situations where there is significant peritumoral inflammation, NIR imaging with ICG is not helpful. This suggests that nontargeted NIR dyes that accumulate in hyperpermeable tissues will have significant limitations in the future, and receptor-specific NIR dyes may be necessary to overcome this problem.

In contrast to passive agents, active fluorescent agents are linked to targeting ligands that are designed to recognize specific receptors at the target tissue. Near-infrared-dye-labeled antibodies (M_W ~ 150 kDa) that are currently used in the clinic for targeted cancer therapy, such as VEGF antibody (bevacizumab), EGFR antibody (cetuximab), and HER2 antibody (trastuzumab), have been evaluated as targeted optical imaging probes in preclinical animal tumor models.[704−706] Several antibody-based imaging probes are approved for clinical trials for image-guided surgery.[707] Potential limitations for antibody-based optical imaging probes include increased background fluorescence resulting from relatively long blood circulation times, as well as low efficiency in penetrating through tumor tissues.[704] To address these issues, smaller antibody fragments, such as affibodies (M_W ~ 7−8 kDa) against HER2 or EGFR, were labeled with NIR dyes for targeted optical imaging. Specificity and sensitivity of those affibody optical imaging probes have been demonstrated in various animal tumor models,[704,708−710] with several groups in the process of conducting clinical trials. For intraoperative imaging of tumor margins, a class of protease activatable optical imaging probes can detect tumor edges since many proteases are highly expressed in the invasive tumor areas that are close to the tumor edge.[711] The first-in-human results have been reported from intraoperative tumor-specific fluorescence imaging by using fluorescein-conjugated agents to target the folate receptors in both ovarian cancer and lung

DOI: 10.1021/acsnano.6b06040
ACS Nano 2017, 11, 2313−2381

cancer.[712,713] In patients with lung cancer, the results show that targeted molecular imaging could identify 46 (92%) of the 50 lung adenocarcinomas, and had no false positive uptake in the chest. *In vivo*, prior to exposing the tumor, molecular imaging could only locate 7 of the lesions. After dissecting the lung parenchyma, 39 more nodules could be detected. Four nodules were not fluorescent, and immunohistochemistry showed these nodules did not express FRα (folate receptor alpha). In 46 positive nodules, tumor fluorescence was independent of size, metabolic activity, histology, and tumor differentiation. Tumors closer to the pleural surface were more fluorescent than tumors deep in the parenchyma. In two cases, this strategy was able to discover tumor nodules that were not located preoperatively or intraoperatively by standard techniques. These pilot clinical trials have demonstrated that targeted intraoperative imaging may lead to more complete surgical resections and potentially better staging.

Fluorescent NPs can be used for similar image-guided applications as organic fluorophores. Targeted NP-based optical imaging probes have been developed by conjugating peptides, natural ligands, antibodies, antibody fragments, and small molecules, to NPs that have optical imaging properties or are labeled with fluorescence dyes. Results of preclinical studies were promising, showing increased specificity and sensitivity in tumor imaging by systemic delivery of targeted NP optical imaging probes as opposed to nontargeted probes.[714,715] It has been shown that optical imaging probes can be targeted to highly expressed tumor cell receptors and active tumor stromal fibroblasts and macrophages, such as urokinase plasminogen activator receptor (uPAR). They are good imaging probes for sensitive detection of tumor margins.[716] In many solid tumors, active tumor stromal cells with a high level of uPAR expression are found in the peripheral tumor areas. Even at the early stage of tumor development, for example in ductal carcinoma *in situ* of the breast, small tumor lesions were surrounded by uPAR expressing macrophages and fibroblasts. Therefore, optical imaging probes targeting active tumor stromal cells offer the opportunity of intraoperative detection of small tumor lesions (<1 mm) that lack tumor vessels that may enable EPR effect to occur or that cannot be delivered to tumor cells.[717] However, clinical translation of targeted NP imaging probes has been a challenging task. The preclinical studies required for filing an Investigational New Drug Application to the FDA for a clinical trial are much more extensive compared to those required for developing small-molecule, peptide, or antibody-based imaging probes. Additionally, the cost of production of targeting ligand-conjugated imaging NPs in good manufacturing practice (GMP)-grade for human use is higher than those of peptide and antibody-based imaging probes.

Tracing of Drug Delivery. Nanoparticles can be engineered to observe the delivery process directly. Theranostic nanocarriers offer high capacity drug loading as well as the ability to track and image the *in vivo* pathway of both the transporter and the drug in the body. Human tumors are highly heterogeneous in their tumor vascular structures, microenvironment, and tumor cells. Efficiency of intratumoral drug delivery and distribution varies among different tumors. Drug delivery using theranostic NPs enables noninvasive *in vivo* imaging of the NP delivery process and may enable assessment of treatment responses at an early stage. As a tool to visualize cellular uptake and cargo release, fluorescent NPs/polymers have been widely used. Quantum dots, AuNPs, iron oxide NPs, and NDs have emerged as valuable tools for combined therapy and diagnostic imaging due to their high stability *in vivo*. DNA, as well as drug transport and release of polycationic QDs and NDs into cells has been visualized by confocal imaging, which, in principle, offers monitoring of the entire gene delivery pathway inside cells.[363,718]

Drug delivery using theranostic NPs enables noninvasive *in vivo* imaging of the NP delivery process and may enable assessment of treatment responses at an early stage.

Polymer NPs with intrinsic imaging properties that do not require conjugation of imaging groups have recently been developed. For instance, the weakly fluorescent polyethylenimine (PEI) polymer was conjugated to hydrophobic polylactide (PLA), yielding amphiphilic PEI with a high payload capacity for the antitumor drug paclitaxel. After conjugation with PLA, the formed NPs exhibited bright and multicolor fluorescence, which could be tuned to the NIR region. Although fluorescence enables spatially resolved imaging at the cellular and tissue levels, it is not applicable for *in vivo* imaging deep inside the body. The high background autofluorescence from the organism, the poor penetration of the fluorescent signal in and out of the animal, and the risk of tissue damage by high intensity excitation light limit the application of fluorescence-based imaging *in vivo*. Magnetic resonance imaging, PET, and CT imaging are considered more attractive and promising for clinical applications. Nanoparticles can be designed to contain MRI contrast agents (*e.g.*, Gd-DOTA) or magnetic iron oxide NPs and to carry drugs using polymers to construct a theranostic agent.

Vasiljeva and co-workers developed an effective delivery system for targeting both tumors and their stromal components based on ferrimagnetic nanoclusters.[719] This multiplexed targeting strategy is important for imaging and treating tumors as the tumor microenvironment has many diverse components including extracellular matrix components and stroma cells. The universal lipidated magnetic NPs (called ferri-liposomes by the authors) enhance the MRI contrast properties and are effectively taken up by tumors and their stromal components. Chemical compounds within the ferri-liposomes are successfully released when administered *in vivo* and can be visualized at both the cellular and tissue levels. Furthermore, this theranostic agent offers an exciting possibility to deliver and to detect therapeutic agents simultaneously *in vivo*. As such, the cathepsin inhibitor JPM-565 was targeted by ferri-liposomes to the peri-tumoral region of mouse breast cancer, which resulted in a significant reduction in tumor size.

Another class of theranostic NPs uses light for activation. One example incorporates a second-generation PDT drug, Pc 4, with a cancer-targeting ligand and iron oxide NPs as a MRI-guided PDT platform (see Figure 36).[720] The delivery of Pc 4 by NPs enhanced the treatment efficacy and reduced the required PDT drug dose. The targeted IO-Pc 4 NPs have potential to serve as both an MRI agent and PDT drug.

Other NP materials may also be used for simultaneous imaging and therapy. One example involves chlorin e6-conjugated C-dots as the light-triggered theranostics NP platform. This platform uses simultaneous enhanced photosensitizer fluorescence detection (PFD) and PDT by FRET.[721] Huang *et al.* reported folic acid-conjugated silica-modified gold nanorods, showing highly selective targeting, enhanced radiation therapy, and PTT effects on MGC803 gastric cancer cells, and also strong X-ray

DOI: 10.1021/acsnano.6b06040
ACS Nano 2017, 11, 2313−2381

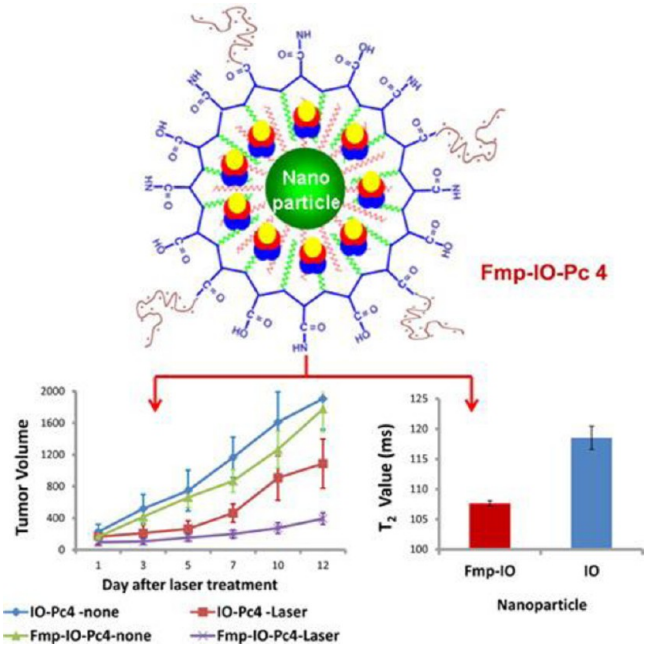

Figure 36. Construction of targeted NPs carrying the PDT drug Pc 4. Quantitative measures of T_2 values show that the cells with Fmp-iron oxide (IO) NPs had lower T_2 values as compared to those with only SPIONs. Reprinted from ref 720. Copyright 2014 American Chemical Society.

attenuation for *in vivo* X-ray and CT imaging.[722] In a similar strategy, multifunctional PEGylated gold nanostar NPs were prepared with CD44v6 monoclonal antibodies conjugated as the targeting ligands.[723] The prepared NPs had high affinity toward gastric cancer stem cell spheroid colonies. Upon NIR laser treatment with a low power density (790 nm, 1.5 W/cm^2, 5 min), those spheroid colonies could be completely destroyed *in vitro*, while being simultaneously observed with X-ray/CT imaging and photoacoustic imaging. Orthotopic and subcutaneous xenografted nude mice models of human gastric cancer were established. Computed tomography imaging observed *in situ* gastric cancer clearly at 4 h postinjection, and photoacoustic imaging revealed that CD44v6-modified NPs could actively target the gastric cancer vascular system at 4 h postinjection, while the NPs inhibited tumor growth upon NIR laser irradiation, and even extended survivability of the gastric cancer-bearing mice. These NPs exhibited good potential for applications of gastric cancer targeted imaging and PTT treatment.

Hybrid materials are increasingly attracting attention since they enable the combination of different properties and functions in one multipurpose material with high adaptability. Phosphate-based inorganic−organic hybrid NPs (IOH-NPs) are attractive tools as imaging and therapeutic drugs.[724] The NPs are generally composed of $[ZrO]^{2+}[R_{function}(O)PO_3]^{2-}$ ($R_{function}$ = functional organic group such as drug and/or fluorescent dye) and enable multipurpose and multifunctional combination of a wide range of properties such as drug delivery (*e.g.*, chemotherapeutic agents or anti-inflammatory drugs) as well as optical and CT-based detection or MRI. For example, the anti-inflammatory potential of $[ZrO]^{2+}[BMP]^{2-}{}_{0.996}[DUT]^{2-}{}_{0.004}$ was tested *in vitro* on an alveolar macrophage cell line, where MHS cells were treated with the endotoxin lipopolysaccharide (LPS, 200 ng/mL) to provoke an inflammatory response. Cells were simultaneously incubated either with IOH-NPs (10^{-10} to 10^{-5} M) or the control drug dexamethasone (DM, 10^{-7} M). Incubation of LPS-stimulated macrophages with increasing amounts of $[ZrO]^{2+}[BMP]^{2-}{}_{0.996}[DUT]^{2-}{}_{0.004}$ resulted in a dose-dependent reduction in TNFα, IL-6, and NO secretion, with an efficacy of 10^{-5} M IOH-NPs comparable to 10^{-7} M of dissolved molecular DM. Fluorescence microscopy confirmed these results.

Another efficient way to implement theranostic delivery carriers is to design multicompartment nanomedicine vehicles.[725] This approach is based on multicompartment capsules, which can be designed in the form of concentric, pericentric, innercentric, and anisotropic or acentric structures.[726] The multicompartments are composed of smaller nanocapsules or NPs, which are often assembled around a bigger nano- or microcapsule or particle. In such an arrangement, some multicompartments are responsible for diagnostics by, for example, incorporating sensing molecules,[727] while other subcompartments are constructed for therapy and treatment, *i.e.*, for on-demand delivery of biomedicine. Among other alternative structures are capsosomes and polymersomes. Capsosomes represent delivery carriers formed by adsorbing liposomes and polymers on a particle template, followed by removal of template cores. A number of interesting applications have been demonstrated for capsosomes, including controlling the rates of enzyme-catalyzed reactions, and pH- and temperature triggered release.[728] Polymersomes, on the other hand, are delivery carriers based on block copolymers.[729] The versatility of controlling their properties makes them, together with polymeric vesicles,[730] an indispensable class of drug delivery vehicles.

Theranostic NPs not only provide signals for imaging the locations of drug delivery vehicles, they also may respond to the local environment and thus report delivery by a change in the read-out signal. A first look at delivery *in vitro* helps to demonstrate this concept. When NPs are incorporated into cells *via* endocytotic pathways, the NPs experience radical changes in their ambient environments. This involves a change in pH from neutral/slightly alkaline extracellular medium, to highly acidic endosomes/lysosomes, which, for example, enables reporting cellular internalization by observing pH changes by pH-sensitive fluorophores integrated into the NPs.[128,171] Endosomes and lysosomes are also rich in proteolytic enzymes, which act on internalized NPs. Fluorescence markers that change signal upon proteolytic activity enable the detection of intracellular internalization.[731,732] These principles have been applied for online observation of the delivery of micelles. Here, a color change reports successful delivery upon degradation of the micelles. The delivery of embedded drugs can be imaged directly.[9,733,734] Murakami and co-workers demonstrated this approach using micelles of BODIPY FL-PEG-*b*-poly(glutamic acid)-BODIPY TR loaded with 1,2-(diaminocyclohexane)platinum(II). The micelles were built to emit due to the shell-conjugated dye, while the core-conjugated dye was quenched. The micelle degradation is triggered by changes in pH and concentration of chloride ions, *i.e.*, changes that occur in late endosomes. The last approach was tested *in vivo* using confocal laser scanning microscopy. Despite rapid progress in this field, theranostic NPs are still at an early stage of development.

Nanoparticle-Labeled Stem Cells for Targeted Imaging and Therapy. Stem cell nanotechnology, as a newly emerging interdisciplinary field, refers to the application of nanotechnology in stem-cell research and development. Hundreds of clinical trials with autologous or allogeneic MSCs are currently ongoing, with efforts being made to ensure the safety and efficacy of these advanced therapy medicinal products. Although

DOI: 10.1021/acsnano.6b06040
ACS Nano 2017, 11, 2313−2381

significant advances in the field of stem cells have been, and are continuously being made, several obstacles must be overcome before their therapeutic application can be realized. These steps include the development of advanced techniques to understand and to control functions of microenvironment signals as well as novel methods to track and to guide transplanted stem cells. The application of nanomaterials and nanotechnology in stem-cell research and development exhibits attractive technological prospects to solve current problems of stem-cell research and development.[735] Mesenchymal stem cells are multipotent stem cells that can differentiate into a variety of cell types, including osteoblasts (bone cells), chondrocytes (cartilage cells), and adipocytes (fat cells). In addition, MSCs possess immunosuppressive or immunomodulatory properties and have the tendency to home to the sites of active tumorigenesis. Thus, MSCs can be considered as a candidate cell type for cell-based tissue engineering, cancer therapeutics, and regenerative medicine applications.

One fascinating and upcoming application is the generation of induced pluripotent stem cells (iPSC) from MSCs with potential in regenerative medicine. Combining negatively charged nucleic acids such as transcription factors and siRNA with cationized NP formulations provided superior reprogramming efficiency compared to conventional "Yamanaka factors" (see Figure 37).[736]

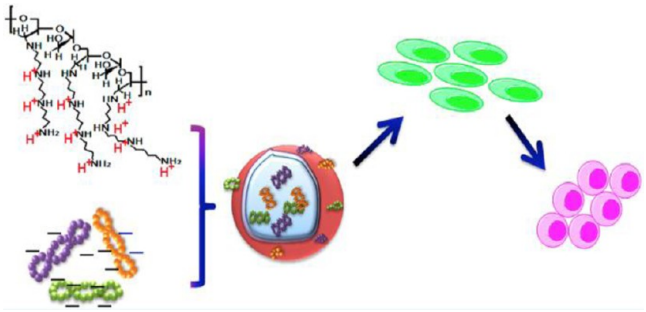

Figure 37. Negatively charged plasmid mixture (encoding Oct4, Sox2, miR302-367) and the positively charged cationized *Pleurotus eryngii* polysaccharide (CPEPS) self-assembled into NPs, named as CPEPS- OS-miR NPs, which were applied to human umbilical cord mesenchymal stem cells for iPSCs generation. Adapted from ref 736. Copyright 2015 American Chemical Society.

The highly tumorigenic c-MYC and KLF4 oncogenes were dispensable in this approach, which employed polysaccharides to form self-assembling NPs instead of lentiviral transduction for iPSC generation from MSCs.

However, the distribution and final fate of MSCs inside the human body have still not been clarified, for which novel labeling and *in vivo* tracking technologies are urgently needed. Nanoparticles are potentially suitable labels. However, little is known about alteration of MSC biology after exposure or uptake of NPs. As an example, silica-coated fluorescent supermagnetic NPs were evaluated for their effects on MSCs, and then used to label MSCs. The distribution and final sites of the labeled MSCs were observed *in vivo* in nude mice models with gastric cancer. Mesenchymal stem cells were efficiently labeled with NPs, yielding stable fluorescent signals and magnetic properties within 14 days. The NP-labeled MSCs targeted and could be used to image *in vivo* gastric cancer cells after being intravenously injected for 14 days (see Figure 38).[737] Nanoparticle-labeled MSCs could significantly inhibit the growth of gastric cancer *in vivo* based on hyperthermia effects of the NPs, and the CCL19/CCR7 and CXCL12/CXCR4 axis loops may play key roles in targeting MSCs to gastric cancer *in vivo*. This NP-based labeling and tracking technology has potential in applications such as labeling and tracking in implanted cells, evaluating cell therapeutic effects, and recognizing and mapping early gastric cancer cells.

Dendritic cells (DCs) also display promising potential in cancer immunity. However, enhancing DCs' immunotherapeutic effect in cancer-targeted immunotherapy and prevention remains a challenge. Li *et al.* reported an allogenic DC and tumor cell fused vaccine combined with cytokine-induced killing cells (CIKs) for targeted imaging and enhanced immunotherapeutic efficacy of gastric cancer (GC).[738] The fused vaccine was prepared by PEG-mediated fusion between mature DCs and inactive GC MGC803 cells. The immunotherapeutic and prophylactic potentials of the fused cells (FCs) were evaluated in tumor-bearing, postsurgery, and tumor-free mice models. The migration and homing process of NIR-QD-labeled FCs were investigated with a real-time animal-imaging system. Results showed that the FCs and FC + CIKs could trigger the tumor-specific cytotoxic T lymphocytes against GC cells. They target the tumor tissue, enhance the prophylactic effects, and suppress

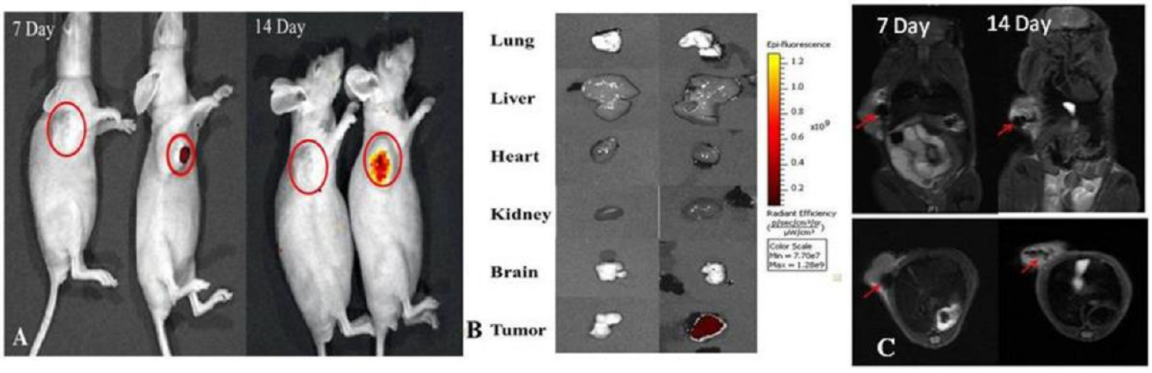

Figure 38. Fluorescence and MR imaging of NP-labeled MSCs targeting gastric cancer cells *in vivo*. (A) *In vivo* fluorescence images show that (right) tumor sites of the mice in the test group had fluorescence signals of NP-labeled MSCs postinjection after 7 and 14 days, and (left) tumor sites of the mice in the control group had no fluorescence signal of NPs postinjection after 7 and 14 days. (B) Fluorescence images of major organs show that (left) no signal was detected in the tumor and organs of the control group, and (right) obvious fluorescence signals were detected in the tumor tissues of the test group. (C) MR imaging of NP-labeled MSCs targeting gastric cancer cells after 7 and 14 days postinjection. Adapted with permission from ref 737. Copyright 2012 Ruan *et al.*

DOI: 10.1021/acsnano.6b06040
ACS Nano 2017, 11, 2313−2381

the tumor growth *in vivo*. These allogenic DC and tumor cell fused vaccine can be used for targeted imaging and enhanced immunotherapeutic efficacy of GC. Similarly, the FC + CIK strategy shows potential in clinical applications, such as early therapy and prevention of tumor metastasis and relapse in near future.

REDUCING SIDE EFFECTS WITH SAFE-BY-DESIGN APPROACHES

Potential Risks of Nanomedicines. While there are many applications of nanomedicines, there are concerns over their potential side effects when they are used in patients. These concerns may limit their translation to patients. Thus, the questions of how to reduce risks and to increase benefits are vital for the development of safe and effective nanomedicines. First, we need to understand how physicochemical properties of nanocarriers and nanomedicine relate to their biological behavior and fate *in vivo*.[577,739] These physicochemical properties include size, shape, surface chemistry, hydrophobicity and hydrophilicity, chirality, aggregation, degradability, and catalytic ability. All of these properties may influence their fate and subsequent biological responses. The other issue to take into consideration is the protein corona. When nanocarriers and nanomedicine are injected in the blood, they can quickly adsorb blood proteins, such as albumin, fibrinogen, transferrin, immunoglobulin, lipoproteins, and so on.[740−743] This corona determines the distribution and transport behavior of such NBCDs.[744] Altered biokinetics, which are dependent on the types of polymer used and on surface chemistry, may enhance the transport velocity but, at the same time, they may cause the NPs to enrich undesirably in some specific tissues, thereby leading to high local concentrations at these parts of the body.[745,746] These distribution and metabolism changes may induce new and unpredictable effects that must be taken into consideration. Second, we need to design and to utilize those properties rationally to optimize their application for therapeutic efficacy and safety. As an example, if the NPs are coated with "stealth" components to keep them in the bloodstream longer, the release of the drug molecules should be low at this stage in order not to treat the blood cells and endothelium with the drug.

> The questions of how to reduce risks and to increase benefits are vital for the development of safe and effective nanomedicines.

The much more complex structure of nanomedicines compared to simple drug molecules makes it important to characterize them carefully. This is relevant not only for the understanding of their activity and effects but also for the responsible production of such structures. For this purpose, in Europe, the "Nanomedicine Characterization Laboratory" (http://www.euncl.eu) was founded and is funded by the European Council.

A further critical issue and major problem for nanomedicine is the quick uptake by cells typically in the reticuloendothelial system (RES), which results in their high accumulation in the liver and spleen.[747−749] Toxicity against these cells and tissues should be carefully tested. Besides these "normal" distribution kinetics, NPs may have novel metabolic and excretion profiles which arise due to the interactions of NPs with tissue microstructure and specific biomicroenvironments.[750−752] Small NPs might be removed from the blood by renal clearance (<5 nm) or rapid liver uptake (10−200 nm),[753] whereas large NPs are filtered in the sinusoidal spleen (>200 nm)[754] or are recognized and cleared by the RES.[755] Renal clearance studies in mice using QDs with zwitterionic cysteine demonstrated that the size threshold for glomerular filtration of QDs was about 5.5 nm, while renal excretion was prevented when the diameter was above this value.[123] Therefore, NPs between 20 and 200 nm can remain in the circulation for extended periods of time,[754] though there is still debate in the literature on this front.[756]

Usually, the increased drug uptake by cells and favorable drug release profiles can be easily achieved using nanodelivery systems. However, toxicity, stability, and degradation properties of such NPs are yet to be well evaluated. Moreover, toxicity testing with NPs is not easy, as good models for testing are not available and most simple *in vitro* systems have not been suitable so far.[757] There are significant variabilities in how different organs interact with NPs and this variability is difficult to capture *in vitro*. It is well accepted that the transport of NPs across tissue barriers is clearly size-dependent. This has been demonstrated for various uptake pathways and different tissues such as the gastrointestinal tract,[758] the lung,[759] the blood−brain barrier,[760,761] or the human placenta.[762,763] Logically, these tissues have to be tested intensely in toxicity assays.[747,758−764]

For assessment of the safety and therapeutic efficacy, proper methodology and state-of-art techniques are necessary to study biological behaviors and transformation of nanomaterials and nanomedicine *in vivo* and *in vitro*. Systemic and quantitative information from proteomics, genomics, transcriptomics, and metabolomics can capture the changes on metabolism, signaling pathways, and biological functions as well.[765,766]

Safe-by-Design Approaches. An important consideration in the development of new nanotherapeutics is the intrinsic safety of the design platform, from conception to implementation. Appropriate consideration should be given to material compositions that are already considered safe by the FDA and contain degradable ingredients that do not lead to biopersistance or bioaccumulation. It is also important to consider intrinsic nanomaterial properties that are generally known to be more hazardous for nanomaterial profiling studies, including high cationic density, high surface reactivity, dissolution and shedding of potentially toxic metal ions (*e.g.*, gadolinium[522,523]), high aspect ratio, *etc*. One approach involves the selection of the initial NP composition and subjecting its components to multiparametric high-throughput screening. This screening would enable one to discern possible effects on cells of potential target tissues and could be used to eliminate hazardous *in vitro* effects such as cytotoxicity, membrane disruption, organellar damage (*e.g.*, mitochondria and lysosomes), unwanted redox activity leading to oxidative stress, biopersistance, off target genotoxicity, *etc*. Attempts are made to relate any adverse *in vitro* effects to specific physicochemical properties, which could then be adapted, eliminated, or redesigned to render a safer *in vitro* profile. This approach reduces the number of subsequent animal studies to be performed, if the intrinsic material design is intended to be safe. However, ultimately, the design's efficacy and safety need to be demonstrated through the performance of *in vivo* studies, including making use of well-established safety screening procedures as well as screening for specific material properties that cannot be assessed *in vitro*, *e.g.*, immunogenicity of PEG-coated particles.

DOI: 10.1021/acsnano.6b06040
ACS Nano 2017, 11, 2313−2381

Carbon nanomaterials, including one-dimensional CNTs and 2D graphene, exhibit unique physical, chemical, and electrical properties, that make them attractive candidates for electronics, energy technologies, medical diagnostics, and drug delivery.[767] Due to this significant potential for industrial applications, methods for safe handling and use of these nanomaterials are of critical importance. Furthermore, emerging biomedical uses of these nanomaterials[768,769] necessitate the development of strategies to minimize toxicity. For example, in a series of studies involving SWCNTs,[770] MWCNTs,[771] and graphene,[772] it was shown that stable aqueous dispersions of carbon nanomaterials can be achieved with the amphiphilic block copolymer surfactant Pluronic F108.[773] In contrast to aggregated samples, carbon nanomaterials that are effectively dispersed with Pluronic F108 further minimize toxicity *in vivo*.[770−774] This same dispersion strategy also minimizes negative environmental outcomes of these nanomaterials in aquatic environments.[775−778] The positive benefits of Pluronic block copolymer surfactants have also recently been realized for related 2D nanomaterials,[779] such as transition metal dichalcogenides (*e.g.*, MoS_2), both *in vivo*[780] and in aquatic environments.[781]

Challenges to Clinical Translation. To reach the patient and to contribute to the benefit of society, medical nanomaterials need to succeed in an industrial technology transfer phase and in clinical translation. This translation is a lengthy, costly, and complex process that should be considered early on in the development process of novel nanotechnology-based therapies.[308] For nanomedicine to be considered for "from the benchtop to the bedside", clinical translation, high therapeutic efficacy alone is not sufficient.[782−785] The nanomedicine must simultaneously meet the basic requirement triangles—high therapeutic efficacy, material excipientability, and scale-up ability[313]—to meet the safety, effectiveness, and producibility requirements for a drug (see Figure 39). Typical roadblocks for clinical translation of academic research projects into nanomedicine include: (i) the failure either to target an unmet clinical need, or to do so beyond what can be expected with simpler products in the near future; (ii) reproducibility and characterization problems of the nanomaterials involved; (iii) design complexity forbidding economic production; (iv) scale-up challenges; (v) lack of efficacy in humans; (vi) unexpected clinical toxicity; (vii) lack of a convincing business case; (viii) a fragile patent situation; (ix) a delay in the registration process of nanomaterials and nanodevices; and (x) crowding of research project topics toward specific disease groups (cancer) while other important disease classes (*e.g.*, poverty diseases, metabolic disease, vascular diseases) are neglected.

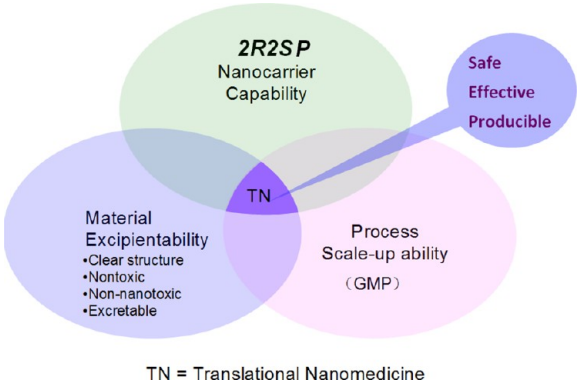

Figure 39. Essential requirements for a nanomedicine to be translational. Adapted with permission from ref 313. Copyright 2012 Elsevier.

Lack of efficacy is frequently seen in humans, despite success in animal models of disease, because the physiology of humans differs from that of small animals in many aspects. This is particularly important in cancer, where the usual xenograft models of human cancer in mice are often curable by nanotechnologies, while current clinical success in cancer therapy remains limited with differences in tumor vascularization playing a key role.[786] To achieve rational, prospective design criteria for the development of future nanomaterials for particular tasks, a strong scientific understanding of nano−bio interactions will be required. Predictive models of such interactions can be used to design novel materials *in silico*, where their interaction with blood components, biological barriers, cell membranes, and intracellular structures can be predicted using the model. This goal can be achieved in part by utilizing the combined power of macromolecule modeling, supramolecular modeling, cell modeling, pharmacokinetic modeling, and computational toxicology.

Toxicity, as discussed in the prior section, is a second key reason for the pharmaceutical industry to abandon a therapy after it has reached first-in-human and phase 1 or phase 2 clinical trials. Excipientability, *i.e.*, the feasibility of the carrier material(s) to be finally proven as an excipient used in humans, is directly related to the safety of the nanomedicine.[313] To have good excipientability, the carrier material itself should be nontoxic and easy to excrete completely from the body *via* the liver (into bile) or the kidneys (into urine) or both. According to Choi and Frangioni,[782] safety and clearance (renal or hepatic) should be included among the basic criteria for clinical translation of formulation/materials administered to humans. Accumulation of any foreign material in the body, even inert polymers like PVP, can cause health problems.[787−789] Additionally, in order to expedite and to increase the probability of successful translation, the carrier materials should have a clear and simple structure with known degradation products. An even better case, as mentioned earlier, would be for the carrier material to be made of FDA-approved building blocks. In addition to concerns surrounding accumulation, complement activation upon intravenous injection by nanomaterials is a frequent and potentially dangerous event.[790] The potential for complement activation of novel nanomaterials can be assessed by combining *in vitro* tests and *in vivo* models,[791] but a full mechanistic understanding of complement activation on nanosurfaces is still missing. Rational design of nanomaterials that will not react with complement by design is highly desirable but not yet reality.

For the pharmaceutical industry, the lack of clear and standardized pathways to regulatory approval for nanosystems renders development riskier and therefore less attractive, unless highly convincing first-in-human studies can be demonstrated by academia. Patent protection is also of key importance for industry, but the flooding of the patent field by a myriad of nanoscience patents in the past decade, with content that is often overlapping and insufficiently examined, has rendered the business case for nanomaterials more difficult. Too many open-ended promises of new technologies may paradoxically reduce the propensity of managers and regulators to act.[792] Joint efforts by the scientific community, industry, and international regulatory bodies to find a common ground through annual, interdisciplinary discussion of the challenges of nanomedicine design and toxicity, and regulation in the CLINAM conferences

DOI: 10.1021/acsnano.6b06040
ACS Nano 2017, 11, 2313−2381

(http:/www.clinam.org) have contributed to streamlining the regulatory aspects of nanomedicine in recent years.

Process scale-up ability is the feasibility of making large volumes of NPs with consistent and reproducible quality to establish GMP.[313] For instance, a nanomedicine of drug-loaded micelles made of block copolymers must be produced with reproducible NP size, NP size distribution, and drug-loading efficiency and content. As the nanomedicine structures become more complex, the number of quality-control parameters dramatically increases,[793,794] which makes it increasingly difficult to produce acceptably consistent formulations. A nanomedicine requiring only simple production processes is more favorable for the establishment of a GMP process. For instance, self-assembling prodrugs can spontaneously form nanomedicines with advantages that include clear and well-characterized molecular structures, fixed drug loading contents, 100% loading efficiency, no burst-release problems, and easy fabrication, all of which are favorable for clinical translation.[441,795,796] For nanomedicine aimed at clinical translation, it is advisable to look into excipientability and scale-up ability issues early at the bench to expedite the process.

CONCLUSIONS AND PROSPECTS

New NPs tuned for nanomedicine applications are emerging, especially in the fields of drug delivery, antibiotic resistance, imaging, diagnostics, and cancer therapies. Recent studies have shown that the use of multiple nanomaterials (*i.e.*, NDs and proteins) or a single nanoplatform functionalized with several therapeutic agents can successfully image and treat tumors with improved efficacy. NPs-based drug delivery has been included in the rational, biomimetic, and systematic design of optimal therapeutic combinations.

Nanomedicine in cellular, preclinical, and clinical studies has led to many important advances, both fundamental and translational. Many of these advances, however, have been in the field of cancer diagnosis and treatment. This disproportionate focus is expected to be addressed in upcoming years with research focuses expanding to other medical challenges such as antibiotic resistance and artificial organs. Nanomedicine is poised to be of benefit in these areas by virtue of the versatility of the nanomaterial platform design, be it through multimodal therapeutic approaches or through highly specialized multifaceted design for relevant biological applications.

Although nanomedicine has raised exciting expectations for many medical problems, scientific challenges have arisen as well, mainly due to the lack of knowledge about the behavior of nanomaterials inside living organisms. However, due to the basic research focused on these issues, we are now closer to solving them and to reaching "real" medical solutions based on nanomedicine.

AUTHOR INFORMATION

Corresponding Author

*E-mail: wolfgang.parak@physik.uni-marburg.de.

ORCID

Beatriz Pelaz: 0000-0002-4626-4576
Anne M. Andrews: 0000-0002-1961-4833
Laura Ballerini: 0000-0001-8420-0787
Monica Carril: 0000-0002-1232-8658
Warren C. W. Chan: 0000-0001-5435-4785
Chunying Chen: 0000-0002-6027-0315
Xiaodong Chen: 0000-0002-3312-1664
Xiaoyuan Chen: 0000-0002-9622-0870
Jianzhong Du: 0000-0003-1889-5669
Alberto Escudero: 0000-0002-0850-6589
Mingyuan Gao: 0000-0002-7360-3684
Yury Gogotsi: 0000-0001-9423-4032
Zhongwei Gu: 0000-0003-1547-6880
Naomi J. Halas: 0000-0002-8461-8494
Norbert Hampp: 0000-0003-1614-2698
Mark C. Hersam: 0000-0003-4120-1426
Ji Jian: 0000-0001-9870-4038
Xingyu Jiang: 0000-0002-5008-4703
Ali Khademhosseini: 0000-0002-2692-1524
Jindřich Kopeček: 0000-0002-4451-6944
Nicholas A. Kotov: 0000-0002-6864-5804
Xing-Jie Liang: 0000-0002-4793-1705
Luis M. Liz-Marzán: 0000-0002-6647-1353
Paul Mulvaney: 0000-0002-8007-3247
Shuming Nie: 0000-0002-7328-1144
Tai Hyun Park: 0000-0003-4254-0657
Reginald M. Penner: 0000-0003-2831-3028
Vincent M. Rotello: 0000-0002-5184-5439
Raymond E. Schaak: 0000-0002-7468-8181
Youqing Shen: 0000-0003-1837-7976
Molly M. Stevens: 0000-0002-7335-266X
J. Scott VanEpps: 0000-0002-5437-3123
Tanja Weil: 0000-0002-5906-7205
Paul S. Weiss: 0000-0001-5527-6248
Itamar Willner: 0000-0001-9710-9077
Yuliang Zhao: 0000-0002-9586-9360
Xin Zhou: 0000-0002-5580-7907
Wolfgang J. Parak: 0000-0003-1672-6650

Notes

The authors declare no competing financial interest.

ACKNOWLEDGMENTS

This report is partly based on presentations held at the Sino-German Symposium Nanomaterials for Biomedical Applications, October 27−31, 2013, Hangzhou, China, ChinaNanomedicine 2015, April 6−9, 2015, Hangzhou, China, the third International Symposium on Molecular Imaging and Nanomedicine, April 25−29, Suzhou, China, and the 5th Asian Biomaterials Congress (ABMC5), May 6−9, 2015, Taipei, Taiwan (ROC), and the Micro- and Nanotechnologies for Medicine: Emerging Frontiers and Applications, July 27−31, 2015, Cambridge, MA, United States. This work was supported by the Deutscher Akademischer Austauschdienst (DAAD to Philipps Universität Marburg and Zhejiang University, Hangzhou), the Chinesisch Deutsches Zentrum für Wissenschaftsförderung ("CDZ" to Z.G. and W.J.P.), and the Chinese Academy of Science (CAS). Part of this work was supported by the National Natural Science Foundation (51390481, 81227902, 81625011), National Basic Research Program (2014CB931900) of China (to Y.S.), by the European Commission grant Futurenanoneeds (to V.P. and W.J.P.), by the Spanish Ministerio de Economia y Competitividad (CTQ2011-23167 and CTQ2014-59808R to R.A.A.P.), the Generalitat of Catalunya (2014-SGR-612 to R.A.A.P.), the Deutsche Forschungsgemeinschaft (DFG) (AL552/8-1 to R.T.), the Swiss National Science Foundation (NRP62 to P.H.), the Claude & Julianna Foundation (grant to P.H.), the National Science Foundation (NSF) grants CHE-1306928 (to R.P.) and ECS-0601345; CBET 0933384; CBET 0932823; and CBET

DOI: 10.1021/acsnano.6b06040
ACS Nano 2017, 11, 2313−2381

1036672 (to N.A.K.), Canadian Institute of Health Research (grant to W.C.W.C.), and Natural Sciences and Engineering Research Council of Canada (grant to W.C.W.C.). S.A. and B.P. acknowledge a fellowship from the Alexander von Humboldt Foundation. N.F. acknowledges the Lars Hiertas Minne Foundation. M.C. acknowledges Ikerbasque for a Research Fellow position. X.C. acknowledges the Intramural Research Program (IRP), National Institute of Biomedical Imaging and Bioengineering (NIBIB), National Institutes of Health (NIH). B.Z.T. acknowledges the Innovation and Technology Commission of Hong Kong (ITC-CNERC14SC01). The Pancreatic Cancer research of A.E.N. and H.M. was funded by the U.S. National Cancer Institute, NIH grant # U01CA198846. A.E. acknowledges Junta de Andalucía (Spain) for a Talentia Postdoc Fellowship, co-financed by the European Union's Seventh Framework Programme, grant agreement no 267226. A.G.S. acknowledges support by BOF (UGent) and FWO (Research Foundation Flanders). Part of this work was supported by the National Natural Science Foundation of China (81625011).

REFERENCES

(1) Min, Y.; Caster, J. M.; Eblan, M. J.; Wang, A. Z. Clinical Translation of Nanomedicine. *Chem. Rev.* **2015**, *115*, 11147−11190.
(2) Kim, B. Y. S.; Rutka, J. T.; Chan, W. C. W. Nanomedicine. *N. Engl. J. Med.* **2010**, *363*, 2434−2443.
(3) Lobatto, M. E.; Fuster, V.; Fayad, Z. A.; Mulder, W. J. M. Perspectives and Opportunities for Nanomedicine in the Management of Atherosclerosis. *Nat. Rev. Cancer* **2011**, *10*, 963−963.
(4) Langer, R.; Weissleder, R. Nanotechnology. *J. Am. Med. Assoc.* **2015**, *313*, 135−136.
(5) Shao, K.; Singha, S.; Clemente-Casares, X.; Tsai, S.; Yang, Y.; Santamaria, P. Nanoparticle-Based Immunotherapy for Cancer. *ACS Nano* **2015**, *9*, 16−30.
(6) Kotov, N. A. Inorganic Nanoparticles as Protein Mimics. *Science* **2010**, *330*, 188−189.
(7) Torchilin, V. P. Micellar Nanocarriers: Pharmaceutical Perspectives. *Pharm. Res.* **2007**, *24*, 1−16.
(8) Zhang, R.; Yang, J.; Sima, M.; Zhou, Y.; Kopeček, J. Sequential Combination Therapy of Ovarian Cancer with Degradable N-(2-hydroxypropyl)methacrylamide Copolymer Paclitaxel and Gemcitabine Conjugates. *Proc. Natl. Acad. Sci. U. S. A.* **2014**, *111*, 12181−12186.
(9) Lee, Y.; Fukushima, S.; Bae, Y.; Hiki, S.; Ishii, T.; Kataoka, K. A Protein Nanocarrier from Charge-Conversion Polymer in Response to Endosomal pH. *J. Am. Chem. Soc.* **2007**, *129*, 5362−5363.
(10) Guo, P. The Emerging Field of RNA Nanotechnology. *Nat. Nanotechnol.* **2010**, *5*, 833−842.
(11) Baker, S. N.; Baker, G. A. Luminescent Carbon Nanodots: Emergent Nanolights. *Angew. Chem., Int. Ed.* **2010**, *49*, 6726−6744.
(12) Yu, S. J.; Kang, M. W.; Chang, H. C.; Chen, K. M.; Yu, Y. C. Bright Fluorescent Nanodiamonds: No Photobleaching and Low Cytotoxicity. *J. Am. Chem. Soc.* **2005**, *127*, 17604−17605.
(13) Baughman, R. H.; Zakhidov, A. A.; de Heer, W. A. Carbon Nanotubes—The Route toward Applications. *Science* **2002**, *297*, 787−792.
(14) Nurunnabi, M.; Khatun, Z.; Reeck, G. R.; Lee, D. Y.; Lee, Y.-k. Photoluminescent Graphene Nanoparticles for Cancer Phototherapy and Imaging. *ACS Appl. Mater. Interfaces* **2014**, *6*, 12413−12421.
(15) Colombo, M.; Carregal-Romero, S.; Casula, M. F.; Gutiérrez, L.; Morales, M. P.; Böhm, I. B.; Heverhagen, J. T.; Prosperi, D.; Parak, W. J. Biological Applications of Magnetic Nanoparticles. *Chem. Soc. Rev.* **2012**, *41*, 4306−4334.
(16) Parak, W. J.; Pellegrino, T.; Plank, C. Labelling of Cells with Quantum Dots. *Nanotechnology* **2005**, *16*, R9−R25.
(17) Sperling, R. A.; Rivera Gil, P.; Zhang, F.; Zanella, M.; Parak, W. J. Biological Applications of Gold Nanoparticles. *Chem. Soc. Rev.* **2008**, *37*, 1896−1908.
(18) Lin, C.-A. J.; Yang, T.-Y.; Lee, C.-H.; Huang, S. H.; Sperling, R. A.; Zanella, M.; Li, J. K.; Shen, J.-L.; Wang, H.-H.; Yeh, H.-I.; Parak, W. J.; Chang, W. H. Synthesis, Characterization, and Bioconjugation of Fluorescent Gold Nanoclusters toward Biological Labeling Applications. *ACS Nano* **2009**, *3*, 395−401.
(19) Wilhelm, S.; Kaiser, M.; Wuerth, C.; Heiland, J.; Carrillo-Carrion, C.; Muhr, V.; Wolfbeis, O. S.; Parak, W. J.; Resch-Genger, U.; Hirsch, T. Water Dispersible Upconverting Nanoparticles: Effects of Surface Modification on their Luminescence and Colloidal Stability. *Nanoscale* **2015**, *7*, 1403−1410.
(20) Sapsford, K. E.; Tyner, K. M.; Dair, B. J.; Deschamps, J. R.; Medintz, I. L. Analyzing Nanomaterial Bioconjugates: A Review of Current and Emerging Purification and Characterization Techniques. *Anal. Chem.* **2011**, *83*, 4453−4488.
(21) Schaak, R. E.; Williams, M. E. Full Disclosure: The Practical Side of Nanoscale Total Synthesis. *ACS Nano* **2012**, *6*, 8492−8497.
(22) Wolf, L. K. Sweating the Small Stuff. *Chem. Eng. News* **2012**, *90*, 48−50.
(23) Kovalenko, M. V.; Manna, L.; Cabot, A.; Hens, Z.; Talapin, D. V.; Kagan, C. R.; Klimov, V. I.; Rogach, A. L.; Reiss, P.; Milliron, D. J.; Guyot-Sionnnest, P.; Konstantatos, G.; Parak, W. J.; Hyeon, T.; Korgel, B. A.; Murray, C. B.; Heiss, W. Prospects of Nanoscience with Nanocrystals. *ACS Nano* **2015**, *9*, 1012−1057.
(24) Beveridge, J. S.; Buck, M. R.; Bondi, J. F.; Misra, R.; Schiffer, P.; Schaak, R. E.; Williams, M. E. Purification and Magnetic Interrogation of Hybrid Au-Fe_3O_4 and FePt-Fe_3O_4 Nanoparticles. *Angew. Chem., Int. Ed.* **2011**, *50*, 9875−9879.
(25) Kowalczyk, B.; Lagzi, I.; Grzybowski, B. A. Nanoseparations: Strategies for Size and/or Shape-Selective Purification of Nanoparticles. *Curr. Opin. Colloid Interface Sci.* **2011**, *16*, 135−148.
(26) Mulvaney, P.; Parak, W. J.; Caruso, F.; Weiss, P. S. Standardizing Nanomaterials. *ACS Nano* **2016**, *10*, 9763−9764.
(27) Saha, S.; Xiong, X.; Chakraborty, P. K.; Shameer, K.; Arvizo, R. R.; Kudgus, R. A.; Dwivedi, S. K. D.; Hossen, Md. N.; Gillies, E. M.; Robertson, J. D.; Dudley, J. T.; Urrutia, R. A.; Postier, R. G.; Bhattacharya, R.; Mukherjee, P. Gold Nanoparticle Reprograms Pancreatic Tumor Microenvironment and Inhibits Tumor Growth. *ACS Nano* **2016**, *10*, 10636−10651.
(28) Melamed, J. R.; Riley, R. S.; Valcourt, D. M.; Day, E. S. Using Gold Nanoparticles To DIsrupt the Tumor Microenvironment: An Emerging Therapeutic Strategy. *ACS Nano* **2016**, *10*, 10631−10635.
(29) Chow, E. K.; Ho, D. Cancer Nanomedicine: From Drug Delivery to Imaging. *Sci. Transl. Med.* **2013**, *5*, 216rv4.
(30) Singh, R.; Lillard, J. W., Jr Nanoparticle-Based Targeted Drug Delivery. *Exp. Mol. Pathol.* **2009**, *86*, 215−223.
(31) Zhang, Q. W.; Mochalin, V. N.; Neitzel, I.; Hazeli, K.; Niu, J. J.; Kontsos, A.; Zhou, J. G.; Lelkes, P. I.; Gogotsi, Y. Mechanical Properties and Biomineralization of Multifunctional Nanodiamond-PLLA Composites for Bone Tissue Engineering. *Biomaterials* **2012**, *33*, 5067−5075.
(32) Altınoğlu, E. I.; Russin, T. J.; Kaiser, J. M.; Barth, B. M.; Eklund, B. C.; Kester, M.; Adair, J. H. Near-Infrared Emitting Fluorophore-Doped Calcium Phosphate Nanoparticles for *In Vivo* Imaging of Human Breast Cancer. *ACS Nano* **2008**, *2*, 2075−2084.
(33) Matsumura, Y.; Maeda, H. A New Concept for Macromolecular Therapeutics in Cancer Chemotherapy: Mechanism of Tumoritropic Accumulation of Proteins and the Antitumor Agent Smancs. *Cancer Res.* **1986**, *46*, 6387−6392.
(34) Wilhelm, S.; Tavares, A. J.; Dai, Q.; Ohta, S.; Audet, J.; Dvorak, H. F.; Chan, W. C. W. Analysis of Nanoparticle Delivery to Tumours. *Nat. Rev. Mater.* **2016**, *1*, 16014.
(35) Kolosnjaj-Tabi, J.; Javed, Y.; Lartigue, L.; Volatron, J.; Elgrabli, D.; Marangon, I.; Pugliese, G.; Caron, B.; Figuerola, A.; Luciani, N.; Pellegrino, T.; Alloyeau, D.; Gazeau, F. The One Year Fate of Iron Oxide Coated Gold Nanoparticles in Mice. *ACS Nano* **2015**, *9*, 7925−7939.
(36) Chou, L. Y. T.; Zagorovsky, K.; Chan, W. C. W. DNA Assembly of Nanoparticle Superstructures for Controlled Biological Delivery and Elimination. *Nat. Nanotechnol.* **2014**, *9*, 148−155.
(37) Kreyling, W. G.; Abdelmonem, A. M.; Ali, Z.; Alves, F.; Geiser, M.; Haberl, N.; Hartmann, R.; Hirn, S.; de Aberasturi, D. J.; Kantner, K.;

DOI: 10.1021/acsnano.6b06040
ACS Nano 2017, 11, 2313−2381

Khadem-Saba, G.; Montenegro, J. M.; Rejman, J.; Rojo, T.; de Larramendi, I. R.; Ufartes, R.; Wenk, A.; Parak, W. J. *In Vivo* Integrity of Polymer-Coated Gold Nanoparticles. *Nat. Nanotechnol.* **2015**, *10*, 619−623.
(38) Peteiro-Cartelle, J.; Rodríguez-Pedreira, M.; Zhang, F.; Rivera Gil, P.; del Mercato, L. L.; Parak, W. J. One Example on how Colloidal Nano- and Microparticles could Contribute to Medicine. *Nanomedicine* **2009**, *4*, 967−979.
(39) OECD, OECD Health Statistics 2014 − Frequently Requested Data. 2014. http://www.oecd.org/els/health-systems/oecd-health-statistics-2014-frequently-requested-data.htm (Accessed January 12, 2017).
(40) Bao, C.; Conde, J.; Polo, E.; del Pino, P.; Moros, M.; Baptista, P.; Grazu, V.; Cui, D.; de la Fuente, J. A Promising Road with Challenges: Where are Gold Nanoparticles in Translational Research? *Nanomedicine* **2014**, *9*, 2353−2370.
(41) Zhou, Z. J.; Zhang, C. L.; Qian, Q. R.; Ma, J. B.; Huang, P.; Zhang, X.; Pan, L. Y.; Gao, G.; Fu, H. L.; Fu, S.; Song, H.; Zhi, X.; Ni, J.; Cui, D. X. Folic Acid-Conjugated Silica Capped Gold Nanoclusters for Targeted Fluorescence/X-Ray Computed Tomography Imaging. *J. Nanobiotechnol.* **2013**, *11*, 17.
(42) Zhang, C. L.; Li, C.; Liu, Y. L.; Zhang, J. P.; Bao, C. C.; Liang, S. J.; Wang, Q.; Yang, Y.; Fu, H. L.; Wang, K.; Cui, D. X. Gold Nanoclusters-Based Nanoprobes for Simultaneous Fluorescence Imaging and Targeted Photodynamic Therapy with Superior Penetration and Retention Behavior in Tumors. *Adv. Funct. Mater.* **2015**, *25*, 1314−1325.
(43) Qiu, P. Y.; Sun, R. J.; Gao, G.; Yin, T.; Shen, Y. L.; Chen, B.; Wang, K.; Zhang, C. L.; Qian, X. Q.; Cui, D. X. Crystal Cell Oriented-Rotation Triggered Phase Transition of Porous Upconversion Nanocrystals Synthesis in Hydrothermal System. *J. Mater. Chem. B* **2015**, *3*, 3948−3958.
(44) Momose, A.; Takeda, T.; Itai, Y.; Hirano, K. Phase-Contrast X-Ray Computed Tomography for Observing Biological Soft Tissues. *Nat. Med.* **1996**, *2*, 473−475.
(45) Chapman, D.; Thomlinson, W.; Johnston, R.; Washburn, D.; Pisano, E.; Gmür, N.; Zhong, Z.; Menk, R.; Arfelli, F.; Sayers, D. Diffraction Enhanced X-Ray Imaging. *Phys. Med. Biol.* **1997**, *42*, 2015.
(46) Cloetens, P.; Ludwig, W.; Baruchel, J.; Van Dyck, D.; Van Landuyt, J.; Guigay, J. P.; Schlenker, M. Holotomography: Quantitative Phase Tomography with Micrometer Resolution using Hard Synchrotron Radiation XRays. *Appl. Phys. Lett.* **1999**, *75*, 2912−2914.
(47) Mohammadi, S.; Larsson, E.; Alves, F.; Dal Monego, S.; Biffi, S.; Garrovo, C.; Lorenzon, A.; Tromba, G.; Dullin, C. Quantitative Evaluation of a Single-Distance Phase-Retrieval Method Applied on In-Line Phase-Contrast Images of a Mouse Lung. *J. Synchrotron Radiat.* **2014**, *21*, 784−789.
(48) Beltran, M. A.; Paganin, D. M.; Uesugi, K.; Kitchen, M. J. 2D and 3D X-Ray Phase Retrieval of Multi-Material Objects using a Single Defocus Distance. *Opt. Express* **2010**, *18*, 6423−6436.
(49) Dullin, C.; dal Monego, S.; Larsson, E.; Mohammadi, S.; Krenkel, M.; Garrovo, C.; Biffi, S.; Lorenzon, A.; Markus, A.; Napp, J.; Salditt, T.; Accardo, A.; Alves, F.; Tromba, G. Functionalized Synchrotron In-Line Phase-Contrast Computed Tomography: A Novel Approach for Simultaneous Quantification of Structural Alterations and Localization of Barium-Labelled Alveolar Macrophages within Mouse Lung Samples. *J. Synchrotron Radiat.* **2015**, *22*, 143−155.
(50) Krenkel, M.; Markus, A.; Bartels, M.; Dullin, C.; Alves, F.; Salditt, T. Phase-Contrast Zoom Tomography Eeveals Precise Locations of Macrophages in Mouse Lungs. *Sci. Rep.* **2015**, *5*, 9973.
(51) Zhou, S. A.; Brahme, A. Development of Phase-Contrast X-Ray Imaging Techniques and Potential Medical Applications. *Phys. Med.* **2008**, *24*, 129−148.
(52) Cormode, D. P.; Roessl, E.; Thran, A.; Skajaa, T.; Gordon, R. E.; Schlomka, J. P.; Fuster, V.; Fisher, E. A.; Mulder, W. J. M.; Proksa, R.; Fayad, Z. A. Atherosclerotic Plaque Composition: Analysis with Multicolor CT and Targeted Gold Nanoparticles. *Radiology* **2010**, *256*, 774−782.
(53) Tang, R. B.; Xi, Y.; Chai, W. M.; Wang, Y. T.; Guan, Y. J.; Yang, G. Y.; Xie, H. L.; Chen, K. M. Microbubble-Based Synchrotron Radiation Phase Contrast Imaging: Basic Study and Angiography Applications. *Phys. Med. Biol.* **2011**, *56*, 3503−3512.
(54) Statistisches Bundesamt. Wiesbaden, Germany, 2016. Fallpauschalenbezogene Krankenhausstatistik (DRG-Statistik) Operationen und Prozeduren der vollstationären Patientinnen und Patienten in Krankenhäusern. https://www.destatis.de/DE/Publikationen/Thematisch/Gesundheit/Krankenhaeuser/OperationenProzeduren5231401137014.pdf (Accessed January 18, 2016).
(55) Silva, A. C.; Lawder, H. J.; Hara, A.; Kujak, J.; Pavlicek, W. Innovations in CT Dose Reduction Strategy: Application of the Adaptive Statistical Iterative Reconstruction Algorithm. *AJR, Am. J. Roentgenol.* **2010**, *194*, 191−199.
(56) Sidky, E. Y.; Kao, C. M.; Pan, X. H. Accurate Image Reconstruction from Few-Views and Limited-Angle Data in Divergent-Beam CT. *J. X-Ray Sci. Technol.* **2006**, *14*, 119−139.
(57) James, M. L.; Gambhir, S. S. A Molecular Imaging Primer: Modalities, Imaging Agents, and Applications. *Physiol. Rev.* **2012**, *92*, 897−965.
(58) Formica, D.; Silvestri, S. Biological Effects of Exposure to Magnetic Resonance Imaging: An Overview. *Biomed. Eng. Online* **2004**, *3*, 11.
(59) Hartwig, V.; Giovannetti, G.; Vanello, N.; Lombardi, M.; Landini, L.; Simi, S. Biological Effects and Safety in Magnetic Resonance Imaging: A Review. *Int. J. Environ. Res. Public Health* **2009**, *6*, 1778−1798.
(60) Leawoods, J. C.; Yablonskiy, D. A.; Saam, B.; Gierada, D. S.; Conradi, M. S. Hyperpolarized ^{3}He Gas Production and MR Imaging of the Lung. *Concepts Magn. Reson.* **2001**, *13*, 277−293.
(61) Xu, W.; Kattel, K.; Park, J. Y.; Chang, Y.; Kim, T. J.; Lee, G. H. Paramagnetic Nanoparticle T_1 and T_2 MRI Contrast Agents. *Phys. Chem. Chem. Phys.* **2012**, *14*, 12687−12700.
(62) Singh, N.; Jenkins, G. J. S.; Asadi, R.; Doak, S. H. Potential Toxicity of Superparamagnetic Iron Oxide Nanoparticles (SPION). *Nano Rev.* **2010**, *1*, 5358.
(63) Khawaja, A. Z.; Cassidy, D. B.; Al Shakarchi, J.; McGrogan, D. G.; Inston, N. G.; Jones, R. G. Revisiting the Risks of MRI with Gadolinium Based Contrast Agents—Review of Literature and Guidelines. *Insights Imag.* **2015**, *6*, 553−558.
(64) Na, H. B.; Song, I. C.; Hyeon, T. Inorganic Nanoparticles for MRI Contrast Agents. *Adv. Mater.* **2009**, *21*, 2133−2148.
(65) Johnson, N. J. J.; Oakden, W.; Stanisz, G. J.; Scott Prosser, R.; van Veggel, F. C. J. M. Size-Tunable, Ultrasmall NaGdF4 Nanoparticles: Insights into Their T1MRI Contrast Enhancement. *Chem. Mater.* **2011**, *23*, 3714−3722.
(66) Manus, L. M.; Mastarone, D. J.; Waters, E. A.; Zhang, X.-Q.; Schultz-Sikma, E. A.; MacRenaris, K. W.; Ho, D.; Meade, T. J. Gd(III)-Nanodiamond Conjugates for MRI Contrast Enhancement. *Nano Lett.* **2010**, *10*, 484−489.
(67) Fan, Q. L.; Cheng, K.; Hu, X.; Ma, X. W.; Zhang, R. P.; Yang, M.; Lu, X. M.; Xing, L.; Huang, W.; Gambhir, S. S.; Cheng, Z. Transferring Biomarker into Molecular Probe: Melanin Nanoparticle as a Naturally Active Platform for Multimodality Imaging. *J. Am. Chem. Soc.* **2014**, *136*, 15185−15194.
(68) Qin, C. X.; Cheng, K.; Chen, K.; Hu, X.; Liu, Y.; Lan, X. L.; Zhang, Y. X.; Liu, H. G.; Xu, Y. D.; Bu, L. H.; Su, X. H.; Zhu, X. H.; Meng, S. X.; Cheng, Z. Tyrosinase as a Multifunctional Reporter Gene for Photoacoustic/MRI/PET Triple Modality Molecular Imaging. *Sci. Rep.* **2013**, *3*, 1490.
(69) Liu, Q. M.; Chen, S.; Chen, J.; Du, J. Z. An Asymmetrical Polymer Vesicle Strategy for Significantly Improving T_1 MRI Sensitivity and Cancer-Targeted Drug Delivery. *Macromolecules* **2015**, *48*, 739−749.
(70) Zhao, Z. H.; Zhou, Z. J.; Bao, J. F.; Wang, Z. Y.; Hu, J.; Chi, X. Q.; Ni, K. Y.; Wang, R. F.; Chen, X. Y.; Chen, Z.; Gao, J. H. Octapod Iron Oxide Nanoparticles as High-Performance T-2 Contrast Agents for Magnetic Resonance Imaging. *Nat. Commun.* **2013**, *4*, 2266.
(71) Ali, Z.; Abbasi, A. Z.; Zhang, F.; Arosio, P.; Lascialfari, A.; Casula, M. F.; Wenk, A.; Kreyling, W.; Plapper, R.; Seidel, M.; Niessner, R.; Knoll, J.; Seubert, A.; Parak, W. J. Multifunctional Nanoparticles for Dual Imaging. *Anal. Chem.* **2011**, *83*, 2877−2882.

DOI: 10.1021/acsnano.6b06040
ACS Nano 2017, 11, 2313−2381

(72) Shin, T. H.; Choi, J. S.; Yun, S.; Kim, I. S.; Song, H. T.; Kim, Y.; Park, K. I.; Cheon, J. T(1) and T(2) Dual-Mode MRI Contrast Agent for Enhancing Accuracy by Engineered Nanomaterials. *ACS Nano* **2014**, *8*, 3393−3401.
(73) Choi, J. S.; Lee, J. H.; Shin, T. H.; Song, H. T.; Kim, E. Y.; Cheon, J. Self-Confirming "AND" Logic Nanoparticles for Fault-Free MRI. *J. Am. Chem. Soc.* **2010**, *132*, 11015−11017.
(74) Cheng, K.; Yang, M.; Zhang, R.; Qin, C.; Su, X.; Cheng, Z. Hybrid Nanotrimers for Dual T1 and T2-Weighted Magnetic Resonance Imaging. *ACS Nano* **2014**, *8*, 9884−9896.
(75) Tassa, C.; Shaw, S. Y.; Weissleder, R. Dextran-Coated Iron Oxide Nanoparticles: A Versatile Platform for Targeted Molecular Imaging, Molecular Diagnostics, and Therapy. *Acc. Chem. Res.* **2011**, *44*, 842−852.
(76) Hu, F. Q.; Wei, L.; Zhou, Z.; Ran, Y. L.; Li, Z.; Gao, M. Y. Preparation of Biocompatible Magnetite Nanocrystals for *in Vivo* Magnetic Resonance Detection of Cancer. *Adv. Mater.* **2006**, *18*, 2553−2556.
(77) Lee, W. W.; Marinelli, B.; van der Laan, A. M.; Sena, B. F.; Gorbatov, R.; Leuschner, F.; Dutta, P.; Iwamoto, Y.; Ueno, T.; Begieneman, M. P. V.; Niessen, H. W. M.; Piek, J. J.; Vinegoni, C.; Pittet, M. J.; Swirski, F. K.; Tawakol, A.; Di Carli, M.; Weissleder, R.; Nahrendorf, M. PET/MRI of Inflammation in Myocardial Infarction. *J. Am. Coll. Cardiol.* **2012**, *59*, 153−163.
(78) Kleijn, A.; Chen, J. W.; Buhrman, J. S.; Wojtkiewicz, G. R.; Iwamoto, Y.; Lamfers, M. L.; Stemmer-Rachamimov, A. O.; Rabkin, S. D.; Weissleder, R.; Martuza, R. L.; Fulci, G. Distinguishing Inflammation from Tumor and Peritumoral Edema by Myeloperoxidase Magnetic Resonance Imaging. *Clin. Cancer Res.* **2011**, *17*, 4484−4493.
(79) Breckwoldt, M. O.; Chen, J. W.; Stangenberg, L.; Aikawa, E.; Rodriguez, E.; Qiu, S.; Moskowitz, M. A.; Weissleder, R. Tracking the Inflammatory Response in Stroke *in Vivo* by Sensing the Enzyme Myeloperoxidase. *Proc. Natl. Acad. Sci. U. S. A.* **2008**, *105*, 18584−18589.
(80) Delcea, M.; Möhwald, H.; Skirtach, A. G. Stimuli Responsive LbL Capsules and Nanoshells for Drug Delivery. *Adv. Drug Deliv. Rev.* **2011**, *63*, 730−747.
(81) Huang, X.; Huang, G.; Zhang, S.; Sagiyama, K.; Togao, O.; Ma, X.; Wang, Y.; Li, Y.; Soesbe, T. C.; Sumer, B. D.; Takahashi, M.; Sherry, A. D.; Gao, J. Multi-Chromatic pH-Activatable ^{19}F-MRI Nanoprobes with Binary ON/OFF pH Transitions and Chemical Shift Barcodes. *Angew. Chem., Int. Ed.* **2013**, *52*, 8074−8078.
(82) Chen, S. Z.; Yang, Y. Q.; Li, H. D.; Zhou, X.; Liu, M. L. pH-Triggered Au-Fluorescent Mesoporous Silica Nanoparticles for ^{19}F MR/Fluorescent Multimodal Cancer Cellular Imaging. *Chem. Commun.* **2014**, *50*, 283−285.
(83) Zhu, X. L.; Chen, S. Z.; Luo, Q.; Ye, C. H.; Liu, M. L.; Zhou, X. Body Temperature Sensitive Micelles for MRI Enhancement. *Chem. Commun.* **2015**, *51*, 9085−9088.
(84) Langereis, S.; Keupp, J.; van Velthoven, J. L. J.; de Roos, I. H. C.; Burdinski, D.; Pikkemaat, J. A.; Grull, H. A Temperature-Sensitive Liposomal H-1 CEST and F-19 Contrast Agent for MR Image-Guided Drug Delivery. *J. Am. Chem. Soc.* **2009**, *131*, 1380−1381.
(85) Rivlin, M.; Horev, J.; Tsarfaty, I.; Navon, G. Molecular Imaging of Tumors and Metastases Using Chemical Exchange Saturation Transfer (CEST) MRI. *Sci. Rep.* **2013**, *3*, 3045.
(86) Nakamura, T.; Matsushita, H.; Sugihara, F.; Yoshioka, Y.; Mizukami, S.; Kikuchi, K. Activatable F-19 MRI Nanoparticle Probes for the Detection of Reducing Environments. *Angew. Chem., Int. Ed.* **2015**, *54*, 1007−1010.
(87) Lee, D. S.; Im, H. J.; Lee, Y. S. Radionanomedicine: Widened Perspectives of Molecular Theragnosis. *Nanomedicine* **2015**, *11*, 795−810.
(88) Lee, Y. K.; Jeong, J. M.; Hoigebazar, L.; Yang, B. Y.; Lee, Y. S.; Lee, B. C.; Youn, H.; Lee, D. S.; Chung, J. K.; Lee, M. C. Nanoparticles Modified by Encapsulation of Ligands with a Long Alkyl Chain to Affect Multispecific and Multimodal Imaging. *J. Nucl. Med.* **2012**, *53*, 1462−1470.
(89) Sun, X. L.; Cai, W. B.; Chen, X. Y. Positron Emission Tomography Imaging Using Radio labeled Inorganic Nanomaterials. *Acc. Chem. Res.* **2015**, *48*, 286−294.
(90) Bartlett, D. W.; Su, H.; Hildebrandt, I. J.; Weber, W. A.; Davis, M. E. Impact of Tumor-Specific Targeting on the Biodistribution and Efficacy of siRNA Nanoparticles Measured by Multimodality *in Vivo* Imaging. *Proc. Natl. Acad. Sci. U. S. A.* **2007**, *104*, 15549−15554.
(91) Rivera Gil, P.; Jimenez de Aberasturi, D.; Wulf, V.; Pelaz, B.; del Pino, P.; Zhao, Y.; de la Fuente, J.; Ruiz de Larramendi, I.; Rojo, T.; Liang, X.-J.; Parak, W. J. The Challenge to Relate the Physicochemical Properties of Colloidal Nanoparticles to Their Cytotoxicity. *Acc. Chem. Res.* **2013**, *46*, 743−749.
(92) Pelaz, B.; Charron, G.; Pfeiffer, C.; Zhao, Y.; de la Fuente, J. M.; Liang, X.-J.; Parak, W. J.; del Pino, P. Interfacing Engineered Nanoparticles with Biological Systems: Anticipating Adverse Nano−Bio Interactions. *Small* **2013**, *9*, 1573−1584.
(93) Mei, J.; Hong, Y. N.; Lam, J. W. Y.; Qin, A. J.; Tang, Y. H.; Tang, B. Z. Aggregation-Induced Emission: The Whole Is More Brilliant than the Parts. *Adv. Mater.* **2014**, *26*, 5429−5479.
(94) Ding, D.; Li, K.; Liu, B.; Tang, B. Z. Bioprobes Based on AIE Fluorogens. *Acc. Chem. Res.* **2013**, *46*, 2441−2453.
(95) Ding, D.; Mao, D.; Li, K.; Wang, X. M.; Qin, W.; Liu, R. R.; Chiam, D. S.; Tomczak, N.; Yang, Z. M.; Tang, B. Z.; Kong, D. L.; Liu, B. Precise and Long-Term Tracking of Adipose-Derived Stem Cells and Their Regenerative Capacity *via* Superb Bright and Stable Organic Nanodots. *ACS Nano* **2014**, *8*, 12620−12631.
(96) Liang, J.; Tang, B. Z.; Liu, B. Specific Light-up Bioprobes Based on AIEgen Conjugates. *Chem. Soc. Rev.* **2015**, *44*, 2798−2811.
(97) Kwok, R. T.; Leung, C. W.; Lam, J. W.; Tang, B. Z. Biosensing by Luminogens with Aggregation-Induced Emission Characteristics. *Chem. Soc. Rev.* **2015**, *44*, 4228−4238.
(98) Derfus, A. M.; Chan, W. C. W.; Bhatia, S. N. Probing the Cytotoxicity of Semiconductor Quantum Dots. *Nano Lett.* **2004**, *4*, 11−18.
(99) Kirchner, C.; Liedl, T.; Kudera, S.; Pellegrino, T.; Muñoz Javier, A.; Gaub, H. E.; Stölzle, S.; Fertig, N.; Parak, W. J. Cytotoxicity of Colloidal CdSe and CdSe/ZnS Nanoparticles. *Nano Lett.* **2005**, *5*, 331−338.
(100) Zhang, C. Q.; Jin, S. B.; Li, S. L.; Xue, X. D.; Liu, J.; Huang, Y. R.; Jiang, Y. G.; Chen, W. Q.; Zou, G. Z.; Liang, X. J. Imaging Intracellular Anticancer Drug Delivery by Self-Assembly Micelles with Aggregation-Induced Emission (AIE Micelles). *ACS Appl. Mater. Interfaces* **2014**, *6*, 5212−5220.
(101) Xue, X. D.; Zhao, Y. Y.; Dai, L. R.; Zhang, X.; Hao, X. H.; Zhang, C. Q.; Huo, S. D.; Liu, J.; Liu, C.; Kumar, A.; Chen, W. Q.; Zou, G. Z.; Liang, X. J. Spatiotemporal Drug Release Visualized through a Drug Delivery System with Tunable Aggregation-Induced Emission. *Adv. Mater.* **2014**, *26*, 712−717.
(102) Bruchez, M., Jr.; Moronne, M.; Gin, P.; Weiss, S.; Alivisatos, A. P. Semiconductor Nanocrystals as Fluorescent Biological Labels. *Science* **1998**, *281*, 2013−2016.
(103) Chan, W. C. W.; Nie, S. Quantum Dot Bioconjugates for Ultrasensitive Nonisotopic Detection. *Science* **1998**, *281*, 2016−2018.
(104) Akinfieva, O.; Nabiev, I.; Sukhanova, A. New Directions in Quantum Dot-Based Cytometry Detection of Cancer Serum Markers and Tumor Cells. *Crit. Rev. Oncol. Hematol.* **2013**, *86*, 1−14.
(105) Xu, H.; Sha, M. Y.; Wong, E. Y.; Uphoff, J.; Xu, Y.; Treadway, J. A.; Truong, A.; O'Brien, E.; Asquith, S.; Stubbins, M.; Spurr, N. K.; Lai, E. H.; Mahoney, W. Multiplexed SNP Genotyping Using the Qbead() System: A Quantum Dot-Encoded Microsphere-Based Assay. *Nucleic Acids Res.* **2003**, *31*, 43e.
(106) Chang, Y.; Pinaud, F.; Antelman, J.; Weiss, S. Tracking Bio-Molecules in Live Cells Using Quantum Dots. *J. Biophotonics* **2008**, *1*, 287−298.
(107) Pinaud, F.; Clarke, S.; Sittner, A.; Dahan, M. Probing Cellular Events, One Quantum Dot at a Time. *Nat. Methods* **2010**, *7*, 275−285.
(108) Clarke, S.; Pinaud, F.; Beutel, O.; You, C. J.; Piehler, J.; Dahan, M. Covalent Monofunctionalization of Peptide-Coated Quantum Dots for Single-Molecule Assays. *Nano Lett.* **2010**, *10*, 2147−2154.

DOI: 10.1021/acsnano.6b06040
ACS Nano 2017, 11, 2313−2381

(109) Hoshino, A.; Hanaki, K.-i.; Suzuki, K.; Yamamoto, K. Applications of T-Lymphoma Labeled with Fluorescent Quantum Dots to Cell Tracing Markers in Mouse Body. *Biochem. Biophys. Res. Commun.* **2004**, *314*, 46−53.
(110) Parak, W. J.; Boudreau, R.; Le Gros, M.; Gerion, D.; Zanchet, D.; Micheel, C. M.; Williams, S. C.; Alivisatos, A. P.; Larabell, C. A. Cell Motility and Metastatic Potential Studies Based on Quantum Dot Imaging of Phagokinetic Tracks. *Adv. Mater.* **2002**, *14*, 882−885.
(111) Pinaud, F.; King, D.; Moore, H.-P.; Weiss, S. Bioactivation and Cell Targeting of Semiconductor CdSe/ZnS Nanocrystals with Phytochelatin-Related Peptides. *J. Am. Chem. Soc.* **2004**, *126*, 6115−6123.
(112) Wang, G. F.; Peng, Q.; Li, Y. D. Lanthanide-Doped Nanocrystals: Synthesis, Optical-Magnetic Properties, and Applications. *Acc. Chem. Res.* **2011**, *44*, 322−332.
(113) Wisser, M. D.; Chea, M.; Lin, Y.; Wu, D. M.; Mao, W. L.; Salleo, A.; Dionne, J. A. Strain-Induced Modification of Optical Selection Rules in Lanthanide-Based Upconverting Nanoparticles. *Nano Lett.* **2015**, *15*, 1891−1897.
(114) Escudero, A.; Carrillo-Carrión, C.; Zyuzin, M. V.; Ashraf, S.; Hartmann, R.; Núñez, N. O.; Ocaña, M.; Parak, W. J. Synthesis and Functionalization of Monodispers near-Ultraviolet and Visible Excitable Multifunctional Eu^{3+}, Bi^{3+}:$REVO_4$ Nanophosphors for Bioimaging and Biosensing Applications. *Nanoscale* **2016**, *8*, 12221−12236.
(115) Li, H.; He, X.; Kang, Z.; Huang, H.; Liu, Y.; Liu, J.; Lian, S.; Tsang, C. H. A.; Yang, X.; Lee, S.-T. Water-Soluble Fluorescent Carbon Quantum Dots and Photocatalyst Design. *Angew. Chem., Int. Ed.* **2010**, *49*, 4430−4434.
(116) Sahu, S.; Behera, B.; Maiti, T. K.; Mohapatra, S. Simple One-Step Synthesis of Highly Luminescent Carbon Dots from Orange Juice: Application as Excellent Bio-Imaging Agents. *Chem. Commun.* **2012**, *48*, 8835−8837.
(117) Wang, K.; Gao, Z. C.; Gao, G.; Wo, Y.; Wang, Y. X.; Shen, G. X.; Cui, D. X. Systematic Safety Evaluation on Photoluminescent Carbon Dots. *Nanoscale Res. Lett.* **2013**, *8*, 122.
(118) Mochalin, V. N.; Shenderova, O.; Ho, D.; Gogotsi, Y. The Properties and Applications of Nanodiamonds. *Nat. Nanotechnol.* **2011**, *7*, 11−23.
(119) Chow, E. K.; Zhang, X. Q.; Chen, M.; Lam, R.; Robinson, E.; Huang, H. J.; Schaffer, D.; Osawa, E.; Goga, A.; Ho, D. Nanodiamond Therapeutic Delivery Agents Mediate Enhanced Chemoresistant Tumor Treatment. *Sci. Transl. Med.* **2011**, *3*, 73ra21.
(120) Chang, Y. R.; Lee, H. Y.; Chen, K.; Chang, C. C.; Tsai, D. S.; Fu, C. C.; Lim, T. S.; Tzeng, Y. K.; Fang, C. Y.; Han, C. C.; Chang, H. C.; Fann, W. Mass Production and Dynamic Imaging of Fluorescent Nanodiamonds. *Nat. Nanotechnol.* **2008**, *3*, 284−288.
(121) Wu, Y.; Jelezko, F.; Plenio, M. B.; Weil, T. Diamond Quantum Devices in Biology. *Angew. Chem., Int. Ed.* **2016**, *55*, 6586−6598.
(122) Mochalin, V. N.; Gogotsi, Y. Wet Chemistry Route to Hydrophobic Blue Fluorescent Nanodiamond. *J. Am. Chem. Soc.* **2009**, *131*, 4594−4595.
(123) Soo Choi, H.; Liu, W.; Misra, P.; Tanaka, E.; Zimmer, J. P.; Itty Ipe, B.; Bawendi, M. G.; Frangioni, J. V. Renal Clearance of Quantum Dots. *Nat. Biotechnol.* **2007**, *25*, 1165−1170.
(124) Liu, J.; Yu, M.; Ning, X.; Zhou, C.; Yang, S.; Zheng, J. PEGylation and Zwitterionization: Pros and Cons in the Renal Clearance and Tumor Targeting of Near-IR-Emitting Gold Nanoparticles. *Angew. Chem., Int. Ed.* **2013**, *52*, 12572−12576.
(125) Mochalin, V. N.; Pentecost, A.; Li, X. M.; Neitzel, I.; Nelson, M.; Wei, C. Y.; He, T.; Guo, F.; Gogotsi, Y. Adsorption of Drugs on Nanodiamond: Toward Development of a Drug Delivery Platform. *Mol. Pharmaceutics* **2013**, *10*, 3728−3735.
(126) Giammarco, J.; Mochalin, V. N.; Haeckel, J.; Gogotsi, Y. The Adsorption of Tetracycline and Vancomycin onto Nanodiamond with Controlled Release. *J. Colloid Interface Sci.* **2016**, *468*, 253−261.
(127) Semmling, M.; Kreft, O.; Muñoz Javier, A.; Sukhorukov, G. B.; Käs, J.; Parak, W. J. A Novel Flow-Cytometry-based Assay for Cellular Uptake Studies of Polyelectrolyte Microcapsules. *Small* **2008**, *4*, 1763−1768.
(128) Hartmann, R.; Weidenbach, M.; Neubauer, M.; Fery, A.; Parak, W. J. Stiffness-Dependent *in Vitro* Uptake and Lysosomal Acidification of Colloidal Particles. *Angew. Chem., Int. Ed.* **2015**, *54*, 1365−1368.
(129) Riedinger, A.; Zhang, F.; Dommershausen, F.; Röcker, C.; Brandholt, S.; Nienhaus, G. U.; Koert, U.; Parak, W. J. Ratiometric Optical Sensing of Chloride Ions with Organic Fluorophore - Gold Nanoparticle Hybrids: A Systematic Study of Distance Dependency and the Influence of Surface Charge. *Small* **2010**, *6*, 2590−2597.
(130) Kantner, K.; Ashraf, S.; Carregal-Romero, S.; Carrillo-Carrion, C.; Collot, M.; del Pino, P.; Heimbrodt, W.; Jimenez de Aberasturi, D.; Kaiser, U.; Kazakova, L. I.; Lelle, M.; Martinez de Baroja, N.; Montenegro, J.-M.; Nazarenus, M.; Pelaz, B.; Peneva, K.; Rivera Gil, P.; Sabir, N.; Schneider, L. M.; Shabarchina, L. I.; et al. Particle-Based Optical Sensing of Intracellular Ions at the Example of Calcium - What are the Experimental Pitfalls? *Small* **2015**, *11*, 896−904.
(131) Shi, H. B.; Kwok, R. T. K.; Liu, J. Z.; Xing, B. G.; Tang, B. Z.; Liu, B. Real-Time Monitoring of Cell Apoptosis and Drug Screening Using Fluorescent Light-Up Probe with Aggregation-Induced Emission Characteristics. *J. Am. Chem. Soc.* **2012**, *134*, 17972−17981.
(132) Zhou, K.; Liu, H.; Zhang, S.; Huang, X.; Wang, Y.; Huang, G.; Sumer, B. D.; Gao, J. Multicolored pH-Tunable and Activatable Fluorescence Nanoplatform Responsive to Physiologic pH Stimuli. *J. Am. Chem. Soc.* **2012**, *134*, 7803−7811.
(133) Wang, Y.; Zhou, K.; Huang, G.; Hensley, C.; Huang, X.; Ma, X.; Zhao, T.; Sumer, B. D.; DeBerardinis, R. J.; Gao, J. A Nanoparticle-Based Strategy for the Imaging of a Broad Range of Tumours by Nonlinear Amplification of Microenvironment Signals. *Nat. Mater.* **2013**, *13*, 204−212.
(134) Leuvering, J. H. W.; Thal, P. J. H. M.; Waart, M. v. d.; Schuurs, A. H. W. M. Sol Particle Agglutination Immunoassay For Human Chorionic-Gonadotropin. *Fresenius' Z. Anal. Chem.* **1980**, *301*, 132.
(135) Leuvering, J. H. W.; Thal, P.; Vanderwaart, M.; Schuurs, A. A Sol Particle Agglutination Assay For Human Chorionic-Gonadotropin. *J. Immunol. Methods* **1981**, *45*, 183−194.
(136) Elghanian, R.; Storhoff, J. J.; Mucic, R. C.; Letsinger, R. L.; Mirkin, C. A. Selective Colorimetric Detection of Polynucleotides Based on the Distance-Dependent Optical Properties of Gold Nanoparticles. *Science* **1997**, *277*, 1078−1081.
(137) Stehr, J.; Hrelescu, C.; Sperling, R. A.; Raschke, G.; Wunderlich, M.; Nichtl, A.; Heindl, D.; Kürzinger, K.; Parak, W. J.; Klar, T. A.; Feldmann, J. Gold Nano-Stoves for Microsecond DNA Melting Analysis. *Nano Lett.* **2008**, *8*, 619−623.
(138) Xu, X. Y.; Daniel, W. L.; Wei, W.; Mirkin, C. A. Colorimetric Cu^{2+} Detection Using DNA-Modified Gold-Nanoparticle Aggregates as Probes and Click Chemistry. *Small* **2010**, *6*, 623−626.
(139) Meng, Z. J.; Song, R. H.; Chen, Y.; Zhu, Y.; Tian, Y. H.; Li, D.; Cui, D. X. Rapid Screening and Identification of Dominant B Cell Epitopes of HBV Surface Antigen by Quantum Dot-Based Fluorescence Polarization Assay. *Nanoscale Res. Lett.* **2013**, *8*, 118.
(140) Han, M.; Gao, X.; Su, J. Z.; Nie, S. Quantum-Dot-Tagged Microbeads for Multiplexed Optical Coding of Biomolecules. *Nat. Biotechnol.* **2001**, *19*, 631−635.
(141) Wang, D.; Rogach, A. L.; Caruso, F. Semiconductor Quantum Dot-Labeled Microsphere Bioconjugates Prepared by Stepwise Self-Assembly. *Nano Lett.* **2002**, *2*, 857−861.
(142) Sheng, W.; Kim, S.; Lee, J.; Kim, S. W.; Jensen, K.; Bawendi, M. G. *In-Situ* Encapsulation of Quantum Dots into Polymer Microspheres. *Langmuir* **2006**, *22*, 3782−3790.
(143) O'Brien, P.; Cummins, S. S.; Darcy, D.; Dearden, A.; Masala, O.; Pickett, N. L.; Ryley, S.; Sutherland, A. J. Quantum Dot-Labelled Polymer Beads by Suspension Polymerisation. *Chem. Commun.* **2003**, 2532−2533.
(144) Fournier-Bidoz, S.; Jennings, T. L.; Klostranec, J. M.; Fung, W.; Rhee, A.; Li, D.; Chan, W. C. W. Facile and Rapid One-Step Mass Preparation of Quantum-Dot Barcodes. *Angew. Chem., Int. Ed.* **2008**, *47*, 5577−5581.
(145) Wang, G.; Leng, Y. K.; Dou, H. J.; Wang, L.; Li, W. W.; Wang, X. B.; Sun, K.; Shen, L. S.; Yuan, X. L.; Li, J. Y.; Sun, K.; Han, J. S.; Xiao, H. S.; Li, Y. Highly Efficient Preparation of Multiscaled Quantum Dot

DOI: 10.1021/acsnano.6b06040
ACS Nano 2017, 11, 2313−2381

Barcodes for Multiplexed Hepatitis B Detection. *ACS Nano* **2013**, *7*, 471−481.
(146) Chen, K.; Chou, L. Y. T.; Song, F. Y.; Chan, W. C. W. Fabrication of Metal Nanoshell Quantum-Dot Barcodes for Biomolecular Detection. *Nano Today* **2013**, *8*, 228−234.
(147) Lee, J. A.; Mardyani, S.; Hung, A.; Rhee, A.; Klostranec, J.; Mu, Y.; Li, D.; Chan, W. C. W. Toward the Accurate Read-out of Quantum Dot Barcodes: Design of Deconvolution Algorithms and Assessment of Fluorescence Signals in Buffer. *Adv. Mater.* **2007**, *19*, 3113−3118.
(148) Giri, S.; Sykes, E. A.; Jennings, T. L.; Chan, W. C. Rapid Screening of Genetic Biomarkers of Infectious Agents Using Quantum Dot Barcodes. *ACS Nano* **2011**, *5*, 1580−1587.
(149) Ming, K.; Kim, J.; Biondi, M. J.; Syed, A.; Chen, K.; Lam, A.; Ostrowski, M.; Rebbapragada, A.; Feld, J. J.; Chan, W. C. W. Integrated Quantum Dot Barcode Smartphone Optical Device for Wireless Multiplexed Diagnosis of Infected Patients. *ACS Nano* **2015**, *9*, 3060−3074.
(150) Kim, J.; Biondi, M. J.; Feld, J. J.; Chan, W. C. W. Clinical Validation of Quantum Dot Barcode Diagnostic Technology. *ACS Nano* **2016**, *10*, 4742−4753.
(151) Pregibon, D. C.; Toner, M.; Doyle, P. S. Multifunctional Encoded Particles for High-Throughput Biomolecule Analysis. *Science* **2007**, *315*, 1393−1396.
(152) Fenniri, H.; Chun, S.; Ding, L. H.; Zyrianov, Y.; Hallenga, K. Preparation, Physical Properties, on-Bead Binding Assay and Spectroscopic Reliability of 25 Barcoded Polystyrene-Poly(ethylene Glycol) Graft Copolymers. *J. Am. Chem. Soc.* **2003**, *125*, 10546−10560.
(153) Pan, W. Y.; Chen, W.; Jiang, X. Y. Microfluidic Western Blot. *Anal. Chem.* **2010**, *82*, 3974−3976.
(154) Zhang, Y.; Zhang, L.; Sun, J.; Liu, Y.; Ma, X.; Cui, S.; Ma, L.; Xi, J. J.; Jiang, X. Point-of-Care Multiplexed Assays of Nucleic Acids Using Microcapillary-based Loop-Mediated Isothermal Amplification. *Anal. Chem.* **2014**, *86*, 7057−7062.
(155) Zhang, Y.; Sun, J.; Zou, Y.; Chen, W.; Zhang, W.; Xi, J. J.; Jiang, X. Barcoded Microchips for Biomolecular Assays. *Anal. Chem.* **2015**, *87*, 900−906.
(156) Anslyn, E. V.; Rotello, V. M. Chemosensory Models: Approaches and Applications of Differential Sensing Editorial Overview. *Curr. Opin. Chem. Biol.* **2010**, *14*, 683−684.
(157) De, M.; Rana, S.; Akpinar, H.; Miranda, O. R.; Arvizo, R. R.; Bunz, U. H. F.; Rotello, V. M. Sensing of Proteins in Human Serum Using Conjugates of Nanoparticles and Green Fluorescent Protein. *Nat. Chem.* **2009**, *1*, 461−465.
(158) Miranda, O. R.; Li, X. N.; Garcia-Gonzalez, L.; Zhu, Z. J.; Yan, B.; Bunz, U. H. F.; Rotello, V. M. Colorimetric Bacteria Sensing Using a Supramolecular Enzyme-Nanoparticle Biosensor. *J. Am. Chem. Soc.* **2011**, *133*, 9650−9653.
(159) Bajaj, A.; Miranda, O.; Kim, I.; Phillips, R.; Jerry, D.; Bunz, U.; Rotello, V. Detection and Differentiation of Normal, Cancerous, and Metastatic Cells Using Nanoparticle-Polymer Sensor Arrays. *Proc. Natl. Acad. Sci. U. S. A.* **2009**, *106*, 10912−10916.
(160) Rana, S.; Le, N. D. B.; Mout, R.; Saha, K.; Tonga, G. Y.; Bain, R. E. S.; Miranda, O. R.; Rotello, C. M.; Rotello, V. M. A Multichannel Nanosensor for Instantaneous Readout of Cancer Drug Mechanisms. *Nat. Nanotechnol.* **2014**, *10*, 65−69.
(161) Li, X. N.; Kong, H.; Mout, R.; Saha, K.; Moyano, D. F.; Robinson, S. M.; Rana, S.; Zhang, X. R.; Riley, M. A.; Rotello, V. M. Rapid Identification of Bacterial Biofilms and Biofilm Wound Models Using a Multichannel Nanosensor. *ACS Nano* **2014**, *8*, 12014−12019.
(162) Stark, W. J. Nanoparticles in Biological Systems. *Angew. Chem., Int. Ed.* **2011**, *50*, 1242−1258.
(163) Wegner, K. D.; Hildebrandt, N. Quantum Dots: Bright and Versatile *in Vitro* and *in Vivo* Fluorescence Imaging Biosensors. *Chem. Soc. Rev.* **2015**, *44*, 4792−834.
(164) Ruedas-Rama, M. J.; Walters, J. D.; Orte, A.; Hall, E. A. H. Fluorescent Nanoparticles for Intracellular Sensing: A Review. *Anal. Chim. Acta* **2012**, *751*, 1−23.
(165) Gill, R.; Zayats, M.; Willner, I. Semiconductor Quantum Dots for Bioanalysis. *Angew. Chem., Int. Ed.* **2008**, *47*, 7602−7625.
(166) Freeman, R.; Willner, B.; Willner, I. Integrated Biomolecule-Quantum Dot Hybrid Systems for Bioanalytical Applications. *J. Phys. Chem. Lett.* **2011**, *2*, 2667−2677.
(167) Medintz, I. L.; Stewart, M. H.; Trammell, S. A.; Susumu, K.; Delehanty, J. B.; Mei, B. C.; Melinger, J. S.; Blanco-Canosa, J. B.; Dawson, P. E.; Mattoussi, H. Quantum-Dot/Dopamine Bioconjugates Function as Redox Coupled Assemblies for *in Vitro* and Intracellular pH Sensing. *Nat. Mater.* **2010**, *9*, 676−684.
(168) Li, D.-W.; Qin, L.-X.; Li, Y.; Nia, R. P.; Long, Y.-T.; Chen, H.-Y. CdSe/ZnS Quantum Dot−Cytochrome c Bioconjugates for Selective Intracellular $O_2\bullet^-$ Sensing. *Chem. Commun.* **2011**, *47*, 8539−8541.
(169) Freeman, R.; Gill, R.; Shweky, I.; Kotler, M.; Banin, U.; Willner, I. Biosensing and Probing of Intracellular Metabolic Pathways by NADH-Sensitive Quantum Dots. *Angew. Chem., Int. Ed.* **2009**, *48*, 309−313.
(170) Du, F.; Ming, Y.; Zeng, F.; Yu, C.; Wu, S. A Low Cytotoxic and Ratiometric Fluorescent Nanosensor Based on Carbon-Dots for Intracellular pH Sensing and Mapping. *Nanotechnology* **2013**, *24*, 365101.
(171) Zhang, F.; Lees, E.; Amin, F.; Rivera-Gil, P.; Yang, F.; Mulvaney, P.; Parak, W. J. Polymer-Coated Nanoparticles: A Universal Tool for Biolabelling Experiments. *Small* **2011**, *7*, 3113−3127.
(172) Shi, W.; Li, X.; Ma, H. A Tunable Ratiometric pH Sensor Based on Carbon Nanodots for the Quantitative Measurement of the Intracellular pH of Whole Cells. *Angew. Chem., Int. Ed.* **2012**, *51*, 6432−6435.
(173) Kong, B.; Zhu, A.; Ding, C.; Zhao, X.; Li, B.; Tian, Y. Carbon Dot-Based Inorganic−Organic Nanosystem for Two-Photon Imaging and Biosensing of pH Variation in Living Cells and Tissues. *Adv. Mater.* **2012**, *24*, 5844−5848.
(174) Izumi, H.; Torigoe, T.; Ishiguchi, H.; Uramoto, H.; Yoshida, Y.; Tanabe, M.; Ise, T.; Murakami, T.; Yoshida, T.; Nomoto, M.; Kohno, K. Cellular pH Regulators: Potentially Promising Molecular Targets for Cancer Chemotherapy. *Cancer Treat. Rev.* **2003**, *29*, 541−549.
(175) Davies, T. A.; Fine, R. E.; Johnson, R. J.; Levesque, C. A.; Rathbun, W. H.; Seetoo, K. F.; Smith, S. J.; Strohmeier, G.; Volicer, L.; Delva, L.; Simons, E. R. Non-Age Related Differences in Thrombin Responses by Platelets from Male Patients with Advanced Alzheimer's Disease. *Biochem. Biophys. Res. Commun.* **1993**, *194*, 537−543.
(176) Jiang, Y.; Wang, Z.; Dai, Z. Preparation of Silicon−Carbon-Based Dots@Dopamine and Its Application in Intracellular Ag+ Detection and Cell Imaging. *ACS Appl. Mater. Interfaces* **2016**, *8*, 3644−3650.
(177) Zhang, Z.; Shi, Y.; Pan, Y.; Cheng, X.; Zhang, L.; Chen, J.; Li, M.-J.; Yi, C. Quinoline Derivative-Functionalized Carbon Dots as a Fluorescent Nanosensor for Sensing and Intracellular Imaging of Zn^{2+}. *J. Mater. Chem. B* **2014**, *2*, 5020−5027.
(178) Koo, Y. E. L.; Cao, Y. F.; Kopelman, R.; Koo, S. M.; Brasuel, M.; Philbert, M. A. Real-Time Measurements of Dissolved Oxygen inside Live Cells by Organically Modified Silicate Fluorescent Nanosensors. *Anal. Chem.* **2004**, *76*, 2498−2505.
(179) Wu, S.; Li, Z.; Han, J.; Han, S. Dual Colored Mesoporous Silica Nanoparticles with pH Activable Rhodamine-Lactam for Ratiometric Sensing of Lysosomal Acidity. *Chem. Commun.* **2011**, *47*, 11276−11278.
(180) He, C.; Zhu, W.; Xu, Y.; Zhong, Y.; Zhou, J.; Qian, X. Ratiometric and Reusable Fluorescent Nanoparticles for Zn^{2+} and $H_2PO_4^-$ Detection in Aqueous Solution and Living Cells. *J. Mater. Chem.* **2010**, *20*, 10755−10764.
(181) Peng, J.; He, X.; Wang, K.; Tan, W.; Wang, Y.; Liu, Y. Noninvasive Monitoring of Intracellular pH Change Induced by Drug Stimulation Using Silica Nanoparticle Sensors. *Anal. Bioanal. Chem.* **2007**, *388*, 645−654.
(182) Park, E. J.; Brasuel, M.; Behrend, C.; Philbert, M. A.; Kopelman, R. Ratiometric Optical PEBBLE Nanosensors for Real-Time Magnesium Ion Concentrations Inside Viable Cells. *Anal. Chem.* **2003**, *75*, 3784−3791.
(183) Sumner, J.; Aylott, J. W.; Monson, E.; Kopelman, R. A Fluorescent PEBBLE Nanosensor for Intracellular Free Zinc. *Analyst* **2002**, *127*, 11−16.

DOI: 10.1021/acsnano.6b06040
ACS Nano 2017, 11, 2313−2381

(184) Seo, S.; Lee, H. Y.; Park, M.; Lim, J. M.; Kang, D.; Yoon, J.; Jung, J. H. Fluorescein-Functionalized Silica Nanoparticles as a Selective Fluorogenic Chemosensor for Cu^{2+} in Living Cells. *Eur. J. Inorg. Chem.* **2010**, *2010*, 843−847.
(185) Oh, W.-K.; Jeong, Y. S.; Kim, S.; Jang, J. Fluorescent Polymer Nanoparticle for Selective Sensing of Intracellular Hydrogen Peroxide. *ACS Nano* **2012**, *6*, 8516−8524.
(186) Kim, S.-H.; Kim, B.; Yadavalli, V. K.; Pishko, M. V. Encapsulation of Enzymes within Polymer Spheres To Create Optical Nanosensors for Oxidative Stress. *Anal. Chem.* **2005**, *77*, 6828−6833.
(187) Xu, H.; Aylott, J. W.; Kopelman, R. Fluorescent Nano-PEBBLE Sensors for the Real-Time Measurement of Glucose Inside Living Cells. *Analyst* **2002**, *127*, 1471−1477.
(188) Chapman, R.; Lin, Y.; Burnapp, M.; Bentham, A.; Hillier, D.; Zabron, A.; Khan, S.; Tyreman, M.; Stevens, M. M. Multivalent Nanoparticle Networks Enable Point-of-Care Detection of Human Phospholipase-A2 in Serum. *ACS Nano* **2015**, *9*, 2565−2573.
(189) Valentini, P.; Fiammengo, R.; Sabella, S.; Gariboldi, M.; Maiorano, G.; Cingolani, R.; Pompa, P. P. Gold-Nanoparticle-Based Colorimetric Discrimination of Cancer-Related Point Mutations with Picomolar Sensitivity. *ACS Nano* **2013**, *7*, 5530−5538.
(190) Aili, D.; Mager, M.; Roche, D.; Stevens, M. M. Hybrid Nanoparticle-Liposome Detection of Phospholipase Activity. *Nano Lett.* **2011**, *11*, 1401−1405.
(191) Liu, G. D.; Mao, X.; Phillips, J. A.; Xu, H.; Tan, W. H.; Zeng, L. W. Aptamer-Nanoparticle Strip Biosensor for Sensitive Detection of Cancer Cells. *Anal. Chem.* **2009**, *81*, 10013−10018.
(192) Endo, T.; Kerman, K.; Nagatani, N.; Hiepa, H. M.; Kim, D.-K.; Yonezawa, Y.; Nakano, K.; Tamiya, E. Multiple Label-Free Detection of Antigen-Antibody Reaction Using Localized Surface Plasmon Resonance-Based Core-Shell Structured Nanoparticle Layer Nanochip. *Anal. Chem.* **2006**, *78*, 6465−6475.
(193) Leuvering, J. H. W.; Thal, P.; Schuurs, A. Optimization Of A Sandwich Sol Particle Immunoassay For Human Chorionic-Gonadotropin. *J. Immunol. Methods* **1983**, *62*, 175−184.
(194) Storhoff, J. J.; Elghanian, R.; Mucic, R. C.; Mirkin, C. A.; Letsinger, R. L. One-Pot Colorimetric Differentiation of Polynucleotides with Single Base Imperfections Using Gold Nanoparticle Probes. *J. Am. Chem. Soc.* **1998**, *120*, 1959−1964.
(195) Reynolds, R. A.; Mirkin, C. A.; Letsinger, R. L. Homogeneous, Nanoparticle-Based Quantitative Colorimetric Detection of Oligonucleotides. *J. Am. Chem. Soc.* **2000**, *122*, 3795−3796.
(196) Qin, Z. P.; Chan, W. C. W.; Boulware, D. R.; Akkin, T.; Butler, E. K.; Bischof, J. C. Significantly Improved Analytical Sensitivity of Lateral Flow Immunoassays by Using Thermal Contrast. *Angew. Chem., Int. Ed.* **2012**, *51*, 4358−4361.
(197) Polo, E.; del Pino, P.; Pelaz, B.; Grazu, V.; de la Fuente, J. M. Plasmonic-Driven Thermal Sensing: Ultralow Detection of Cancer Markers. *Chem. Commun.* **2013**, *49*, 3676−3678.
(198) Chen, W.; Bian, A.; Agarwal, A.; Liu, L.; Shen, H.; Wang, L.; Xu, C.; Kotov, N. A. Nanoparticle Superstructures Made by Polymerase Chain Reaction: Collective Interactions of Nanoparticles and a New Principle for Chiral Materials. *Nano Lett.* **2009**, *9*, 2153−2159.
(199) Ma, M.; Kuang, H.; Xu, L.; Ding, L.; Xu, C.; Wang, L.; Kotov, N. A. Attomolar DNA Detection with Chiral Nanorod Assemblies. *Nature Comm* **2013**, *4*, 2689.
(200) Zhao, Y.; Xu, L.; Ma, W.; Wang, L.; Kuang, H.; Xu, C.; Kotov, N. A. Shell-Engineered Chiroplasmonic Assemblies of Nanoparticles for Zeptomolar DNA Detection. *Nano Lett.* **2014**, *14*, 3908−3913.
(201) Ma, M.; Kuang, H.; Xu, L.; Ding, L.; Xu, C.; Wang, L.; Kotov, N. A. Attomolar DNA Detection with Chiral Nanorod Assemblies. *Nature Comm.* **2013**, *4*, 2689.
(202) Wu, X.; Xu, L.; Liu, L.; Ma, W.; Yin, H.; Kuang, H.; Wang, L.; Xu, C.; Kotov, N.A. Unexpected Chirality of Nanoparticle Dimers and Ultrasensitive Chiroplasmonic Bioanalysis. *J. Am. Chem. Soc.* **2014**, *135*, 18629−18636.
(203) Li, S.; Xu, L.; Ma, W.; Wu, X.; Sun, M.; Kuang, H.; Wang, L.; Kotov, N. A.; Xu, C. Dual-Mode Ultrasensitive Quantification of MicroRNA in Living Cells by Chiroplasmonic Nanopyramids Self-Assembled from Gold and Upconversion Nanoparticles. *J. Am. Chem. Soc.* **2016**, *138*, 306−312.
(204) Alvarez-Puebla, R. A.; Zubarev, E. R.; Kotov, N. A.; Liz-Marzan, L. M. Self-Assembled Nanorod Supercrystals for Ultrasensitive SERS Diagnostics. *Nano Today* **2012**, *7*, 6−9.
(205) Alvarez-Puebla, R. A.; Agarwal, A.; Manna, P.; Khanal, B. P.; Aldeanueva-Potel, P.; Carbo-Argibay, E.; Pazos-Perez, N.; Vigderman, L.; Zubarev, E. R.; Kotov, N. A.; Liz-Marzan, L. M. Gold Nanorods 3D-Supercrystals as Surface Enhanced Raman Scattering Spectroscopy Substrates for the Rapid Detection of Scrambled Prions. *Proc. Natl. Acad. Sci. U. S. A.* **2011**, *108*, 8157−8161.
(206) Nie, S. M.; Emery, S. R. Probing Single Molecules and Single Nanoparticles by Surface-Enhanced Raman Scattering. *Science* **1997**, *275*, 1102−1106.
(207) Alvarez-Puebla, R. A.; Liz-Marzan, L. M. Traps and Cages for Universal SERS Detection. *Chem. Soc. Rev.* **2012**, *41*, 43−51.
(208) Sanles-Sobrido, M.; Rodriguez-Lorenzo, L.; Lorenzo-Abalde, S.; Gonzalez-Fernandez, A.; Correa-Duarte, M. A.; Alvarez-Puebla, R. A.; Liz-Marzan, L. M. Label-Free SERS Detection of Relevant Bioanalytes on Silver-Coated Carbon Nanotubes: The Case of Cocaine. *Nanoscale* **2009**, *1*, 153−158.
(209) Guerrini, L.; Arenal, R.; Mannini, B.; Chiti, F.; Pini, R.; Matteini, P.; Alvarez-Puebla, R. A. SERS Detection of Amyloid Oligomers on Metallorganic-Decorated Plasmonic Beads. *ACS Appl. Mater. Interfaces* **2015**, *7*, 9420−9428.
(210) Stuart, D. A.; Yuen, J. M.; Shah, N.; Lyandres, O.; Yonzon, C. R.; Glucksberg, M. R.; Walsh, J. T.; Van Duyne, R. P. *In Vivo* Glucose Measurement by Surface-Enhanced Raman Spectroscopy. *Anal. Chem.* **2006**, *78*, 7211−7215.
(211) Guerrini, L.; Rodriguez-Loureiro, I.; Correa-Duarte, M. A.; Lee, Y. H.; Ling, X. Y.; Garcia de Abajo, F. J.; Alvarez-Puebla, R. A. Chemical Speciation of Heavy Metals by Surface-Enhanced Raman Scattering Spectroscopy: Identification and Quantification of Inorganic- and Methyl-Mercury in Water. *Nanoscale* **2014**, *6*, 8368−8375.
(212) Rivera Gil, P.; Vazquez-Vazquez, C.; Giannini, V.; Callao, M. P.; Parak, W. J.; Correa-Duarte, M. A.; Alvarez-Puebla, R. A. Plasmonic Nanoprobes for Real-Time Optical Monitoring of Nitric Oxide inside Living Cells. *Angew. Chem., Int. Ed.* **2013**, *52*, 13694−13698.
(213) Kneipp, K.; Kneipp, H.; Kneipp, J. Surface-Enhanced Raman Scattering in Local Optical Fields of Silver and Gold Nanoaggregates-From Single-Molecule Raman Spectroscopy to Ultrasensitive Probing in Live Cells. *Acc. Chem. Res.* **2006**, *39*, 443−450.
(214) Milde-Langosch, K. The Fos Family of Transcription Factors and Their Role in Tumourigenesis. *Eur. J. Cancer* **2005**, *41*, 2449−2461.
(215) Guerrini, L.; Pazos, E.; Penas, C.; Vazquez, M. E.; Mascarenas, J. L.; Alvarez-Puebla, R. A. Highly Sensitive SERS Quantification of the Oncogenic Protein c-Jun in Cellular Extracts. *J. Am. Chem. Soc.* **2013**, *135*, 10314−10317.
(216) Qian, X. M.; Peng, X. H.; Ansari, D. O.; Yin-Goen, Q.; Chen, G. Z.; Shin, D. M.; Yang, L.; Young, A. N.; Wang, M. D.; Nie, S. M. *In Vivo* Tumor Targeting and Spectroscopic Detection with Surface-Enhanced Raman Nanoparticle Tags. *Nat. Biotechnol.* **2007**, *26*, 83−90.
(217) Lutz, B.; Dentinger, C.; Sun, L.; Nguyen, L.; Zhang, J.; Chmura, A.; Allen, A.; Chan, S.; Knudsen, B. Raman Nanoparticle Probes for Antibody-Based Protein Detection in Tissues. *J. Histochem. Cytochem.* **2008**, *56*, 371−379.
(218) Bodelon, G.; Montes-Garcia, V.; Fernandez-Lopez, C.; Pastoriza-Santos, I.; Perez-Juste, J.; Liz-Marzan, L. M. Au@pNIPAM SERRS Tags for Multiplex Immunophenotyping Cellular Receptors and Imaging Tumor Cells. *Small* **2015**, *11*, 4149−4157.
(219) Wang, X.; Qian, X. M.; Beitler, J. J.; Chen, Z. G.; Khuri, F. R.; Lewis, M. M.; Shin, H. J. C.; Nie, S. M.; Shin, D. M. Detection of Circulating Tumor Cells in Human Peripheral Blood Using Surface-Enhanced Raman Scattering Nanoparticles. *Cancer Res.* **2011**, *71*, 1526−1532.
(220) So, H. Y.; Lee, K.; Murthy, N.; Pisano, A. P. All-in-One Nanowire-Decorated Multifunctional Membrane for Rapid Cell Lysis and Direct DNA Isolation. *ACS Appl. Mater. Interfaces* **2014**, *6*, 20693−20699.

DOI: 10.1021/acsnano.6b06040
ACS Nano 2017, 11, 2313−2381

(221) Lu, N.; Dai, P. F.; Gao, A. R.; Valiaho, J.; Kallio, P.; Wang, Y. L.; Li, T. Label-Free and Rapid Electrical Detection of hTSH with CMOS-Compatible Silicon Nanowire Transistor Arrays. *ACS Appl. Mater. Interfaces* **2014**, *6*, 20378−20384.
(222) Cai, B. J.; Wang, S. T.; Huang, L.; Ning, Y.; Zhang, Z. Y.; Zhang, G. J. Ultrasensitive Label-Free Detection of PNA-DNA Hybridization by Reduced Graphene Oxide Field-Effect Transistor Biosensor. *ACS Nano* **2014**, *8*, 2632−2638.
(223) Kulkarni, G. S.; Zhong, Z. H. Detection beyond the Debye Screening Length in a High-Frequency Nanoelectronic Biosensor. *Nano Lett.* **2012**, *12*, 719−723.
(224) Dorvel, B. R.; Reddy, B.; Go, J.; Duarte Guevara, C.; Salm, E.; Alam, M. A.; Bashir, R. Silicon Nanowires with High-k Hafnium Oxide Dielectrics for Sensitive Detection of Small Nucleic Acid Oligomers. *ACS Nano* **2012**, *6*, 6150−6164.
(225) Chua, J. H.; Chee, R. E.; Agarwal, A.; Wong, S. M.; Zhang, G. J. Label-Free Electrical Detection of Cardiac Biomarker with Complementary Metal-Oxide Semiconductor-Compatible Silicon Nanowire Sensor Arrays. *Anal. Chem.* **2009**, *81*, 6266−6271.
(226) Bangar, M. A.; Shirale, D. J.; Chen, W.; Myung, N. V.; Mulchandani, A. Single Conducting Polymer Nanowire Chemiresistive Label-Free Immunosensor for Cancer Biomarker. *Anal. Chem.* **2009**, *81*, 2168−2175.
(227) Gao, Z. Q.; Agarwal, A.; Trigg, A. D.; Singh, N.; Fang, C.; Tung, C. H.; Fan, Y.; Buddharaju, K. D.; Kong, J. M. Silicon Nanowire Arrays for Label-Free Detection of DNA. *Anal. Chem.* **2007**, *79*, 3291−3297.
(228) Arter, J. A.; Taggart, D. K.; McIntire, T. M.; Penner, R. M.; Weiss, G. A. Virus-PEDOT Nanowires for Biosensing. *Nano Lett.* **2010**, *10*, 4858−4862.
(229) Arter, J. A.; Diaz, J. E.; Donavan, K. C.; Yuan, T.; Penner, R. M.; Weiss, G. A. Virus-Polymer Hybrid Nanowires Tailored to Detect Prostate-Specific Membrane Antigen. *Anal. Chem.* **2012**, *84*, 2776−2783.
(230) Gao, N.; Zhou, W.; Jiang, X. C.; Hong, G. S.; Fu, T. M.; Lieber, C. M. General Strategy for Biodetection in High Ionic Strength Solutions Using Transistor-Based Nanoelectronic Sensors. *Nano Lett.* **2015**, *15*, 2143−2148.
(231) Li, J. S.; Zhang, Y. L.; To, S.; You, L. D.; Sun, Y. Effect of Nanowire Number, Diameter, and Doping Density on Nano-FET Biosensor Sensitivity. *ACS Nano* **2011**, *5*, 6661−6668.
(232) Mu, L. Y.; Droujinine, I. A.; Rajan, N. K.; Sawtelle, S. D.; Reed, M. A. Direct, Rapid, and Label-Free Detection of Enzyme Substrate Interactions in Physiological Buffers Using CMOS-Compatible Nanoribbon Sensors. *Nano Lett.* **2014**, *14*, 5315−5322.
(233) Duan, X. X.; Rajan, N. K.; Routenberg, D. A.; Huskens, J.; Reed, M. A. Regenerative Electronic Biosensors Using Supramolecular Approaches. *ACS Nano* **2013**, *7*, 4014−4021.
(234) Bergveld, P. Development, Operation, and Application of the Ion-Sensitive Field-Effect Transistor as a Tool for Electrophysiology. *IEEE Trans. Biomed. Eng.* **1972**, *BME-19*, 342−351.
(235) Bergveld, P. The Development and Application of FET-based Biosensors. *Biosensors* **1986**, *2*, 15−33.
(236) van der Schoot, B. H.; Bergveld, P. ISFET Based Enzyme Sensors. *Biosensors* **1987**, *3*, 161−186.
(237) Stern, E.; Wagner, R.; Sigworth, F. J.; Breaker, R.; Fahmy, T. M.; Reed, M. A. Importance of the Debye Screening Length on Nanowire Field Effect Transistor Sensors. *Nano Lett.* **2007**, *7*, 3405−3409.
(238) Kim, J.; Rim, Y. S.; Chen, H.; Cao, H. H.; Nakatsuka, N.; Hinton, H. L.; Zhao, C.; Andrews, A. M.; Yang, Y.; Weiss, P. S. Fabrication of High-Performance Ultrathin In203 Film Field-Effect Transistors and Biosensors Using Chemical Lift-Off Lithography. *ACS Nano* **2015**, *9*, 4572−4582.
(239) Rim, Y. S.; Bae, S.-H.; Chen, H.; Yang, J. L.; Kim, J.; Andrews, A. M.; Weiss, P. A.; Yang, Y.; Tseng, H.-R. Printable Ultrathin Metal Oxide Semiconductor-Based Conformal Biosensors. *ACS Nano* **2015**, *9*, 12174−12181.
(240) Gangopadhyay, R.; Chowdhury, A. D.; De, A. Functionalized Polyaniline Nanowires for Biosensing. *Sens. Actuators, B* **2012**, *171*, 777−785.
(241) Penner, R. M. Chemical Sensing with Nanowires. *Annu. Rev. Anal. Chem.* **2012**, *5*, 461−485.
(242) Luo, X. L.; Lee, I.; Huang, J. Y.; Yun, M. H.; Cui, X. Y. T. Ultrasensitive Protein Detection Using an Aptamer-Functionalized Single Polyaniline Nanowire. *Chem. Commun.* **2011**, *47*, 6368−6370.
(243) Fan, Y.; Chen, X. T.; Trigg, A. D.; Tung, C. H.; Kong, J. M.; Gao, Z. Q. Detection of microRNAs Using Target-Guided Formation of Conducting Polymer Nanowires in Nanogaps. *J. Am. Chem. Soc.* **2007**, *129*, 5437−5443.
(244) Bangar, M. A.; Chen, W.; Myung, N. V.; Mulchandani, A. Conducting Polymer 1-Dimensional Nanostructures for FET Sensors. *Thin Solid Films* **2010**, *519*, 964−973.
(245) Shirale, D. J.; Bangar, M. A.; Chen, W.; Myung, N. V.; Mulchandani, A. Effect of Aspect Ratio (Length:Diameter) on a Single Polypyrrole Nanowire FET Device. *J. Phys. Chem. C* **2010**, *114*, 13375−13380.
(246) Zelada-Guillen, G. A.; Riu, J.; Duzgun, A.; Rius, F. X. Immediate Detection of Living Bacteria at Ultralow Concentrations Using a Carbon Nanotube Based Potentiometric Aptasensor. *Angew. Chem., Int. Ed.* **2009**, *48*, 7334−7337.
(247) Liu, G. D.; Lin, Y. Y.; Wang, J.; Wu, H.; Wai, C. M.; Lin, Y. H. Disposable Electrochemical Immunosensor Diagnosis Device Based on Nanoparticle Probe and Immunochromatographic Strip. *Anal. Chem.* **2007**, *79*, 7644−7653.
(248) Chikkaveeraiah, B. V.; Bhirde, A. A.; Morgan, N. Y.; Eden, H. S.; Chen, X. Y. Electrochemical Immunosensors for Detection of Cancer Protein Biomarkers. *ACS Nano* **2012**, *6*, 6546−6561.
(249) Stoll, C.; Kudera, S.; Parak, W. J.; Lisdat, F. Quantum Dots on Gold:Electrodes For Photoswitchable Cytochrome c Electrochemistry. *Small* **2006**, *2*, 741−743.
(250) Katz, E.; Zayats, M.; Willner, I.; Lisdat, F. Controlling the Direction of Photocurrents by Means of CdS Nanoparticles and Cytochrome c-Mediated Biocatalytic Cascades. *Chem. Commun.* **2006**, 1395−1397.
(251) Stoll, C.; Gehring, C.; Schubert, K.; Zanella, M.; Parak, W. J.; Lisdat, F. Photoelectrochemical Signal Chain Based on Quantum Dots on Gold-Sensitive to Superoxide Radicals in Solution. *Biosens. Bioelectron.* **2008**, *24*, 260−265.
(252) Khalid, W.; El Helou, M.; Murböck, T.; Yue, Z.; Montenegro, J.-M.; Schubert, K.; Göbel, G.; Lisdat, F.; Witte, G.; Parak, W. J. Immobilization of Quantum Dots *via* Conjugated Self-Assembled Monolayers and Their Application as a Light-Controlled Sensor for the Detection of Hydrogen Peroxide. *ACS Nano* **2011**, *5*, 9870−9876.
(253) Yue, Z.; Lisdat, F.; Parak, W. J.; Hickey, S. G.; Tu, L. P.; Sabir, N.; Dorfs, D.; Bigall, N. C. Quantum-Dot-Based Photoelectrochemical Sensors for Chemical and Biological Detection. *ACS Appl. Mater. Interfaces* **2013**, *5*, 2800−2814.
(254) Sabir, N.; Khan, N.; Völkner, J.; Widdascheck, F.; del Pino, P.; Witte, G.; Riedel, M.; Lisdat, F.; Konrad, M.; Parak, W. J. Photo-Electrochemical Bioanalysis of Guanosine Monophosphate Using Coupled Enzymatic Reactions at a CdS/ZnS Quantum Dot Electrode. *Small* **2015**, *11*, 5844−5850.
(255) Stieve, H. Sensors of Biological Organisms—Biological Transducers. *Sens. Actuators* **1983**, *4*, 689−704.
(256) Jones, D. T.; Reed, R. R. Golf: An Olfactory Neuron Specific-G Protein Involved in Odorant Signal Transduction. *Science* **1989**, *244*, 790−795.
(257) Malnic, B.; Godfrey, P. A.; Buck, L. B. The Human Olfactory Receptor Gene Family. *Proc. Natl. Acad. Sci. U. S. A.* **2004**, *101*, 2584−2589.
(258) Spehr, M.; Schwane, K.; Riffell, J. A.; Zimmer, R. K.; Hatt, H. Odorant Receptors and Olfactory-like Signaling Mechanisms in Mammalian Sperm. *Mol. Cell. Endocrinol.* **2006**, *250*, 128−136.
(259) Machado, R. F.; Laskowski, D.; Deffenderfer, O.; Burch, T.; Zheng, S.; Mazzone, P. J.; Mekhail, T.; Jennings, C.; Stoller, J. K.; Pyle, J.; Duncan, J.; Dweik, R. A.; Erzurum, S. C. Detection of Lung Cancer by Sensor Array Analyses of Exhaled Breath. *Am. J. Respir. Crit. Care Med.* **2005**, *171*, 1286−1291.

DOI: 10.1021/acsnano.6b06040
ACS Nano 2017, 11, 2313−2381

(260) Nakhleh, M.; Amal, H.; Jeries, R.; Broza, Y.; Aboud, M.; Gharra, A.; Ivgi, H.; Khatib, S.; Badarneh, S.; Har-Shai, L.; Glass-Marmor, L.; Lejbkowicz, I.; Miller, A.; Badarny, S.; Winer, R.; Finberg, J.; Cohen-Kaminsky, S.; Perros, F.; Montani, D.; Girerd, B. Diagnosis and Classification of 17 diseases from 1404 Subjects *via* Pattern Analysis of Exhaled Molecules. *ACS Nano* **2017**, *11*, 112.
(261) Ko, H. J.; Park, T. H. Piezoelectric Olfactory Biosensor: Ligand Specificity and Dose-Dependence of an Olfactory Receptor Expressed in a Heterologous Cell System. *Biosens. Bioelectron.* **2005**, *20*, 1327−1332.
(262) Sung, J. H.; Ko, H. J.; Park, T. H. Piezoelectric Biosensor Using Olfactory Receptor Protein Expressed in *Escherichia coli*. *Biosens. Bioelectron.* **2006**, *21*, 1981−1986.
(263) Ko, H. J.; Park, T. H. Enhancement of Odorant Detection Sensitivity by the Expression of Odorant-Binding Protein. *Biosens. Bioelectron.* **2008**, *23*, 1017−1023.
(264) Lee, S. H.; Ko, H. J.; Park, T. H. Real-Time Monitoring of Odorant-Induced Cellular Reactions Using Surface Plasmon Resonance. *Biosens. Bioelectron.* **2009**, *25*, 55−60.
(265) Lee, J. Y.; Ko, H. J.; Lee, S. H.; Park, T. H. Cell-Based Measurement of Odorant Molecules Using Surface Plasmon Resonance. *Enzyme Microb. Technol.* **2006**, *39*, 375−380.
(266) Lee, S. H.; Jun, S. B.; Ko, H. J.; Kim, S. J.; Park, T. H. Cell-Based Olfactory Biosensor Using Microfabricated Planar Electrode. *Biosens. Bioelectron.* **2009**, *24*, 2659−2664.
(267) Lee, S. H.; Jeong, S. H.; Jun, S. B.; Kim, S. J.; Park, T. H. Enhancement of Cellular Olfactory Signal by Electrical Stimulation. *Electrophoresis* **2009**, *30*, 3283−3288.
(268) Kwon, O. S.; Ahn, S. R.; Park, S. J.; Song, H. S.; Lee, S. H.; Lee, J. S.; Hong, J. Y.; Lee, J. S.; You, S. A.; Yoon, H.; Park, T. H.; Jang, J. Ultrasensitive and Selective Recognition of Peptide Hormone Using Close-Packed Arrays of hPTHR-Conjugated Polymer Nanoparticles. *ACS Nano* **2012**, *6*, 5549−5558.
(269) Park, S. J.; Kwon, O. S.; Lee, S. H.; Song, H. S.; Park, T. H.; Jang, J. Ultrasensitive Flexible Graphene Based Field-Effect Transistor (FET)-Type Bioelectronic Nose. *Nano Lett.* **2012**, *12*, 5082−5090.
(270) Kwon, O. S.; Lee, S. H.; Park, S. J.; An, J. H.; Song, H. S.; Kim, T.; Oh, J. H.; Bae, J.; Yoon, H.; Park, T. H.; Jang, J. Large-Scale Graphene Micropattern Nano-Biohybrids: High-Performance Transducers for FET-Type Flexible Fluidic HIV Immunoassays. *Adv. Mater.* **2013**, *25*, 4177−4185.
(271) Kim, T. H.; Lee, S. H.; Lee, J.; Song, H. S.; Oh, E. H.; Park, T. H.; Hong, S. Single-Carbon-Atomic-Resolution Detection of Odorant Molecules using a Human Olfactory Receptor-Based Bioelectronic Nose. *Adv. Mater.* **2009**, *21*, 91−94.
(272) Yoon, H.; Lee, S. H.; Kwon, O. S.; Song, H. S.; Oh, E. H.; Park, T. H.; Jang, J. Polypyrrole Nanotubes Conjugated with Human Olfactory Receptors: High-Performance Transducers for FET-Type Bioelectronic Noses. *Angew. Chem., Int. Ed.* **2009**, *48*, 2755−2758.
(273) Lee, S. H.; Kwon, O. S.; Song, H. S.; Park, S. J.; Sung, J. H.; Jang, J.; Park, T. H. Mimicking the Human Smell Sensing Mechanism with an Artificial Nose Platform. *Biomaterials* **2012**, *33*, 1722−1729.
(274) Lee, S. H.; Jin, H. J.; Song, H. S.; Hong, S.; Park, T. H. Bioelectronic Nose with High Sensitivity and Selectivity Using Chemically Functionalized Carbon Nanotube Combined with Human Olfactory Receptor. *J. Biotechnol.* **2012**, *157*, 467−472.
(275) Park, J.; Lim, J. H.; Jin, H. J.; Namgung, S.; Lee, S. H.; Park, T. H.; Hong, S. A Bioelectronic Sensor Based on Canine Olfactory Nanovesicle-Carbon Nanotube Hybrid Structures for the Fast Assessment of Food Quality. *Analyst* **2012**, *137*, 3249−3254.
(276) Jin, H. J.; Lee, S. H.; Kim, T. H.; Park, J.; Song, H. S.; Park, T. H.; Hong, S. Nanovesicle-Based Bioelectronic Nose Platform Mimicking Human Olfactory Signal Transduction. *Biosens. Bioelectron.* **2012**, *35*, 335−341.
(277) Lim, J. H.; Park, J.; Oh, E. H.; Ko, H. J.; Hong, S.; Park, T. H. Nanovesicle-Based Bioelectronic Nose for the Diagnosis of Lung Cancer from Human Blood. *Adv. Healthcare Mater.* **2014**, *3*, 360−366.
(278) Song, H. S.; Kwon, O. S.; Lee, S. H.; Park, S. J.; Kim, U. K.; Jang, J.; Park, T. H. Human Taste Receptor-Functionalized Field Effect Transistor as a Human-Like Nanobioelectronic Tongue. *Nano Lett.* **2013**, *13*, 172−178.
(279) Song, H. S.; Jin, H. J.; Ahn, S. R.; Kim, D.; Lee, S. H.; Kim, U. K.; Simons, C. T.; Hong, S.; Park, T. H. Bioelectronic Tongue Using Heterodimeric Human Taste Receptor for the Discrimination of Sweeteners with Human-like Performance. *ACS Nano* **2014**, *8*, 9781−9789.
(280) Lim, J. H.; Park, J.; Ahn, J. H.; Jin, H. J.; Hong, S.; Park, T. H. A Peptide Receptor-Based Bioelectronic Nose for the Real-Time Determination of Seafood Quality. *Biosens. Bioelectron.* **2013**, *39*, 244−249.
(281) Norton, J. J. S.; Lee, D. S.; Lee, J. W.; Lee, W.; Kwon, O.; Won, P.; Jung, S.-Y.; Cheng, H.; Jeong, J.-W.; Akce, A.; Umunna, S.; Na, I.; Kwon, Y. H.; Wang, X.-Q.; Liu, Z.; Paik, U.; Huang, Y.; Bretl, T.; Yeo, W.-H.; Rogers, J. A. Soft, Curved Electrode Systems Capable of Integration on the Auricle as a Persistent Brain−Computer Interface. *Proc. Natl. Acad. Sci. U. S. A.* **2015**, *112*, 3920−3925.
(282) Rim, Y. S.; Bae, S.-H.; Chen, H.; Yang, J. L.; Kim, J.; Andrews, A. M.; Weiss, P. S.; Yang, Y.; Tseng, H.-R. Printable Ultrathin Metal Oxide Semiconductor-Based Conformal Biosensors. *ACS Nano* **2015**, *9*, 12174−12181.
(283) Liu, Q.; Cai, H.; Xu, Y.; Li, Y.; Li, R.; Wang, P. Olfactory Cell-Based Biosensor: A First Step towards a Neurochip of Bioelectronic Nose. *Biosens. Bioelectron.* **2006**, *22*, 318−322.
(284) Milligan, C. J.; Li, J.; Sukumar, P.; Majeed, Y.; Dallas, M. L.; English, A.; Emery, P.; Porter, K. E.; Smith, A. M.; McFadzean, I.; Beccano-Kelly, D.; Bahnasi, Y.; Cheong, A.; Naylor, J.; Zeng, F.; Liu, X.; Gamper, N.; Jiang, L. H.; Pearson, H. A.; Peers, C.; et al. Robotic Multiwell Planar Patch-Clamp for Native and Primary Mammalian Cells. *Nat. Protoc.* **2009**, *4*, 244−255.
(285) Haythornthwaite, A.; Stoelzle, S.; Hasler, A.; Kiss, A.; Mosbacher, J.; George, M.; Bruggemann, A.; Fertig, N. Characterizing Human Ion Channels in Induced Pluripotent Stem Cell-Derived Neurons. *J. Biomol. Screening* **2012**, *17*, 1264−1272.
(286) Yao, X.; Kwan, H. Y. Activity of Voltage-Gated K^+ Channels Is Associated with Cell Proliferation and Ca^{2+} Influx in Carcinoma Cells of Colon Cancer. *Life Sci.* **1999**, *65*, 55−62.
(287) Oblatt-Montal, M.; Reddy, G. L.; Iwamoto, T.; Tomich, J. M.; Montal, M. Identification of an Ion Channel-Forming Motif in the Primary Structure of CFTR, the Cystic Fibrosis Chloride Channel. *Proc. Natl. Acad. Sci. U. S. A.* **1994**, *91*, 1495−1499.
(288) Abbott, G. W.; Pitt, G. S. Ion Channels under the Sun. *FASEB J.* **2014**, *28*, 1957−1962.
(289) Sakurai, Y.; Kolokoltsov, A. A.; Chen, C. C.; Tidwell, M. W.; Bauta, W. E.; Klugbauer, N.; Grimm, C.; Wahl-Schott, C.; Biel, M.; Davey, R. A. Two-Pore Channels Control Ebola Virus Host Cell Entry and Are Drug Targets for Disease Treatment. *Science* **2015**, *347*, 995−998.
(290) Neher, E.; Sakmann, B. Single-Channel Currents Recorded from Membrane of Denervated Frog Muscle Fibres. *Nature* **1976**, *260*, 799−802.
(291) Farre, C.; Stoelzle, S.; Haarmann, C.; George, M.; Bruggemann, A.; Fertig, N. Automated Ion Channel Screening: Patch Clamping Made Easy. *Expert Opin. Ther. Targets* **2007**, *11*, 557−565.
(292) Farre, C.; Fertig, N. HTS Techniques for Patch Clamp-Based Ion Channel Screening - Advances and Economy. *Expert Opin. Drug Discovery* **2012**, *7*, 515−524.
(293) Ang, Y. S.; Yung, L. Y. L. Rapid and Label-Free Single-Nucleotide Discrimination *via* an Integrative Nanoparticle-Nanopore Approach. *ACS Nano* **2012**, *6*, 8815−8823.
(294) Polonchuk, L. Toward a new gold standard for early safety: automated temperature-controlled hERG test on the Patch Liner (R). *Front. Pharmacol.* **2012**, *3*, 3.
(295) Sager, P. T.; Gintant, G.; Turner, J. R.; Pettit, S.; Stockbridge, N. Rechanneling the Cardiac Proarrhythmia Safety Paradigm: A Meeting Report from the Cardiac Safety Research Consortium. *Am. Heart J.* **2014**, *167*, 292−300.
(296) Becker, N.; Stoelzle, S.; Gopel, S.; Guinot, D.; Mumm, P.; Haarmann, C.; Malan, D.; Bohlen, H.; Kossolov, E.; Kettenhofen, R.;

DOI: 10.1021/acsnano.6b06040
ACS Nano 2017, 11, 2313−2381

George, M.; Fertig, N.; Bruggemann, A. Minimized Cell Usage for Stem Cell-Derived and Primary Cells on an Automated Patch Clamp System. *J. Pharmacol. Toxicol. Methods* **2013**, *68*, 82−87.
(297) Qi, D.; Liu, Z.; Yu, M.; Liu, Y.; Tang, Y.; Lv, J.; Li, Y.; Wei, J.; Liedberg, B.; Yu, Z.; Chen, X. Highly Stretchable Gold Nanobelts with Sinusoidal Structures for Recording Electrocorticograms. *Adv. Mater.* **2015**, *27*, 3145−3151.
(298) Viventi, J.; Kim, D.-H.; Vigeland, L.; Frechette, E. S.; Blanco, J. A.; Kim, Y.-S.; Avrin, A. E.; Tiruvadi, V. R.; Hwang, S. W.; Vanleer, A. C.; et al. Flexible, Foldable, Actively Multiplexed, High-Density Electrode Array for Mapping Brain Activity *in Vivo*. *Nat. Neurosci.* **2011**, *14*, 1599−1605.
(299) Di Carlo, D. A Mechanical Biomarker of Cell State in Medicine. *J. Lab. Autom.* **2012**, *17*, 32−42.
(300) Albrecht-Buehler, G. The Phagokinetic Tracks of 3T3 Cells. *Cell* **1977**, *11*, 395−404.
(301) Bernstein, L. R.; Antoniades, H.; Zetter, B. R. Migration of Cultured Vascular Cells in Response to Plasma and Platelet-Derived Factors. *J. Cell Sci.* **1982**, *56*, 71−82.
(302) Pellegrino, T.; Parak, W. J.; Boudreau, R.; LeGros, M.; Gerion, D.; Alivisatos, A. P.; Larabell, C. Quantum Dot-Based Cell Motility Assay. *Differentiation* **2003**, *71*, 542−548.
(303) Tijore, A.; Cai, P.; Nai, M. H.; Zhuyun, L.; Yu, W.; Tay, C. Y.; Lim, C. T.; Chen, X.; Tan, L. P. Role of Cytoskeletal Tension in the Induction of Cardiomyogenic Differentiation in Micropatterned Human Mesenchymal Stem Cell. *Adv. Healthcare Mater.* **2015**, *4*, 1399−1407.
(304) Lam, C. R.; Tan, C.; Teo, Z.; Tay, C. Y.; Phua, T.; Wu, Y. L.; Cai, P. Q.; Tan, L. P.; Chen, X.; Zhu, P.; Tan, N. S. Loss of TAK1 Increases Cell Traction Force in a ROS-Dependent Manner to Drive Epithelial-Mesenchymal Transition of Cancer Cells. *Cell Death Dis.* **2013**, *4*, e848.
(305) Tay, C. Y.; Wu, Y. L.; Cai, P.; Tan, N. S.; Venkatraman, S. S.; Chen, X.; Tan, L. P. Bio-Inspired Micropatterned Hydrogel to Direct and Deconstruct Hierarchical Processing of Geometry-Force Signals by Human Mesenchymal Stem Cells during Smooth Muscle Cell Differentiation. *NPG Asia Mater.* **2015**, *7*, e199.
(306) Tay, C. Y.; Cai, P.; Setyawati, M. I.; Fang, W.; Tan, L. P.; Hong, C. H.; Chen, X.; Leong, D. T. Nanoparticles Strengthen Intracellular Tension and Retard Cellular Migration. *Nano Lett.* **2014**, *14*, 83−88.
(307) Berridge, M. V.; Herst, P. M.; Tan, A. S. Tetrazolium Dyes as Tools in Cell Biology: New Insights into Their Cellular Reduction. *Biotechnol. Annu. Rev.* **2005**, *11*, 127−152.
(308) Lehner, R.; Wang, X. Y.; Marsch, S.; Hunziker, P. Intelligent Nanomaterials for Medicine: Carrier Platforms and Targeting Strategies in the Context of Clinical Application. *Nanomedicine* **2013**, *9*, 742−757.
(309) Barenholz, Y. Doxil® - The First FDA-Approved Nano-Drug: Lessons learned. *J. Controlled Release* **2012**, *160*, 117−134.
(310) Stirland, D. L.; Nichols, J. W.; Miura, S.; Bae, Y. H. Mind the Gap: A Survey of How Cancer Drug Carriers Are Susceptible to the Gap between Research and Practice. *J. Controlled Release* **2013**, *172*, 1045−1064.
(311) Cheng, Z.; Al Zaki, A.; Hui, J. Z.; Muzykantov, V. R.; Tsourkas, A. Multifunctional Nanoparticles: Cost *versus* Benefit of Adding Targeting and Imaging Capabilities. *Science* **2012**, *338*, 903−910.
(312) Sun, Q. H.; Sun, X. R.; Ma, X. P.; Zhou, Z. X.; Jin, E. L.; Zhang, B.; Shen, Y. Q.; Van Kirk, E. A.; Murdoch, W. J.; Lott, J. R.; Lodge, T. P.; Radosz, M.; Zhao, Y. L. Integration of Nanoassembly Functions for an Effective Delivery Cascade for Cancer Drugs. *Adv. Mater.* **2014**, *26*, 7615−7621.
(313) Sun, Q. H.; Radosz, M.; Shen, Y. Q. Challenges in Design of Translational Nanocarriers. *J. Controlled Release* **2012**, *164*, 156−169.
(314) Ma, X. P.; Tang, J. B.; Shen, Y. Q.; Fan, M. H.; Tang, H. D.; Radosz, M. Facile Synthesis of Polyester Dendrimers from Sequential Click Coupling of Asymmetrical Monomers. *J. Am. Chem. Soc.* **2009**, *131*, 14795−14803.
(315) Shen, Y. Q.; Ma, X. P.; Zhang, B.; Zhou, Z. X.; Sun, Q. H.; Jin, E. L.; Sui, M. H.; Tang, J. B.; Wang, J. Q.; Fan, M. H. Degradable Dual pH- and Temperature-Responsive Photoluminescent Dendrimers. *Chem. - Eur. J.* **2011**, *17*, 5319−5326.
(316) Fan, Y.; Zhang, Q. Development of Liposomal Formulations: From Concept to Clinical Investigations. *Asian J. Pharm. Sci.* **2013**, *8*, 81−87.
(317) Huynh, N. T.; Passirani, C.; Saulnier, P.; Benoit, J. P. Lipid Nanocapsules: A New Platform for Nanomedicine. *Int. J. Pharm.* **2009**, *379*, 201−209.
(318) Nishiyama, N.; Okazaki, S.; Cabral, H.; Miyamoto, M.; Kato, Y.; Sugiyama, Y.; Nishio, K.; Matsumura, Y.; Kataoka, K. Novel Cisplatin-Incorporated Polymeric Micelles Can Eradicate Solid Tumors in Mice. *Cancer Res.* **2003**, *63*, 8977−8983.
(319) Mochida, Y.; Cabral, H.; Miura, Y.; Albertini, F.; Fukushima, S.; Osada, K.; Nishiyama, N.; Kataoka, K. Bundled Assembly of Helical Nanostructures in Polymeric Micelles Loaded with Platinum Drugs Enhancing Therapeutic Efficiency against Pancreatic Tumor. *ACS Nano* **2014**, *8*, 6724−6738.
(320) Cabral, H.; Kataoka, K. 22. The Impact of "Development of the Polymer Micelles Carrier System for Doxorubicin" on the Nanomedicine Realm: Original Research Article: Development of the Polymer Micelle Carrier System for Doxorubicin, 2001 References. *J. Controlled Release* **2014**, *190*, 70−72.
(321) Zhang, L.; Feng, Q.; Wang, J. L.; Sun, J. S.; Shi, X. H.; Jiang, X. Y. Microfluidic Synthesis of Rigid Nanovesicles for Hydrophilic Reagents Delivery. *Angew. Chem., Int. Ed.* **2015**, *54*, 3952−3956.
(322) Sun, J. S.; Zhang, L.; Wang, J. L.; Feng, Q.; Liu, D. B.; Yin, Q. F.; Xu, D. Y.; Wei, Y. J.; Ding, B. Q.; Shi, X. H.; Jiang, X. Y. Tunable Rigidity of (Polymeric Core)-(Lipid Shell) Nanoparticles for Regulated Cellular Uptake. *Adv. Mater.* **2015**, *27*, 1402−1407.
(323) Sun, H. L.; Wong, E. H. H.; Yan, Y.; Cui, J. W.; Dai, Q.; Guo, J. L.; Qiao, G. G.; Caruso, F. The Role of Capsule Stiffness on Cellular Processing. *Chem. Sci.* **2015**, *6*, 3505−3514.
(324) Donath, E.; Sukhorukov, G. B.; Caruso, F.; Davis, S. A.; Möhwald, H. Novel Hollow Polymer Shells by Colloid-Templated Assembly of Polyelectrolytes. *Angew. Chem., Int. Ed.* **1998**, *37*, 2201−2205.
(325) Sukhorukov, G. B.; Donath, E.; Lichtenfeld, H.; Knippel, E.; Knippel, M.; Budde, A.; Mohwald, H. Layer-by-Layer Self Assembly of Polyelectrolytes on Colloidal Particles. *Colloids Surf., A* **1998**, *137*, 253−266.
(326) Sukhorukov, G. B.; Rogach, A. L.; Parak, W. J.; Winterhalter, M. Nanoengineered Polymer Capsules: Tools for Detection, Controlled Delivery and Site Specific Manipulation. *Small* **2005**, *1*, 194−200.
(327) Köhler, K.; Shchukin, D. G.; Mohwald, H.; Sukhorukov, G. B. Thermal Behavior of Polyelectrolyte Multilayer Microcapsules. 1. The Effect of Odd and Even Layer Number. *J. Phys. Chem. B* **2005**, *109*, 18250−18259.
(328) Willms, E.; Johansson, H. J.; Mäger, I.; Lee, Y.; Blomberg, K. E. M.; Sadik, M.; Alaarg, A.; Smith, C. I. E.; Lehtiö, J.; El Andaloussi, S.; Wood, M. J. A.; Vader, P. Cells Release Subpopulations of Exosomes with Distinct Molecular and Biological Properties. *Sci. Rep.* **2016**, *6*, 22519.
(329) Tran, T.-H.; Mattheolabakis, G.; Aldawsari, H.; Amiji, M. Exosomes as Nanocarriers for Immunotherapy of Cancer and Inflammatory Diseases. *Clin. Immunol.* **2015**, *160*, 46−58.
(330) El Andaloussi, S.; Lakhal, S.; Mäger, I.; Wood, M. J. A. Exosomes for Targeted siRNA Delivery across Biological Barriers. *Adv. Drug Delivery Rev.* **2013**, *65*, 391−397.
(331) Kopeček, J. Polymer−drug Conjugates: Origins, Progress to Date and Future Directions. *Adv. Drug Delivery Rev.* **2013**, *65*, 49−59.
(332) Yang, J.; Zhang, R.; Radford, D. C.; Kopeček, J. FRET-Trackable Biodegradable HPMA Copolymer-Epirubicin Conjugates for Ovarian Carcinoma Therapy. *J. Controlled Release* **2015**, *218*, 36−44.
(333) Pan, H.; Sima, M.; Yang, J.; Kopeček, J. Synthesis of Long-Circulating, Backbone Degradable HPMA Copolymer−Doxorubicin Conjugates and Evaluation of Molecular-Weight-Dependent Antitumor Efficacy. *Macromol. Biosci.* **2013**, *13*, 155−160.
(334) Wei, T.; Chen, C.; Liu, J.; Liu, C.; Posocco, P.; Liu, X. X.; Cheng, Q.; Huo, S. D.; Liang, Z. C.; Fermeglia, M.; Pricl, S.; Liang, X. J.; Rocchi, P.; Peng, L. Anticancer Drug Nanomicelles Formed by Self-Assembling

DOI: 10.1021/acsnano.6b06040
ACS Nano 2017, 11, 2313−2381

Amphiphilic Dendrimer to Combat Cancer Drug Resistance. *Proc. Natl. Acad. Sci. U. S. A.* **2015**, *112*, 2978−2983.
(335) Mintzer, M. A.; Grinstaff, M. W. Biomedical Applications of Dendrimers: A Tutorial. *Chem. Soc. Rev.* **2011**, *40*, 173−190.
(336) Rolland, O.; Turrin, C.-O.; Caminade, A.-M.; Majoral, J.-P. Dendrimers and Nanomedicine: Multivalency in Action. *New J. Chem.* **2009**, *33*, 1809−1824.
(337) Bussy, C.; Alexiou, C.; Petros, R. A.; Nyström, A. M.; Methven, L.; Kostarelos, K. Therapeutic Applications. In *Adverse Effects of Engineered Nanomaterials*; Fadeel, B., Pietroiusti, A., Shvedova, A. A., Eds.; Boston Academic Press: Boston, 2012; pp 285−313.
(338) Raghupathi, K. R.; Guo, J.; Munkhbat, O.; Rangadurai, P.; Thayumanavan, S. Supramolecular Disassembly of Facially Amphiphilic Dendrimer Assemblies in Response to Physical, Chemical, and Biological Stimuli. *Acc. Chem. Res.* **2014**, *47*, 2200−2211.
(339) Nyström, A. M.; Wooley, K. L. The Importance of Chemistry in Creating Well-Defined Nanoscopic Embedded Therapeutics: Devices Capable of the Dual Functions of Imaging and Therapy. *Acc. Chem. Res.* **2011**, *44*, 969−978.
(340) Sung, H. W.; Sonaje, K.; Liao, Z. X.; Hsu, L. W.; Chuang, E. Y. pH-Responsive Nanoparticles Shelled with Chitosan for Oral Delivery of Insulin: From Mechanism to Therapeutic Applications. *Acc. Chem. Res.* **2012**, *45*, 619−629.
(341) Sung, H. W.; Sonaje, K.; Feng, S. S. Nanomedicine for Diabetes Treatment. *Nanomedicine* **2011**, *6*, 1297−1300.
(342) Hsu, L. W.; Ho, Y. C.; Chuang, E. Y.; Chen, C. T.; Juang, J. H.; Su, F. Y.; Hwang, S. M.; Sung, H. W. Effects of pH on Molecular Mechanisms of Chitosan-Integrin Interactions and Resulting Tight-Junction Disruptions. *Biomaterials* **2013**, *34*, 784−793.
(343) Chen, M. C.; Mi, F. L.; Liao, Z. X.; Hsiao, C. W.; Sonaje, K.; Chung, M. F.; Hsu, L. W.; Sung, H. W. Recent Advances in Chitosan-Based Nanoparticles for Oral Delivery of Macromolecules. *Adv. Drug Delivery Rev.* **2013**, *65*, 865−879.
(344) Chuang, E. Y.; Lin, K. J.; Su, F. Y.; Chen, H. L.; Maiti, B.; Ho, Y. C.; Yen, T. C.; Panda, N.; Sung, H. W. Calcium Depletion-Mediated Protease Inhibition and Apical-Junctional-Complex Disassembly *via* an EGTA-Conjugated Carrier for Oral Insulin Delivery. *J. Controlled Release* **2013**, *169*, 296−305.
(345) Liao, Z. X.; Chuang, E. Y.; Hsiao, C. W.; Sung, H. W. 21. pH-Sensitive Chitosan-Based Nanoparticles for Protein Drug Delivery: Oral Approaches: Original Research Article: A Novel pH-Sensitive Hydrogel Composed of Carboxymethyl Chitosan and Alginate Cross-Linked by Genipin for Protein Drug Delivery, 2004. *J. Controlled Release* **2014**, *190*, 68−70.
(346) MaHam, A.; Tang, Z.; Wu, H.; Wang, J.; Lin, Y. Protein-Based Nanomedicine Platforms for Drug Delivery. *Small* **2009**, *5*, 1706−1721.
(347) Gradishar, W. J. Albumin-Bound Paclitaxel: A Next-Generation Taxane. *Expert Opin. Pharmacother.* **2006**, *7*, 1041−1053.
(348) Wang, J.; Wu, W.; Zhang, Y. J.; Wang, X.; Qian, H. Q.; Liu, B. R.; Jiang, X. Q. The Combined Effects of Size and Surface Chemistry on the Accumulation of Boronic Acid-Rich Protein Nanoparticles in Tumors. *Biomaterials* **2014**, *35*, 866−878.
(349) Elzoghby, A. O.; Abo El-Fotoh, W. S.; Elgindy, N. A. Casein-Based Formulations as Promising Controlled Release Drug Delivery Systems. *J. Controlled Release* **2011**, *153*, 206−216.
(350) Liang, M. M.; Fan, K. L.; Zhou, M.; Duan, D. M.; Zheng, J. Y.; Yang, D. L.; Feng, J.; Yan, X. Y. H-Ferritin-Nanocaged Doxorubicin Nanoparticles Specifically Target and Kill Tumors with a Single-Dose Injection. *Proc. Natl. Acad. Sci. U. S. A.* **2014**, *111*, 14900−14905.
(351) Wu, Y. Z.; Ihme, S.; Feuring-Buske, M.; Kuan, S. L.; Eisele, K.; Lamla, M.; Wang, Y. R.; Buske, C.; Weil, T. A Core-Shell Albumin Copolymer Nanotransporter for High Capacity Loading and Two-Step Release of Doxorubicin with Enhanced Anti-Leukemia Activity. *Adv. Healthcare Mater.* **2013**, *2*, 884−894.
(352) Jones, M.-C.; Leroux, J.-C. Polymeric Micelles−A New Generation of Colloidal Drug Carriers. *Eur. J. Pharm. Biopharm.* **1999**, *48*, 101−111.
(353) Torchilin, V. P. Structure and Design of Polymeric Surfactant-Based Drug Delivery Systems. *J. Controlled Release* **2001**, *73*, 137−172.
(354) Sukhorukov, G. B.; Rogach, A. L.; Zebli, B.; Liedl, T.; Skirtach, A. G.; Köhler, K.; Antipov, A. A.; Gaponik, N.; Susha, A. S.; Winterhalter, M.; Parak, W. J. Nanoengineered Polymer Capsules: Tools for Detection, Controlled Delivery and Site Specific Manipulation. *Small* **2005**, *1*, 194−200.
(355) Pan, H.; Yang, J.; Kopečková, P.; Kopeček, J. Backbone Degradable Multiblock N-(2-Hydroxypropyl)methacrylamide Copolymer Conjugates *via* Reversible Addition−Fragmentation Chain Transfer Polymerization and Thiol−ene Coupling Reaction. *Biomacromolecules* **2011**, *12*, 247−252.
(356) Agnihotri, S. A.; Mallikarjuna, N. N.; Aminabhavi, T. M. Recent Advances on Chitosan-Based Micro- and Nanoparticles in Drug Delivery. *J. Controlled Release* **2004**, *100*, 5−28.
(357) Pouton, C. W. Lipid Formulations for Oral Administration of Drugs: Non-Emulsifying, Self-Emulsifying and "Self-Microemulsifying" Drug Delivery Systems. *Eur. J. Pharm. Sci.* **2000**, *11*, S93−8.
(358) Yeh, T.-H.; Hsu, L.-W.; Tseng, M. T.; Lee, P.-L.; Sonjae, K.; Ho, Y.-C.; Sung, H.-W. Mechanism and Consequence of Chitosan-Mediated Reversible Epithelial Tight Junction Opening. *Biomaterials* **2011**, *32*, 6164−6173.
(359) Nicolì, E.; Syga, M. I.; Bosetti, M.; Shastri, V. P. Enhanced Gene Silencing through Human Serum Albumin-Mediated Delivery of Polyethylenimine-siRNA Polyplexes. *PLoS One* **2015**, *10*, e0122581.
(360) Cui, D. X.; Zhang, C. L.; Liu, B.; Shu, Y.; Du, T.; Shu, D.; Wang, K.; Dai, F. P.; Liu, Y. L.; Li, C.; Pan, F.; Yang, Y. M.; Ni, J.; Li, H.; Brand-Saberi, B.; Guo, P.X. Regression of Gastric Cancer by Systemic Injection of RNA Nanoparticles Carrying both Ligand and siRNA. *Sci. Rep.* **2015**, *5*, 10726.
(361) Conde, J.; Tian, F. R.; Hernandez, Y.; Bao, C. C.; Baptista, P. V.; Cui, D. X.; Stoeger, T.; de la Fuente, J. M. RNAi-Based Glyconanoparticles Trigger Apoptotic Pathways for *in Vitro* and *in Vivo* Enhanced Cancer-Cell Killing. *Nanoscale* **2015**, *7*, 9083−9091.
(362) Shu, D.; Shu, Y.; Haque, F.; Abdelmawla, S.; Guo, P. X. Thermodynamically Stable RNA Three-Way Junction for Constructing Multifunctional Nanoparticles for Delivery of Therapeutics. *Nat. Nanotechnol.* **2011**, *6*, 658−667.
(363) Wu, Y.; Ermakova, A.; Liu, W.; Pramanik, G.; Vu, T. M.; Kurz, A.; McGuinness, L.; Naydenov, B.; Hafner, S.; Reuter, R.; Wrachtrup, J.; Isoya, J.; Förtsch, C.; Barth, H.; Simmet, T.; Jelezko, F.; Weil, T. Programmable Biopolymers for Advancing Biomedical Applications of Fluorescent Nanodiamonds. *Adv. Funct. Mater.* **2015**, *25*, 6576−6585.
(364) Alhaddad, A.; Adam, M. P.; Botsoa, J.; Dantelle, G.; Perruchas, S.; Gacoin, T.; Mansuy, C.; Lavielle, S.; Malvy, C.; Treussart, F.; Bertrand, J. R. Nanodiamond as a Vector for siRNA Delivery to Ewing Sarcoma Cells. *Small* **2011**, *7*, 3087−3095.
(365) Shimkunas, R. A.; Robinson, E.; Lam, R.; Lu, S.; Xu, X. Y.; Zhang, X. Q.; Huang, H. J.; Osawa, E.; Ho, D. Nanodiamond-Insulin Complexes as pH-Dependent Protein Delivery Vehicles. *Biomaterials* **2009**, *30*, 5720−5728.
(366) Knapinska, A. M.; Tokmina-Roszyk, D.; Amar, S.; Tokmina-Roszyk, M.; Mochalin, V. N.; Gogotsi, Y.; Cosme, P.; Terentis, A. C.; Fields, G. B. Solid-Phase Synthesis, Characterization, and Cellular Activities of Collagen-Model Nanodiamond-Peptide Conjugates. *Biopolymers* **2015**, *104*, 186−195.
(367) Cabral, H.; Matsumoto, Y.; Mizuno, K.; Chen, Q.; Murakami, M.; Kimura, M.; Terada, Y.; Kano, M. R.; Miyazono, K.; Uesaka, M.; Nishiyama, N.; Kataoka, K. Accumulation of Sub-100 nm Polymeric Micelles in Poorly Permeable Tumours Depends on Size. *Nat. Nanotechnol.* **2011**, *6*, 815−823.
(368) Sugahara, K. N.; Teesalu, T.; Karmali, P. P.; Kotamraju, V. R.; Agemy, L.; Greenwald, D. R.; Ruoslahti, E. Coadministration of a Tumor-Penetrating Peptide Enhances the Efficacy of Cancer Drugs. *Science* **2010**, *328*, 1031−1035.
(369) Frese, K. K.; Neesse, A.; Cook, N.; Bapiro, T. E.; Lolkema, M. P.; Jodrell, D. I.; Tuveson, D. A. Nab-Paclitaxel Potentiates Gemcitabine Activity by Reducing Cytidine Deaminase Levels in a Mouse Model of Pancreatic Cancer. *Cancer Discovery* **2012**, *2*, 260−269.
(370) Liu, J.; Liao, S.; Diop-Frimpong, B.; Chen, W.; Goel, S.; Naxerova, K.; Ancukiewicz, M.; Boucher, Y.; Jain, R. K.; Xu, L. TGF-β

DOI: 10.1021/acsnano.6b06040
ACS Nano 2017, 11, 2313−2381

Blockade Improves the Distribution and Efficacy of Therapeutics in Breast Carcinoma by Normalizing the Tumor Stroma. *Proc. Natl. Acad. Sci. U. S. A.* **2012**, *109*, 16618−16623.
(371) Meng, H.; Zhao, Y.; Dong, J.; Xue, M.; Lin, Y.-S.; Ji, Z.; Mai, W. X.; Zhang, H.; Chang, C. H.; Brinker, C. J.; Zink, J. I.; Nel, A. E. Two-Wave Nanotherapy To Target the Stroma and Optimize Gemcitabine Delivery To a Human Pancreatic Cancer Model in Mice. *ACS Nano* **2013**, *7*, 10048−10065.
(372) Meng, H.; Wang, M.; Liu, H.; Liu, X.; Situ, A.; Wu, B.; Ji, Z.; Chang, C. H.; Nel, A. E. Use of a Lipid-Coated Mesoporous Silica Nanoparticle Platform for Synergistic Gemcitabine and Paclitaxel Delivery to Human Pancreatic Cancer in Mice. *ACS Nano* **2015**, *9*, 3540−3557.
(373) Liu, X.; Situ, A.; Kang, Y.; Villabroza, K. R.; Liao, Y.; Chang, C. H.; Donahue, T.; Nel, A. E.; Meng, H. Irinotecan Delivery by Lipid-Coated Mesoporous Silica Nanoparticles Shows Improved Efficacy and Safety over Liposomes for Pancreatic Cancer. *ACS Nano* **2016**, *10*, 2702−2715.
(374) Torchilin, V. Tumor Delivery of Macromolecular Drugs Based on the EPR Effect. *Adv. Drug Delivery Rev.* **2011**, *63*, 131−135.
(375) Zhang, J.; Yuan, Z. F.; Wang, Y.; Chen, W. H.; Luo, G. F.; Cheng, S. X.; Zhuo, R. X.; Zhang, X. Z. Multifunctional Envelope-Type Mesoporous Silica Nanoparticles for Tumor-Triggered Targeting Drug Delivery. *J. Am. Chem. Soc.* **2013**, *135*, 5068−5073.
(376) Quan, C. Y.; Chen, J. X.; Wang, H. Y.; Li, C.; Chang, C.; Zhang, X. Z.; Zhuo, R. X. Core-Shell Nanosized Assemblies Mediated by the Alpha-Beta Cyclodextrin Dimer with a Tumor-Triggered Targeting Property. *ACS Nano* **2010**, *4*, 4211−4219.
(377) Zhong, Y. N.; Yang, W. J.; Sun, H. L.; Cheng, R.; Meng, F. H.; Deng, C.; Zhong, Z. Y. Ligand-Directed Reduction-Sensitive Shell-Sheddable Biodegradable Micelles Actively Deliver Doxorubicin into the Nuclei of Target Cancer Cells. *Biomacromolecules* **2013**, *14*, 3723−3730.
(378) Chen, W.; Zou, Y.; Meng, F.; Cheng, R.; Deng, C.; Feijen, J.; Zhong, Z. Glyco-Nanoparticles with Sheddable Saccharide Shells: A Unique and Potent Platform for Hepatoma-Targeting Delivery of Anticancer Drugs. *Biomacromolecules* **2014**, *15*, 900−907.
(379) Yuan, Y. Y.; Mao, C. Q.; Du, X. J.; Du, J. Z.; Wang, F.; Wang, J. Surface Charge Switchable Nanoparticles Based on Zwitterionic Polymer for Enhanced Drug Delivery to Tumor. *Adv. Mater.* **2012**, *24*, 5476−5480.
(380) Liu, X. S.; Li, H.; Jin, Q.; Ji, J. Surface Tailoring of Nanoparticles *via* Mixed-Charge Monolayers and Their Biomedical Applications. *Small* **2014**, *10*, 4230−4242.
(381) Marradi, M.; Chiodo, F.; Garcia, I.; Penades, S. Glyconanoparticles as Multifunctional and Multimodal Carbohydrate Systems. *Chem. Soc. Rev.* **2013**, *42*, 4728−4745.
(382) Garcia, I.; Sanchez-Iglesias, A.; Henriksen-Lacey, M.; Grzelczak, M.; Penades, S.; Liz-Marzan, L. M. Glycans as Biofunctional Ligands for Gold Nanorods: Stability and Targeting in Protein-Rich Media. *J. Am. Chem. Soc.* **2015**, *137*, 3686−3692.
(383) Liu, X. S.; Chen, Y. J.; Li, H.; Huang, N.; Jin, Q.; Ren, K. F.; Ji, J. Enhanced Retention and Cellular Uptake of Nanoparticles in Tumors by Controlling Their Aggregation Behavior. *ACS Nano* **2013**, *7*, 6244−6257.
(384) Liu, X. S.; Li, H.; Chen, Y. J.; Jin, Q.; Ren, K. F.; Ji, J. Mixed-Charge Nanoparticles for Long Circulation, Low Reticuloendothelial System Clearance, and High Tumor Accumulation. *Adv. Healthcare Mater.* **2014**, *3*, 1439−1447.
(385) Li, H.; Liu, X. S.; Huang, N.; Ren, K. F.; Jin, Q.; Ji, J. Mixed-Charge Self-Assembled Monolayers″ as a Facile Method to Design pH-induced Aggregation of Large Gold Nanoparticles for Near-Infrared Photothermal Cancer Therapy. *ACS Appl. Mater. Interfaces* **2014**, *6*, 18930−18937.
(386) Wang, Y. C.; Bahng, J. H.; Che, Q. T.; Han, J. S.; Kotov, N. A. Anomalously Fast Diffusion of Targeted Carbon Nanotubes in Cellular Spheroids. *ACS Nano* **2015**, *9*, 8231−8238.
(387) Wang, J. Q.; Mao, W. W.; Lock, L. L.; Tang, J. B.; Sui, M. H.; Sun, W. L.; Cui, H. G.; Xu, D.; Shen, Y. Q. The Role of Micelle Size in Tumor Accumulation, Penetration, and Treatment. *ACS Nano* **2015**, *9*, 7195−7206.
(388) Huo, S. D.; Ma, H. L.; Huang, K. Y.; Liu, J.; Wei, T.; Jin, S. B.; Zhang, J. C.; He, S. T.; Liang, X. J. Superior Penetration and Retention Behavior of 50 nm Gold Nanoparticles in Tumors. *Cancer Res.* **2013**, *73*, 319−330.
(389) Xiong, X. B.; Huang, Y.; Lu, W. L.; Zhang, X.; Zhang, H.; Nagai, T.; Zhang, Q. Enhanced Intracellular Delivery and Improved Antitumor Efficacy of Doxorubicin by Sterically Stabilized Liposomes Modified with a Synthetic RGD Mimetic. *J. Controlled Release* **2005**, *107*, 262−275.
(390) Mei, D.; Lin, Z. Q.; Fu, J. J.; He, B.; Gao, W.; Ma, L.; Dai, W. B.; Zhang, H.; Wang, X. Q.; Wang, J. C.; Zhang, X.; Lu, W. L.; Zhou, D. M.; Zhang, Q. The Use of Alpha-Conotoxin ImI to Actualize the Targeted Delivery of Paclitaxel Micelles to Alpha 7 nAChR-Overexpressing Breast Cancer. *Biomaterials* **2015**, *42*, 52−65.
(391) Dai, W. B.; Yang, T. Y.; Wang, Y. G.; Wang, X. Q.; Wang, J. C.; Zhang, X.; Zhang, Q. Peptide PHSCNK as an Integrin alpha(5)beta(1) Antagonist Targets Stealth Liposomes to Integrin-Overexpressing Melanoma. *Nanomedicine* **2012**, *8*, 1152−1161.
(392) Zheng, N.; Dai, W.; Du, W.; Zhang, H.; Lei, L.; Zhang, H.; Wang, X.; Wang, J.; Zhang, X.; Gao, J.; Zhang, Q. A Novel Lanreotide-Encoded Micelle System Targets Paclitaxel to the Tumors with Overexpression of Somatostatin Receptors. *Mol. Pharmaceutics* **2012**, *9*, 1175−1188.
(393) Zhang, J. L.; Jin, W.; Wang, X. Q.; Wang, J. C.; Zhang, X. A.; Zhang, Q. A. A Novel Octreotide Modified Lipid Vesicle Improved the Anticancer Efficacy of Doxorubicin in Somatostatin Receptor 2 Positive Tumor Models. *Mol. Pharmaceutics* **2010**, *7*, 1159−1168.
(394) Xiang, Y.; Liang, L.; Wang, X.; Wang, J.; Zhang, X.; Zhang, Q. Chloride Channel-Mediated Brain Glioma Targeting of Chlorotoxin-Modified Doxorubicine-Loaded Liposomes. *J. Controlled Release* **2011**, *152*, 402−410.
(395) Guo, Z. M.; He, B.; Jin, H. W.; Zhang, H. R.; Dai, W. B.; Zhang, L. R.; Zhang, H.; Wang, X. Q.; Wang, J. C.; Zhang, X.; Zhang, Q. Targeting Efficiency of RGD-Modified Nanocarriers with Different Ligand Intervals in Response to Integrin Alpha v Beta 3 Clustering. *Biomaterials* **2014**, *35*, 6106−6117.
(396) Cai, D.; Gao, W.; He, B.; Dai, W.; Zhang, H.; Wang, X.; Wang, J.; Zhang, X.; Zhang, Q. Hydrophobic Penetrating Peptide PFVYLI-Modified Stealth Liposomes for Doxorubicin Delivery in Breast Cancer Therapy. *Biomaterials* **2014**, *35*, 2283−2294.
(397) Sykes, E. A.; Chen, J.; Zheng, G.; Chan, W. C. W. Investigating the Impact of Nanoparticle Size on Active and Passive Tumor Targeting Efficiency. *ACS Nano* **2014**, *8*, 5696−5706.
(398) Laurent, S.; Saei, A. A.; Behzadi, S.; Panahifar, A.; Mahmoudi, M. Superparamagnetic Iron Oxide Nanoparticles for Delivery of Therapeutic Agents: Opportunities and Challenges. *Expert Opin. Drug Delivery* **2014**, *11*, 1449−1470.
(399) Alexiou, C.; Arnold, W.; Klein, R. J.; Parak, F. G.; Hulin, P.; Bergemann, C.; Erhardt, W.; Wagenpfeil, S.; Lübbe, A. S. Locoregional Cancer Treatment with Magnetic Drug Targeting. *Cancer Res.* **2000**, *60*, 6641−6648.
(400) Lueshen, E.; Venugopal, I.; Soni, T.; Alaraj, A.; Linninger, A. Implant-Assisted Intrathecal Magnetic Drug Targeting to Aid in Therapeutic Nanoparticle Localization for Potential Treatment of Central Nervous System Disorders. *J. Biomed. Nanotechnol.* **2015**, *11*, 253−261.
(401) Hournkumnuard, K.; Natenapit, M. Magnetic Drug Targeting by Ferromagnetic Microwires Implanted within Blood Vessels. *Med. Phys.* **2013**, *40*, 062302.
(402) He, W.; Ji, Y.; Luo, C.; Xu, Z. Development of Single-Side Magnet Array for Super Paramagnetic Nano-Particle Targeting. *Res. J. Appl. Sci., Eng. Technol.* **2014**, *7*, 3022−3029.
(403) Nacev, A.; Weinberg, I. N.; Stepanov, P. Y.; Kupfer, S.; Mair, L. O.; Urdaneta, M. G.; Shimoji, M.; Fricke, S. T.; Shapiro, B. Dynamic Inversion Enables External Magnets To Concentrate Ferromagnetic Rods to a Central Target. *Nano Lett.* **2015**, *15*, 359−364.
(404) Tietze, R.; Lyer, S.; Durr, S.; Struffert, T.; Engelhorn, T.; Schwarz, M.; Eckert, E.; Goen, T.; Vasylyev, S.; Peukert, W.; Wiekhorst,

DOI: 10.1021/acsnano.6b06040
ACS Nano 2017, 11, 2313−2381

F.; Trahms, L.; Dorfler, A.; Alexiou, C. Efficient Drug-Delivery Using Magnetic Nanoparticles – Biodistribution and Therapeutic Effects in Tumour Bearing Rabbits. *Nanomedicine* **2013**, *9*, 961–971.
(405) Karamipour, S.; Sadjadi, M. S.; Farhadyar, N. Fabrication and Spectroscopic Studies of Folic Acid-Conjugated Fe_3O_4@Au Core-Shell for Targeted Drug Delivery Application. *Spectrochim. Acta, Part A* **2015**, *148*, 146–155.
(406) Unterweger, H.; Tietze, R.; Janko, C.; Zaloga, J.; Lyer, S.; Durr, S.; Taccardi, N.; Goudouri, O. M.; Hoppe, A.; Eberbeck, D.; Schubert, D. W.; Boccaccini, A. R.; Alexiou, C. Development and Characterization of Magnetic Iron Oxide Nanoparticles with a Cisplatin-Bearing Polymer Coating for Targeted Drug Delivery. *Int. J. Nanomed.* **2014**, *9*, 3659–3676.
(407) Hamarat Sanlier, S.; Yasa, M.; Cihnioglu, A. O.; Abdulhayoglu, M.; Yilmaz, H.; Ak, G. Development of Gemcitabine-Adsorbed Magnetic Gelatin Nanoparticles for Targeted Drug Delivery in Lung Cancer. *Artif. Cells, Nanomed., Biotechnol.* **2016**, 1–7.
(408) Huang, J.; Shu, Q.; Wang, L. Y.; Wu, H.; Wang, A. Y.; Mao, H. Layer-by-Layer Assembled Milk Protein Coated Magnetic Nanoparticle Enabled Oral Drug Delivery with High Stability in Stomach and Enzyme-Responsive Release in Small Intestine. *Biomaterials* **2015**, *39*, 105–113.
(409) Halupka-Bryl, M.; Asai, K.; Thangavel, S.; Bednarowicz, M.; Krzyminiewski, R.; Nagasaki, Y. Synthesis and *in Vitro* and *in Vivo* Evaluations of Poly(ethylene Glycol)-Block-poly(4-Vinylbenzyl-phosphonate) Magnetic Nanoparticles Containing Doxorubicin as a Potential Targeted Drug Delivery System. *Colloids Surf., B* **2014**, *118*, 140–147.
(410) Wang, N.; Guan, Y. P.; Yang, L. R.; Jia, L. W.; Wei, X. T.; Liu, H. Z.; Guo, C. Magnetic Nanoparticles (MNPs) Covalently Coated by PEO-PPO-PEO Block Copolymer for Drug Delivery. *J. Colloid Interface Sci.* **2013**, *395*, 50–57.
(411) Zaloga, J.; Janko, C.; Nowak, J.; Matuszak, J.; Knaup, S.; Eberbeck, D.; Tietze, R.; Unterweger, H.; Friedrich, R. P.; Duerr, S.; Heimke-Brinck, R.; Baum, E.; Cicha, I.; Dorje, F.; Odenbach, S.; Lyer, S.; Lee, G.; Alexiou, C. Development of a Lauric Acid/Albumin Hybrid Iron Oxide Nanoparticle System with Improved Biocompatibility. *Int. J. Nanomed.* **2014**, *9*, 4847–4866.
(412) Zaloga, J.; Janko, C.; Agarwal, R.; Nowak, J.; Muller, R.; Boccaccini, A. R.; Lee, G.; Odenbach, S.; Lyer, S.; Alexiou, C. Different Storage Conditions Influence Biocompatibility and Physicochemical Properties of Iron Oxide Nanoparticles. *Int. J. Mol. Sci.* **2015**, *16*, 9368–9384.
(413) Lepeltier, E. A.; Nuhn, L.; Lehr, C. M.; Zentel, R. Not Just for Tumor Targeting: Unmet Medical Needs and Opportunities for Nanomedicine. *Nanomedicine* **2015**, *10*, 3147–3166.
(414) de Souza Carvalho, C.; Daum, N.; Lehr, C. M. Carrier Interactions with the Biological Barriers of the Lung: Advanced *in Vitro* Models and Challenges for Pulmonary Drug Delivery. *Adv. Drug Delivery Rev.* **2014**, *75*, 129–140.
(415) Mitragotri, S.; Burke, P. A.; Langer, R. Overcoming the Challenges in Administering Biopharmaceuticals: Formulation and Delivery Strategies. *Nat. Rev. Drug Discovery* **2014**, *13*, 655–672.
(416) Schmidt, C.; Lautenschlaeger, C.; Collnot, E. M.; Schumann, M.; Bojarski, C.; Schulzke, J. D.; Lehr, C. M.; Stallmach, A. Nano- and Microscaled Particles for Drug Targeting to Inflamed Intestinal Mucosa-A First *in Vivo* Study in Human Patients. *J. Controlled Release* **2013**, *165*, 139–145.
(417) Ali, H.; Weigmann, B.; Collnot, E. M.; Khan, S. A.; Windbergs, M.; Lehr, C. M. Budesonide Loaded PLGA Nanoparticles for Targeting the Inflamed Intestinal Mucosa-Pharmaceutical Characterization and Fluorescence Imaging. *Pharm. Res.* **2016**, *33*, 1085–1092.
(418) Ali, H.; Weigmann, B.; Neurath, M. F.; Collnot, E. M.; Windbergs, M.; Lehr, C. M. Budesonide Loaded Nanoparticles with pH-Sensitive Coating for Improved Mucosal Targeting in Mouse Models of Inflammatory Bowel Diseases. *J. Controlled Release* **2014**, *183*, 167–177.
(419) Mittal, A.; Schulze, K.; Ebensen, T.; Weissmann, S.; Hansen, S.; Guzman, C. A.; Lehr, C. M. Inverse Micellar Sugar Glass (IMSG) Nanoparticles for Transfollicular Vaccination. *J. Controlled Release* **2015**, *206*, 140–152.
(420) Mittal, A.; Schulze, K.; Ebensen, T.; Weissmann, S.; Hansen, S.; Lehr, C. M.; Guzman, C. A. Efficient Nanoparticle-Mediated Needle-Free Transcutaneous Vaccination *via* Hair Follicles Requires Adjuvantation. *Nanomedicine* **2015**, *11*, 147–154.
(421) Mittal, A.; Raber, A. S.; Schaefer, U. F.; Weissmann, S.; Ebensen, T.; Schulze, K.; Guzman, C. A.; Lehr, C. M.; Hansen, S. Non-Invasive Delivery of Nanoparticles to Hair Follicles: A Perspective for Transcutaneous Immunization. *Vaccine* **2013**, *31*, 3442–3451.
(422) Paranjpe, M.; Müller-Goymann, C. Nanoparticle-Mediated Pulmonary Drug Delivery: A Review. *Int. J. Mol. Sci.* **2014**, *15*, 5852–5873.
(423) Nafee, N.; Husari, A.; Maurer, C. K.; Lu, C. B.; de Rossi, C.; Steinbach, A.; Hartmann, R. W.; Lehr, C. M.; Schneider, M. Antibiotic-Free Nanotherapeutics: Ultra-Small, Mucus-Penetrating Solid Lipid Nanoparticles Enhance the Pulmonary Delivery and Anti-Virulence Efficacy of Novel Quorum Sensing Inhibitors. *J. Controlled Release* **2014**, *192*, 131–140.
(424) Mahiny, A. J.; Dewerth, A.; Mays, L. E.; Alkhaled, M.; Mothes, B.; Malaeksefat, E.; Loretz, B.; Rottenberger, J.; Brosch, D. M.; Reautschnig, P.; Surapolchai, P.; Zeyer, F.; Schams, A.; Carevic, M.; Bakele, M.; Griese, M.; Schwab, M.; Nurnberg, B.; Beer-Hammer, S.; Handgretinger, R.; et al. *In Vivo* Genome Editing Using Nuclease-Encoding mRNA Corrects SP-B Deficiency. *Nat. Biotechnol.* **2015**, *33*, 584–586.
(425) Zhang, X.; Malhotra, S.; Molina, M.; Haag, R. Micro- and Nanogels with Labile Crosslinks - from Synthesis to Biomedical Applications. *Chem. Soc. Rev.* **2015**, *44*, 1948–1973.
(426) Kakizawa, Y.; Harada, A.; Kataoka, K. Environment-Sensitive Stabilization of Core–Shell Structured Polyion Complex Micelle by Reversible Cross-Linking of the Core through Disulfide Bond. *J. Am. Chem. Soc.* **1999**, *121*, 11247–11248.
(427) Cheng, R.; Feng, F.; Meng, F. H.; Deng, C.; Feijen, J.; Zhong, Z. Y. Glutathione-Responsive Nano-Vehicles as a Promising Platform for Targeted Intracellular Drug and Gene Delivery. *J. Controlled Release* **2011**, *152*, 2–12.
(428) Sun, Y.; Yan, X. L.; Yuan, T. M.; Liang, J.; Fan, Y. J.; Gu, Z. W.; Zhang, X. D. Disassemblable Micelles Based on Reduction-Degradable Amphiphilic Graft Copolymers for Intracellular Delivery of Doxorubicin. *Biomaterials* **2010**, *31*, 7124–7131.
(429) Sun, H. L.; Guo, B. N.; Cheng, R.; Meng, F. H.; Liu, H. Y.; Zhong, Z. Y. Biodegradable Micelles with Sheddable Poly(Ethylene Glycol) Shells for Triggered Intracellular Release of Doxorubicin. *Biomaterials* **2009**, *30*, 6358–6366.
(430) Zhang, J.; Jiang, X.; Zhang, Y.; Li, Y.; Liu, S. Facile Fabrication of Reversible Core Cross-Linked Micelles Possessing Thermosensitive Swellability. *Macromolecules* **2007**, *40*, 9125–9132.
(431) Xu, H. P.; Cao, W.; Zhang, X. Selenium-Containing Polymers: Promising Biomaterials for Controlled Release and Enzyme Mimics. *Acc. Chem. Res.* **2013**, *46*, 1647–1658.
(432) He, Y. Y.; Nie, Y.; Cheng, G.; Xie, L.; Shen, Y. Q.; Gu, Z. W. Viral Mimicking Ternary Polyplexes: A Reduction-Controlled Hierarchical Unpacking Vector for Gene Delivery. *Adv. Mater.* **2014**, *26*, 1534–1540.
(433) Wang, T.; Ng, D. Y. W.; Wu, Y. Z.; Thomas, J.; TamTran, T.; Weil, T. Bis-Sulfide Bioconjugates for Glutathione Triggered Tumor Responsive Drug Release. *Chem. Commun.* **2014**, *50*, 1116–1118.
(434) Marusyk, A.; Polyak, K. Tumor Heterogeneity: Causes and Consequences. *Biochim. Biophys. Acta, Rev. Cancer* **2010**, *1805*, 105–117.
(435) van Vlerken, L. E.; Amiji, M. M. Multi-Functional Polymeric Nanoparticles for Tumour-Targeted Drug Delivery. *Expert Opin. Drug Delivery* **2006**, *3*, 205–216.
(436) Lee, F. Y. F.; Vessey, A.; Rofstad, E.; Siemann, D. W.; Sutherland, R. M. Heterogeneity of Glutathione Content in Human Ovarian-Cancer. *Cancer Res.* **1989**, *49*, 5244–5248.
(437) Konstantinov, A. A.; Peskin, A. V.; Popova, E. Y.; Khomutov, G. B.; Ruuge, E. K. Superoxide Generation by the Respiratory-Chain of Tumor Mitochondria. *Biochim. Biophys. Acta, Bioenerg.* **1987**, *894*, 1–10.

DOI: 10.1021/acsnano.6b06040
ACS Nano 2017, 11, 2313–2381

(438) Fang, J.; Seki, T.; Maeda, H. Therapeutic Strategies by Modulating Oxygen Stress in Cancer and Inflammation. *Adv. Drug Delivery Rev.* **2009**, *61*, 290−302.
(439) Grek, C. L.; Tew, K. D. Redox Metabolism and Malignancy. *Curr. Opin. Pharmacol.* **2010**, *10*, 362−368.
(440) Ray, P. D.; Huang, B. W.; Tsuji, Y. Reactive Oxygen Species (ROS) Homeostasis and Redox Regulation in Cellular Signaling. *Cell. Signalling* **2012**, *24*, 981−990.
(441) Wang, J. R.; Sun, X. R.; Mao, W. W.; Sun, W. L.; Tang, J. B.; Sui, M. H.; Shen, Y. Q.; Gu, Z. W. Tumor Redox Heterogeneity-Responsive Prodrug Nanocapsules for Cancer Chemotherapy. *Adv. Mater.* **2013**, *25*, 3670−3676.
(442) Lu, C.-H.; Willner, I. Stimuli-Responsive DNA-Functionalized Nano-/Microcontainers for Switchable and Controlled Release. *Angew. Chem., Int. Ed.* **2015**, *54*, 12212−12235.
(443) Zhang, Z. X.; Balogh, D.; Wang, F. A.; Sung, S. Y.; Nechushtai, R.; Willner, I. Biocatalytic Release of an Anticancer Drug from Nucleic-Acids-Capped Mesoporous SiO2 Using DNA or Molecular Biomarkers as Triggering Stimuli. *ACS Nano* **2013**, *7*, 8455−8468.
(444) Zhang, P.; Cheng, F.; Zhou, R.; Cao, J.; Li, J.; Burda, C.; Min, Q.; Zhu, J.-J. DNA-Hybrid-Gated Multifunctional Mesoporous Silica Nanocarriers for Dual-Targeted and MicroRNA-Responsive Controlled Drug Delivery. *Angew. Chem.* **2014**, *126*, 2403−2407.
(445) He, D.; He, X.; Wang, K.; Cao, J.; Zhao, Y. A Photon-Fueled Gate-Like Delivery System Using i-Motif DNA Functionalized Mesoporous Silica Nanoparticles. *Adv. Funct. Mater.* **2012**, *22*, 4704−4710.
(446) Zhang, Z. X.; Balogh, D.; Wang, F. A.; Willner, I. Smart Mesoporous SiO_2 Nanoparticles for the DNAzyme-Induced Multiplexed Release of Substrates. *J. Am. Chem. Soc.* **2013**, *135*, 1934−1940.
(447) Chen, C.; Zhou, L.; Geng, J.; Ren, J.; Qu, X. Photosensitizer-Incorporated Quadruplex DNA-Gated Nanovechicles for Light-Triggered, Targeted Dual Drug Delivery to Cancer Cells. *Small* **2013**, *9*, 2793−2800.
(448) Eastoe, J.; Vesperinas, A.; Donnewirth, A.-C.; Wyatt, P.; Grillo, I.; Heenan, R. K.; Davis, S. Photodestructible Vesicles. *Langmuir* **2006**, *22*, 851−853.
(449) Brazel, C. S. Magnetothermally-Responsive Nanomaterials: Combining Magnetic Nanostructures and Thermally-Sensitive Polymers for Triggered Drug Release. *Pharm. Res.* **2009**, *26*, 644−656.
(450) Carregal-Romero, S.; Guardia, P.; Yu, X.; Hartmann, R.; Pellegrino, T.; Parak, W. J. Magnetically Triggered Release of Molecular Cargo from Iron Oxide Nanoparticle Loaded Microcapsules. *Nanoscale* **2015**, *7*, 570−576.
(451) Rai, P.; Mallidi, S.; Zheng, X.; Rahmanzadeh, R.; Mir, Y.; Elrington, S.; Khurshid, A.; Hasan, T. Development and Applications of Photo-Triggered Theranostic Agents. *Adv. Drug Delivery Rev.* **2010**, *62*, 1094−1124.
(452) Sykes, E. A.; Dai, Q.; Tsoi, K. M.; Hwang, D. M.; Chan, W. C. W. Nanoparticle Exposure in Animals Can Be Visualized in the Skin and Analysed *via* Skin Biopsy. *Nat. Commun.* **2014**, *5*, 3796.
(453) Pass, H. I. Photodynamic Therapy in Oncology: Mechanisms and Clinical Use. *J. Natl. Cancer Inst.* **1993**, *85*, 443−456.
(454) Chen, C. J.; Liu, G. Y.; Liu, X. S.; Pang, S. P.; Zhu, C. S.; Lv, L. P.; Ji, J. Photo-Responsive, Biocompatible Polymeric Micelles Self-Assembled from Hyperbranched Polyphosphate-Based Polymers. *Polym. Chem.* **2011**, *2*, 1389−1397.
(455) Chen, C. J.; Liu, G. Y.; Shi, Y. T.; Zhu, C. S.; Pang, S. P.; Liu, X. S.; Ji, J. Biocompatible Micelles Based on Comb-like PEG Derivates: Formation, Characterization, and Photo-Responsiveness. *Macromol. Rapid Commun.* **2011**, *32*, 1077−1081.
(456) Liu, G. Y.; Chen, C. J.; Li, D. D.; Wang, S. S.; Ji, J. Near-Infrared Light-Sensitive Micelles for Enhanced Intracellular Drug Delivery. *J. Mater. Chem.* **2012**, *22*, 16865−16871.
(457) Skirtach, A. G.; Dejugnat, C.; Braun, D.; Susha, A. S.; Parak, W. J.; Möhwald, H.; Sukhorukov, G. B.; Rogach, A. L. The Role of Metal Nanoparticles in Remote Release of Encapsulated Materials. *Nano Lett.* **2005**, *5*, 1371−1377.
(458) Carregal-Romero, S.; Ochs, M.; Rivera Gil, P.; Ganas, C.; Pavlov, A. M.; Sukhorukov, G. B.; Parak, W. J. NIR-Light Triggered Delivery of Macromolecules into the Cytosol. *J. Controlled Release* **2012**, *159*, 120−127.
(459) Muñoz Javier, A.; del Pino, P.; Bedard, M. F.; Skirtach, A. G.; Ho, D.; Sukhorukov, G. B.; Plank, C.; Parak, W. J. Photoactivated Release of Cargo from the Cavity of Polyelectrolyte Capsules to the Cytosol of Cells. *Langmuir* **2008**, *24*, 12517−12520.
(460) Skirtach, A. G.; Javier, A. M.; Kreft, O.; Köhler, K.; Alberola, A. P.; Möhwald, H.; Parak, W. J.; Sukhorukov, G. B. Laser-Induced Release of Encapsulated Materials inside Living Cells. *Angew. Chem., Int. Ed.* **2006**, *45*, 4612−4617.
(461) Ochs, M.; Carregal-Romero, S.; Rejman, J.; Braeckmans, K.; De Smedt, S. C.; Parak, W. J. Light-Addressable Capsules as Caged Compound Matrix for Controlled *in Vitro* Release. *Angew. Chem., Int. Ed.* **2013**, *52*, 695−699.
(462) Ambrosone, A.; Marchesano, V.; Carregal-Romero, S.; Intartaglia, D.; Parak, W. J.; Tortiglione, C. Control of Wnt/β-Catenin Signaling Pathway *in Vivo via* Light Responsive Capsules. *ACS Nano* **2016**, *10*, 4828−4834.
(463) Kim, H.-C.; Härtner, S.; Behe, M.; Behr, T. M.; Hampp, N. A. Two-Photon Absorption-Controlled Multidose Drug Release: A Novel Approach for Secondary Cataract Treatment. *J. Biomed. Opt.* **2006**, *11*, 034024.
(464) Rahimi, M.; Kilaru, S.; Hajj Sleiman, G. E. L.; Saleh, A.; Rudkevich, D.; Nguyen, K. Synthesis and Characterization of Thermo-Sensitive Nanoparticles for Drug Delivery Applications. *J. Biomed. Nanotechnol.* **2008**, *4*, 482−490.
(465) Au, K. M.; Min, Y.; Tian, X.; Zhang, L.; Perello, V.; Caster, J. M.; Wang, A. Z. Improving Cancer Chemoradiotherapy Treatment by Dual Controlled Release of Wortmannin and Docetaxel in Polymeric Nanoparticles. *ACS Nano* **2015**, *9*, 8976−8996.
(466) Goldman, A.; Kulkarni, A.; Kohandel, M.; Pandey, P.; Rao, P.; Natarajan, S. K.; Sabbisetti, V.; Sengupta, S. Rationally Designed 2-in-1 Nanoparticles Can Overcome Adaptive Resistance in Cancer. *ACS Nano* **2016**, *10*, 5823−5834.
(467) Li, J.; Wang, Y.; Zhu, Y.; Oupický, D. Recent Advances in Delivery of Drug-Nucleic Acid Combinations for Cancer Treatment. *J. Controlled Release* **2013**, *172*, 589−600.
(468) Zhang, Y.; Zhang, H.; Wang, X. Q.; Wang, J. C.; Zhang, X.; Zhang, Q. The Eradication of Breast Cancer and Cancer Stem Cells Using Octreotide Modified Paclitaxel Active Targeting Micelles and Salinomycin Passive Targeting Micelles. *Biomaterials* **2012**, *33*, 679−691.
(469) Zhou, Y.; Yang, J.; Rhim, J. S.; Kopeček, J. HPMA Copolymer-Based Combination Therapy Toxic to Both Prostate Cancer Stem/Progenitor Cells and Differentiated Cells Induces Durable Anti-Tumor Effects. *J. Controlled Release* **2013**, *172*, 946−953.
(470) Dai, W. B.; Yang, F.; Ma, L.; Fan, Y. C.; He, B.; He, Q. H.; Wang, X. Q.; Zhang, H.; Zhang, Q. Combined mTOR Inhibitor Rapamycin and Doxorubicin-Loaded Cyclic Octapeptide Modified Liposomes for Targeting Integrin Alpha 3 in Triple-Negative Breast Cancer. *Biomaterials* **2014**, *35*, 5347−5358.
(471) Feng, Q.; Yu, M. Z.; Wang, J. C.; Hou, W. J.; Gao, L. Y.; Ma, X. F.; Pei, X. W.; Niu, Y. J.; Liu, X. Y.; Qiu, C.; Pang, W. H.; Du, L. L.; Zhang, Q. Synergistic Inhibition of Breast Cancer by Co-Delivery of VEGF siRNA and Paclitaxel *via* Vapreotide-Modified Core-Shell Nanoparticles. *Biomaterials* **2014**, *35*, 5028−5038.
(472) Fan, Y. C.; Du, W. W.; He, B.; Fu, F. Y.; Yuan, L.; Wu, H. N.; Dai, W. B.; Zhang, H.; Wang, X. Q.; Wang, J. C.; Zhang, X.; Zhang, Q. The Reduction of Tumor Interstitial Fluid Pressure by Liposomal Imatinib and Its Effect on Combination Therapy with Liposomal Doxorubicin. *Biomaterials* **2013**, *34*, 2277−2288.
(473) Wang, Y. G.; Yang, T. Y.; Wang, X.; Dai, W. B.; Wang, J. C.; Zhang, X. A.; Li, Z. Q.; Zhang, Q. A. Materializing Sequential Killing of Tumor Vasculature and Tumor Cells *via* Targeted Polymeric Micelle System. *J. Controlled Release* **2011**, *149*, 299−306.
(474) Lin, Z. Q.; Gao, W.; Hu, H. X.; Ma, K.; He, B.; Dai, W. B.; Wang, X. Q.; Wang, J. C.; Zhang, X.; Zhang, Q. Novel Thermo-Sensitive

DOI: 10.1021/acsnano.6b06040
ACS Nano 2017, 11, 2313−2381

Hydrogel System with Paclitaxel Nanocrystals: High Drug-Loading, Sustained Drug Release and Extended Local Retention Guaranteeing Better Efficacy and Lower Toxicity. *J. Controlled Release* **2014**, *174*, 161−170.
(475) Yang, Y.; Wang, J.; Zhang, X.; Lu, W.; Zhang, Q. A Novel Mixed Micelle Gel with Thermo-Sensitive Property for the Local Delivery of Docetaxel. *J. Controlled Release* **2009**, *135*, 175−182.
(476) Wang, Z.; Yu, Y.; Dai, W.; Cui, J.; Wu, H.; Yuan, L.; Zhang, H.; Wang, X.; Wang, J.; Zhang, X.; Zhang, Q. A Specific Peptide Ligand-Modified Lipid Nanoparticle Carrier for the Inhibition of Tumor Metastasis Growth. *Biomaterials* **2013**, *34*, 756−764.
(477) Wang, Z. H.; Yu, Y.; Dai, W. B.; Lu, J. K.; Cui, J. R.; Wu, H. N.; Yuan, L.; Zhang, H.; Wang, X. Q.; Wang, J. C.; Zhang, X.; Zhang, Q. The Use of a Tumor Metastasis Targeting Peptide to Deliver Doxorubicin-Containing Liposomes to Highly Metastatic Cancer. *Biomaterials* **2012**, *33*, 8451−8460.
(478) Wang, Z. H.; Yu, Y.; Ma, J.; Zhang, H. R.; Zhang, H.; Wang, X. Q.; Wang, J. C.; Zhang, X.; Zhang, Q. LyP-1 Modification To Enhance Delivery of Artemisinin or Fluorescent Probe Loaded Polymeric Micelles to Highly Metastatic Tumor and Its Lymphatics. *Mol. Pharmaceutics* **2012**, *9*, 2646−2657.
(479) Qin, C.; He, B.; Dai, W. B.; Zhang, H.; Wang, X. Q.; Wang, J. C.; Zhang, X.; Wang, G. J.; Yin, L. F.; Zhang, Q. Inhibition of Metastatic Tumor Growth and Metastasis *via* Targeting Metastatic Breast Cancer by Chlorotoxin-Modified Liposomes. *Mol. Pharmaceutics* **2014**, *11*, 3233−3241.
(480) Zhang, H.; Wang, X.; Dai, W.; Gemeinhart, R. A.; Zhang, Q.; Li, T. Pharmacokinetics and Treatment Efficacy of Camptothecin Nanocrystals on Lung Metastasis. *Mol. Pharmaceutics* **2014**, *11*, 226−233.
(481) Fu, J. J.; Wang, D.; Mei, D.; Zhang, H. R.; Wang, Z. Y.; He, B.; Dai, W. B.; Zhang, H.; Wang, X. Q.; Zhang, Q. Macrophage Mediated Biomimetic Delivery System for the Treatment of Lung Metastasis of Breast Cancer. *J. Controlled Release* **2015**, *204*, 11−19.
(482) Borel, F.; Kay, M. A.; Mueller, C. Recombinant AAV as a Platform for Translating the Therapeutic Potential of RNA Interference. *Mol. Ther.* **2014**, *22*, 692−701.
(483) Liu, Y. P.; Berkhout, B. Lentiviral Delivery of RNAi Effectors Against HIV-1. *Curr. Top. Med. Chem.* **2009**, *9*, 1130−1143.
(484) Liu, Y. P.; Berkhout, B. Gene Silencing Methods Using Vector-Encoded siRNAs or miRNAs. *Handbook of RNA Biochemistry*, 2nd ed.; Hartmann, R. K., Bindereif, A., Schön, A., Westhof, E., Eds.; Wiley-VCH: Weinheim, Germany, 2014; pp 1221−1242.
(485) Grunweller, A.; Hartmann, R. K. RNA Interference as a Gene-Specific Approach for Molecular Medicine. *Curr. Med. Chem.* **2005**, *12*, 3143−3161.
(486) Zhou, J.; Shum, K.-T.; Burnett, J.; Rossi, J. Nanoparticle-Based Delivery of RNAi Therapeutics: Progress and Challenges. *Pharmaceuticals* **2013**, *6*, 85−107.
(487) Krutzfeldt, J.; Rajewsky, N.; Braich, R.; Rajeev, K. G.; Tuschl, T.; Manoharan, M.; Stoffel, M. Silencing of mMcroRNAs *in Vivo* with "Antagomirs. *Nature* **2005**, *438*, 685−689.
(488) Nishina, K.; Unno, T.; Uno, Y.; Kubodera, T.; Kanouchi, T.; Mizusawa, H.; Yokota, T. Efficient *in Vivo* Delivery of siRNA to the Liver by Conjugation of Alpha-Tocopherol. *Mol. Ther.* **2008**, *16*, 734−740.
(489) Matsuda, S.; Keiser, K.; Nair, J. K.; Charisse, K.; Manoharan, R. M.; Kretschmer, P.; Peng, C. G.; Kel'in, A. V.; Kandasamy, P.; Willoughby, J. L. S.; Liebow, A.; Querbes, W.; Yucius, K.; Nguyen, T.; Milstein, S.; Maier, M. A.; Rajeev, K. G.; Manoharan, M. siRNA Conjugates Carrying Sequentially Assembled Trivalent N-Acetylgalactosamine Linked Through Nucleosides Elicit Robust Gene Silencing *in Vivo* in Hepatocytes. *ACS Chem. Biol.* **2015**, *10*, 1181−1187.
(490) Zhou, J. H.; Li, H. T.; Li, S.; Zaia, J.; Rossi, J. J. Novel Dual Inhibitory Function Aptamer-siRNA Delivery System for HIV-1 Therapy. *Mol. Ther.* **2008**, *16*, 1481−1489.
(491) Stein, C. A.; Hansen, J. B.; Lai, J.; Wu, S. J.; Voskresenskiy, A.; Hog, A.; Worm, J.; Hedtjarn, M.; Souleimanian, N.; Miller, P.; Soifer, H. S.; Castanotto, D.; Benimetskaya, L.; Orum, H.; Koch, T. Efficient Gene Silencing by Delivery of Locked Nucleic Acid Antisense Oligonucleotides, Unassisted by Transfection Reagents. *Nucleic Acids Res.* **2010**, *38*, e3.
(492) Bramsen, J. B.; Grünweller, A.; Hartmann, R. K.; Kjems, J. Using Chemical Modification To Enhance siRNA Performance. *Handbook of RNA Biochemistry*, 2nd ed.; Hartmann, R. K., Bindereif, A., Schön, A., Westhof, E., Eds.; Wiley-VCH: Weinheim, Germany, 2014; pp 1243−1277.
(493) Grunweller, A.; Hartmann, R. K. Locked Nucleic Acid Oligonucleotides − The Next Generation of Antisense Agents? *BioDrugs* **2007**, *21*, 235−243.
(494) Sarvestani, S. T.; Stunden, H. J.; Behlke, M. A.; Forster, S. C.; McCoy, C. E.; Tate, M. D.; Ferrand, J.; Lennox, K. A.; Latz, E.; Williams, B. R. G.; Gantier, M. P. Sequence-Dependent off-Target Inhibition of TLR7/8 Sensing by Synthetic microRNA Inhibitors. *Nucleic Acids Res.* **2015**, *43*, 1177−1188.
(495) Grunweller, A.; Wyszko, E.; Bieber, B.; Jahnel, R.; Erdmann, V. A.; Kurreck, J. Comparison of Different Antisense Strategies in Mammalian Cells Using Locked Nucleic Acids, 2 ′-O-Methyl RNA, Phosphorothioates and Small Interfering RNA. *Nucleic Acids Res.* **2003**, *31*, 3185−3193.
(496) Rinn, J. L.; Chang, H. Y. Genome Regulation by Long Noncoding RNAs. *Annu. Rev. Biochem.* **2012**, *81*, 145−166.
(497) Uchida, S.; Dimmeler, S. Long Noncoding RNAs in Cardiovascular Diseases. *Circ. Res.* **2015**, *116*, 737−750.
(498) Yang, G. D.; Lu, X. Z.; Yuan, L. J. LncRNA: A Link between RNA and cancer. *Biochim. Biophys. Acta, Gene Regul. Mech.* **2014**, *1839*, 1097−1109.
(499) Goraczniak, R.; Behlke, M. A.; Gunderson, S. I. Gene Silencing by Synthetic U1 Adaptors. *Nat. Biotechnol.* **2009**, *27*, 257−263.
(500) Grunweller, A.; Hartmann, R. K. Expanding RNA Silencing Approaches by U1 Adaptors. *ChemBioChem* **2009**, *10*, 1599−1601.
(501) ter Brake, O.; 't Hooft, K.; Liu, Y. P.; Centlivre, M.; von Eije, K. J.; Berkhout, B. Lentiviral Vector Design for Multiple shRNA Expression and Durable HIV-1 Inhibition. *Mol. Ther.* **2008**, *16*, 557−564.
(502) Stenvang, J.; Petri, A.; Lindow, M.; Obad, S.; Kauppinen, S. Inhibition of microRNA Function by antimiR Oligonucleotides. *Silence* **2012**, *3*, 1.
(503) Elmen, J.; Lindow, M.; Schutz, S.; Lawrence, M.; Petri, A.; Obad, S.; Lindholm, M.; Hedtjarn, M.; Hansen, H. F.; Berger, U.; Gullans, S.; Kearney, P.; Sarnow, P.; Straarup, E. M.; Kauppinen, S. LNA-Mediated microRNA Silencing in Non-Human Primates. *Nature* **2008**, *452*, 896−899.
(504) Lennox, K. A.; Behlke, M. A. Chemical Modification and Design of Anti-miRNA Oligonucleotides. *Gene Ther.* **2011**, *18*, 1111−1120.
(505) Lindow, M.; Kauppinen, S. Discovering the First microRNA-Targeted Drug. *J. Cell Biol.* **2012**, *199*, 407−412.
(506) Obad, S.; dos Santos, C. O.; Petri, A.; Heidenblad, M.; Broom, O.; Ruse, C.; Fu, C. X.; Lindow, M.; Stenvang, J.; Straarup, E. M.; Hansen, H. F.; Koch, T.; Pappin, D.; Hannon, G. J.; Kauppinen, S. Silencing of microRNA Families by Seed-Targeting Tiny LNAs. *Nat. Genet.* **2011**, *43*, 371−378.
(507) Thomas, M.; Lange-Grunweller, K.; Dayyoub, E.; Bakowsky, U.; Weirauch, U.; Aigner, A.; Hartmann, R. K.; Grunweller, A. PEI-Complexed LNA Antiseeds as miRNA Inhibitors. *RNA Biol.* **2012**, *9*, 1088−1098.
(508) Weirauch, U.; Grunweller, A.; Cuellar, L.; Hartmann, R. K.; Aigner, A. U1 Adaptors for the Therapeutic Knockdown of the Oncogene Pim-1 Kinase in Glioblastoma. *Nucleic Acid Ther.* **2013**, *23*, 264−272.
(509) Chen, C.; Xing, G.; Wang, J.; Zhao, Y.; Li, B.; Tang, J.; Jia, G.; Wang, T.; Sun, J.; Xing, L.; Yuan, H.; Gao, Y.; Meng, H.; Chen, Z.; Zhao, F.; Chai, Z.; Fang, X. Multihydroxylated [Gd@C82(OH)22]n Nanoparticles: Antineoplastic Activity of High Efficiency and Low Toxicity. *Nano Lett.* **2005**, *5*, 2050−2057.
(510) Yang, D.; Zhao, Y.; Guo, H.; Li, Y.; Tewary, P.; Xing, G.; Hou, W.; Oppenheim, J. J.; Zhang, N. [Gd@C(82) (OH)(22)](n) Nanoparticles Induce Dendritic Cell Maturation and Activate Th1 Immune Responses. *ACS Nano* **2010**, *4*, 1178−1186.

DOI: 10.1021/acsnano.6b06040
ACS Nano 2017, 11, 2313−2381

(511) Liu, Y.; Jiao, F.; Qiu, Y.; Li, W.; Lao, F.; Zhou, G.; Sun, B.; Xing, G.; Dong, J.; Zhao, Y.; Chai, Z.; Chen, C. The Effect of Gd@C82(OH)22 Nanoparticles on the Release of Th1/Th2 Cytokines and Induction of TNF-Alpha Mediated Cellular Immunity. *Biomaterials* **2009**, *30*, 3934−3945.
(512) Kang, S. G.; Zhou, G.; Yang, P.; Liu, Y.; Sun, B.; Huynh, T.; Meng, H.; Zhao, L.; Xing, G.; Chen, C.; Zhao, Y.; Zhou, R. Molecular Mechanism of Pancreatic Tumor Metastasis Inhibition by Gd@$C_{82}(OH)_{22}$ and Its Implication for *de Novo* Design of Nanomedicine. *Proc. Natl. Acad. Sci. U. S. A.* **2012**, *109*, 15431−15436.
(513) Liang, X. J.; Meng, H.; Wang, Y.; He, H.; Meng, J.; Lu, J.; Wang, P. C.; Zhao, Y.; Gao, X.; Sun, B.; Chen, C.; Xing, G.; Shen, D.; Gottesman, M. M.; Wu, Y.; Yin, J. J.; Jia, L. Metallofullerene Nanoparticles Circumvent Tumor Resistance to Cisplatin by Reactivating Endocytosis. *Proc. Natl. Acad. Sci. U. S. A.* **2010**, *107*, 7449−7454.
(514) Meng, H.; Xing, G.; Sun, B.; Zhao, F.; Lei, H.; Li, W.; Song, Y.; Chen, Z.; Yuan, H.; Wang, X.; Long, J.; Chen, C.; Liang, X.; Zhang, N.; Chai, Z.; Zhao, Y. Potent Angiogenesis Inhibition by the Particulate Form of Fullerene Derivatives. *ACS Nano* **2010**, *4*, 2773−2783.
(515) Meng, H.; Xing, G. M.; Blanco, E.; Song, Y.; Zhao, L. N.; Sun, B. Y.; Li, X. D.; Wang, P. C.; Korotcov, A.; Li, W.; Liang, X. J.; Chen, C. Y.; Yuan, H.; Zhao, F.; Chen, Z.; Sun, T.; Chai, Z. F.; Ferrari, M.; Zhao, Y. L. Gadolinium Metallofullerenol Nanoparticles Inhibit Cancer Metastasis through Matrix Metalloproteinase Inhibition: Imprisoning instead of Poisoning Cancer Cells. *Nanomedicine* **2012**, *8*, 136−146.
(516) Song, Y.; Zhang, M.; Zhao, L.; Yin, X.; Zhao, J.; Li, J.; He, R.; Chang, Y.; Jin, J.; Zhao, Y.; Li, J.; Xing, G. Regulation on Mechanical Properties of Collagen: Enhanced Bioactivities of Metallofullerol. *Nanomedicine* **2014**, *10*, 783−793.
(517) Wang, J. X.; Chen, C. Y.; Li, B.; Yu, H. W.; Zhao, Y. L.; Sun, J.; Li, Y. F.; Xing, G. M.; Yuan, H.; Tang, J.; Chen, Z.; Meng, H.; Gao, Y. X.; Ye, C.; Chai, Z. F.; Zhu, C. F.; Ma, B. C.; Fang, X. H.; Wan, L. J. Antioxidative Function and Biodistribution of $[Gd@C_{82}(OH)_{22}]_n$ Nanoparticles in Tumor-Bearing Mice. *Biochem. Pharmacol.* **2006**, *71*, 872−881.
(518) Yin, J. J.; Lao, F.; Meng, J.; Fu, P. P.; Zhao, Y. L.; Xing, G. M.; Gao, X. Y.; Sun, B. Y.; Wang, P. C.; Chen, C. Y.; Liang, X. J. Inhibition of Tumor Growth by Endohedral Metallofullerenol Nanoparticles Optimized as Reactive Oxygen Species Scavenger. *Mol. Pharmacol.* **2008**, *74*, 1132−1140.
(519) Yin, J. J.; Lao, F.; Fu, P. P.; Wamer, W. G.; Zhao, Y.; Wang, P. C.; Qiu, Y.; Sun, B.; Xing, G.; Dong, J.; Liang, X. J.; Chen, C. The Scavenging of Reactive Oxygen Species and the Potential for Cell Protection by Functionalized Fullerene Materials. *Biomaterials* **2009**, *30*, 611−621.
(520) Liu, Y.; Chen, C. Y.; Qian, P. X.; Lu, X. F.; Sun, B. Y.; Zhang, X.; Wang, L. M.; Gao, X. F.; Li, H.; Chen, Z. Y.; Tang, J. L.; Zhang, W. J.; Dong, J. Q.; Bai, R.; Lobie, P. E.; Wu, Q. F.; Liu, S. L.; Zhang, H. F.; Zhao, F.; Wicha, M. S.; Zhu, T.; Zhao, Y. L. Gd-Metallofullerenol Nanomaterial as Non-Toxic Breast Cancer Stem Cell-Specific Inhibitor. *Nat. Commun.* **2015**, *6*, 5988.
(521) Balogh, L. P. Caging Cancer. *Nanomedicine* **2015**, *11*, 867−896.
(522) Thomsen, H. S. Nephrogenic Systemic Fibrosis: A Serious Adverse Reaction to Gadolinium − 1997−2006−2016. Part 2. *Acta Radiol.* **2016**, *57*, 643.
(523) Thomsen, H. S. Nephrogenic Systemic Fibrosis: A Serious Adverse Reaction to Gadolinium − 1997−2006−2016. Part 1. *Acta Radiol.* **2016**, *57*, 515.
(524) Cha, S. H.; Hong, J.; McGuffie, M.; Yeom, B.; VanEpps, J. S.; Kotov, N. A. Shape-Dependent Biomimetic Inhibition of Enzyme by Nanoparticles and Their Antibacterial Activity. *ACS Nano* **2015**, *9*, 9097−9105.
(525) Wu, K.; Liu, J.; Johnson, R. N.; Yang, J.; Kopeček, J. Drug-Free Macromolecular Therapeutics: Induction of Apoptosis by Coiled-Coil-Mediated Cross-Linking of Antigens on the Cell Surface. *Angew. Chem., Int. Ed.* **2010**, *49*, 1451−1455.
(526) Wu, K.; Yang, J.; Liu, J.; Kopeček, J. Coiled-Coil Based Drug-Free Macromolecular Therapeutics: *In Vivo* Efficacy. *J. Controlled Release* **2012**, *157*, 126−131.
(527) Chu, T.-W.; Yang, J.; Zhang, R.; Sima, M.; Kopeček, J. Cell Surface Self-Assembly of Hybrid Nanoconjugates *via* Oligonucleotide Hybridization Induces Apoptosis. *ACS Nano* **2014**, *8*, 719−730.
(528) Zhang, R.; Yang, J.; Chu, T.-W.; Hartley, J. M.; Kopeček, J. Multimodality Imaging of Coiled-Coil Mediated Self-Assembly in a "Drug-Free" Therapeutic System. *Adv. Healthcare Mater.* **2015**, *4*, 1054−1065.
(529) Hartley, J. M.; Chu, T.-W.; Peterson, E. M.; Zhang, R.; Yang, J.; Harris, J.; Kopeček, J. Super-Resolution Imaging and Quantitative Analysis of Membrane Protein/Lipid Raft Clustering Mediated by Cell-Surface Self-Assembly of Hybrid Nanoconjugates. *ChemBioChem* **2015**, *16*, 1725−1729.
(530) Chu, T.-W.; Kosak, K. M.; Shami, P. J.; Kopeček, J. Drug-Free Macromolecular Therapeutics Induce Apoptosis of Patient Chronic Lymphocytic Leukemia Cells. *Drug Delivery Transl. Res.* **2014**, *4*, 389−394.
(531) Chu, T.-W.; Zhang, R.; Yang, J.; Chao, M. P.; Shami, P. J.; Kopeček, J. A Two-Step Pretargeted Nanotherapy for CD20 Cross-linking May Achieve Superior Anti-Lymphoma Efficacy to Rituximab. *Theranostics* **2015**, *5*, 834−846.
(532) Chu, T.-W.; Kopecek, J. Drug-Free Macromolecular Therapeutics − A New Paradigm in Polymeric Nanomedicines. *Biomater. Sci.* **2015**, *3*, 908−922.
(533) Lucky, S. S.; Soo, K. C.; Zhang, Y. Nanoparticles in Photodynamic Therapy. *Chem. Rev.* **2015**, *115*, 1990−2042.
(534) Jaque, D.; Martinez Maestro, L.; del Rosal, B.; Haro-Gonzalez, P.; Benayas, A.; Plaza, J. L.; Martin Rodriguez, E.; Garcia Sole, J. Nanoparticles for Photothermal Therapies. *Nanoscale* **2014**, *6*, 9494−9530.
(535) Deatsch, A. E.; Evans, B. A. Heating Efficiency in Magnetic Nanoparticle Hyperthermia. *J. Magn. Magn. Mater.* **2014**, *354*, 163−172.
(536) Castano, A. P.; Demidova, T. N.; Hamblin, M. R. Mechanisms in Photodynamic Therapy: Part One—Photosensitizers, Photochemistry and Cellular Localization. *Photodiagn. Photodyn. Ther.* **2004**, *1*, 279−293.
(537) Redmond, R. W.; Gamlin, J. N. A Compilation of Singlet Oxygen Yields from Biologically Relevant Molecules. *Photochem. Photobiol.* **1999**, *70*, 391−475.
(538) DeRosa, M. C.; Crutchley, R. J. Photosensitized Singlet Oxygen and Its Applications. *Coord. Chem. Rev.* **2002**, *233*, 351−371.
(539) GarciaFresnadillo, D.; Georgiadou, Y.; Orellana, G.; Braun, A. M.; Oliveros, E. Singlet-Oxygen $^1\Delta_g$ Production by ruthenium(II) Complexes Containing Polyazaheterocyclic Ligands in Methanol and in Water. *Helv. Chim. Acta* **1996**, *79*, 1222−1238.
(540) Ibanez, J. A.; Litter, M. I.; Pizarro, R. A. Photocatalytic Bactericidal Effect of TiO2 on Enterobacter Cloacae. Comparative Study with Other Gram (−) Bacteria. *J. Photochem. Photobiol., A* **2003**, *157*, 81−85.
(541) Dolmans, D.; Fukumura, D.; Jain, R. Photodynamic Therapy for Cancer. *Nat. Rev. Cancer* **2003**, *3*, 380−387.
(542) Wohrle, D.; Hirth, A.; Bogdahn-Rai, T.; Schnurpfeil, G.; Shopova, M. Photodynamic Therapy of Cancer: Second and Third Generations of Photosensitizers. *Russ. Chem. Bull.* **1998**, *47*, 807−816.
(543) Dolmans, D. E. J. G. J.; Kadambi, A.; Hill, J. S.; Waters, C. A.; Robinson, B. C.; Walker, J. P.; Fukumura, D.; Jain, R. K. Vascular Accumulation of a Novel Photosensitizer, MV6401, Causes Selective Thrombosis in Tumor Vessels after Photodynamic Therapy. *Cancer Res.* **2002**, *62*, 2151−2156.
(544) Wilson, B. C.; Patterson, M. S. The Physics, Biophysics and Technology of Photodynamic Therapy. *Phys. Med. Biol.* **2008**, *53*, R61−R109.
(545) Wust, P.; Hegewisch-Becker, S.; Issels, R. Hyperthermia: Current Status and Therapeutic Results. *Dtsch. Med. Wochenschr.* **2003**, *128*, 2023−2029.
(546) Hirsch, L. R.; Stafford, R. J.; Bankson, J. A.; Sershen, S. R.; Rivera, B.; Price, R. E.; Hazle, J. D.; Halas, N. J.; West, J. L. Nanoshell-Mediated Near-Infrared Thermal Therapy of Tumors Under Magnetic Resonance Guidance. *Proc. Natl. Acad. Sci. U. S. A.* **2003**, *100*, 13549−13554.

DOI: 10.1021/acsnano.6b06040
ACS Nano 2017, 11, 2313−2381

(547) Weissleder, R. A Clearer Vision for *in Vivo* Imaging. *Nat. Biotechnol.* **2001**, *19*, 316−317.
(548) Huang, X. H.; Jain, P. K.; El-Sayed, I. H.; El-Sayed, M. A. Determination of the Minimum Temperature Required for Selective Photothermal Destruction of Cancer Cells with the Use of Immunotargeted Gold Nanoparticles. *Photochem. Photobiol.* **2006**, *82*, 412−417.
(549) Huang, X.; El-Sayed, I. H.; Qian, W.; El-Sayed, M. A. Cancer Cell Imaging and Photothermal Therapy in the Near-Infrared Region by Using Gold Nanorods. *J. Am. Chem. Soc.* **2006**, *128*, 2115−2120.
(550) Jain, P. K.; El-Sayed, I. H.; El-Sayed, M. A. Au Nanoparticles Target Cancer. *Nano Today* **2007**, *2*, 18−29.
(551) Perez-Hernandez, M.; Del Pino, P.; Mitchell, S. G.; Moros, M.; Stepien, G.; Pelaz, B.; Parak, W. J.; Galvez, E. M.; Pardo, J.; de la Fuente, J. M. Dissecting the Molecular Mechanism of Apoptosis during Photothermal Therapy Using Gold Nanoprisms. *ACS Nano* **2015**, *9*, 52−61.
(552) Pelaz, B.; Grazu, V.; Ibarra, A.; Magen, C.; del Pino, P.; de la Fuente, J. M. Tailoring the Synthesis and Heating Ability of Gold Nanoprisms for Bioapplications. *Langmuir* **2012**, *28*, 8965−8970.
(553) O'Neal, D. P.; Hirsch, L. R.; Halas, N. J.; Payne, J. D.; West, J. L. Photo-Thermal Tumor Ablation in Mice Using near Infrared-Absorbing Nanoparticles. *Cancer Lett.* **2004**, *209*, 171−176.
(554) Loo, C.; Lin, A.; Hirsch, L.; Lee, M. H.; Barton, J.; Halas, N. J.; West, J.; Drezek, R. Nanoshell-Enabled Photonics-Based Imaging and Therapy of Cancer. *Technol. Cancer Res. Treat.* **2004**, *3*, 33−40.
(555) Loo, C.; Lowery, A.; Halas, N.; West, J.; Drezek, R. Immunotargeted Nanoshells for Integrated Cancer Imaging and Therapy. *Nano Lett.* **2005**, *5*, 709−711.
(556) Chen, J.; Wang, D.; Xi, J.; Au, L.; Siekkinen, A.; Warsen, A.; Li, Z. Y.; Zhang, H.; Xia, Y.; Li, X. Immuno Gold Nanocages with Tailored Optical Properties for Targeted Photothermal Destruction of Cancer Cells. *Nano Lett.* **2007**, *7*, 1318−1322.
(557) Gad, S. C.; Sharp, K. L.; Montgomery, C.; Payne, J. D.; Goodrich, G. P. Evaluation of the Toxicity of Intravenous Delivery of Auroshell Particles (Gold-Silica Nanoshells). *Int. J. Toxicol.* **2012**, *31*, 584−594.
(558) Bardhan, R.; Chen, W. X.; Perez-Torres, C.; Bartels, M.; Huschka, R. M.; Zhao, L. L.; Morosan, E.; Pautler, R. G.; Joshi, A.; Halas, N. J. Nanoshells with Targeted Simultaneous Enhancement of Magnetic and Optical Imaging and Photothermal Therapeutic Response. *Adv. Funct. Mater.* **2009**, *19*, 3901−3909.
(559) Bardhan, R.; Chen, W. X.; Bartels, M.; Perez-Torres, C.; Botero, M. F.; McAninch, R. W.; Contreras, A.; Schiff, R.; Pautler, R. G.; Halas, N. J.; Joshi, A. Tracking of Multimodal Therapeutic Nanocomplexes Targeting Breast Cancer *in Vivo*. *Nano Lett.* **2010**, *10*, 4920−4928.
(560) Bardhan, R.; Lal, S.; Joshi, A.; Halas, N. J. Theranostic Nanoshells: From Probe Design to Imaging and Treatment of Cancer. *Acc. Chem. Res.* **2011**, *44*, 936−946.
(561) Ayala-Orozco, C.; Liu, J. G.; Knight, M. W.; Wang, Y. M.; Day, J. K.; Nordlander, P.; Halas, N. J. Fluorescence Enhancement of Molecules Inside a Gold Nanomatryoshka. *Nano Lett.* **2014**, *14*, 2926−2933.
(562) Ayala-Orozco, C.; Urban, C.; Bishnoi, S.; Urban, A.; Charron, H.; Mitchell, T.; Shea, M.; Nanda, S.; Schiff, R.; Halas, N.; Joshi, A. Sub-100 Nm Gold Nanomatryoshkas Improve Photo-Thermal Therapy Efficacy in Large and Highly Aggressive Triple Negative Breast Tumors. *J. Controlled Release* **2014**, *191*, 90−97.
(563) Ayala-Orozco, C.; Urban, C.; Knight, M. W.; Urban, A. S.; Neumann, O.; Bishnoi, S. W.; Mukherjee, S.; Goodman, A. M.; Charron, H.; Mitchell, T.; Shea, M.; Roy, R.; Nanda, S.; Schiff, R.; Halas, N. J.; Joshi, A. Au Nanomatryoshkas as Efficient Near-Infrared Photothermal Transducers for Cancer Treatment: Benchmarking against Nanoshells. *ACS Nano* **2014**, *8*, 6372−6381.
(564) Pankhurst, Q. A.; Connolly, J.; Jones, S. K.; Dobson, J. Applications of Magnetic Nanoparticles in Biomedicine. *J. Phys. D: Appl. Phys.* **2003**, *36*, R167−R181.
(565) Pankhurst, Q. A.; Thanh, N. K. T.; Jones, S. K.; Dobson, J. Progress in Applications of Magnetic Nanoparticles in Biomedicine. *J. Phys. D: Appl. Phys.* **2009**, *42*, 224001.
(566) Fortin, J. P.; Wilhelm, C.; Servais, J.; Menager, C.; Bacri, J. C.; Gazeau, F. Size-Sorted Anionic Iron Oxide Nanomagnets as Colloidal Mediators for Magnetic Hyperthermia. *J. Am. Chem. Soc.* **2007**, *129*, 2628−2635.
(567) Guardia, P.; Di Corato, R.; Lartigue, L.; Wilhelm, C.; Espinosa, A.; Garcia-Hernandez, M.; Gazeau, F.; Manna, L.; Pellegrino, T. Water-Soluble Iron Oxide Nanocubes with High Values of Specific Absorption Rate for Cancer Cell Hyperthermia Treatment. *ACS Nano* **2012**, *6*, 3080−3091.
(568) Hergt, R.; Andrä, W.; d'Ambly, C. G.; Hilger, I.; Kaiser, W. A.; Richter, U.; Schmidt, H.-G. Physical Limits of Hyperthermia Using Magnetite Fine Particles. *IEEE Trans. Magn.* **1998**, *34*, 3745−3754.
(569) Kettering, M.; Winter, J.; Zeisberger, M.; Alexiou, C.; Bremer-Streck, S.; Bergemann, C.; Kaiser, W. A.; Hilger, I. Magnetically Based Enhancement of Nanoparticle Uptake in Tumor Cells: Combination of Magnetically Induced Cell Labeling and Magnetic Heating. *Rofo-Fortschritte Auf Dem Gebiet Der Rontgenstrahlen Und Der Bildgebenden Verfahren* **2006**, *178*, 1255−1260.
(570) Zhang, Q.; Castellanos-Rubio, I.; Munshi, R.; Orue, I.; Pelaz, B.; Gries, K. I.; Parak, W. J.; del Pino, P.; Pralle, A. Model Driven Optimization of Magnetic Anisotropy of Exchange-Coupled Core-Shell Ferrite Nanoparticles for Maximal Hysteretic Loss. *Chem. Mater.* **2015**, *27*, 7380−7387.
(571) Hergt, R.; Hiergeist, R.; Hilger, I.; Kaiser, W. A.; Lapatnikov, Y.; Margel, S.; Richter, U. Maghemite Nanoparticles with Very High AC-Losses for Application in RF-Magnetic Hyperthermia. *J. Magn. Magn. Mater.* **2004**, *270*, 345−357.
(572) Hergt, R.; Hiergeist, R.; Zeisberger, M.; Glockl, G.; Weitschies, W.; Ramirez, P.; Hilger, I.; Kaiser, W. A. Enhancement of AC-Losses of Magnetic Nanoparticles for Heating Applications. *J. Magn. Magn. Mater.* **2004**, *280*, 358−368.
(573) Hergt, R.; Hiergeist, R.; Zeisberger, M.; Schuler, D.; Heyen, U.; Hilger, I.; Kaiser, W. A. Magnetic Properties of Bacterial Magnetosomes as Potential Diagnostic and Therapeutic Tools. *J. Magn. Magn. Mater.* **2005**, *293*, 80−86.
(574) Dutz, S.; Hergt, R. Magnetic Particle Hyperthermia-a Promising Tumour Therapy? *Nanotechnology* **2014**, *25*, 452001.
(575) Alphandery, E.; Faure, S.; Seksek, O.; Guyot, F.; Chebbi, I. Chains of Magnetosomes Extracted from AMB-1 Magnetotactic Bacteria for Application in Alternative Magnetic Field Cancer Therapy. *ACS Nano* **2011**, *5*, 6279−6296.
(576) Raaphorst, G. P.; Li, L. F.; Yang, D. P.; LeBlanc, J. M. Cisplatin Sensitization by Concurrent Mild Hyperthermia in Parental and Mutant Cell Lines Deficient in Homologous Recombination and Non-Homologous Endjoining Repair. *Oncol. Rep.* **2005**, *14*, 281−285.
(577) Feliu, N.; Docter, D.; Heine, M.; del Pino, P.; Ashraf, S.; Kolosnjaj-Tabi, J.; Macchiarini, P.; Nielsen, P.; Alloyeau, D.; Gazeau, F.; Stauber, R. H.; Parak, W. J. *In Vivo* Degradation and the Fate of Inorganic Nanoparticles. *Chem. Soc. Rev.* **2016**, *45*, 2440−2457.
(578) Yu, M.; Zheng, J. Clearance Pathways and Tumor Targeting of Imaging Nanoparticles. *ACS Nano* **2015**, *9*, 6655−6674.
(579) Shiah, J. G.; Dvořák, M.; Kopečková, P.; Sun, Y.; Peterson, C. M.; Kopeček, J. Biodistribution and Antitumour Efficacy of Long-Circulating N-(2-Hydroxypropyl)methacrylamide Copolymer−doxorubicin Conjugates in Nude Mice. *Eur. J. Cancer* **2001**, *37*, 131−139.
(580) Seymour, L. W.; Duncan, R.; Strohalm, J.; Kopeček, J. Effect of Molecular Weight (Mw) of N-(2-Hydroxypropyl)methacrylamide Copolymers on Body Distribution and Rate of Excretion after Subcutaneous, Intraperitoneal, and Intravenous Administration to Rats. *J. Biomed. Mater. Res.* **1987**, *21*, 1341−1358.
(581) Yang, J.; Luo, K.; Pan, H.; Kopečková, P.; Kopeček, J. Synthesis of Biodegradable Multiblock Copolymers by Click Coupling of RAFT-Generated Heterotelechelic polyHPMA Conjugates. *React. Funct. Polym.* **2011**, *71*, 294−302.
(582) Luo, K.; Yang, J.; Kopečková, P.; Kopeček, J. Biodegradable Multiblock Poly[N-(2-hydroxypropyl)methacrylamide] *via* Reversible Addition−Fragmentation Chain Transfer Polymerization and Click Chemistry. *Macromolecules* **2011**, *44*, 2481−2488.

DOI: 10.1021/acsnano.6b06040
ACS Nano 2017, 11, 2313−2381

(583) Kricheldorf, H. R. In *Models of Biopolymers by Ring-Opening Polymerization*; Penczek, S., Ed.; CRC Press: Boca Raton, FL, 1990.
(584) Maurer, P. H.; Subrahmanyam, D.; Katchalski, E.; Blout, E. R. Antigenicity of Polypeptides (Poly Alpha Amino Acids). *J. Immunol.* **1959**, *83*, 193−197.
(585) Sela, M. Immunological Studies with Synthetic Polypeptides. *Adv. Immunol.* **1966**, *5*, 29−129.
(586) Hara, E.; Ueda, M.; Kim, C. J.; Makino, A.; Hara, I.; Ozeki, E.; Kimura, S. Suppressive Immune Response of Poly-(Sarcosine) Chains in Peptide-Nanosheets in Contrast to Polymeric Micelles. *J. Pept. Sci.* **2014**, *20*, 570−577.
(587) Lau, K. H. A.; Ren, C. L.; Sileika, T. S.; Park, S. H.; Szleifer, I.; Messersmith, P. B. Surface-Grafted Polysarcosine as a Peptoid Antifouling Polymer Brush. *Langmuir* **2012**, *28*, 16099−16107.
(588) Hortz, C.; Birke, A.; Kaps, L.; Decker, S.; Wachtersbach, E.; Fischer, K.; Schuppan, D.; Barz, M.; Schmidt, M. Cylindrical Brush Polymers with Polysarcosine Side Chains: A Novel Biocompatible Carrier for Biomedical Applications. *Macromolecules* **2015**, *48*, 2074−2086.
(589) Huesmann, D.; Sevenich, A.; Weber, B.; Barz, M. A Head-to-Head Comparison of Poly(sarcosine) and Poly(ethylene Glycol) in Peptidic, Amphiphilic Block Copolymers. *Polymer* **2015**, *67*, 240−248.
(590) Heller, P.; Birke, A.; Huesmann, D.; Weber, B.; Fischer, K.; Reske-Kunz, A.; Bros, M.; Barz, M. Introducing PeptoPlexes: Polylysine-block-Polysarcosine Based Polyplexes for Transfection of HEK 293T Cells. *Macromol. Biosci.* **2014**, *14*, 1380−1395.
(591) Ho, D.; Wang, C.-H. K.; Chow, E. K.-H. Nanodiamonds: The Intersection of Nanotechnology, Drug Development, and Personalized Medicine. *Sci. Adv.* **2015**, *1*, e1500439.
(592) Fischer, H. C.; Hauck, T. S.; Gomez-Aristizabal, A.; Chan, W. C. W. Exploring Primary Liver Macrophages for Studying Quantum Dot Interactions with Biological Systems. *Adv. Mater.* **2010**, *22*, 2520−2524.
(593) Ballou, B.; Lagerholm, B. C.; Ernst, L. A.; Bruchez, M. P.; Waggoner, A. S. Noninvasive Imaging of Quantum Dots in Mice. *Bioconjugate Chem.* **2004**, *15*, 79−86.
(594) Fischer, H. C.; Liu, L.; Pang, K. S.; Chan, W. C. W. Pharmacokinetics of Nanoscale Quantum Dots: *In Vivo* Distribution,-sequestration, and Clearance in the Rat. *Adv. Funct. Mater.* **2006**, *16*, 1299−1305.
(595) Goodman, A.; Cao, Y.; Urban, C.; Neumann, O.; Ayala-Orozco, C.; Knight, M.; Joshi, A.; Nordlander, P.; Halas, N. The Surprising *in Vivo* Instability of Near-IR-Absorbing Hollow Au-Ag Nanoshells. *ACS Nano* **2014**, *8*, 3222−3231.
(596) Hauck, T. S.; Anderson, R. E.; Fischer, H. C.; Newbigging, S.; Chan, W. C. W. *In Vivo* Quantum-Dot Toxicity Assessment. *Small* **2010**, *6*, 138−144.
(597) Van Haute, D.; Longmate, J. M.; Berlin, J. M. Controlled Assembly of Biocompatible Metallic Nanoaggregates Using a Small Molecule Crosslinker. *Adv. Mater.* **2015**, *27*, 5158−5164.
(598) Chou, L. Y. T.; Song, F.; Chan, W. C. W. Engineering the Structure and Properties of DNA-Nanoparticle Superstructures Using Polyvalent Counterions. *J. Am. Chem. Soc.* **2016**, *138*, 4565−4572.
(599) Bruinink, A.; Bitar, M.; Pleskova, M.; Wick, P.; Krug, H. F.; Maniura-Weber, K. Addition of Nanoscaled Bioinspired Surface Features: A Revolution for Bone-Related Implants and Scaffolds? *J. Biomed. Mater. Res., Part A* **2014**, *102*, 275−294.
(600) Marchesan, S.; Prato, M. Nanomaterials for (Nano)medicine. *ACS Med. Chem. Lett.* **2013**, *4*, 147−149.
(601) Marchesan, S.; Melchionna, M.; Prato, M. Wire Up on Carbon Nanostructures! How To Play a Winning Game. *ACS Nano* **2015**, *9*, 9441−9450.
(602) Ku, S. H.; Lee, M.; Park, C. B. Carbon-Based Nanomaterials for Tissue Engineering. *Adv. Healthcare Mater.* **2013**, *2*, 244−260.
(603) Marchesan, S.; Kostarelos, K.; Bianco, A.; Prato, M. The Winding Road for Carbon Nanotubes in Nanomedicine. *Mater. Today* **2015**, *18*, 12−19.
(604) Battigelli, A.; Ménard-Moyon, C.; Da Ros, T.; Prato, M.; Bianco, A. Endowing Carbon Nanotubes with Biological and Biomedical Properties by Chemical Modifications. *Adv. Drug Delivery Rev.* **2013**, *65*, 1899−1920.
(605) Saito, N.; Haniu, H.; Usui, Y.; Aoki, K.; Hara, K.; Takanashi, S.; Shimizu, M.; Narita, N.; Okamoto, M.; Kobayashi, S.; Nomura, H.; Kato, H.; Nishimura, N.; Taruta, S.; Endo, M. Safe Clinical Use of Carbon Nanotubes as Innovative Biomaterials. *Chem. Rev.* **2014**, *114*, 6040−6079.
(606) Zhang, Q. W.; Mochalin, V. N.; Neitzel, I.; Knoke, I. Y.; Han, J. J.; Klug, C. A.; Zhou, J. G.; Lelkes, P. I.; Gogotsi, Y. Fluorescent PLLA-Nanodiamond Composites for Bone Tissue Engineering. *Biomaterials* **2011**, *32*, 87−94.
(607) Shalek, A. K.; Robinson, J. T.; Karp, E. S.; Lee, J. S.; Ahn, D. R.; Yoon, M. H.; Sutton, A.; Jorgolli, M.; Gertner, R. S.; Gujral, T. S.; MacBeath, G.; Yang, E. G.; Park, H. Vertical Silicon Nanowires as a Universal Platform for Delivering Biomolecules into Living Cells. *Proc. Natl. Acad. Sci. U. S. A.* **2010**, *107*, 1870−1875.
(608) Chiappini, C.; Campagnolo, P.; Almeida, C. S.; Abbassi-Ghadi, N.; Chow, L. W.; Hanna, G. B.; Stevens, M. M. Mapping Local Cytosolic Enzymatic Activity in Human Esophageal Mucosa with Porous Silicon Nanoneedles. *Adv. Mater.* **2015**, *27*, 5147−5152.
(609) Chiappini, C.; Martinez, J. O.; De Rosa, E.; Almeida, C. S.; Tasciotti, E.; Stevens, M. M. Biodegradable Nanoneedles for Localized Delivery of Nanoparticles *in Vivo*: Exploring the Biointerface. *ACS Nano* **2015**, *9*, 5500−5509.
(610) Chiappini, C.; De Rosa, E.; Martinez, J. O.; Liu, X.; Steele, J.; Stevens, M. M.; Tasciotti, E. Biodegradable Silicon Nanoneedles Delivering Nucleic Acids Intracellularly Induce Localized *in Vivo* Neovascularization. *Nat. Mater.* **2015**, *14*, 532−539.
(611) Gross, G. W.; Rieske, E.; Kreutzberg, G. W.; Meyer, A. A New Fixed-Array Multi-Microelectrode System Designed for Long-Term Monitoring of Extracellular Single Unit Neuronal Activity *in Vitro*. *Neurosci. Lett.* **1977**, *6*, 101−105.
(612) Fromherz, P.; Offenhäusser, A.; Vetter, T.; Weis, J. A Neuron-Silicon Junction: A Retzius Cell of the Leech on an Insulated-Gate Filed-Effect Transistor. *Science* **1991**, *252*, 1290−1293.
(613) Stein, B.; George, M.; Parak, W. J.; Gaub, H. E. Extracellular Measurements of Averaged Ionic Currents with the Light-Addressable Potentiometric Sensor (LAPS). *Sens. Actuators, B* **2004**, *98*, 299−304.
(614) Patolsky, F.; Timko, B. P.; Yu, G. H.; Fang, Y.; Greytak, A. B.; Zheng, G. F.; Lieber, C. M. Detection, Stimulation, and Inhibition of Neuronal Signals with High-Density Nanowire Transistor Arrays. *Science* **2006**, *313*, 1100−1104.
(615) George, M.; Parak, W. J.; Gaub, H. E. Highly Integrated Surface Potential Sensors. *Sens. Actuators, B* **2000**, *69*, 266−275.
(616) Kotov, N. A.; Winter, J. O.; Clements, I. P.; Jan, E.; Timko, B. P.; Campidelli, S.; Pathak, S.; Mazzatenta, A.; Lieber, C. M.; Prato, M.; Bellamkonda, R. V.; Silva, G. A.; Kam, N. W. S.; Patolsky, F.; Ballerini, L. Nanomaterials for Neural Interfaces. *Adv. Mater.* **2009**, *21*, 3970−4004.
(617) Zhang, H. N.; Patel, P. R.; Xie, Z. X.; Swanson, S. D.; Wang, X. D.; Kotov, N. A. Tissue-Compliant Neural Implants from Micro-fabricated Carbon Nanotube Multilayer Composite. *ACS Nano* **2013**, *7*, 7619−7629.
(618) Kim, Y.; Zhu, J.; Yeom, B.; Di Prima, M.; Su, X. L.; Kim, J. G.; Yoo, S. J.; Uher, C.; Kotov, N. A. Stretchable Nanoparticle Conductors with Self-Organized Conductive Pathways. *Nature* **2013**, *500*, 59−63.
(619) Zhu, J.; Zhang, H. N.; Kotov, N. A. Thermodynamic and Structural Insights into Nanocomposites Engineering by Comparing Two Materials Assembly Techniques for Graphene. *ACS Nano* **2013**, *7*, 4818−4829.
(620) Kang, M.; Jung, S.; Zhang, H. N.; Kang, T.; Kang, H.; Yoo, Y.; Hong, J. P.; Ahn, J. P.; Kwak, J.; Jeon, D.; Kotov, N. A.; Kim, B. Subcellular Neural Probes from Single-Crystal Gold Nanowires. *ACS Nano* **2014**, *8*, 8182−8189.
(621) Mattson, M. P.; Haddon, R. C.; Rao, A. M. Molecular Functionalization of Carbon Nanotubes and Use as Substrates for Neuronal Growth. *J. Mol. Neurosci.* **2000**, *14*, 175−182.
(622) Lovat, V.; Pantarotto, D.; Lagostena, L.; Cacciari, B.; Grandolfo, M.; Righi, M.; Spalluto, G.; Prato, M.; Ballerini, L. Carbon Nanotube

DOI: 10.1021/acsnano.6b06040
ACS Nano 2017, 11, 2313−2381

Substrates Boost Neuronal Electrical Signaling. *Nano Lett.* **2005**, *5*, 1107−1110.
(623) Cellot, G.; Cilia, E.; Cipollone, S.; Rancic, V.; Sucapane, A.; Giordani, S.; Gambazzi, L.; Markram, H.; Grandolfo, M.; Scaini, D.; Gelain, F.; Casalis, L.; Prato, M.; Giugliano, M.; Ballerini, L. Carbon Nanotubes Might Improve Neuronal Performance by Favouring Electrical Shortcuts. *Nat. Nanotechnol.* **2009**, *4*, 126−133.
(624) Cellot, G.; Toma, F. M.; Kasap Varley, Z.; Laishram, J.; Villari, A.; Quintana, M.; Cipollone, S.; Prato, M.; Ballerini, L. Carbon Nanotube Scaffolds Tune Synaptic Strength in Cultured Neural Circuits: Novel Frontiers in Nanomaterial−Tissue Interactions. *J. Neurosci.* **2011**, *31*, 12945−12953.
(625) Fabbro, A.; Villari, A.; Laishram, J.; Scaini, D.; Toma, F. M.; Turco, A.; Prato, M.; Ballerini, L. Spinal Cord Explants Use Carbon Nanotube Interfaces To Enhance Neurite Outgrowth and To Fortify Synaptic Inputs. *ACS Nano* **2012**, *6*, 2041−2055.
(626) Huang, Y.-C.; Hsu, S.-H.; Kuo, W.-C.; Chang-Chien, C.-L.; Cheng, H.; Huang, Y.-Y. Effects of Laminin-Coated Carbon Nanotube/Chitosan Fibers on Guided Neurite Growth. *J. Biomed. Mater. Res., Part A* **2011**, *99A*, 86−93.
(627) Lewitus, D. Y.; Landers, J.; Branch, J.; Smith, K. L.; Callegari, G.; Kohn, J.; Neimark, A. V. Biohybrid Carbon Nanotube/Agarose Fibers for Neural Tissue Engineering. *Adv. Funct. Mater.* **2011**, *21*, 2624−2632.
(628) Lee, H. J.; Yoon, O. J.; Kim, D. H.; Jang, Y. M.; Kim, H. W.; Lee, W. B.; Lee, N.-E.; Kim, S. S. Neurite Outgrowth on Nanocomposite Scaffolds Synthesized from PLGA and Carboxylated Carbon Nanotubes. *Adv. Eng. Mater.* **2009**, *11*, B261−B266.
(629) Jin, G.-Z.; Kim, M.; Shin, U. S.; Kim, H.-W. Neurite Outgrowth of Dorsal Root Ganglia Neurons Is Enhanced on Aligned Nanofibrous Biopolymer Scaffold with Carbon Nanotube Coating. *Neurosci. Lett.* **2011**, *501*, 10−14.
(630) Bosi, S.; Rauti, R.; Laishram, J.; Turco, A.; Lonardoni, D.; Nieus, T.; Prato, M.; Scaini, D.; Ballerini, L. From 2D to 3D: Novel Nanostructured Scaffolds to Investigate Signalling in Reconstructed Neuronal Networks. *Sci. Rep.* **2015**, *5*, 9562.
(631) Tyler, W. J. The Mechanobiology of Brain Function. *Nat. Rev. Neurosci.* **2012**, *13*, 867−878.
(632) Martinelli, V.; Cellot, G.; Toma, F. M.; Long, C. S.; Caldwell, J. H.; Zentilin, L.; Giacca, M.; Turco, A.; Prato, M.; Ballerini, L.; Mestroni, L. Carbon Nanotubes Promote Growth and Spontaneous Electrical Activity in Cultured Cardiac Myocytes. *Nano Lett.* **2012**, *12*, 1831−1838.
(633) Pok, S.; Vitale, F.; Eichmann, S. L.; Benavides, O. M.; Pasquali, M.; Jacot, J. G. Biocompatible Carbon Nanotube−Chitosan Scaffold Matching the Electrical Conductivity of the Heart. *ACS Nano* **2014**, *8*, 9822−9832.
(634) Shin, S. R.; Jung, S. M.; Zalabany, M.; Kim, K.; Zorlutuna, P.; Kim, S. B.; Nikkhah, M.; Khabiry, M.; Azize, M.; Kong, J.; Wan, K. T.; Palacios, T.; Dokmeci, M. R.; Bae, H.; Tang, X. S.; Khademhosseini, A. Carbon-Nanotube-Embedded Hydrogel Sheets for Engineering Cardiac Constructs and Bioactuators. *ACS Nano* **2013**, *7*, 2369−2380.
(635) Kharaziha, M.; Shin, S. R.; Nikkhah, M.; Topkaya, S. N.; Masoumi, N.; Annabi, N.; Dokmeci, M. R.; Khademhosseini, A. Tough and Flexible CNT−polymeric Hybrid Scaffolds for Engineering Cardiac Constructs. *Biomaterials* **2014**, *35*, 7346−7354.
(636) Martinelli, V.; Cellot, G.; Toma, F. M.; Long, C. S.; Caldwell, J. H.; Zentilin, L.; Giacca, M.; Turco, A.; Prato, M.; Ballerini, L.; Mestroni, L. Carbon Nanotubes Instruct Physiological Growth and Functionally Mature Syncytia: Nongenetic Engineering of Cardiac Myocytes. *ACS Nano* **2013**, *7*, 5746−5756.
(637) Sheng, Z. Y.; Fu, X. B.; Cai, S.; Lei, Y. H.; Sun, T. Z.; Bai, X. D.; Chen, M. L. Regeneration of Functional Sweat Gland-Like Structures by Transplanted Differentiated Bone Marrow Mesenchymal Stem Cells. *Wound Repair Regen.* **2009**, *17*, 427−435.
(638) Li, H. H.; Fu, X. B.; Ouyang, Y. S.; Cai, C. L.; Wang, J.; Sun, T. Z. Adult Bone-Marrow-Derived Mesenchymal Stem Cells Contribute to Wound Healing of Skin Appendages. *Cell Tissue Res.* **2006**, *326*, 725−736.
(639) Kushida, A.; Yamato, M.; Konno, C.; Kikuchi, A.; Sakurai, Y.; Okano, T. Decrease in Culture Temperature Releases Monolayer Endothelial Cell Sheets Together with Deposited Fibronectin Matrix from Temperature-Responsive Culture Surfaces. *J. Biomed. Mater. Res.* **1999**, *45*, 355−362.
(640) Giner-Casares, J. J.; Henriksen-Lacey, M.; García, I.; Liz-Marzán, L. M. Plasmonic Surfaces for Cell Growth and Retrieval Triggered by Near-Infrared Light. *Angew. Chem., Int. Ed.* **2016**, *55*, 974−978.
(641) Haraguchi, Y.; Shimizu, T.; Yamato, M.; Kikuchi, A.; Okano, T. Electrical Coupling of Cardiomyocyte Sheets Occurs Rapidly *via* Functional Gap Junction Formation. *Biomaterials* **2006**, *27*, 4765−4774.
(642) Shimizu, T.; Yamato, M.; Isoi, Y.; Akutsu, T.; Setomaru, T.; Abe, K.; Kikuchi, A.; Umezu, M.; Okano, T. Fabrication of Pulsatile Cardiac Tissue Grafts Using a Novel 3-Dimensional Cell Sheet Manipulation Technique and Temperature-Responsive Cell Culture Surfaces. *Circ. Res.* **2002**, *90*, 40e−48.
(643) Iwata, T.; Yamato, M.; Ishikawa, I.; Ando, T.; Okano, T. Tissue Engineering in Periodontal Tissue. *Anat. Rec.* **2014**, *297*, 16−25.
(644) Matsuura, K.; Utoh, R.; Nagase, K.; Okano, T. Cell Sheet Approach for Tissue Engineering and Regenerative Medicine. *J. Controlled Release* **2014**, *190*, 228−239.
(645) Folkman, J.; Hochberg, M. Self-Regulation of Growth in 3 Dimensions. *J. Exp. Med.* **1973**, *138*, 745−753.
(646) Haraguchi, Y.; Shimizu, T.; Sasagawa, T.; Sekine, H.; Sakaguchi, K.; Kikuchi, T.; Sekine, W.; Sekiya, S.; Yamato, M.; Umezu, M.; Okano, T. Fabrication of Functional Three-Dimensional Tissues by Stacking Cell Sheets. *Nat. Protoc.* **2012**, *7*, 850−858.
(647) Sekine, H.; Shimizu, T.; Sakaguchi, K.; Dobashi, I.; Wada, M.; Yamato, M.; Kobayashi, E.; Umezu, M.; Okano, T. *In Vitro* Fabrication of Functional Three-Dimensional Tissues with Perfusable Blood Vessels. *Nat. Commun.* **2013**, *4*, 1399.
(648) Mahmoudi, M.; Bonakdar, S.; Shokrgozar, M. A.; Aghaverdi, H.; Hartmann, R.; Pick, A.; Witte, G.; Parak, W. J. Cell-Imprinted Substrates Direct the Fate of Stem Cells. *ACS Nano* **2013**, *7*, 8379−8384.
(649) Ott, H. C.; Matthiesen, T. S.; Goh, S.-K.; Black, L. D.; Kren, S. M.; Netoff, T. I.; Taylor, D. A. Perfusion-Decellularized Matrix: Using Nature's Platform To Engineer a Bioartificial Heart. *Nat. Med.* **2008**, *14*, 213−221.
(650) Liu, A.; Xue, G.-h.; Sun, M.; Shao, H.-f.; Ma, C.-y.; Gao, Q.; Gou, Z.-r.; Yan, S.-g.; Liu, Y.-m.; He, Y. 3D Printing Surgical Implants at the Clinic: A Experimental Study on Anterior Cruciate Ligament Reconstruction. *Sci. Rep.* **2016**, *6*, 21704.
(651) Liu, N. B.; Huang, S.; Yao, B.; Xie, J. F.; Wu, X.; Fu, X. B. 3D Bioprinting Matrices with Controlled Pore Structure and Release Function Guide *In Vitro* Self-Organization of Sweat Gland. *Sci. Rep.* **2016**, *6*, 34410.
(652) Mansfield, E. G.; Greene, V. K., Jr.; Auguste, D. T. Patterned, Tubular Scaffolds Mimic Longitudinal and Radial Mechanics of the Neonatal Trachea. *Acta Biomater.* **2016**, *33*, 176−182.
(653) Dua, K. S.; Hogan, W. J.; Aadam, A. A.; Gasparri, M. *In-Vivo* Oesophageal Regeneration in a Human Being by Use of a Non-Biological Scaff Old and Extracellular Matrix. *Lancet* **2016**, *388*, 55−61.
(654) Delaere, P. R. Stem-Cell "Hype" in Tracheal Transplantation? *Transplantation* **2010**, *90*, 927−928.
(655) Delaere, P. R. Tracheal Transplantation. *Curr. Opin. Pulm. Med.* **2012**, *18*, 313−320.
(656) Abbott, A. Culture of Silence and Nonchalance Protected Disgraced Trachea Surgeon. *Nature* **2016**, DOI: 10.1038/nature.2016.20533.
(657) Delaere, P. R.; Hermans, R. Clinical Transplantation of a Tissue-Engineered Airway. *Lancet* **2009**, *373*, 717−718.
(658) Delaere, P.; Raemdonck, D. V. Tracheal Replacement. *J. Thorac. Dis.* **2016**, *8*, S186−S196.
(659) Murphy, S. V.; Atala, A. 3D Bioprinting of Tissues and Organs. *Nat. Biotechnol.* **2014**, *32*, 773−785.
(660) Bhise, N. S.; Ribas, J.; Manoharan, V.; Zhang, Y. S.; Polini, A.; Massa, S.; Dokmeci, M. R.; Khademhosseini, A. Organ-on-a-Chip Platforms for Studying Drug Delivery Systems. *J. Controlled Release* **2014**, *190*, 82−93.

DOI: 10.1021/acsnano.6b06040
ACS Nano 2017, 11, 2313−2381

(661) Cha, C. Y.; Shin, S. R.; Annabi, N.; Dokmeci, M. R.; Khademhosseini, A. Carbon-Based Nanomaterials: Multifunctional Materials for Biomedical Engineering. *ACS Nano* **2013**, *7*, 2891−2897.
(662) Gaharwar, A. K.; Peppas, N. A.; Khademhosseini, A. Nanocomposite Hydrogels for Biomedical Applications. *Biotechnol. Bioeng.* **2014**, *111*, 441−453.
(663) Hassanzadeh, P.; Kharaziha, M.; Nikkhah, M.; Shin, S. R.; Jin, J.; He, S.; Sun, W.; Zhong, C.; Dokmeci, M. R.; Khademhosseini, A.; Rolandi, M. Chitin Nanofiber Micropatterned Flexible Substrates for Tissue Engineering. *J. Mater. Chem. B* **2013**, *1*, 4217−4224.
(664) Kharaziha, M.; Nikkhah, M.; Shin, S. R.; Annabi, N.; Masoumi, N.; Gaharwar, A. K.; Camci-Unal, G.; Khademhosseini, A. PGS:Gelatin Nanofibrous Scaffolds with Tunable Mechanical and Structural Properties for Engineering Cardiac Tissues. *Biomaterials* **2013**, *34*, 6355−6366.
(665) Kang, H.-W.; Lee, S. J.; Ko, I. K.; Kengla, C.; Yoo, J. J.; Atala, A. A 3D Bioprinting System to Produce Human-Scale Tissue Constructs with Structural Integrity. *Nat. Biotechnol.* **2016**, *34*, 312−316.
(666) Tamayol, A.; Akbari, M.; Annabi, N.; Paul, A.; Khademhosseini, A.; Juncker, D. Fiber-Based Tissue Engineering: Progress, Challenges, and Opportunities. *Biotechnol. Adv.* **2013**, *31*, 669−687.
(667) Hasan, A.; Memic, A.; Annabi, N.; Hossain, M.; Paul, A.; Dokmeci, M. R.; Dehghani, F.; Khademhosseini, A. Electrospun Scaffolds for Tissue Engineering of Vascular Grafts. *Acta Biomater.* **2014**, *10*, 11−25.
(668) Ifkovits, J. L.; Devlin, J. J.; Eng, G.; Martens, T. P.; Vunjak-Novakovic, G.; Burdick, J. A. Biodegradable Fibrous Scaffolds with Tunable Properties Formed from Photo-Cross-Linkable Poly(glycerol sebacate). *ACS Appl. Mater. Interfaces* **2009**, *1*, 1878−1886.
(669) Seidlits, S. K.; Lee, J. Y.; Schmidt, C. E. Nanostructured Scaffolds for Neural Applications. *Nanomedicine* **2008**, *3*, 183−199.
(670) Kotov, N. A.; Liu, Y. F.; Wang, S. P.; Cumming, C.; Eghtedari, M.; Vargas, G.; Motamedi, M.; Nichols, J.; Cortiella, J. Inverted Colloidal Crystals as Three-Dimensional Cell Scaffolds. *Langmuir* **2004**, *20*, 7887−7892.
(671) Liu, Y. F.; Wang, S. P.; Krouse, J.; Kotov, N. A.; Eghtedari, M.; Vargas, G.; Motamedi, M. Rapid Aqueous Photo-Polymerization Route to Polymer and Polymer-Composite Hydrogel 3D Inverted Colloidal Crystal Scaffolds. *J. Biomed. Mater. Res., Part A* **2007**, *83A*, 1−9.
(672) Zhang, Y. J.; Wang, S. P.; Eghtedari, M.; Motamedi, M.; Kotov, N. A. Inverted-Colloidal-Crystal Hydrogel Matrices as Three-Dimensional Cell Scaffolds. *Adv. Funct. Mater.* **2005**, *15*, 725−731.
(673) Cuddihy, M. J.; Kotov, N. A. Poly(lactic-co-glycolic acid) Bone Scaffolds with Inverted Colloidal Crystal Geometry. *Tissue Eng., Part A* **2008**, *14*, 1639−1649.
(674) Nichols, J. E.; Cortiella, J. Q.; Lee, J.; Niles, J. A.; Cuddihy, M.; Wang, S. P.; Bielitzki, J.; Cantu, A.; Mlcak, R.; Valdivia, E.; Yancy, R.; McClure, M. L.; Kotov, N. A. *In Vitro* Analog of Human Bone Marrow from 3D Scaffolds with Biomimetic Inverted Colloidal Crystal Geometry. *Biomaterials* **2009**, *30*, 1071−1079.
(675) Lee, J.; Kotov, N. A. Notch Ligand Presenting Acellular 3D Microenvironments for ex vivo Human Hematopoietic Stem-Cell Culture made by Layer-By-Layer Assembly. *Small* **2009**, *5*, 1008−1013.
(676) Lee, J.; Shanbhag, S.; Kotov, N. A. Inverted Colloidal Crystals as Three-Dimensional Microenvironments for Cellular Co-Cultures. *J. Mater. Chem.* **2006**, *16*, 3558−3564.
(677) Lee, J.; Lilly, G. D.; Doty, R. C.; Podsiadlo, P.; Kotov, N. A. *In Vitro* Toxicity Testing of Nanoparticles in 3D Cell Culture. *Small* **2009**, *5*, 1213−1221.
(678) Gaharwar, A. K.; Mihaila, S. M.; Swami, A.; Patel, A.; Sant, S.; Reis, R. L.; Marques, A. P.; Gomes, M. E.; Khademhosseini, A. Bioactive Silicate Nanoplatelets for Osteogenic Differentiation of Human Mesenchymal Stem Cells. *Adv. Mater.* **2013**, *25*, 3329−3336.
(679) Ahadian, S.; Ramon-Azcon, J.; Estili, M.; Liang, X. B.; Ostrovidov, S.; Shiku, H.; Ramalingam, M.; Nakajima, K.; Sakka, Y.; Bae, H.; Matsue, T.; Khademhosseini, A. Hybrid Hydrogels Containing Vertically Aligned Carbon Nanotubes with Anisotropic Electrical Conductivity for Muscle Myofiber Fabrication. *Sci. Rep.* **2014**, *4*, 4271.
(680) Shin, S. R.; Bae, H.; Cha, J. M.; Mun, J. Y.; Chen, Y. C.; Tekin, H.; Shin, H.; Farshchi, S.; Dokmeci, M. R.; Tang, S.; Khademhosseini, A. Carbon Nanotube Reinforced Hybrid Microgels as Scaffold Materials for Cell Encapsulation. *ACS Nano* **2012**, *6*, 362−372.
(681) Qi, H.; Ghodousi, M.; Du, Y.; Grun, C.; Bae, H.; Yin, P.; Khademhosseini, A. DNA-Directed Self-Assembly of Shape-Controlled Hydrogels. *Nat. Commun.* **2013**, *4*, 2275.
(682) Wang, B.; Ren, K.; Wang, H.; Ji, J.; Chang, H. Construction of Degradable Multilayer Films for Enhanced Antibacterial Properties. *ACS Appl. Mater. Interfaces* **2013**, *5*, 4136−4143.
(683) Paulo, C. S. O.; Vidal, M.; Ferreira, L. S. Antifungal Nanoparticles and Surfaces. *Biomacromolecules* **2010**, *11*, 2810−2817.
(684) Botequim, D.; Maia, J.; Lino, M. M. F.; Lopes, L. M. F.; Simoes, P. N.; Ilharco, L. M.; Ferreira, L. Nanoparticles and Surfaces Presenting Antifungal, Antibacterial and Antiviral Properties. *Langmuir* **2012**, *28*, 7646−7656.
(685) Jones, N.; Ray, B.; Ranjit, K. T.; Manna, A. C. Antibacterial Activity of ZnO Nanoparticle Suspensions on a Broad Spectrum of Microorganisms. *FEMS Microbiol. Lett.* **2008**, *279*, 71−76.
(686) Raghupathi, K. R.; Koodali, R. T.; Manna, A. C. Size-Dependent Bacterial Growth Inhibition and Mechanism of Antibacterial Activity of Zinc Oxide Nanoparticles. *Langmuir* **2011**, *27*, 4020−4028.
(687) Zhang, L. L.; Jiang, Y. H.; Ding, Y. L.; Povey, M.; York, D. Investigation into the Antibacterial Behaviour of Suspensions of ZnO Nanoparticles (ZnO Nanofluids). *J. Nanopart. Res.* **2007**, *9*, 479−489.
(688) Applerot, G.; Lipovsky, A.; Dror, R.; Perkas, N.; Nitzan, Y.; Lubart, R.; Gedanken, A. Enhanced Antibacterial Activity of Nanocrystalline ZnO Due to Increased ROS-Mediated Cell Injury. *Adv. Funct. Mater.* **2009**, *19*, 842−852.
(689) Applerot, G.; Perkas, N.; Amirian, G.; Girshevitz, O.; Gedanken, A. Coating of Glass with ZnO *via* Ultrasonic Irradiation and a Study of Its Antibacterial Properties. *Appl. Surf. Sci.* **2009**, *256*, S3−S8.
(690) Politano, A. D.; Campbell, K. T.; Rosenberger, L. H.; Sawyer, R. G. Use of Silver in the Prevention and Treatment of Infections: Silver Review. *Surg. Infect.* **2013**, *14*, 8−20.
(691) Schierholz, J. M.; Lucas, L. J.; Rump, A.; Pulverer, G. Efficacy of Silver-Coated Medical Devices. *J. Hosp. Infect.* **1998**, *40*, 257−262.
(692) Darouiche, R. O. Anti-Infective Efficacy of Silver-Coated Medical Prostheses. *Clin. Infect. Dis.* **1999**, *29*, 1371−1377.
(693) Premanathan, M.; Karthikeyan, K.; Jeyasubramanian, K.; Manivannan, G. Selective Toxicity of ZnO Nanoparticles toward Gram-Positive Bacteria and Cancer Cells by Apoptosis through Lipid Peroxidation. *Nanomedicine* **2011**, *7*, 184−192.
(694) Hanley, C.; Layne, J.; Punnoose, A.; Reddy, K. M.; Coombs, I.; Coombs, A.; Feris, K.; Wingett, D. Preferential Killing of Cancer Cells and Activated Human T Cells Using ZnO Nanoparticles. *Nanotechnology* **2008**, *19*, 295103.
(695) Bressler, A. M.; Kaye, K. S.; LiPuma, J. J.; Alexander, B. D.; Moore, C. M.; Reller, L. B.; Woods, C. W. Risk Factors for Burkholderia Cepacia Complex Bacteremia among Intensive Care Unit Patients without Cystic Fibrosis: A Case-Control Study. *Infect. Control Hosp. Epidemiol.* **2007**, *28*, 951−958.
(696) Lai, C. C.; Teng, L. J.; Hsueh, P. R.; Yuan, A.; Tsai, K. C.; Tang, J. L.; Tien, H. F. Clinical and Microbiological Characteristics of Rhizobium Radiobacter Infections. *Clin. Infect. Dis.* **2004**, *38*, 149−153.
(697) Zhou, C. C.; Wang, M. Z.; Zou, K. D.; Chen, J.; Zhu, Y. Q.; Du, J. Z. Antibacterial Polypeptide-Grafted Chitosan-Based Nanocapsules As an "Armed" Carrier of Anticancer and Antiepileptic Drugs. *ACS Macro Lett.* **2013**, *2*, 1021−1025.
(698) Wang, M. Z.; Zhou, C. C.; Chen, J.; Xiao, Y. F.; Du, J. Z. Multifunctional Biocompatible and Biodegradable Folic Acid Conjugated Poly(epsilon-caprolactone)-Polypeptide Copolymer Vesicles with Excellent Antibacterial Activities. *Bioconjugate Chem.* **2015**, *26*, 725−734.
(699) Kim, S.; Lim, Y. T.; Soltesz, E. G.; De Grand, A. M.; Lee, J.; Nakayama, A.; Parker, J. A.; Mihaljevic, T.; Laurence, R. G.; Dor, D. M.; Cohn, L. H.; Bawendi, M. G.; Frangioni, J. V. Near-Infrared Fluorescent Type II Quantum Dots for Sentinel Lymph Node Mapping. *Nat. Biotechnol.* **2004**, *22*, 93−97.

DOI: 10.1021/acsnano.6b06040
ACS Nano 2017, 11, 2313−2381

(700) Xie, J.; Lee, S.; Chen, X. Y. Nanoparticle-Based Theranostic Agents. *Adv. Drug Delivery Rev.* **2010**, *62*, 1064−1079.
(701) Okusanya, O. T.; Holt, D.; Heitjan, D.; Deshpande, C.; Venegas, O.; Jiang, J.; Judy, R.; DeJesus, E.; Madajewski, B.; Oh, K.; Wang, M.; Albelda, S. M.; Nie, S. M.; Singhal, S. Intraoperative Near-Infrared Imaging Can Identify Pulmonary Nodules. *Ann. Thorac. Surg.* **2014**, *98*, 1223−1230.
(702) Keating, J. J.; Kennedy, G. T.; Singhal, S. Identification of a Subcentimeter Pulmonary Adenocarcinoma Using Intraoperative near-Infrared Imaging during Video-Assisted Thoracoscopic Surgery. *J. Thorac. Cardiovasc. Surg.* **2015**, *149*, e51−e53.
(703) Keating, J.; Crisman, E.; Singhal, S. Indocyanine Green (ICG) Extraction and Quantification for Intraoperative Molecular Imaging of Tumors. *J. Nucl. Med.* **2015**, *56*, 1218.
(704) Freise, A. C.; Wu, A. M. *In Vivo* Imaging with Antibodies and Engineered Fragments. *Mol. Immunol.* **2015**, *67*, 142−152.
(705) Sampath, L.; Kwon, S.; Ke, S.; Wang, W.; Schiff, R.; Mawad, M. E.; Sevick-Muraca, E. M. Dual-Labeled Trastuzumab-Based Imaging Agent for the Detection of Human Epidermal Growth Factor Receptor 2 Overexpression in Breast Cancer. *J. Nucl. Med.* **2007**, *48*, 1501−1510.
(706) van Scheltinga, A. G. T. T.; van Dam, G. M.; Nagengast, W. B.; Ntziachristos, V.; Hollema, H.; Herek, J. L.; Schroder, C. P.; Kosterink, J. G. W.; Lub-de Hoog, M. N.; de Vries, E. G. E. Intraoperative Near-Infrared Fluorescence Tumor Imaging with Vascular Endothelial Growth Factor and Human Epidermal Growth Factor Receptor 2 Targeting Antibodies. *J. Nucl. Med.* **2011**, *52*, 1778−1785.
(707) Rosenthal, E. L.; Warram, J. M.; de Boer, E.; Chung, T. K.; Korb, M. L.; Brandwein-Gensler, M.; Strong, T. V.; Schmalbach, C. E.; Morlandt, A. B.; Agarwal, G.; Hartman, Y. E.; Carroll, W. R.; Richman, J. S.; Clemons, L. K.; Nabell, L. M.; Zinn, K. R. Safety and Tumor Specificity of Cetuximab-IRDye800 for Surgical Navigation in Head and Neck Cancer. *Clin. Cancer Res.* **2015**, *21*, 3658−3666.
(708) van de Ven, S. M. W. Y.; Elias, S. G.; Chan, C. T.; Miao, Z.; Cheng, Z.; De, A.; Gambhir, S. S. Optical Imaging with Her2-Targeted Affibody Molecules Can Monitor Hsp90 Treatment Response in a Breast Cancer Xenograft Mouse Model. *Clin. Cancer Res.* **2012**, *18*, 1073−1081.
(709) Lee, S. B.; Hassan, M.; Fisher, R.; Chertov, O.; Chernomordik, V.; Kramer-Marek, G.; Gandjbakhche, A.; Capala, J. Affibody Molecules for *in Vivo* Characterization of HER2-Positive Tumors by near-Infrared Imaging. *Clin. Cancer Res.* **2008**, *14*, 3840−3849.
(710) Gong, H. B.; Kovar, J.; Little, G.; Chen, H. X.; Olive, D. M. *In Vivo* Imaging of Xenograft Tumors Using an Epidermal Growth Factor Receptor-Specific Affibody Molecule Labeled with a Near-Infrared Fluorophore. *Neoplasia* **2010**, *12*, 139−149.
(711) Nguyen, Q. T.; Olson, E. S.; Aguilera, T. A.; Jiang, T.; Scadeng, M.; Ellies, L. G.; Tsien, R. Y. Surgery with Molecular Fluorescence Imaging Using Activatable Cell-Penetrating Peptides Decreases Residual Cancer and Improves Survival. *Proc. Natl. Acad. Sci. U. S. A.* **2010**, *107*, 4317−4322.
(712) Holt, D.; Okusanya, O.; Judy, R.; Venegas, O.; Jiang, J.; DeJesus, E.; Eruslanov, E.; Quatromoni, J.; Bhojnagarwala, P.; Deshpande, C.; Albelda, S.; Nie, S.; Singhal, S. Intraoperative near-Infrared Imaging Can Distinguish Cancer from Normal Tissue but Not Inflammation. *PLoS One* **2014**, *9*, e103342.
(713) van Dam, G. M.; Themelis, G.; Crane, L. M.; Harlaar, N. J.; Pleijhuis, R. G.; Kelder, W.; Sarantopoulos, A.; de Jong, J. S.; Arts, H. J.; van der Zee, A. G.; Bart, J.; Low, P. S.; Ntziachristos, V. Intraoperative Tumor-Specific Fluorescence Imaging in Ovarian Cancer by Folate Receptor-Alpha Targeting: First in-Human Results. *Nat. Med.* **2011**, *17*, 1315−1319.
(714) Nielsen, B.; Rank, F.; Illemann, M.; Lund, L.; Dano, K. Stromal Cells Associated with Early Invasive Foci in Human Mammary Ductal Carcinoma *in Situ* Coexpress Urokinase and Urokinase Receptor. *Int. J. Cancer* **2007**, *120*, 2086−2095.
(715) Pyke, C.; Graem, N.; Ralfkiaer, E.; Ronne, E.; Hoyerhansen, G.; Brunner, N.; Dano, K. Receptor for Urokinase Is Present in Tumor-Associated Macrophages in Ductal Breast-Carcinoma. *Cancer Res.* **1993**, *53*, 1911−1915.
(716) Yang, L.; Sajja, H. R.; Cao, Z.; Qian, W.; Bender, M.; Marcus, A. I.; Lipowska, M.; Wood, W. C.; Wang, A. uPAR-targeted Optical Imaging Contrasts as Theranostic Agents for Tumor Margin Detection. *Theranostics* **2014**, *4*, 106−118.
(717) Yang, L.; Mao, H.; Cao, Z.; Wang, Y.; Peng, X.; Wang, X.; Sajja, H.; Wang, L.; Duan, H.; Ni, C.; Staley, C.; Wood, W.; Gao, X.; Nie, S. Molecular Imaging of Pancreatic Cancer in an Animal Model Using Targeted Multifunctional Nanoparticles. *Gastroenterology* **2009**, *136*, 1514−1525.
(718) Wu, Y. Z.; Eisele, K.; Doroshenko, M.; Algara-Siller, G.; Kaiser, U.; Koynov, K.; Weil, T. A Quantum Dot Photoswitch for DNA Detection, Gene Transfection, and Live-Cell Imaging. *Small* **2012**, *8*, 3465−3475.
(719) Mikhaylov, G.; Mikac, U.; Magaeva, A. A.; Itin, V. I.; Naiden, E. P.; Psakhye, I.; Babes, L.; Reinheckel, T.; Peters, C.; Zeiser, R.; Bogyo, M.; Turk, V.; Psakhye, S. G.; Turk, B.; Vasiljeva, O. Ferri-Liposomes as an MRI-Visible Drug-Delivery System for Targeting Tumours and Their Microenvironment. *Nat. Nanotechnol.* **2011**, *6*, 594−602.
(720) Wang, D. S.; Fei, B. W.; Halig, L. V.; Qin, X. L.; Hu, Z. L.; Xu, H.; Wang, Y. A.; Chen, Z. J.; Kim, S.; Shin, D. M.; Chen, Z. Targeted Iron-Oxide Nanoparticle for Photodynamic Therapy and Imaging of Head and Neck Cancer. *ACS Nano* **2014**, *8*, 6620−6632.
(721) Huang, P.; Lin, J.; Wang, X. S.; Wang, Z.; Zhang, C. L.; He, M.; Wang, K.; Chen, F.; Li, Z. M.; Shen, G. X.; Cui, D. X.; Chen, X. Y. Light-Triggered Theranostics Based on Photosensitizer-Conjugated Carbon Dots for Simultaneous Enhanced-Fluorescence Imaging and Photodynamic Therapy. *Adv. Mater.* **2012**, *24*, 5104−5110.
(722) Huang, P.; Bao, L.; Zhang, C.; Lin, J.; Luo, T.; Yang, D.; He, M.; Li, Z.; Gao, G.; Gao, B.; Fu, S.; Cui, D. Folic Acid-Conjugated Silica-Modified Gold Nanorods for X-Ray/CT Imaging-Guided Dual-Mode Radiation and Photo-Thermal Therapy. *Biomaterials* **2011**, *32*, 9796−9809.
(723) Liang, S. J.; Li, C.; Zhang, C. L.; Chen, Y. S.; Xu, L.; Bao, C. C.; Wang, X. Y.; Liu, G.; Zhang, F. C.; Cui, D. X. CD44v6Monoclonal Antibody-Conjugated Gold Nanostars for Targeted Photoacoustic Imaging and Plasmonic Photothermal Therapy of Gastric Cancer Stem-like Cells. *Theranostics* **2015**, *5*, 970−984.
(724) Heck, J. G.; Napp, J.; Simonato, S.; Mollmer, J.; Lange, M.; Reichardt, H. M.; Staudt, R.; Alves, F.; Feldmann, C. Multifunctional Phosphate-Based Inorganic-Organic Hybrid Nanoparticles. *J. Am. Chem. Soc.* **2015**, *137*, 7329−7336.
(725) Xiong, R.; Soenen, S. J.; Braeckmans, K.; Skirtach, A. G. Towards Theranostic Multicompartment Microcapsules: In-Situ Diagnostics and Laser-Induced Treatment. *Theranostics* **2013**, *3*, 141−151.
(726) Delcea, M.; Yashchenok, A.; Videnova, K.; Kreft, O.; Mohwald, H.; Skirtach, A. G. Multicompartmental Micro- and Nanocapsules: Hierarchy and Applications in Biosciences. *Macromol. Biosci.* **2010**, *10*, 465−474.
(727) Kreft, O.; Muñoz Javier, A.; Sukhorukov, G. B.; Parak, W. J. Polymer Microcapsules as Mobile Local pH-Sensors. *J. Mater. Chem.* **2007**, *17*, 4471−4476.
(728) Chandrawati, R.; Hosta-Rigau, L.; Vanderstraaten, D.; Lokuliyana, S. A.; Stadler, B.; Albericio, F.; Caruso, F. Engineering Advanced Capsosomes: Maximizing the Number of Subcompartments, Cargo Retention, and Temperature-Triggered Reaction. *ACS Nano* **2010**, *4*, 1351−1361.
(729) Discher, B. M.; Bermudez, H.; Hammer, D. A.; Discher, D. E.; Won, Y. Y.; Bates, F. S. Cross-Linked Polymersome Membranes: Vesicles with Broadly Adjustable Properties. *J. Phys. Chem. B* **2002**, *106*, 2848−2854.
(730) Discher, D. E.; Eisenberg, A. Polymer Vesicles. *Science* **2002**, *297*, 967−973.
(731) Rivera Gil, P.; De Koker, S.; De Geest, B. G.; Parak, W. J. Intracellular Processing of Proteins Mediated by Biodegradable Polyelectrolyte Capsules. *Nano Lett.* **2009**, *9*, 4398−4402.
(732) Chanana, M.; Rivera Gil, P.; Correa-Duarte, M. A.; Parak, W. J.; Liz-Marzán, L. M. Physicochemical Properties of Protein-Coated Gold Nanoparticles in Biological Fluids and Cells before and after Proteolytic Digestion. *Angew. Chem., Int. Ed.* **2013**, *52*, 4179−4183.

DOI: 10.1021/acsnano.6b06040
ACS Nano 2017, 11, 2313−2381

(733) Suma, T.; Miyata, K.; Anraku, Y.; Watanabe, S.; Christie, R. J.; Takemoto, H.; Shioyama, M.; Gouda, N.; Ishii, T.; Nishiyama, N.; Kataoka, K. Smart Multilayered Assembly for Biocompatible siRNA Delivery Featuring Dissolvable Silica, Endosome-Disrupting Polycation, and Detachable PEG. *ACS Nano* **2012**, *6*, 6693−6705.
(734) Kim, H.; Ishii, T.; Zheng, M.; Watanabe, S.; Toh, K.; Matsumoto, Y.; Nishiyama, N.; Miyata, K.; Kataoka, K. Multifunctional Polyion Complex Micelle Featuring Enhanced Stability, Targetability, and Endosome Escapability for Systemic siRNA Delivery to Subcutaneous Model of Lung Cancer. *Drug Delivery Transl. Res.* **2014**, *4*, 50−60.
(735) Wang, Z.; Ruan, J.; Cui, D. X. Advances and Prospect of Nanotechnology in Stem Cells. *Nanoscale Res. Lett.* **2009**, *4*, 593−605.
(736) Deng, W.; Cao, X.; Chen, J.; Zhang, Z.; Yu, Q.; Wang, Y.; Shao, G.; Zhou, J.; Gao, X.; Yu, J.; Xu, X. MicroRNA Replacing Oncogenic Klf4 and c-Myc for Generating iPS Cells *via* Cationized *Pleurotus eryngii* Polysaccharide-based Nanotransfection. *ACS Appl. Mater. Interfaces* **2015**, *7*, 18957−18966.
(737) Ruan, J.; Ji, J. J.; Song, H.; Qian, Q. R.; Wang, K.; Wang, C.; Cui, D. X. Fluorescent Magnetic Nanoparticle-Labeled Mesenchymal Stem Cells for Targeted Imaging and Hyperthermia Therapy of *in Vivo* Gastric Cancer. *Nanoscale Res. Lett.* **2012**, *7*, 309.
(738) Li, C.; Liang, S. J.; Zhang, C. L.; Liu, Y. L.; Yang, M.; Zhang, J. P.; Zhi, X.; Pan, F.; Cui, D. X. Allogenic Dendritic Cell and Tumor Cell Fused Vaccine for Targeted Imaging and Enhanced Immunotherapeutic Efficacy of Gastric Cancer. *Biomaterials* **2015**, *54*, 177−187.
(739) Rivera Gil, P.; Oberdorster, G.; Elder, A.; Puntes, V. F.; Parak, W. J. Correlating Physico-Chemical with Toxicological Properties of Nanoparticles: The Present and the Future. *ACS Nano* **2010**, *4*, 5527−5531.
(740) Ge, C.; Du, J.; Zhao, L.; Wang, L.; Liu, Y.; Li, D.; Yang, Y.; Zhou, R.; Zhao, Y.; Chai, Z.; Chen, C. Binding of Blood Proteins to Carbon Nanotubes Reduces Cytotoxicity. *Proc. Natl. Acad. Sci. U. S. A.* **2011**, *108*, 16968−16973.
(741) Wang, L.; Jiang, X.; Ji, Y.; Bai, R.; Zhao, Y.; Wu, X.; Chen, C. Surface Chemistry of Gold Nanorods: Origin of Cell Membrane Damage and Cytotoxicity. *Nanoscale* **2013**, *5*, 8384−8391.
(742) Walkey, C. D.; Olsen, J. B.; Song, F. Y.; Liu, R.; Guo, H. B.; Olsen, D. W. H.; Cohen, Y.; Emili, A.; Chan, W. C. W. Protein Corona Fingerprinting Predicts the Cellular Interaction of Gold and Silver Nanoparticles. *ACS Nano* **2014**, *8*, 2439−2455.
(743) Lundqvist, M.; Stigler, J.; Elia, G.; Lynch, I.; Cedervall, T.; Dawson, K. A. Nanoparticle Size and Surface Properties Determine the Protein Corona with Possible Implications for Biological Impacts. *Proc. Natl. Acad. Sci. U. S. A.* **2008**, *105*, 14265−14270.
(744) Tinkle, S.; McNeil, S. E.; Muhlebach, S.; Bawa, R.; Borchard, G.; Barenholz, Y.; Tamarkin, L.; Desai, N. Nanomedicines: Addressing the Scientific and Regulatory Gap. *Ann. N. Y. Acad. Sci.* **2014**, *1313*, 35−56.
(745) Qiu, Y.; Liu, Y.; Wang, L. M.; Xu, L. G.; Bai, R.; Ji, Y. L.; Wu, X. C.; Zhao, Y. L.; Li, Y. F.; Chen, C. Y. Surface Chemistry and Aspect Ratio Mediated Cellular Uptake of Au Nanorods. *Biomaterials* **2010**, *31*, 7606−7619.
(746) Zhang, Z.; Wang, J.; Nie, X.; Wen, T.; Ji, Y.; Wu, X.; Zhao, Y.; Chen, C. Near Infrared Laser-Induced Targeted Cancer Therapy Using Thermoresponsive Polymer Encapsulated Gold Nanorods. *J. Am. Chem. Soc.* **2014**, *136*, 7317−7326.
(747) Wang, Y. W.; Grainger, D. W. Barriers to Advancing Nanotechnology to Better Improve and Translate Nanomedicines. *Front. Chem. Sci. Eng.* **2014**, *8*, 265−275.
(748) He, X.; Zhang, H.; Ma, Y.; Bai, W.; Zhang, Z.; Lu, K.; Ding, Y.; Zhao, Y.; Chai, Z. Lung Deposition and Extrapulmonary Translocation of Nano-Ceria after Intratracheal Instillation. *Nanotechnology* **2010**, *21*, 285103.
(749) Wang, B.; Feng, W.; Zhu, M.; Wang, Y.; Wang, M.; Gu, Y.; Ouyang, H.; Wang, H.; Li, M.; Zhao, Y.; Chai, Z.; Wang, H. Neurotoxicity of Low-Dose Repeatedly Intranasal Instillation of Nano- and Submicron-Sized Ferric Oxide Particles in Mice. *J. Nanopart. Res.* **2009**, *11*, 41−53.
(750) Zhu, M. T.; Nie, G. J.; Meng, H.; Xia, T.; Nel, A.; Zhao, Y. L. Physicochemical Properties Determine Nanomaterial Cellular Uptake, Transport, and Fate. *Acc. Chem. Res.* **2013**, *46*, 622−631.
(751) Wang, B.; He, X.; Zhang, Z. Y.; Zhao, Y. L.; Feng, W. Y. Metabolism of Nanomaterials *in Vivo*: Blood Circulation and Organ Clearance. *Acc. Chem. Res.* **2013**, *46*, 761−769.
(752) Ernsting, M. J.; Murakami, M.; Roy, A.; Li, S. D. Factors Controlling the Pharmacokinetics, Biodistribution and Intratumoral Penetration of Nanoparticles. *J. Controlled Release* **2013**, *172*, 782−794.
(753) Longmire, M.; Choyke, P. L.; Kobayashi, H. Clearance Properties of Nano-Sized Particles and Molecules as Imaging Agents: Considerations and Caveats. *Nanomedicine* **2008**, *3*, 703−717.
(754) Petros, R. A.; DeSimone, J. M. Strategies in the Design of Nanoparticles for Therapeutic Applications. *Nat. Rev. Drug Discovery* **2010**, *9*, 615−627.
(755) Koo, H.; Huh, M. S.; Sun, I. C.; Yuk, S. H.; Choi, K.; Kim, K.; Kwon, I. C. *In Vivo* Targeted Delivery of Nanoparticles for Theranosis. *Acc. Chem. Res.* **2011**, *44*, 1018−1028.
(756) He, X. X.; Nie, H. L.; Wang, K. M.; Tan, W. H.; Wu, X.; Zhang, P. F. *In Vivo* Study of Biodistribution and Urinary Excretion of Surface-Modified Silica Nanoparticles. *Anal. Chem.* **2008**, *80*, 9597−9603.
(757) Hartung, T. Toxicology for the Twenty-First Century. *Nature* **2009**, *460*, 208−212.
(758) Schleh, C.; Semmler-Behnke, M.; Lipka, J.; Wenk, A.; Hirn, S.; Schaeffler, M.; Schmid, G.; Simon, U.; Kreyling, W. G. Size and Surface Charge of Gold Nanoparticles Determine Absorption across Intestinal Barriers and Accumulation in Secondary Target Organs after Oral Administration. *Nanotoxicology* **2012**, *6*, 36−46.
(759) Kreyling, W. G.; Hirn, S.; Möller, W.; Schleh, C.; Wenk, A.; Celik, G.; Lipka, J.; Schäffler, M.; Haberl, N.; Johnston, B. D.; Sperling, R.; Schmid, G.; Simon, U.; Parak, W. J.; Semmler-Behnke, M. Air−Blood Barrier Translocation of Tracheally Instilled Gold Nanoparticles Inversely Depends on Particle Size. *ACS Nano* **2014**, *8*, 222−233.
(760) Kreuter, J. Drug Delivery to the Central Nervous System by Polymeric Nanoparticles: What Do We Know? *Adv. Drug Delivery Rev.* **2014**, *71*, 2−14.
(761) Wang, B.; Feng, W. Y.; Wang, M.; Shi, J. W.; Zhang, F.; Ouyang, H.; Zhao, Y. L.; Chai, Z. F.; Huang, Y. Y.; Xie, Y. N.; Wang, H. F.; Wang, J. Transport of Intranasally Instilled Fine Fe2O3 Particles into the Brain: Micro-distribution, Chemical States, and Histopathological Observation. *Biol. Trace Elem. Res.* **2007**, *118*, 233−243.
(762) Wick, P.; Malek, A.; Manser, P.; Meili, D.; Maeder-Althaus, X.; Diener, L.; Diener, P. A.; Zisch, A.; Krug, H. F.; von Mandach, U. Barrier Capacity of Human Placenta for Nanosized Materials. *Environ. Health Perspect.* **2009**, *118*, 432−436.
(763) Grafmuller, S.; Manser, P.; Krug, H. F.; Wick, P.; von Mandach, U. Determination of the Transport Rate of Xenobiotics and Nanomaterials Across the Placenta using the *ex Vivo* Human Placental Perfusion Model. *J. Visualized Exp.* **2013**, *76*, e50401.
(764) Batrakova, E. V.; Kabanov, A. V. Pluronic Block Copolymers: Evolution of Drug Delivery Concept from Inert Nanocarriers to Biological Response Modifiers. *J. Controlled Release* **2008**, *130*, 98−106.
(765) Zhou, T.; Yu, M.; Zhang, B.; Wang, L.; Wu, X.; Zhou, H.; Du, Y.; Hao, J.; Tu, Y.; Chen, C.; Wei, T. Inhibition of Cancer Cell Migration by Gold Nanorods: Molecular Mechanisms and Implications for Cancer Therapy. *Adv. Funct. Mater.* **2014**, *24*, 6922−6932.
(766) Chen, C.; Li, Y.-F.; Qu, Y.; Chai, Z.; Zhao, Y. Advanced Nuclear Analytical and Related Techniques for the Growing Challenges in Nanotoxicology. *Chem. Soc. Rev.* **2013**, *42*, 8266−8303.
(767) Jariwala, D.; Sangwan, V. K.; Lauhon, L. J.; Marks, T. J.; Hersam, M. C. Carbon Nanomaterials for Electronics, Optoelectronics, Photovoltaics, and Sensing. *Chem. Soc. Rev.* **2013**, *42*, 2824−2860.
(768) Hung, A. H.; Duch, M. C.; Parigi, G.; Rotz, M. W.; Manus, L. M.; Mastarone, D. J.; Dam, K. T.; Gits, C. C.; MacRenaris, K. W.; Luchinat, C.; Hersam, M. C.; Meade, T. J. Mechanisms of Gadographene-Mediated Proton Spin Relaxation. *J. Phys. Chem. C* **2013**, *117*, 16263−16273.
(769) Hung, A. H.; Holbrook, R. J.; Rotz, M. W.; Glasscock, C. J.; Mansukhani, N. D.; MacRenaris, K. W.; Manus, L. M.; Duch, M. C.;

DOI: 10.1021/acsnano.6b06040
ACS Nano 2017, 11, 2313−2381

Dam, K. T.; Hersam, M. C.; Meade, T. J. Graphene Oxide Enhances Cellular Delivery of Hydrophilic Small Molecules by Co-Incubation. *ACS Nano* **2014**, *8*, 10168−10177.
(770) Mutlu, G. M.; Budinger, G. R. S.; Green, A. A.; Urich, D.; Soberanes, S.; Chiarella, S. E.; Alheid, G. F.; McCrimmon, D. R.; Szleifer, I.; Hersam, M. C. Biocompatible Nanoscale Dispersion of Single-Walled Carbon Nanotubes Minimizes *in Vivo* Pulmonary Toxicity. *Nano Lett.* **2010**, *10*, 1664−1670.
(771) Wang, X.; Xia, T.; Duch, M. C.; Ji, Z. X.; Zhang, H. Y.; Li, R. B.; Sun, B. B.; Lin, S. J.; Meng, H.; Liao, Y. P.; Wang, M. Y.; Song, T. B.; Yang, Y.; Hersam, M. C.; Nel, A. E. Pluronic F108 Coating Decreases the Lung Fibrosis Potential of Multiwall Carbon Nanotubes by Reducing Lysosomal Injury. *Nano Lett.* **2012**, *12*, 3050−3061.
(772) Duch, M. C.; Budinger, G. R. S.; Liang, Y. T.; Soberanes, S.; Urich, D.; Chiarella, S. E.; Campochiaro, L. A.; Gonzalez, A.; Chandel, N. S.; Hersam, M. C.; Mutlu, G. M. Minimizing Oxidation and Stable Nanoscale Dispersion Improves the Biocompatibility of Graphene in the Lung. *Nano Lett.* **2011**, *11*, 5201−5207.
(773) Wang, X.; Duch, M. C.; Mansukhani, N.; Ji, Z. X.; Liao, Y. P.; Wang, M. Y.; Zhang, H. Y.; Sun, B. B.; Chang, C. H.; Li, R. B.; Lin, S. J.; Meng, H.; Xia, T.; Hersam, M. C.; Nel, A. E. Use of a Pro-Fibrogenic Mechanism-Based Predictive Toxicological Approach for Tiered Testing and Decision Analysis of Carbonaceous Nanomaterials. *ACS Nano* **2015**, *9*, 3032−3043.
(774) Wick, P.; Manser, P.; Limbach, L. K.; Dettlaff-Weglikowska, U.; Krumeich, F.; Roth, S.; Stark, W. J.; Bruinink, A. The Degree and Kind of Agglomeration Affect Carbon Nanotube Cytotoxicity. *Toxicol. Lett.* **2007**, *168*, 121−131.
(775) Chowdhury, I.; Duch, M. C.; Gits, C. C.; Hersam, M. C.; Walker, S. L. Impact of Synthesis Methods on the Transport of Single Walled Carbon Nanotubes in the Aquatic Environment. *Environ. Sci. Technol.* **2012**, *46*, 11752−11760.
(776) Chowdhury, I.; Duch, M. C.; Mansukhani, N. D.; Hersam, M. C.; Bouchard, D. Colloidal Properties and Stability of Graphene Oxide Nanomaterials in the Aquatic Environment. *Environ. Sci. Technol.* **2013**, *47*, 6288−6296.
(777) Chowdhury, I.; Duch, M. C.; Mansukhani, N. D.; Hersam, M. C.; Bouchard, D. Deposition and Release of Graphene Oxide Nanomaterials Using a Quartz Crystal Microbalance. *Environ. Sci. Technol.* **2014**, *48*, 961−969.
(778) Chowdhury, I.; Duch, M. C.; Mansukhani, N. D.; Hersam, M. C.; Bouchard, D. Interactions of Graphene Oxide Nanomaterials with Natural Organic Matter and Metal Oxide Surfaces. *Environ. Sci. Technol.* **2014**, *48*, 9382−9390.
(779) Jariwala, D.; Sangwan, V. K.; Lauhon, L. J.; Marks, T. J.; Hersam, M. C. Emerging Device Applications for Semiconducting Two-Dimensional Transition Metal Dichalcogenides. *ACS Nano* **2014**, *8*, 1102−1120.
(780) Wang, X.; Mansukhani, N. D.; Guiney, L. M.; Ji, Z.; Chang, C. H.; Wang, M.; Liao, Y.-P.; Song, T.-B.; Sun, B.; Li, R.; Xia, T.; Hersam, M. C.; Nel, A. E. Differences in the Toxicological Potential of Two-Dimensional *versus* Aggregated Molybdenum Disulfide in the Lung. *Small* **2015**, *11*, 5079−5087.
(781) Lanphere, J. D.; Luth, C. J.; Guiney, L. M.; Mansukhani, N. D.; Hersam, M. C.; Walker, S. L. Fate and Transport of Molybdenum Disulfide Nanomaterials in Sand Columns. *Environ. Eng. Sci.* **2015**, *32*, 163−173.
(782) Choi, H. S.; Frangioni, J. V. Nanoparticles for Biomedical Imaging: Fundamentals of Clinical Translation. *Mol. Imaging* **2010**, *9*, 291−310.
(783) Lavik, E.; von Recum, H. The Role of Nanomaterials in Translational Medicine. *ACS Nano* **2011**, *5*, 3419−3424.
(784) Stern, S. T.; Hall, J. B.; Yu, L. L.; Wood, L. J.; Paciotti, G. F.; Tamarkin, L.; Long, S. E.; McNeil, S. E. Translational Considerations for Cancer Nanomedicine. *J. Controlled Release* **2010**, *146*, 164−174.
(785) Dodson, B. P.; Levine, A. D. Challenges in the Translation and Commercialization of Cell Therapies. *BMC Biotechnol.* **2015**, *15*, 70.
(786) Prabhakar, U.; Maeda, H.; Jain, R. K.; Sevick-Muraca, E. M.; Zamboni, W.; Farokhzad, O. C.; Barry, S. T.; Gabizon, A.; Grodzinski, P.; Blakey, D. C. Challenges and Key Considerations of the Enhanced Permeability and Retention Effect for Nanomedicine Drug Delivery in Oncology. *Cancer Res.* **2013**, *73*, 2412−2417.
(787) Dunn, P.; Kuo, T. T.; Shih, L. Y.; Wang, P. N.; Sun, C. F.; Chang, M. W. J. Bone Marrow Failure and Myelofibrosis in a Case of PVP Storage Disease. *Am. J. Hematol.* **1998**, *57*, 68−71.
(788) Kuo, T. T.; Hu, S.; Huang, C. L.; Chan, H. L.; Chang, M. J. W.; Dunn, P.; Chen, Y. J. Cutaneous Involvement in Polyvinylpyrrolidone Storage Disease: A Clinicopathologic Study of Five Patients, Including Two Patients with Severe Anemia. *Am. J. Surg. Pathol.* **1997**, *21*, 1361−1367.
(789) Schneider, P.; Korolenko, T. A.; Busch, U. A Review of Drug-Induced Lysosomal Disorders of the Liver in Man and Laboratory Animals. *Microsc. Res. Tech.* **1997**, *36*, 253−275.
(790) Urbanics, R.; Bedocs, P.; Szebeni, J. Lessons Learned from the Porcine CARPA Model: Constant and Variable Responses to Different Nanomedicines and Administration Protocols. *Eur. J. Nanomed.* **2015**, *7*, 219−231.
(791) Dézsi, L.; Fülöp, T.; Mészáros, T.; Szénási, G.; Urbanics, R.; Vázsonyi, C.; Őrfi, E.; Rosivall, L.; Nemes, R.; Kok, R. J.; Metselaar, J. M.; Storm, G.; Szebeni, J. Features of Complement Activation-Related Pseudoallergy to Liposomes with Different Surface Charge and PEGylation: Comparison of the Porcine and Rat Responses. *J. Controlled Release* **2014**, *195*, 2−10.
(792) Parandian, A.; Rip, A.; Te Kulve, H. Dual Dynamics of Promises, and Waiting Games around Emerging Nanotechnologies. *Technol. Anal. Strateg.* **2012**, *24*, 565−582.
(793) Irfan, M.; Seiler, M. Encapsulation Using Hyperbranched Polymers: From Research and Technologies to Emerging Applications. *Ind. Eng. Chem. Res.* **2010**, *49*, 1169−1196.
(794) Tyrrell, Z. L.; Shen, Y.; Radosz, M. Fabrication of Micellar Nanoparticles for Drug Delivery through the Self-Assembly of Block Copolymers. *Prog. Polym. Sci.* **2010**, *35*, 1128−1143.
(795) Shen, Y. Q.; Jin, E. L.; Zhang, B.; Murphy, C. J.; Sui, M. H.; Zhao, J.; Wang, J. Q.; Tang, J. B.; Fan, M. H.; Van Kirk, E.; Murdoch, W. J. Prodrugs Forming High Drug Loading Multifunctional Nanocapsules for Intracellular Cancer Drug Delivery. *J. Am. Chem. Soc.* **2010**, *132*, 4259−4265.
(796) Tang, H. D.; Murphy, C. J.; Zhang, B.; Shen, Y. Q.; Sui, M. H.; Van Kirk, E. A.; Feng, X. W.; Murdoch, W. J. Amphiphilic Curcumin Conjugate-Forming Nanoparticles as Anticancer Prodrug and Drug Carriers: *In Vitro* and *in Vivo* Effects. *Nanomedicine* **2010**, *5*, 855−865.

DOI: 10.1021/acsnano.6b06040
ACS Nano 2017, 11, 2313−2381